

https://dspace.org/

Development of a biophysical system based on bentonite, zeolite and micro-organisms for remediating gold mine wastewaters and tailings ponds

Nsimba, Elisee Bakatula

2013-04-22
http://hdl.handle.net/10539/12672

Downloaded from a DSpace repository. https://dspace.org/

DEVELOPMENT OF A BIOPHYSICAL SYSTEM BASED ON BENTONITE, ZEOLITE AND MICRO-ORGANISMS FOR REMEDIATING GOLD MINE WASTEWATERS AND TAILINGS PONDS

Elisee Bakatula Nsimba

A thesis submitted to the Faculty of Science, University of the Witwatersrand, Johannesburg, in fulfilment of the requirements for the degree of

Doctor of Philosophy

Johannesburg 2012

Declaration

I declare that this thesis is my own, unaided work. It is being submitted for the award of the Degree of Doctor of Philosophy to the University of the Witwatersrand, Johannesburg. It has not been submitted before for any degree or examination to any other University.

(Signature of candidate)

……day of…….2012

Abstract

Wastes from mining operations usually contain a suite of pollutants, among them cyanide and its complexes; heavy metals; metalloids and radionuclides. The pollution plume can affect public health through contamination of drinking water supplies, aquatic ecosystems and agricultural soils. As such, waste management and remediation has become an important integral component of mining. Conventional chemical and physical methods are often expensive and ineffective when the pollutant concentrations are very high, so the challenge of developing cost-effective materials with high adsorption efficiencies for pollutants still remains.

This research was dedicated to the development of biosorbents with high metal loading capacity for the remediation of mine wastewater, namely: zeolite/bentonite functionalised with microbial components such as histidine, cysteine, sorbitol and mannitol; zeolite/bentonite functionalised with *Penicillium-simplicissimum* and zeolite-alginate complex generated by impregnating natural zeolite into alginate gel beads. The ability of the fresh water algae, *Oedogonium* sp. to remove heavy metals from aqueous solutions in batch systems was also assessed.

Optimum biosorption conditions for the removal of Co, Cu, Cr, Fe, Hg, Ni, Zn and U (in a single-ion and multi-ion systems) were determined as a function of pH, initial concentration, contact time, temperature, and mass of biosorbent. An increase of adsorption capacity was observed following modification of natural zeolite/bentonite by microbial components with a maximum adsorption capacity obtained at low pH. The FTIR results of the developed biosorbents showed that the biomass has different functional groups that are able to react with metal ions in aqueous solution.

Immobilisation of fungi (*Penicillium-simplicissimum*) on zeolite/bentonite yielded biomass of 600 mg g^{-1} (10-fold higher than the non-immobilised one) at a pH 4, showing the potential of this sorbent towards remediation of AMD-polluted mine sites. The maximum uptake of metals ions (in a multi-ion system) was higher and constant (40-50 mg g^{-1}) in the inactive fungal biomass (heat-killed) from pH 2 to 7. The uptake of U and Hg increased significantly in the zeolite/bentonite-*P.simplicissimum* compared to their natural forms due to the presence of the N-H, S-H and COO^- groups.

The pseudo second-order adsorption model was found to be more suitable in describing the adsorption kinetics of metal ions onto biomasses in single- and multi-ion systems with the sorption of nickel being controlled by film diffusion processes (with the coefficient values of 10^{-7} cm^2 s^{-1}). The thermodynamic parameters showed that the adsorption onto developed biosorbents was feasible and spontaneous under the studied conditions.

The calculated values of the loading capacities in column adsorption for the natural zeolite/bentonite as well as zeolite/bentonite-*P.simplicissimum* were close to those obtained in the batch tests, mainly for U and Ni. The bed depth service time model (BDST) was used successfully to fit the experimental data for Ni and U adsorbed on the natural zeolite. This suggested a linear relationship between bed depth and service time, which could be used for scale-up purpose.

The developed biosorbents could be regenerated using 1 mol L^{-1} HNO_3 solution for potential re-use. The total decrease in biosorption efficiency of zeolite-*Penicillium simplicissimum* after five cycles of adsorption-desorption was $\leq$ 5% which showed that zeolite/bentonite-*Penicillium simplicissimum* had good potential to adsorb metal ions repeatedly from aqueous solution. On applying it to real wastewater samples, the zeolite-*P. simplicissimum* biosorbent removed 97% of the metals. *Penicillium* sp. immobilisation enhanced the potential and makes it an attractive bioremediation agent.

The zeolite-alginate sorbent exhibited elevated adsorption capacities for metals. This showed potential for use of such a system for remediation purposes. It also provides a platform to explore the possibility of using zeolite in conjunction with other polysaccharide-containing materials for heavy metal removal from wastewaters.

The results obtained in this study have shown that zeolite and bentonite are good supports for biomass. The biofunctionalised zeolite/bentonite systems have potential in removal of heavy metals from wastewaters.

Dedicace,

I would like to dedicate this work to many people that were beside me throughout this long exciting journey, without their unrelenting confidence and support I couldn't have come so far.

Acknowledgements

Science is a collaborative enterprise, and this thesis could not exist without the contributions of many people and I would like to offer my deepest thanks to them:

Dr Hlanganani Tutu, my supervisor, for the contributions and ideas to make my PhD experience productive and stimulating. The joy and enthusiasm he has for research was contagious and motivational for me, even during tough times. It has been an honour to be his first PhD student and he has taught me, both consciously and unconsciously, how good scientific research is done.

Prof. Ewa M. Cukrowska, my co-supervisor, for her enthusiasm, encouragement and advice throughout this formation.

Ms Isabel Weiersbye of the School of Animal, Plant and Environmental Sciences, Wits University, for the valuable information that she provided and for her assistance with sample collection at mining sites.

Dr Ing. Leonard Mihaly- Cozmuta (North university of Baia Mare (Romania) for his valuable contribution. Dr Ing. Anca Mihaly, Dr Monica Marian, Dr Anca Peter, Dr Camelia Nicula for their contribution. I really enjoyed the time and experience shared during my stay in Romania.

Prof. Collin Straker of the School of Molecular and Cell Biology, Wits University, for accepting me in his lab and providing the strains of fungi used in this study.

I would like to thank Prof. Boguslaw Buszewski and Dr Miroslav Sprynskyy of the Nicholas Kopernicus University, Poland for their valuable information and discussions.

Many thanks to Richard Mampa for helping with NMR Spectroscopy analysis.

I gratefully acknowledge the funding sources that made my PhD work possible. I was funded by the National Research Foundation (NRF), Thuthuka Programme, the South Africa-Romania Bilateral Programme through the NRF, the Carnegie Corporation, Anglogold Ashanti, Wits University through the Postgraduate Merit Awards and the Friedel Sellschop Award.

To my family, many thanks for being there for me all the time, your love, support and encouragement meant a lot to me.

My mentor, Prof. Fidele Lungungu, thanks for your precious advice as well as the moral and financial support.

My sincere gratitude to Dr Agata Bartyzel, Dr Julien Lusilao and Pierre Kalenga for the encouragement and friendship.

And finally, to my colleagues in the Environmental Analytical Chemistry Research Group, thanks for the collaboration and the time shared together.

At last, I'm thankful to the mighty God for all his blessings, wisdom and guidance throughout my life.

Contents **Page**

Declaration ***i***
Abstract ***ii***
Dedicace ***iv***
Acknowledgements ***v***
Contents ***vii***
List of figures ***xi***
List of tables ***xxi***
Abbreviations ***xxvii***

Chapter 1- Introduction ***1***
1.1 Background and motivation 1
1.2 Problem statement 2
1.3 Objectives of the research 4
1.4 Research approach 5
1.5 Outline of the thesis 6

Chapter 2 - Literature review ***8***
2.1 State of pollution in the Witwatersrand 8
2.1.1 Acid mine drainage 9
2.1.2 Toxic element contamination and leaching 10
2.1.3 Pollution by processing chemicals 11
2.1.4 Erosion and sedimentation 11
2.2 Remediation technology 11
2.2.1 Chemical and physical methods 12
2.2.2 Phytoremediation 23
2.2.3 Microbial remediation process 25
2.2.4 Fungi in bioremediation 35
2.2.5 Algae in bioremediation 39

Chapter 3-Materials and methods ***49***
3.1 Field studies 49
3.1.1 Collecting materials 49
3.1.2 Collecting water samples 51
3.2 Laboratory investigations 53
3.2.1 Biomaterials development 53
3.2.1.1 Natural zeolite/bentonite 53
3.2.1.2 Functionalisation of zeolite/bentonite with the proxy-compounds 53
3.2.1.3 Preparation of Zeolite/Bentonite-*Penicillium simplicissimum* 54
3.2.1.4 Preparation of algal biomass 56
3.2.1.5 Isolation of alginates from *Oedogonium* sp 57
3.2.1.6 Preparation of alginate complex beads 57
3.2.2.Characterisation of the raw materials and the developed biosorbents 58
3.2.2.1 Physical properties 58
3.2.2.2 Chemical properties 59
3.2.3 Analytical procedures 61
3.2.3.1 Chemicals and reagents 61
3.2.3.2 Preparation of standard solutions 61
3.2.3.3 Metals analysis 62
3.2.3.4 Sorption studies 62
3.2.3.5 Metal analysis in fresh algae (Oedogonium sp.) 66

3.2.3.6 Biosorption studies on algal biomass…….....67
3.2.3.7 Biosorption studies on Na-Alginate-zeolite complex……68
3.2.3.8 Desorption studies on Na-Alginate-zeolite complex……69
3.3 Data analysis……...69
3.3.1 Statistical analysis……69
3.3.2 Analytical figures of merit……69
3.4 Fitting data in equilibrium (isotherms), kinetics and thermodynamic models……..70
3.4.1 Isotherm models……...70
3.4.2 Kinetic models……73
3.4.3 Thermodynamic parameters……76

Chapter 4-Results and discussion……78
4.1 Bentonite……..78
4.1.1 Mineral and chemical properties ……...78
4.1.2 Physical surface characteristics ……79
4.1.2.1 Surface area and pore volume analysis ……....79
4.1.2.2 Zeta potential measurements ……...80
4.1.2.3 Thermal analysis……...82
4.1.3 Chemical properties of the surface ……...83
4.1.3.1 Cation exchange capacity and elemental analysis ……..83
4.1.3.2 FT-IR spectral analysis ……...84
4.1.4 Sorption studies ……87
4.1.4.1 Sorption capacities, pH and isotherms of adsorption……..87
4.1.4.2 Effect of contact time and kinetics of adsorption ……...93
4.4.4.3 Effect of temperature and thermodynamic parameters……96

4.2 Functionalised Bentonite with proxy-compounds ……..99
4.2.1 Bentonite-Histidine ……...99
4.2.1.1 Sorption capacities, pH and isotherms of adsorption ……..99
4.2.1.2 Effect of contact time and kinetics of adsorption ……105
4.2.1.3 Effect of temperature and thermodynamic parameters …….....107
4.2.2 Bentonite-Cysteine…… 110
4.2.2.1 Sorption capacities, pH and isotherms of adsorption ……....111
4.2.2.2 Effect of contact time and kinetics of adsorption ……116
4.2.2.3 Effect of temperature and thermodynamic parameters …… 120
4.2.3 Bentonite-Sorbitol……123
4.2.3.1 Sorption capacities, pH and isotherms of adsorption.....124
4.2.3.2 Effect of contact time and kinetics of adsorption……..128
4.2.3.3 Effect of temperature and thermodynamic parameters……. ……131

4.3 Zeolite……135
4.3.1 Mineral and chemical properties…… 135
4.3.2 Physical surface characteristics ……..136
4.3.2.1 Surface area and pore volume analysis ……...136
4.3.2.2 Zeta potential analysis……..137
4.3.2.3 Thermal analysis……...139
4.3.3 Chemical properties of the surface……139
4.3.3.1 Cation exchange capacity and elemental composition……139
4.3.3.2 FTIR spectral analysis ……140
4.3.4 Sorption studies ……143
4.3.4.1 Sorption capacities, pH and isotherms of adsorption……...144
4.3.4.2 Effect of contact time and kinetics of adsorption ……148
4.3.4.3 Effect of temperature and thermodynamic parameters ……151

4.4 Functionalised Zeolite with proxy-compounds ……...154
4.4.1 Zeolite-Histidine ……...154
4.4.1.1 Sorption capacities, pH and isotherms of adsorption ……154
4.4.1.2 Effect of contact time and kinetics of adsorption ……...160
4.4.1.3 Effect of temperature and thermodynamic parameters……162
4.4.2 Zeolite-Cysteine……165
4.4.2.1 Sorption capacities, pH and isotherms of adsorption ……165
4.4.2.2 Effect of contact time and kinetics of adsorption ……...170
4.4.2.3 Effect of temperature and thermodynamic parameters……173
4.4.3 Zeolite-Sorbitol**……*175***
4.4.3.1 Sorption capacities, pH and isotherms of adsorption ……175
4.4.3.2 Effect of contact time and kinetics of adsorption ……...179
4.4.3.3 Effect of temperature and thermodynamic parameters……182
Conclusion……185

4.5 Capacity of metal sorption by Bentonite and Zeolite after biofunctionalisation with *Penicillium simplicissimum*……192
4.5.1 Growth and morphology identification of *Penicillium simplicissimum*……192
4.5.2 Bentonite-*Penicillium simplicissimum*……193
4.5.2.1 Growth curve of *P. simplicissimum* on bentonite……193
4.5.2.2 Characteristics of the biomass……195
4.5.2.3 Sorption studies of metals on Bentonite-*P.simplicissimum* (active or living) in batch mode……198
4.5.2.3.1 Sorption capacities, pH and isotherms of adsorption……198
4.5.2.3.2 Effect of contact time and kinetic of adsorption……208
4.5.2.3.3 Effect of temperature and thermodynamic parameters……214
4.5.2.4 Sorption studies of metals on Bentonite-*P.simplicissimum* (inactive or heat killed) in batch mode……220
4.5.2.4.1 Sorption capacities, pH and isotherms of adsorption……221
4.5.2.4.2 Effect of contact time and kinetic of adsorption……229
4.5.2.4.3 Effect of temperature and thermodynamic parameters……234
4.5.2.4.4 Metal ions biosorption as function of culture age……239
4.5.3 Zeolite-*Penicillium simplicissimum*……241
4.5.3.1 Growth curve of *P. simplicissimum* on zeolite……241
4.5.3.2 Characteristics of the biomass……242
4.5.3.3 Sorption studies of metals on Zeolite-*P.simplicissimum* (active or living) in batch mode……245
4.5.3.3.1 Sorption capacities, pH and isotherms of adsorption……245
4.5.3.3.2 Effect of contact time and kinetic of adsorption……252
4.5.3.3.3 Effect of temperature and thermodynamic parameters……258
4.5.3.4 Sorption studies of metals on Zeolite-*P.simplicissimum* (inactive or heat killed) in batch mode……263
4.5.3.4.1 Sorption capacities, pH and isotherms of adsorption……263
4.5.3.4.2 Effect of contact time and kinetic of adsorption……271
4.5.3.4.3 Effect of temperature and thermodynamic parameters……276
4.5.3.4.4 Metal ions biosorption as function of culture age……281
4.5.3.4.5 Adsorption study of uranium in the presence of other metals……283
4.5.3.4.6 Effect of biorbent mass on the adsorption capacity……284
4.5.3.4.7 Regeneration of the biosorbent……285
4.5.3.4.8 Application of zeolite-*P.simplicissimum* (inactive) in mine wastewater remediation……287
Conclusion……289

4.5.4 Sorption studies of the adsorption of metals on natural and functionalised Bentonite/Zeolite with *P. simplicissimum* (inactive) in column mode.....292
4.5.4.1 Breakthrough curves……292
4.5.4.2 Column performance……293
4.5.4.3 Number of theoretical plates……303
4.5.4.4 Desorption studies and regeneration of the biosorbent……305
4.5.4.5 Mathematical models……...310
Conclusion……...312

4.6 Augmentation of mine water remediation through biofunctionalisation of zeolite and bentonite with alginate extracts and green algae…….....313
4.6.1 Physical properties and elemental composition of the algal biomass…… 313
4.6.2 Metal analysis ……316
4.6.3 Sorption studies of heavy metals on algal biomass…….316
4.6.3.1 Effects of pre-treatment on sorption capacity of the biomass……...317
4.6.3.2 Sorption capacities, pH and isotherms of adsorption……....317
4.6.3.3 Effect of contact time and kinetic of adsorption……..327
4.6.3.4 Effect of temperature and thermodynamic parameters…….333
4.6.3.5 Effect of adsorbent mass……...335
4.6.3.6 Regeneration and reuse of the algal biomass ……...336
4.6.4 Extraction and isolation of alginate from Oedogonium sp.……338
4.6.4.1 Alginate content of Oedogonium sp…….338
4.6.4.2 Estimation of M:G ratios by ^{1}HNMR ……..340
4.6.5 Biosorption of metal ions by zeolite impregnated with Na-alginate complex……345
4.6.5.1 Characteristics of the zeolite-alginate……...345
4.6.5.2 Sorption capacities, pH and isotherms of adsorption……347
4.6.3.3 Effect of contact time and kinetic studies..…….. ……358
4.6.3.4 Effect of temperature and thermodynamic parameters…….363
4.6.5.5 Effect of adsorbent mass……...365
4.6.5.6 Regeneration and reuse of the zeolite-alginate…….366
Conclusion……...370

***Chapter 5 General conclusion and recommendations*……..... 373**

Publications*……..*376
References*……....*378
Appendices* ……..*416

List of figures

Figure 2.1 Schematic illustrations of adsorption steps…….18

Figure 2.2 Layer structure of bentonite……22

Figure2.3 .Mechanisms of biosorption, a) classification according to dependence on cell metabolism, b) classification according to the location within the cell and the metal removed……..28

Figure 2.4 Chemical structure of glutathione (GSH) ……..33

Figure 2.5 Chemical structures of molecules binding heavy metals: A) Natural phytochelatin (PC) and B) Synthetic phytochelatin (EC) - glutamic acid (glu-E) and cysteine (Cys-C) ……34

Figure 2.6 Schematic representations of the outer fungal cell layers …….37

Figure 2.7 Cell wall structures in the brown algae ……...41

Figure 2.8 Alginate structural data: (A) alginate monomers (M versus G); (B) the alginate polymer; (C) chain sequences of the alginate polymer ……41

Figure 2.9 Schematic representation of the calcium-induced gelation of alginate in accordance with the ‘‘egg-box’’ structure ……...44

Figure 3.1 West Wits operations in the regional context……50

Figure 3.2 Mat- forming algae in the West Boundary Dam……...51

Figure 3.3 Filamentous green algae in the Varkenslaagte stream……..51

Figure 3.4 Map of study area and sampling points…….52

Figure 3.5 Photograph of the column experiment set-up……..66

Figure 4.1 XRD spectrum of bentonite powder……...78

Figure 4.2 The zeta potential of: (a) natural bentonite (b) Bentonite-histidine, Bentonite-cysteine, Bentonite-sorbitol……...81

Figure 4.3 Thermogravimetric curve of natural bentonite……82

Figure 4.4 FTIR spectrum of the natural……..84

Figure 4.5 Effect of initial pH on adsorption of (a) Cu, Ni, Zn, Cr and (b) Co, Fe, Hg and U onto natural bentonite in single component solutions (C_i = 100 mg L^{-1}, Temp = 298.15±1^oK, agitation rate = 150 rpm, agitation time = 12h)……...88

Figure 4.6 Effect of concentration on the adsorption of (a) Cu, Ni, Zn, Cr and (b) Co, Fe, Hg and U (in single-component solutions at pH 3) onto natural bentonite (Temp = 298.15±1^oK, agitation rate= 150 rpm, agitation time= 12h)……..90

Figure 4.7 Effect of contact time on adsorption of Cu, Ni, Zn, Co, Fe, Hg and U onto natural bentonite in single component solutions (C_i = 100 mg L^{-1}, Temp = 298.15±1^oK, agitation rate = 150 rpm)……93

Figure 4.8 Effect of temperature on adsorption of Cu, Ni, Zn, Co, Fe, Hg and U onto natural bentonite in single component solutions (Ci = 100 mg L^{-1}, pH 3, agitation rate = 150 rpm, contact time = 12 h)……97

Figure 4.9 Effect of initial pH on adsorption of (a) Cu, Ni, Zn, Cr and (b) Co, Fe, Hg and U onto bentonite-histidine in single component solutions (Ci = 100 mg L^{-1}, Temp = 298.15±1^{o}K, agitation rate = 150 rpm, agitation time = 12h)……..100

Figure 4.10 Illustration of histidine-metal complex…….101

Figure 4.11 Effect of concentration on the adsorption of (a) Cr, Cu, Ni, Zn and (b) Co, Fe, Hg, U (in single-component solutions at pH 3) onto bentonite-histidine (Temp = 298.15±1^{o}K, agitation rate = 150 rpm, agitation time = 12h)……102

Figure 4.12 Effect of contact time on adsorption of (a) Cu, Co, Ni, Zn and (b) Fe, Hg and U onto bentonite-histidine in single component solutions (C_i = 100 mg L^{-1}, Temp = 298.15±1^{o}K, agitation rate = 150 rpm)…….105

Figure 4.13 Effect of temperature on adsorption of (a) Cu, Co, Ni, Zn and (b) Fe, Hg and U onto bentonite-histidine in single component solutions (C_i = 100 mg L^{-1}, pH 3, agitation rate = 150 rpm, contact time = 12 h)…….108

Figure 4.14 Structure of (R)-Cysteine in zwitterionic form at neutral pH…….110

Figure 4.15 Effect of initial pH on adsorption of (a) Cu, Co, Ni, Zn and (b) Cr, Fe, Hg and U onto bentonite-cysteine in single component solutions (C_i = 100 mg L^{-1}, Temp = 298.15±1^{o}K, agitation rate = 150 rpm, agitation time = 12h)……..112

Figure 4.16 Effect of concentration on the adsorption of (a) Cu, Ni, Zn, Co (b) Cr, Fe, Hg and U onto bentonite-cysteine in single-component solutions at pH 3, Temp = 298.15±1^{o}K, agitation rate= 150 rpm, agitation time = 12h)……114

Figure 4.17 Effect of contact time on adsorption of Cu, Ni, Zn, Co, Cr, Fe, Hg and U onto bentonite-cysteine in single component solutions (C_i = 100 mg L^{-1}, Temp = 298.15±1^{o}K, agitation rate = 150 rpm)……..117

Figure 4.18 Effect of temperature on adsorption of (a) Cu, Zn, Hg, Co and (b) Cr, Ni, Fe, and U onto bentonite-cysteine in single component solutions (C_i = 100 mg L^{-1}, pH 3, agitation rate = 150 rpm, contact time = 12 h)…….121

Figure 4.19 Structure of sorbitol……123

Figure 4.20 Effect of initial pH on adsorption of (a) Cu, Ni, Zn, Co and (b) Fe, Cr, Hg and U onto bentonite-sorbitol in single component solutions (Ci = 100 mg L^{-1}, Temp = 298.15±1^{o}K, agitation rate = 150 rpm, agitation time = 12h)……..125

Figure 4.21 Effect of concentration on the adsorption of (a) Cu, Ni, Zn, Co and (b) Fe, Cr, Hg and U onto bentonite-sorbitol in single component solutions (at pH 3, Temp = 298.15±1^{o}K, agitation rate= 150 rpm, agitation time= 12h)……126

Figure 4.22 Effect of contact time on the adsorption of (a) Cu, Ni, Zn, Co and (b) Cr, Fe, Hg and U onto bentonite-sorbitol in single component solutions (C_i = 100 mg L^{-1}, Temp = 298.15±1^{o}K, agitation rate = 150 rpm)……129

Figure 4.23 Effect of temperature on adsorption of (a) Cu, Ni, Zn, Co and (b) Cr, Fe, Hg and U onto bentonite-sorbitol in single component solutions (C_i = 100 mg L^{-1}, pH 3, agitation rate = 150 rpm, contact time = 12 h)……132

Figure 4.24 XRD pattern of natural zeolite……135

Figure 4.25 The zeta potential of: (a) natural zeolite (b) Zeolite-histidine, Zeolite-cysteine, Zeolite-sorbitol 137

Figure 4.26 Thermogravimetric curve of natural zeolite 139

Figure 4.27 FTIR spectrum of natural zeolite 141

Figure 4.28 Effect of initial pH on adsorption of (a) Cu, Ni, Zn, Co and (b) Fe, Hg, Cr and U onto natural zeolite in single component solutions (C_i = 100 mg L^{-1}, Temp = 298.15±1^{o}K, agitation rate = 150 rpm, agitation time = 12h) 145

Figure 4.29 Effect of concentration on the adsorption of (a) Cu, Ni, Zn, Co and (b) Cr, Fe, Hg and U onto natural zeolite in single component solutions (pH 3, Temp = 298.15±1^{o}K, agitation rate = 150 rpm, agitation time = 12h) 146

Figure 4.30 Effect of contact time on adsorption of (a) Cu, Ni, Zn, Co and (b) Cr, Fe, Hg and U onto natural zeolite in single component solutions (pH =3, C_i = 100 mg L^{-1}, Temp = 298.15±1^{o}K, agitation rate = 150 rpm).....149

Figure 4.31 Effect of temperature on adsorption of (a) Cu, Ni, Zn, Co and (b) Cr, Fe, Hg and U onto natural zeolite in single component solutions (C_i = 100 mg L^{-1}, pH 3, agitation rate = 150 rpm, contact time = 12 h) 152

Figure 4.32 Effect of initial pH on adsorption of (a) Cu, Ni, Zn, Co and (b) Cr, Fe, Hg and U onto zeolite-histidine in single component solutions (C_i = 100 mg L^{-1}, Temp = 298.15±1^{o}K, agitation rate = 150 rpm, agitation time = 12h) 156

Figure 4.33 Effect of concentration on the adsorption of (a) Cu, Ni, Zn, Co and (b) Cr, Fe, Hg and U onto zeolite-histidine in single component solutions (pH=3, Temp = 298.15±1^{o}K, agitation rate= 150 rpm, agitation time= 12h) 157

Figure 4.34 Effect of contact time on adsorption of (a) Cu, Ni, Zn, Co and (b) Cr, Fe, Hg and U onto zeolite-histidine in single component solutions (pH=2, C_i = 100 mg L^{-1}, Temp = 298.15±1^{o}K, agitation rate = 150 rpm) 160

Figure 4.35 Effect of temperature on adsorption of Cu, Cr, Ni, Zn, Co, Fe, Hg and U onto zeolite-histidine in single component solutions (Ci = 100 mg L^{-1}, pH 3, agitation rate = 150 rpm, contact time = 12 h) 163

Figure 4.36 Effect of initial pH on adsorption of (a) Cu, Ni, Zn, Co and (b) Cr, Fe, Hg and U onto zeolite-cysteine in single component solutions (C_i = 100 mg L^{-1}, Temp = 298.15±1^oK, agitation rate = 150 rpm, agitation time = 12h) 166

Figure 4.37 Nickel species distribution using Medusa 167

Figure 4.38 Effect of concentration on the adsorption of (a) Cu, Ni, Zn, Co and (b) Cr, Fe, Hg and U onto zeolite-cysteine in single component solutions (pH 3,Temp = 298.15±1^oK, agitation rate= 150 rpm, agitation time= 12h) 168

Figure 4.39 Effect of contact time on adsorption of (a) Cu, Ni, Zn, Co and (b) Cr, Fe, Hg and U onto zeolite-cysteine in single component solutions (pH=3, C_i = 100 mg L^{-1}, Temp = 298.15±1^oK, agitation rate = 150 rpm)..... 171

Figure 4.40 Effect of temperature on adsorption of Cu, Cr, Ni, Zn, Co, Fe, Hg and U onto zeolite-cysteine in single component solutions (C_i = 100 mg L^{-1}, pH 3, agitation rate = 150 rpm, contact time = 12 h) 173

Figure 4.41 Effect of initial pH on adsorption of (a) Cu, Ni, Zn, Co and (b) Cr, Fe, Hg and U onto zeolite-sorbitol in single component solutions (C_i = 100 mg L^{-1}, Temp = 298.15±1^oK, agitation rate = 150 rpm, agitation time = 12h) 176

Figure 4.42 Effect of concentration on the adsorption of (a) Cu, Ni, Zn, Co and (b) Cr, Fe, Hg and U onto zeolite-sorbitol in single component solutions (pH 3, Temp = 298.15±1^oK, agitation rate= 150 rpm, agitation time= 12h) 177

Figure 4.43 Effect of contact time on adsorption of (a) Cu, Ni, Zn, Co and (b) Cr, Fe, Hg and U onto zeolite-sorbitol in single component (pH 3, C_i = 100 mg L^{-1}, Temp = 298.15±1^oK, agitation rate = 150 rpm 180

Figure 4.44 Effect of temperature on adsorption of (a) Cu, Ni, Zn, Co and (b) Cr, Fe, Hg and U onto zeolite-sorbitol in single component solutions (Ci = 100 mg L^{-1}, pH 3, agitation rate = 150 rpm, contact time = 12 h) 183

Figure 4.45 Growth of *P. simplicissimum* (a) left bottle-with zeolite + liquid medium; right bottle-liquid medium without zeolite (b) left bottle: liquid medium without bentonite; right bottle: bentonite + liquid medium 192

Figure 4.46 Light microscope images of sporulating culture of *P. simplicissimum* 193

Figure 4.47 Growth curves of (a) *P. simplicissimum* in liquid medium (b *P.simplicissimum* in liquid medium and supported on bentonite 194

Figure 4.48 Zeta potential plots for bentonite-*P.simplicissimum* and zeolite-*P.simplicissimum* .. 196

Figure 4.49 FTIR spectra of bentonite-P.*simplicissimum* 197

Figure 4.50 Effect of initial pH on adsorption of (a) Cu, Ni, Zn and Co (b) Cr, Fe, Hg and U onto bentonite-*P. simplicissimum* (active) in single component solution (C_i = 100 mg L^{-1}, Temp = 298.15±1^oK, agitation rate = 150 rpm, agitation time = 12h) 199

Figure 4.51 Effect of initial pH on adsorption of (a) Cu, Ni, Zn and Co (b) Cr, Fe, Hg and U onto bentonite-*P.simplicissimum* (active) in multi-component solutions (C_i = 100 mg L^{-1}, Temp = 298.15±1^oK, agitation rate = 150 rpm, agitation time = 12h) 201

Figure 4.52 Effect of concentration on the adsorption of (a) Cu, Ni, Zn, Co and (b) Cr, Fe, Hg and U in single component solutions onto bentonite-*P.simplicissimum*(active) (pH = 3, Temp = 298.15±1^oK, agitation rate = 150 rpm, agitation time = 12h) 202

Figure 4.53 Effect of concentration on the adsorption of (a) Cu, Ni, Zn, Co and (b) Cr, Fe, Hg and U in multi component solutions onto bentonite-*P.simplicissimum* (active) (pH = 3, Temp = 298.15±1^oK, agitation rate = 150 rpm, agitation time = 12h) 204

Figure 4.54 Effect of contact time on the adsorption of (a) Cu, Ni, Zn, Co and (b) Cr, Fe, Hg and U on bentonite-*P. simplicissimum* (active) in single component solutions (pH = 3, C*i* = 100 mg L^{-1}, Temp = 298.15±1^oK, agitation rate = 150 rpm..... 209

Figure 4.55 Effect of contact time on the adsorption of (a) Cu, Ni, Zn, Co, (b) Cr, Fe, Hg and U on bentonite-*P. simplicissimum* (active) in multi-ion solutions (C_i = 100 mg L^{-1}, Temp = 298.15±1^oK, agitation rate = 150 rpm 211

Figure 4.56 Effect of temperature on adsorption of heavy metals onto bentonite-*P.simplicissimum* (active) in single component solutions (pH=3,Ci = 100 mg L^{-1}, agitation rate = 150 rpm, contact time = 12 h) 215

Figure 4.57 Effect of temperature on adsorption of heavy metals onto bentonite-*P. simplicissimum* (active) in multi component solutions (pH = 3, C_i = 100 mg L^{-1}, agitation rate = 150 rpm,contacttime=12h) 217

Figure 4.58 Effect of initial pH on adsorption of (a) Cu, Ni, Zn, Co and (b) Fe, Hg, Cr and U onto bentonite-*P. simplicissimum* (inactive) in single component solutions (C_i = 100 mg L^{-1}, Temp = 298.15±1^oK, agitation rate = 150 rpm, agitation time = 12h) 222

Figure 4.59 Effect of initial pH on adsorption of (a) Cu, Ni, Zn, Co and (b) Fe, Hg, Cr and U onto bentonite-*P. simplicissimum* (inactive) in multi-component solutions (C_i = 100 mg L^{-1}, Temp = 298.15±1^oK, agitation rate = 150 rpm, agitation time = 12h) 223

Figure 4.60 Effect of concentration on the adsorption of (a) Cu, Ni, Zn, Co and (b) Fe, Hg, Cr and Uonto bentonite-*P. simplicissimum* (inactive) (in single-metal solutions (pH 3, Temp = 298.15±1^oK, agitation rate = 150 rpm, agitation time = 12h) 224

Figure 4.61 Effect of concentration on the adsorption of (a) Cu, Ni, Zn, Co and (b) Fe, Hg, Cr and U onto bentonite-*P. simplicissimum* (inactive) in multi-component solutions (pH 3, Temp = 298.15±1^{o}K, agitation rate = 150 rpm, agitation time = 12h) 226

Figure 4.62 Effect of contact time on the adsorption of (a) Cu, Ni, Zn, Co and (b) Fe, Hg, Cr and U onto bentonite-*P.simplicissimum* in single component solutions (pH 3, Temp = 298.15±1^{o}K, agitation rate = 150 rpm) 330

Figure 4.63 Effect of contact time on the adsorption of (a) Cu, Ni, Zn, Co and Fe, Hg, Cr and U onto bentonite-*P.simplicissimum* in multi component solutions (pH 3, Temp = 298.15±1^{o}K, agitation rate = 150 rpm)……..... 331

Figure 4.64 Effect of temperature on the adsorption of (a) Cu, Ni, Zn, Co and (b) Fe, Hg, Cr and Uonto bentonite-*P.simplicissimum* in single component solutions (pH = 3, C_i = 100 mg L^{-1}, agitation rate = 150 rpm)…….. 235

Figure 4.65 Effect of temperature on the adsorption of (a) Cu, Ni, Zn, Co and (b) Fe, Hg, Cr and U onto bentonite-*P.simplicissimum* in multi-component solutions (pH = 3, C_i = 100 mg L^{-1}, agitation rate = 150 rpm)…….. 236

Figure 4.66 Effect of growth days of the biomass on the adsorption of metals (a) Cu, Ni, Zn and Co (b) Fe, Hg, U and Cr…… 240

Figure 4.67 Growth curves for (a) *P. simplicissimum* in liquid medium (b) *P. simplicissimum* in liquid medium supported on zeolite 242

Figure 4.68 FTIR for zeolite-*P.simplicissimum* 244

Figure 4.69 Effect of initial pH on adsorption of (a) Cu, Co, Ni and Zn (b) Cr, Fe, Hg and U onto zeolite-*P. simplicissimum* in single component solution (C_i = 100 mg L^{-1}, Temp = 298.15±1^{o}K, agitation rate = 150 rpm, agitation time = 12h) 246

Figure 4.70 Effect of initial pH on adsorption of (a) Cu, Co, Ni and Zn (b) Cr, Fe, Hg and U zeolite-*P. simplicissimum* in multi component solution (C_i = 100 mg L^{-1}, Temp = 298.15±1^{o}K, agitation rate = 150 rpm, agitation time = 12h) 247

Figure 4.71 Effect of initial concntration on adsorption of (a) Cu, Co, Ni and Zn (b) Cr, Fe, Hg and U onto zeolite-*P. simplicissimum* in single component solution (pH = 3, C_i = 100 mg L^{-1}, Temp = 298.15±1^{o}K, agitation rate = 150 rpm, agitation time = 12h) 248

Figure 4.72 Effect of initial concentration on adsorption of (a) Cu, Co, Ni and Zn (b) Cr, Fe, Hg and U onto zeolite-*P. simplicissimum* (active) in multi component solution (pH = 3, C_i = 100 mg L^{-1}, Temp = 298.15±1^{o}K, agitation rate = 150 rpm, agitation time = 12h)..... 249

Figure 4.73 Effect of contact time on the adsorption of (a) Cu, Ni, Zn and Co (b) Cr, Fe, Hg, U on zeolite-*P. simplicissimum* (active) in single component solutions (pH = 3, C_i = 100 mg L^{-1}, Temp = 298.15±1^{o}K, agitation rate = 150 rpm) 253

Figure 4.74 Effect of contact time on the adsorption of (a) Cu, Ni, Zn and Co (b) Cr, Fe, Hg and U on zeolite-*P. simplicissimum* (active) in multi- component solutions (pH = 3, C_i = 100 mg L^{-1}, Temp = 298.15±1^oK, agitation rate = 150 rpm) 254

Figure 4.75 Effect of temperature on adsorption of (a) Cu, Ni, Zn and Co (b) Cr, Fe, Hg and U onto zeolite-*P.simplicissimum* (active) in single component solutions (pH = 3, C_i = 100 mg L^{-1}, pH 3, agitation rate = 150 rpm, contact time = 12 h)..... 259

Figure 4.76 Effect of temperature on adsorption of (a) Cu, Cr, Ni, Zn, Co and (b) Cr, Fe, Hg, U onto zeolite-*P.simplicissimum* (active) in single component solutions (pH = 3, C_i = 100 mg L^{-1}, pH 3, agitation rate = 150 rpm, contact time = 12 h)..... 260

Figure 4.77 Effect of initial pH on adsorption of (a) Cu, Cr, Ni, Zn and Co (b) Cr, Fe, Hg and U onto zeolite-*P. simplicissimum* (inactive) in single component solutions (C_i = 100 mg L^{-1}, Temp = 298.15±1^oK, agitation rate = 150 rpm, agitation time = 12h) 264

Figure 4.78 Effect of initial pH on adsorption of (a) Cu, Ni, Zn, Co and (b) Cr, Fe, Hg and U onto zeolite-*P. simplicissimum* (inactive) in multi-component solutions (C_i = 100 mg L^{-1}, Temp = 298.15±1^oK, agitation rate = 150 rpm, agitation time = 12h) 265

Figure 4.79 Effect of initial concentration on adsorption of (a) Cu, Ni, Zn and Co (b) Cr, Fe, Hg and U onto zeolite-*P.simplicissimum* (inactive) in single-ion solutions (pH = 3, C_i = 100 mg L^{-1}, Temp = 298.15±1^oK, agitation rate = 150 rpm, agitation time = 12h)..... 267

Figure 4.80 Effect of initial concentration on adsorption of (a) Cu, Ni, Zn and Co (b) Cr, Fe, Hg and U onto zeolite-*P. simplicissimum* (inactive) in multi-component solutions (pH = 3, C_i = 100 mg L^{-1}, Temp = 298.15±1 ^oK, agitation rate = 150 rpm, agitation time = 12h) 268

Figure 4.81 Effect of contact time on the adsorption of (a) Cu, Ni, Zn and Co (b) Cr, Fe, Hg and U in single component solutions onto zeolite-*P. simplicissimum* (pH 3, Temp = 298.15±1^oK, agitation rate = 150 rpm)……..... 272

Figure 4.82 Effect of contact time on the adsorption of (a) Cu, Ni, Zn, Co (b) Cr, Fe, Hg and U in multi-component solutions onto zeolite-*P. simplicissimum* (pH = 3, Temp = 298.15±1^oK, agitation rate = 150 rpm)…….273

Figure 4.83 Effect of temperature on the adsorption of (a) Cu, Ni, Zn and Co (b) Cr, Fe, Hg and U zeolite-*P.simplicissimum* in single component solutions (pH = 3, C_i = 100 mg L^{-1}, agitation rate = 150 rpm)……..277

Figure 4.84 Effect of temperature on the adsorption of (a) Cu, Ni, Zn and Co (b) Cr, Fe, Hg and U onto zeolite-*P.simplicissimum* in multi-component solutions (pH = 3, C_i = 100 mg L^{-1}, agitation rate = 150 rpm)……278

Figure 4.85 Effect of growth days of the zeolite-*P.simplicissimum* on the adsorption of metal…282

Figure 4.86 Adsorption capacity of U in solution with Cu, Co, Fe, Zn, Hg, Cr and Ni..... 283

Figure 4.87 Effect of biomass concentration (a) in a single ion system (b) multi-ion system (Ci = 100 mg L^{-1})……284
Figure 4.88 Regeneration of the zeolite-*P.simplicissimum*……286
Figure 4.89 Desorption of the metal-ions……286
Figure 4.90 Regeneration and reuse of the zeolite-*P.simplicissimum* ……287
Figure 4.91 Breakthrough curves for biosorption of (a) Cu, Co, Ni and Zn (b) Cr, Hg, Fe and U on natural bentonite (concentration = 100 mg L^{-1}, pH 3 at 2 mL min^{-1})……294
Figure 4.92 Breakthrough curves for the biosorption of Cu, Co, Cr, Hg, Fe, Ni, Zn and U on natural zeolite (concentration = 100 mg L^{-1}, pH 3 at 2 mL min^{-1})……296
Figure 4.93 Breakthrough curves for the biosorption of (a) Cu, Co, Ni, and Zn (b) Cr, Hg, Fe and U (single-ion) on bentonite P.*simplicissimum* (concentration = 100 mg L^{-1}, pH 3 at 2 mL min^{-1}) ……297
Figure 4.94 Breakthrough curves biosorption of (a) Cu, Co, Ni and Zn (b) Cr, Hg, Fe and U on natural bentonite (concentration = 100 mg L^{-1}, pH 3 at 2 mL min^{-1})……299
Figure 4.95 Breakthrough curves biosorption of (a) Cu, Co, Ni, and Zn (b) Cr, Hg, Fe and U (single-ion system) zeolite-P.*simplicissimum* (concentration = 100 mg L^{-1}, pH 3 at 2 mL min^{-1}) ….301
Figure 4.96 Breakthrough curves biosorption of (a) Cu, Co, Ni, and Zn (b) Cr, Hg, Fe and U (multi-ion) on zeolite-P.*simplicissimum* (concentration = 100 mg L^{-1}, pH 3 at 2 mL min^{-1}) ……302
Figure 4.97 Breakthrough curve (Daszkiewicz and Voelkel, 2009)…….303
Figure 4.98 FTIR spectra of (q) *Oedogonium* sp. from the stream and (r) *Oedogonium* sp. from the dam……314
Figure 4.99 Effect of pH on the biosorption of (a) Cu, Co, Ni, Zn (b) Cr, Fe, Hg, U for *Oedogonium* sp. in single-component solutions (C_i = 100 mg L^{-1}, pH = 3, algal mass = 1g, Temp = 25 ^oC)……319
Figure 4.100 Eh-pH diagram for aqueous species in the U-O_2-CO_2-H_2O system in pure water at 25^oC (Langmuir, 1997)……320
Figure 4.101 Effect of pH on the biosorption of (a) Cu, Co, Ni and Zn (b) Cr, Fe, Hg and U for *Oedogonium* sp. in multi-component solutions (C_i = 100 mg L^{-1}, pH = 3, algal mass = 1g, Temp = 25 ^oC)……322
Figure 4.102 Effect of concentration on the biosorption of (a) Cu, Co, Ni, Zn (b) Cr, Fe, Hg, U for *Oedogonium* sp. in single component solutions (C_i = 100 mg L^{-1}, pH = 3, algal mass = 1g, Temp = 298.15 ^oK)……323
Figure 4.103 Effect of concentration on the biosorption of (a) Cu, Co, Ni and Zn (b) Cr, Fe, Hg and U for *Oedogonium* sp. in multi- components solutions (C_i = 100 mg L^{-1}, pH = 3, algal mass = 1 g, Temp = 298.15^oK) ……324

Figure 4.104 Effect of contact time on the biosorption of (a) Cu, Co, Ni and Zn (b) Cr, Fe, Hg and U for *Oedogonium* sp. in single-component solutions (C_i = 100 mg L^{-1}, pH = 3, algal mass = 1 g, Temp = 25^oC).....328

Figure 4.105 Effect of contact time on the biosorption of (a) Cu, Co, Ni, Zn (b) Cr, Fe, Hg, U for *Oedogonium* sp. in multi- component solutions (C_i = 100 mg L^{-1}, pH = 3, algal mass = 25 g, Temp = 25^oC) 330

Figure 4.106 Effect of algal mass on the biosorption of (a) Cu, Co, Ni and Zn (b) Cr, Fe, Hg and U for *Oedogonium* sp. in multi- component solutions (C_i = 100 mg L^{-1}, pH = 3, Temp = 25^oC) 335

Figure 4.107 Desorption of metals adsorbed in (a) single-ion (b) multi-ion systems by HCl (0.1 M), contact time 1 h.....336

Figure 4.108 Regeneration and re-use of *Oedogonium* sp. biomass (a) single-ion system (b) multi-ion system 337

Figure 4.109 FTIR Spectra of the alginates extracted from the *Oedogonium* sp. algal 339

Figure 4.110 ^1H NMR spectra of sodium alginates (a) Mannuronic-Guluronic acid from Sigma Aldrich (South Africa) (b) Mannuronic acid (c) Mannuronic-Guluronic acid extracted from *Oedogonium* sp. algal.....342

Figure 4.111 (a) Assignment of the ^1H signals for M and G residues for the commercial Na-alginates 343

Figure 4.111 (b) Assignment of the ^1H signals for M and G residues from *Oedogonium* sp. algal biomass 344

Figure 4.112 FT-IR spectra of the alginates immobilized zeolite.....345

Figure 4.113 Zeta potential of zeolite-alginates.....346

Figure 4.114 Effect of pH on the adsorption of (a) Cu, Co, Ni and Zn (b) Cr, Fe, Hg and U on zeolite-alginate in single-ion system (C_i= 100 mg L^{-1}, Temp= 25±1^oC) 347

Figure 4.115 Effect of pH on the adsorption of (a) Cu, Co, Ni and Zn (b) Cr, Fe, Hg and U on zeolite-alginate in multi-ion system (C_i= 100 mg L^{-1}, Temp = 298.15^oK, algal mass = 1 g) 349

Figure 4.116 Effect of concentration on the adsorption of (a) Cu, Ni, Zn, Co (b) Cr, Fe, Hg, U in single-ion solution on zeolite-alginate (pH = 3, Temp = 298.15±1^oK, agitation rate= 150 rpm, agitation time = 12h, algal mass = 1 g).....351

Figure 4.117 Effect of concentration on the adsorption of (a) Cu, Ni, Zn and Co (b) Cr, Fe, Hg, U in multi- component solutions on zeolite-alginate (pH = 3, Temp = 298.15±1^oK, agitation rate = 150 rpm, agitation time = 12h) 352

Figure 4.118 (a) and (b) R_L values based on Langmuir isotherm at different metals concentrations in single-ion system 357

Figure 4.119 Effect of contact time on the adsorption of (a) Cu, Ni, Zn, Co, (b) Cr, Fe, Hg, U on zeolite-alginates in single component solutions (pH = 3, C_i = 100 mg L^{-1}, Temp = 298.15±1^oK, agitation rate = 150 rpm).....359
Figure 4.120 Effect of contact time on the adsorption of (a) Cu, Ni, Zn, Co (b) Cr, Fe, Hg, U on zeolite-alginates in multi-component solutions (pH = 3, C_i = 100 mg L^{-1}, Temp = 298.15±1^oK, agitation rate = 150 rpm).....360
Figure 4.121 Effect of biosorbent mass on the biosorption of (a) Cu, Co, Ni, Zn (b) Cr, Fe, Hg, U for zeolite-alginates in multi-component solutions (C_i = 100 mg L^{-1}, pH = 3, Temp = 25^oC) 366
Figure 4.122 Regeneration and reuse of zeolite-alginates (a) single-ion system (b) multi-ion system 367
Figure 4.123 Desorption (%) of metal ions from the zeolite-alginates by 0.1 M HCl.....369

List of tables

Table 2.1 Selected oxidation reactions for mine tailing with oxygen and iron (Fe^{3+})……...10
Table 2.2 Properties of physisorption and chemisorption……..16
Table 2.3 The bond energies of various mechanisms for adsorption …….. 17
Table 3.1 CHNS calibration results with corn gluten (Leco)…… 60
Table 3.2 Table of parameters of ICP-OES 62
Table 3.3….Effect of separation factor 71
Table 4.1 Chemical composition of natural Bentonite 79
Table 4.2 Physical properties of natural and functionalised Bentonite 80
Table 4.3 Chemical properties of natural and functionalised Bentonite…… ...83
Table 4.4a IR wavenumbers of natural Bentonite 85
Table 4.4b IR wavenumbers of Bentonite-Histidine..... ...85
Table 4.4c IR wavenumbers of bentonite-Cysteine..... ...85
Table 4.4d IR wavenumbers of bentonite-Sorbitol..... 86
Table 4.4e IR wavenumbers of bentonite-Mannitol..... 86
Table 4.5 Parameters of the Langmuir, Freundlich and D-R models for the adsorption of metals on natural bentonite.....91
Table 4.6 Kinetic constants for the adsorption of metal ions on natural bentonite 95
Table 4.7 Thermodynamic parameters of metal ions adsorption on natural bentonite 98
Table 4.8 The reaction rate of the adsorption of metal ions on natural bentonite 99
Table 4.9 Parameters of the Langmuir, Freundlich and D-R models for the adsorption of metals on the bentonite-histidine.....103
Table 4.10 Kinetic constants for the adsorption of metal ions on bentonite-histidine 107
Table 4.11 Thermodynamic parameters for the adsorption of heavy metals on bentonite-histidine. 109
Table 4.12 Rate of metal ions adsorption on bentonite-histidine 110
Table 4.13 Parameters of the Langmuir, Freundlich and D-R models for the adsorption of metals on the bentonite-cysteine 115
Table 4.14 Kinetic constants for the adsorption of metal ions on bentonite-cysteine.....119
Table 4.15 Thermodynamic parameters for the adsorption of metal ions on bentonite-cysteine.....122
Table 4.16 Rate of the adsorption of metal ions on bentonite-cysteine 123
Table 4.17 Isotherms modelling for the adsorption of metal ions on bentonite-sorbitol 128
Table 4.18 Kinetic modelling for the adsorption of metal ions on bentonite-sorbitol 130
Table 4.19 Thermodynamic parameters for bentonite-sorbitol.....133
Table 4.20 Rate of the adsorption of metal ions on bentonite-sorbitol 134

Table 4.21 Chemical composition of natural zeolite……136
Table 4.22a Physical properties of natural and functionalised zeolite……...136
Table 4.22b Chemical properties of natural and modified zeolite…….....140
Table 4.23a IR vibrations of natural Zeolite……141
Table 4.23b IR vibrations of Zeolite-Histidine……142
Table 4.23c IR vibrations of Zeolite-Cysteine……..142
Table 4.23d IR vibrations of Zeolite-Sorbitol & Zeolite-Mannitol……..143
Table 4.24 Parameters of the Langmuir, Freundlich and D-R models for the adsorption of metals on the natural zeolite……148
Table 4.25 Kinetic constants for the adsorption of metal ions on natural zeolite……150
Table 4.26 Thermodynamic parameters for natural zeolite……153
Table 4.27 Rate of adsorption of metals on natural zeolite……..154
Table 4.28 Parameters of the Langmuir, Freundlich and D-R models for the adsorption of metals on the zeolite-histidine.....158
Table 4.29 Kinetic constants for the adsorption of metal ions on zeolite-histidine 162
Table 4.30 Thermodynamic parameters for the adsorption of heavy metals on zeolite-histidine...164
Table 4.31 Rate of metal ions adsorption on zeolite-histidine 164
Table 4.32 Parameters of the Langmuir, Freundlich and D-R models for the adsorption of metals on the zeolite-cysteine.....169
Table 4.33 Kinetic constants for the adsorption of metal ions on zeolite-cysteine 172
Table 4.34 Thermodynamic parameters for the adsorption of metal ions on zeolite-cysteine.....174
Table 4.35 Rate of the adsorption of metal ions on zeolite-cysteine.....175
Table 4.36 Parameters of the Langmuir, Freundlich and D-R models for the adsorption of metals on the zeolite-sorbitol 178
Table 4.37 Kinetic constants for the adsorption of metal ions on zeolite-sorbitol.....181
Table 4.38 Thermodynamic parameters for the adsorption of metal ions on zeolite- sorbitol.....184
Table 4.39 Rate of the adsorption of metal ions on zeolite-sorbitol 185
Table 4.40 Physical properties and elemental composition of natural and functionalised bentonite with *P. simplicissimum*.....195
Table 4.41 FTIR absorption bands and corresponding possible groups observed on the bentonite-P.*simplicissimum* fungal biomass 198
Table 4.42 Parameters of the Langmuir, Freundlich and D-R and distribution coefficient models for the adsorption of metals on bentonite-*P. simplicissimum* immobilized on bentonite in a single metal system 205

Table 4.43 Parameters of the Langmuir, Freundlich and D-R and distribution coefficient models for the adsorption of metals on the *P. simplicissimum* immobilized on bentonite in multi-ion system ... 208
Table 4.44 Kinetic constants for the adsorption of metal ions on *P. simplicissimum* immobilized on bentonite in single-ion system ... 212
Table 4.45 Kinetic constants for the adsorption of metal ions on *P. simplicissimum* immobilized on bentonite in multi-ion system ... 214
Table 4.46 Thermodynamic parameters of metal ions adsorption on bentonite- *P.simplicissimum* in single-ion system ... 218
Table 4.47 Thermodynamic parameters of metal ions adsorption on bentonite- *P.simplicissimum* in multi-ion system ... 219
Table 4.48 The reaction rate of the adsorption of metal ions on bentonite- *P.simplicissimum* in single-ion system ... 219
Table 4.49 The reaction rate of the adsorption of metal ions onto bentonite-*P.simplicissimum* ... 220
Table 4.50 Parameters of the Langmuir, Freundlich and D-R models for the adsorption of metals on the bentonite-*P. simplicissimum* (inactive) in a single metal system ... 228
Table 4.51 Parameters of the Langmuir, Freundlich and D-R models for the adsorption of metals on the bentonite-*P. simplicissimum* (inactive) in multi-ion metal system ... 229
Table 4.52 Kinetic constants for the adsorption of metal ions on bentonite-*P. simplicissimum* (inactive) in single ion system ... 232
Table 4.53 Kinetic constants for the adsorption of metal ions on bentonite-*P. simplicissimum)* inactive in multi-ion system ... 234
Table 4.54 Thermodynamic parameters of metal ions adsorption on bentonite- *P.simplicissimum* (inactive) in single-ion system ... 237
Table 4.55 Thermodynamic parameters of metal ions adsorption on bentonite- *P.simplicissimum* (inactive) in multi-ion system ... 238
Table 4.56 Rate of adsorption in a single-metal system at different temperatures ... 239l
Table 4.57 Rate of adsorption in a multi-metals system at different temperatures ... 239
Table 4.58 Elemental composition of natural zeolite and zeolite-*P. simplicissimum* ... 243
Table 4.59 FTIR absorption bands and corresponding possible groups observed on the zeolite-P.*simplicissimum* fungal biomass ... 244
Table 4.60 Parameters of the Langmuir, Freundlich and D-R and correlation coefficient for the adsorption of metals on zeolite-*P. simplicissimum* in a single metal system ... 250
Table 4.61 Parameters of the Langmuir, Freundlich and D-R and correlation coefficient models for the adsorption of metals on zeolite-*P. simplicissimum* in multi-ion system ... 252

Table 4.62 Kinetic constants for the adsorption of metal ions on *P. simplicissimum* immobilized on zeolite (in single metal system)..... 255
Table 4.63 Kinetic constants for the adsorption of metal ions on *P.simplicissimum* immobilized on zeolite (in single metal system)..... 257
Table 4.64 Thermodynamic parameters of metal ions adsorption on zeolite- *P.simplicissimum* in single-ion system 261
Table 4.65 Thermodynamic parameters of metal ions adsorption on zeolite- *P.simplicissimum* in multi-ion system..... 262
Table 4.66 The reaction rate of the adsorption of metal ions on zeolite-*P. simplicissimum* 262
Table 4.67 The reaction rate of the adsorption of metal ions on zeolite-*P.simplicissimum* 263
Table 4.68. Parameters of the Langmuir, Freundlich and D-R models for the adsorption of metals on the zeolite-*P. simplicissimum* (inactive) in a single metal system 269
Table 4.69 Parameters of the Langmuir, Freundlich and D-R models for the adsorption of metals on the zeolite-*P. simplicissimum* (inactive) in a multi-ion metal system..... 271
Table 4.70 Kinetic constants for the adsorption of metal ions on zeolite-*P. simplicissimum* (inactive) in a single-ion system 274
Table 4.71 Kinetic constants for the adsorption of metal ions on zeolite-*P. simplicissimum* (inactive) in a multi- ion system 276
Table 4.72 Thermodynamic parameters of metal ions adsorption on zeolite- *P.simplicissimum* (inactive) in single-ion system 279
Table 4.73 Thermodynamic parameters of metal ions adsorption on zeolite- *P.simplicissimum* (inactive) in a multi-ion system 280
Table 4.74 Rate of adsorption in a single-metal system at different temperatures 281
Table 4.75 Rate of adsorption in a metal ion system at different temperatures 281
Table 4.76 Removal of heavy metal ions from wastewater samples by zeolite-*P.simplicissimum*(inactive) 288
Table 4.77 Discharge standards for industrial wastewater (US EPA, 1996)..... 289
Table 4.78 Theoretical number of plate of the column and adsorption capacity of the biosorbents for Ni and U..... 304
Table 4.79a Calculated desorption efficiencies for the desorption of heavy metals from natural Bentonite in fixed bed columns using 0.1 M HNO_3 at 25ºC; bed height 13 cm, flow rate 4 mL/min; contact time 540 minutes 306
Table 4.79b Calculated desorption efficiencies for the desorption of heavy metals from natural Zeolite in fixed bed columns using 0.1 M HNO_3 at 25ºC; bed height 13 cm, flow rate 4 mL/min; contact time 540 minutes……..... 307

Table 4.79c Calculated desorption efficiencies for the desorption of heavy metals from Bentonite-*P.simplicissimum* in fixed bed columns using 0.1 M HNO_3 at 25ºC; bed height 13 cm, flow rate 4 mL/min, contact time 540 minutes.....308
Table 4.79d Calculated desorption efficiencies for the desorption of heavy metals from Zeolite-*P.simplicissimum* in fixed bed columns using 0.1 M HNO_3 at 25ºC; bed height 13 cm, flow rate 4 mL/min; contact time 540 minutes.....309
Table 4.80 Values of BDST model parameters for the adsorption of Ni and U from multi-component solutions by natural and modified zeolite/bentonite at breakthrough, 12 cm column height and a flow rate of 2 mL min^{-1} 311
Table 4.81. IR adsorption bands for *Oedogonium* sp. from the dam and the river and corresponding possible groups observed 315
Table 4.82 Results of metals analysed in water and fresh algae from dams and stream.....316
Table 4.83 Effect of various pre-treatments on metals sorption capacity of *Oedogonium* sp.....317
Table 4.84 Parameters of the Langmuir, Freundlich and D-R models for the adsorption of metals *Oedogonium* sp. in single-ion system 325
Table 4.85 Parameters of the Langmuir, Freundlich and D-R models for the adsorption of metals *Oedogonium* sp. in multi–ions system 327
Table 4.86 Kinetic constants for the adsorption of metal ions on *Oedogonium* sp. (in single-ion system) 331
Table 4.87 Kinetic constants for the adsorption of metal ions on *Oedogonium* sp. (in a multi-ion system) 332
Table 4.88 Thermodynamic parameters of metal ions adsorption on *Oedogonium* sp. in a single-ion system 333
Table 4.89 Thermodynamic parameters of metal ions adsorption on *Oedogonium* sp. in a multi-ion system 334
Table 4.90 IR adsorption bands for Na-alginates extracted from the *Oedogonium* sp.....340
Table 4.91 IR adsorption bands for zeolite-alginates.....346
Table 4.92 Parameters of the Langmuir, Freundlich and D-R models for the adsorption of metals on zeolite-alginate in single-ion system.....353
Table 4.93 Parameters of the Langmuir, Freundlich and D-R models for the adsorption of metals on zeolite-alginate in multi-ons system. 355
Table 4.94 Kinetic constants for the adsorption of metal ions on zeolite-alginates in single-ion system 361

Table 4.95 Kinetic constants for the adsorption of metal ions on zeolite-alginates in multi-ion system 363
Table 4.96 Thermodynamic parameters of metal ions adsorption on zeolite-alginates in a single-ion system. 364
Table 4.97 Thermodynamic parameters of metal ions adsorption on zeolite-alginates in a multi-ion system 365

Acronyms and abbreviations

AMD Acid Mine Drainage

BDST Bed Depth Service Time

BET Brenner-Emmett-Taylor

CCD Coupled Charge Detection

CEC Cation Exchange Capacity

CHNS CarbonNitrogen-Hydrogen-Sulphur

CSIR Council for Scientific and Industrial Research

D_2O Deuterium Oxide

DAF Dissolved-Air Flotation

DEAT Department of Environmental Affairs and Tourism

EEB European Environmental Bureau

FTIR Fourier Transform Infra-red

G Guluronic acid

ICP-OES Inductively Coupled Plasma-Optical Emission Spectroscopy

IUBMB International Union of Biochemistry and Molecular Biology

IUPAC International Union of Pure and Applied Chemistry

LOD Limit of Detection

M Mannuronic acid

MEA Malt Extract Agar

NEESA Novel Energy and Environmental Support Activity

NMR Nuclear Magnetic Resonance

ORP Oxidation-Reduction Potential

PDA Potato Dextrose Agar

PP Polypropylene

PVC Polyvinylchloride

RSD Relative standard deviation

S**AWQG** South African water quality guide

SDWF Safe Drinking Water Foundation

SHE Standard Hydrogen Electrode

SSA Specific Surface Area

TCEC Theorical Cation Exchange Capacity

TGA/DTA Thermal Gravimetry/ Differential Thermogravimetric

UNEP United Nations Environmental Programme

USEPA United States Environmental Protection Agency

USGS United State Geological Survey

VSA Volume Specific Surface Area

XRD X-ray Diffraction

XRF X-ray Fluorescence

ΔS^o Entropy changes (kJ $(mol \cdot K)^{-1}$)

ΔH^o Enthalpy changes (kJ mol^{-1})

Ea Activation energy ((kJ mol^{-1})

Co Initial concentration (mg L^{-1})

C_e Equilibrium concentration (mol L^{-1})

q_e Equilibrium ion exchange capacity (mol kg^{-1})

q_m Theoretical maximum monolayer adsorption capacity (mol kg^{-1})

b Langmuir constant related to the energy of the sorption (L mol^{-1})

ΔG^o Change in Gibbs free energy (kJ mol^{-1})

K_f Freundlich constant (mol g^{-1})/ (mol L^{-1})

1/n Freundlich constant related to the energy heterogeneity of the system and the size of the exchanged molecule

R_L Separator factor

R Gas constant (kJ $(mol\ K)^{-1}$)

T Absolute temperature (^oK)

B Activity coefficient related to mean sorption energy ($mol^2\ (kJ)^{-2}$)

F Polanyi coefficient (D-R isotherm)

Es Sorption energy (kJ mol^{-1})

K_d Distribution coefficient (L kg^{-1})

q_t Amount of adsorbed metal ion on the adsorbent at time t (min) (mol Kg^{-1})

q_e Amount of adsorbed metal ion on the adsorbent at equilibrium (mol Kg^{-1})

k_1 Rate constant of first-order adsorption (min^{-1})

k_2 Aate constant of second-order model (Kg $(mol\ min)^{-1}$)

a Initial adsorption rate (mol $(Kg\ min)^{-1}$)

D_e Effective diffusion coefficient ($cm^2\ min^{-1}$)

d_p Mean diameter particle (cm^{-1})

K_p Initial rate of the intraparticle diffusion (mol $(Kg\ min)^{-0.5}$)

K_f Adsorption rate constant

F Fractional attainment of equilibrium

No Dynamic adsorption capacity (mg L^{-1})

Z Column bed depth (cm)

K Rate constant [L (mg min^{-1})]

μ Linear velocity

Chapter 1: Introduction

1.1 Background and motivation

Water pollution as a result of disposal of heavy metals is of great concern worldwide. Consequently, the treatment of polluted industrial wastewater remains a topical issue since water is a scarce commodity, particularly in South Africa. Here, heavy metal sources include: electroplating facilities; battery manufacturing; production of paints, pigments, ceramics, glass; and mining operations, with the latter contributing by far compared to others. For instance, gold mining wastes in South Africa usually contain elevated concentrations of Pb, Cu, Ni, Zn, Cr, U, Hg, As, Fe, Co, and rare earth metals among others. The toxic characteristics of these elements include: toxicity at low concentrations; transformation from relatively low toxic forms into more toxic forms under certain environmental conditions; bioaccumulation and bio-augmentation; as well as toxicity can last for a long time in nature (Alkorta *et al*., 2004; Volesky, 1990a; Wang and Chen, 2006).

The toxic effects of these elements make it imperative to remove them if safe domestic and industrial water is to be obtained. Worldwide, a number of conventional methods have been used for the removal of heavy metals and other pollutants in water. These include: chemical precipitation, coagulation, ion exchange, reverse osmosis, evaporation and adsorption. These techniques have their inherent advantages and limitations in application (Keleşoğlu, 2007). For instance, they often involve high capital and operational costs and may be associated with the generation of secondary waste which presents treatment problems such as the large quantity of sludge generated by precipitation processes. When applied to lower concentrations of metal ions, these processes are either ineffective or not cost-effective (Huang and Huang, 1996). Ion exchange, reverse osmosis and adsorption are more attractive processes because the metal values can be recovered along with their removal from the effluents. Reverse osmosis and ion exchange are not usually economically feasible because of their relatively high investment and operational cost.

Adsorption has, by far, drawn a lot of interest due to the possibility of using low cost adsorbents. Some of the adsorbents that have been studied include waste materials e.g. fly ash (Hernandez-Ramirez and Holmes, 2007), clay-based materials (Gupta *et al.,* 2006) and

biosorbents e.g. agricultural by-products, algae, fungi and bacteria (Das *et al*., 2007; Wang and Chen, 2008).

Biosorbents based on the use of micro-organisms have recently emerged as better alternatives to the traditional adsorbents due to their high adsorption capacities. Biosorption involves active and non-active uptake of adsorbates by biomass. Adsorption can occur through ionic, chemical and physical processes. A variety of ligands (e.g. carboxyl, amine, phosphate and hydroxyl) located on the microbial biomass tend to increase metal chelation.

The main drawback in most of the work that has explored the use of biosorbents has been an attempt to use them as stand-alone adsorbents. This has made it difficult to control the biomass as well as to get satisfactory results.

This study seeks to address that gap by exploring the use of conventional adsorbents such as bentonite and zeolite as supports for fungal and algal biomass, thus offering a lot more advantages than would the individual adsorbent entities. The use of such a biophysical system would be suited to toxic wastewaters, such as those with elevated concentrations of metals from the processing of gold in South Africa. The country's abundance of bentonite and zeolitic material and environmental conditions that are conducive for the growth and maintenance of an active microbial population makes the pursuit of such a project viable.

1.2 Problem statement

Gold mining in the Witwatersrand Basin, South Africa generated vast volumes of hazardous waste. Since the commencement of extensive mining activities in 1886, about six billion tons of tailings have been produced; thus posing an environmental threat (Winde *et al.,* 2004; Rosner, 2001; Liefferink, 2007). The mineralogy of gold tailings in this basin consists mainly of quartz, pyrite and over 70 other minerals that include uraninite (UO_2), brannerite (UTi_2O_6), arsenopyrite (FeAsS), cobaltite (CoAsS), galena (PbS), pyrrhotite (FeS), gersdofite (NiAsS) and chromite ($FeCr_2O_4$) (Feather and Koen, 1975).

Due to gold resources occurring in greater depths (as low as 4 km in some cases), there are very few shaft mining operations still active. Reprocessing of old tailings is now the main method of gold recovery. This activity, coupled with poor management of most of the tailings storage facilities, results in the release of acid mine drainage (AMD) following oxidation of pyrite (Hallberg and Johnson, 2005). AMD is formed by a series of complex geochemical and microbial reactions which can be simply represented as follows (Stumm and Morgan, 1970):

$$FeS_2 + 7/2O_2 + H_2O \rightarrow Fe^{2+} + 2SO_4^{2-} + 2H^+ \quad (1.1)$$

$$4Fe^{2+} + O_2 + 4H^+ \rightarrow 4Fe^{3+} + 2H_2O \quad (1.2)$$

$$4Fe^{3+} + 12H_2O \rightarrow 4Fe(OH)_3\downarrow + 12H^+ \quad (1.3)$$

$$FeS_2 + 14Fe^{3+} + 8H_2O \rightarrow 15Fe^{2+} + 2SO_4^{2-} + 16H^+ \quad (1.4)$$

Reaction 1.2 is the rate-determining step in the overall acid–generating sequence and is dependent on the presence of *Thiobacillus ferrooxidans* bacteria (which are acidophilic and chemolithotropic), oxygen and pH.

Reaction 1.4 is a self-sustaining reaction and as such renders tailings dumps as sources of AMD for a long time after mining operations have ceased (Nordstrom, 1979; Moses *et al*., 1987; Ehrlich, 1996; Blowes *et al*., 1998).

This has led to the release of most of the elements in the host ores into the receiving water bodies. Some of the elements that have been reported to emanate from AMD and contaminate water systems in the Witwatersrand Basin include: Cu, Co, Cr, Fe, As, U, Ni, Zn, Hg (Ochieng *et al.,* 2010). The migration of these elements into adjacent waterways poses a long-term risk for cattle, crop farming as well as people located in the vicinity of the polluted waterways.

Currently, the removal of toxic elements from water in the area can be viewed as taking place through natural and human-induced processes. The natural process occurs in wetlands which are a common naturally-occurring feature around most water bodies in the area. The main processes of elemental attenuation in wetlands include precipitation on iron and manganese oxyhydroxyoxides; complexation with humic substances and sulphide precipitation (Tutu, 2006). The latter process stems from sulphate reduction in the wetlands which leads to the formation of hydrogen sulphide which, if persistent in solution, will react with metals to form insoluble sulphides.

While they are an important feature as sinks for pollutants, these wetlands do not always occur in pollution-impacted areas. For instance, they do not occur on tailings footprints, tailings storage facilities and tailings ponds which are the main sources of pollutants.

The human-induced process constitutes of attempts to curtail the promulgation of toxic elements through liming using $CaCO_3$ (limestone). This works well in elevating the pH and rendering divalent elements immobile due to precipitation. However, it is not a viable option for oxy-ion forming elements e.g. uranium and arsenic as these tend to be mobilised at

elevated pH regimes (Levinson, 1974; Langmuir, 1997; Zielinski *et al.*, 1997; Tutu, 2006). Notwithstanding, liming tends to form a lot of sludge which becomes difficult to dispose of as indicated before. Also, it is largely a less informed endeavour in that the limestone dosage is not based on the equivalent acid-producing sulphide content in the tailings and as such pH elevation is usually just short-lived as acidity tends to persist thereafter.

The scale of the pollution problem is so large that both of these methods need to be augmented in order to effectively remove heavy metals and toxic elements. Obviously, the remediation system should work *in situ* and *ex situ* in addition to being cost-effective. The biophysical system based on zeolite/bentonite as supports for fungal and algal biomass was assessed to be the best suited to exploit this gap. As indicated earlier, these adsorbents have the advantage of high loading capacities. The added advantage of using zeolite/bentonite is that they exhibits improved adsorption capacities when chemically modified (Panayotova and Velikov, 2003). Also, fungal and algal biomass easily grows in the area while zeolite and bentonite can be sourced cheaply.

1.3 Objectives of the research

The central aim of this work was to develop a biophysical system based on zeolite/bentonite and micro-organisms (fungal and algal) to remediate polluted seepages and wastewaters from gold tailings. This was achieved by addressing the following specific objectives:

1. To investigate and compare the effectiveness of natural zeolite/bentonite and zeolite/bentonite modified with representative amino acid and polysaccharide compounds (cysteine, histidine, sorbitol and mannitol) released by fungi in removing trace elements from mine waste waters.
2. To prepare and investigate the effectiveness of algal biomass based on *Penicillium simplissicimum* immobilized onto zeolite/bentonite in removing trace elements from mine wastewaters.
3. To study the effects of contact time, pH, concentration and temperature on the adsorption capacity of zeolite/bentonite-living fungi as well as zeolite/bentonite-non active fungi systems.

4. To assess the potential of zeolite/bentonite as a support for the preparation of a biosorbent from the polysaccharide extract from green micro algae and to study the kinetics in the uptake of trace elements from gold mine wastewaters.
5. To assess, by use of column experiments, the potential for application of the different biosorbents prepared above for the removal/recovery of trace elements in gold-mine polluted environments.

1.4 Research approach

This project consists of a two-pronged approach, namely immobilisation of metals and metalloids in solution through sorption processes, and assessing the bioremediation potential of two types of biophysical complexes (viz fungal or microalgal-zeolite/bentonite complexes).

The first step in the approach to adsorption studies constitutes using proxy major components of fungi and microalga, namely: histidine, cysteine, sorbitol and mannitol. These are largely the amino acids and alcohol components of the micro-organisms and are important assessment indicators for metal-binding sites.

The second step involves culturing fungal and microalgal biomass into zeolite/bentonite supports (biofunctionalisation). The performance of the proxy compound-functionalised zeolite/bentonite is compared to the fungal and microalgal biofunctionalised zeolite/bentonite.

The approach also includes the following

- Biofunctionalisation of zeolite/bentonite followed by the characterisation of the developed biomass.
- Assessing the different parameters controlling the adsorption process, namely: pH, effect of metal concentration, effect of contact time and temperature of metal solution.
- Use of various models (kinetic and isothermic) to describe the adsorption process.
- The regeneration of the biophysical system for potential re-use.
- The application of the developed biophysical system for the removal of toxic elements from contaminated effluent emanating from tailings dams.

1.5 Outline of the thesis

This thesis is divided into a number of chapters, each explaining different aspects of the investigation. Although each chapter briefly introduces itself, a summary of each chapter is given below.

Chapter 1 gives a brief background on heavy metals, one of the pollutants from the mining operations in South Africa. An outline of the problem statement is briefly discussed. The main objectives of the study are presented with the research approach to achieve these objectives.

Chapter 2 presents briefly the state of pollution related to the gold mining in the Witwatersrand Basin. The techniques used for the wastewater remediation with emphasis on their processes and applications are described. Adsorbents used in mine water including zeolite, bentonite, fungi and algae with their general characteristics are reviewed.

Chapter 3 is dedicated to the research approach, namely: the collection of mine water and algae; the preparation and characterisation of the biosorbents, mainly: zeolite/bentonite functionalised with microbial compounds (i.e., histidine, cysteine, sorbitol and mannitol); zeolite/bentonite functionalised with *Penicillium simplicissimum and* zeolite-alginates. The experimental protocol followed for the sorption studies in batch and column modes is described.

A section is reserved for the quality control and the different models (isotherms, kinetic and thermodynamic) used to fit the experimental data.

Chapter 4 presents the results and discussion of work done in 3 sections:

- Adsoption capacity of bentonite and zeolite after biofunctionalisation with proxy-compounds.
- Capacity of metal sorption by bentonite and zeolite after biofunctionalisation with *Penicillium simplicissimum.*
- Augmentation of mine waste remediation through biofunctionalisation of zeolite and bentonite with green algae and alginate extracts.

Chapter 5 is a general conclusion of the work presented in this thesis. The chapter highlights the successes of the project and the usefulness of its outcomes. Recommendations are included for further studies and new perspective.

Chapter 2: Literature review

As mentioned in Chapter 1, wastewaters emanating from gold tailings dumps in the Witwatersrand Basin contain toxic elements. These elements have the ability of dissolving in wastewaters and upon discharge into surface waters can be concentrated and travel up the food chain. They can also seep into groundwater, hence contaminating drinking water, thereby posing a health threat.

The following chapter gives the state of pollution related to gold mining in this region and the different remediation technology of heavy metals in water, with emphasis on their processes and applications. An overview on the use of adsorbents in mine water treatment is also given.

2.1 State of pollution in the Witwatersrand Basin

The effect of mining on the environment includes the release of many chemical contaminants into water resources, which can cause environmental damage and threaten the health and safety of nearby communities long after mine closure. This pollution is so persistent that, in the absence of available remedies, in many instances the contaminated sites may never be completely restored (CSIR, Briefing note, 2009). Water is a scarce resource in South Africa. The rapid economic and industrial growth has forced the Department of Water Affairs and Forestry to strictly control the consumption of water. The scarcity of water is also exacerbated by pollution of the surface and groundwater resources. Typical pollutants of South Africa's freshwater aquatic environment include industrial effluents, domestic and commercial sewage, acid mine drainage, agricultural runoff, and litter. Acid mine drainage is a recognised problem in the mining areas of the country (especially from coal and gold mines). There is little reliable information on the amount of mining effluent entering water courses. The Minerals Bureau of Statistics has estimated the total number of mines as anything between 1 200 and 2 000, making it difficult to get any reliable estimate of the problem (National State of the Environment Report-South Africa, 1999).

The gold mining industry in South Africa (particularly in the Witwatersrand Goldfield) is in decline, but the post-closure decant of AMD is an enormous threat, and this could become worse if remedial activities are not taken. The potential volume of AMD for the Witwatersrand Goldfield alone amounts to an estimated 350ML/day (1ML = 1000 m^3) (FSE,

2006; Liefferink, 2011). This represents 10% of the potable water supplied daily by Rand Water to municipal authorities for urban distribution in the Gauteng Province and surrounding areas, at a cost of R3000/ML (Liefferink, 2011). These figures place not only the volume, but also the potential economic value of mine water in perspective.

There are four main types of mining impacts on water quality:

2.1.1 Acid mine drainage

This phenomenon has been described under the Problem Statement in Chapter 1. It is a phenomenon that has been extensively researched worldwide by several authors (Sato, 1960; Bryner *et al*., 1967; Singer and Stumm, 1970; Nordstrom, 1977; Heather et al., 1995; IWQS, 1995; Salomons, 1995; Morin and Hutt, 1997; Jambor and Blowes, 1998; Nordstrom and Alpers, 1999; Akcil and Koldas, 2006; Costello, 2003; Da Silva *et al*., 2003; EEB, 2000).

In South Africa, a number of studies have also been conducted (Forstner and Wittmann, 1976; Marsden, 1986; Jones *et al.,* 1988; Funke, 1990; Coetzee, 1995; Davidson, 2003; Naicker, 2003; Mphephu, 2004; Ndasi, 2004; Nengovhela *et al*., 2006; Pinetown *et al*., 2007; Tutu *et al.,* 2008).

Further to the AMD-formation reactions presented in Chapter 1, other sulphide minerals also react with O_2 and produce acidity (Table 2.1).

Other sulphides can oxidize and release metal iron into solution, but may not produce acidity. Examples of such reactions can be seen as reactions (2.3), (2.9), (2.11), (2.13), (2.15) and (2.18) in Table 2.1 (Costello, 2003; Da Silva *et al*., 2003); sphalerite and galena are the most important of these minerals.

AMD is characterized by low pH (high acidity), high salinity levels, elevated concentrations of sulphate, iron, aluminium and manganese, raised levels of toxic heavy metals such as cadmium, cobalt, copper, molybdenum and zinc, and in some instances radionuclides.

Table 2.1 Selected oxidation reactions for mine tailing with oxygen and iron (Fe^{3+}) (modified table from Mine Water Environ, 2009)

Mineral	Oxidation reactions	
Marcasite (by oxygen)	Same as pyrite	(2.1)
Marcasite (by iron)	Same as pyrite	(2.2)
Chalcopyrite (by oxygen)	$CuFeS_2(s) + 4O_2(aq) \rightarrow Cu^{2+} + Fe^{2+} + SO_4^{2-}$	(2.3)
Chalcopyrite (by iron)	$CuFeS_2(s) + 16Fe^{3+} + 8H_2O \rightarrow Cu^{2+} + 17Fe^{2+} + 2SO_4^{2-} + 16H^+$	(2.4)
Pyrrhotite (with oxygen)	$Fe_{(1-x)}S + (2-0.5x)O_2 + xH_2O \rightarrow (1-x)Fe^{2+} + SO_4^{2-} + 2xH^+$	(2.5)
Pyrrhotite (with iron)	$Fe_{(1-x)}S + (8-2x)Fe^{3+} + 2H_2O \rightarrow (9-3x)Fe^{2+} + SO_4^{2-} + 8H^+$	(2.6)
Arsenopyrite (with oxygen)	$FeAsS + 13/4O_2 + 3/2H_2O \rightarrow Fe^{2+} + SO_4^{2-} + H_2AsO_4^- + H^+$	(2.7)
Arsenopyrite (with iron)	$FeAsS(s) + 14Fe^{3+} + 7H_2O \rightarrow 15Fe^{2+} + SO_4^{2-} + H_3AsO_3(aq) + 14H^+$	(2.8)
Sphalerite (with oxygen)	$ZnS(s) + 2O_2(aq) \rightarrow Zn^{2+} + SO_4^{2-}$	(2.9)
Sphalerite (with iron)	$ZnS(s) + 8Fe^{3+} + 4H_2O \rightarrow Zn^{2+} + SO_4^{2-} + 8Fe^{2+} + 8H^+$	(2.10)
Covellite (with oxygen)	$CuS(s) + 2O_2(aq) \rightarrow Cu^{2+} + SO_4^{2-}$	(2.11)
Covellite (with iron)	$CuS(s) + 8Fe^{3+} + 4H_2O \rightarrow Cu^{2+} + SO_4^{2-} + 8Fe^{2+} + 8H^+$	(2.12)
Millerite (with oxygen)	$NiS(s) + 2O_2(aq) \rightarrow Ni^{2+} + SO_4^{2-}$	(2.13)
Millerite (with iron)	$NiS(s) + 8\ Fe^{3+} + 4H_2O \rightarrow Ni^{2+} + SO_4^{2-} + 8Fe^{2+} + 8H^+$	(2.14)
Greenockite (with oxygen)	$CdS(s) + 2O_2(aq) \rightarrow Cd^{2+} + SO_4^{2-}$	(2.15)
Greenockite (with iron)	$CdS(s) + 8Fe^{3+} + 4H_2O \rightarrow Cd^{2+} + SO_4^{2-} + 8Fe^{2+} + 8H^+$	(2.16)
Galena (with oxygen)	$PbS(s) + 2O_2(aq) \rightarrow Pb^{2+} + SO_4^{2-}$	(2.17)
Galena (with iron)	$PbS(s) + 8Fe_{3+} + 4H_2O \rightarrow Pb^{2+} + SO_4^{2-} + 8Fe^{2+} + 8H^+$	(2.18)

2.1.2 Toxic element contamination and leaching

Pollution by toxic elements occurs when elements such as arsenic, cobalt, copper, cadmium, lead, silver and zinc contained in excavated rock or exposed in an underground mine come in contact with water. Metals are leached out and carried downstream as water washes over the rock surface. Although metals can become mobile in neutral pH conditions, leaching is particularly accelerated in the low pH conditions such as created by AMD (Taylor *et al.*, 2005; Gaikward and Gupta, 2007).

2.1.3 Pollution by processing chemicals

This kind of pollution occurs when chemical agents (such as cyanide or sulphuric acid used by mining companies to separate the target mineral from the ore) spill, leak, or leach from the mine site into nearby water bodies. These chemicals can be highly toxic to humans and wildlife. They can also exacerbate the leaching of toxic elements contained in host ores.

2.1.4 Erosion and sedimentation

Mineral development disturbs soil and rock in the course of constructing and maintaining roads, open pits, and waste impoundments. In the absence of adequate prevention and control strategies, erosion of the exposed earth may carry substantial amounts of sediment into streams, rivers and lakes. Excessive sediment can clog riverbeds and smother watershed vegetation, wildlife habitat and aquatic organisms (Environmental mine council, 2000; De Rosa and Lyon, 1997).

Water has been called "mining's most common casualty" (James Lyon, interview, Mineral Policy Center, Washington DC). There is growing awareness of the environmental legacy of mining activities that have been undertaken with little concern for the environment. Mining by its nature consumes, diverts and can seriously pollute water resources. Water pollution from mine waste rock and tailings may need to be managed for decades, if not centuries, after closure. As mine technologies are developed to make it more profitable to mine low grade ore, even more waste will be generated in the future thus prompting a need for remediation efforts to be pursued more seriously.

2.2 Remediation technology

Conventional techniques commonly applied for the remediation of heavy metals in wastewater treatment systems include physicochemical remediation, phytoremediation and microbial remediation (Matheickal *et al*., 1987; Atkison *et al*., 1998).

The common physicochemical treatment processes for metal remediation include chemical precipitation, coagulation–flocculation, reverse osmosis, ultra-filtration, electro-dialysis flotation, ion exchange and activated carbon adsorption. They have their inherent advantages and limitations in application (Keleşoğlu, 2007). For instance, they often involve high capital

and operational costs and may be associated with the generation of secondary waste which presents treatment problems such as the large quantity of sludge generated by precipitation processes. When applied to dilute metal waste or lower concentrations of metal ions, these processes are either ineffective or not cost-effective (Huang and Huang, 1996). Ion exchange, reverse osmosis and adsorption are more attractive processes because the metal values can be recovered along with their removal from the effluents. Reverse osmosis and ion exchange are not usually economically feasible because of their relatively high investment and operational cost. Adsorption has advantages over the other methods because of simple design with a sludge free environment and can involve low investment in terms of both initial cost and space required (Viraraghavan and Dronamrajum, 1993; Volesky, 2003). The process description of each method is presented below.

2.2.1 Chemical and physical methods

a. Chemical precipitation

The precipitation of heavy metals in water has been practiced as a prime method of treatment in industrial waters for many years. The process involves the transformation of dissolved contaminants into insoluble solids, thereby facilitating the contaminant's subsequent removal from the liquid phase by physical methods, such as filtration (NEESA, 1993; Nomanbhay and Palanisamy, 2005). In a precipitation process, chemical precipitants (also known as coagulants and flocculants) are used to increase particle size through aggregation.

The amount of chemical that is required during treatment is dependent on pH and alkalinity of the water. Usually, heavy metals in water are precipitated by adding sodium hydroxide or lime during neutralization. However, the results of this process are far from satisfying in many cases. A complete hydroxide precipitation does not take place especially in the presence of complexing agents (NEESA, 1993; EPA, 2000; Xu and Xu, 2008).

The conceptual mechanism of heavy metal removal by chemical precipitation is:

$$M^{2+} + 2OH^{-} \rightleftharpoons M(OH)_2\downarrow \qquad (2.19)$$

In practice, the minimum achievable residual metal concentrations are also dependent on the nature and concentration of the organic matter in the wastewater as well as the temperature.

Precipitation is inappropriate for large solution volumes with very low concentrations of metal ions. Addition of an anionic polymer after pH adjustment and formation of hydroxide particles usually results in the rapid growth of a large flocculant which sweeps smaller particles out of solution and quickly settles.

Chemical precipitation of metals can be justified by its low cost and can be performed by a simple pH adjustment. Other advantages include:

- It is a well-established technology with ready availability of equipment and many chemicals.
- It is a completely enclosed system and as such is convenient, self-operating and requires low maintenance since only replenishment of chemicals is needed, with no need for sophisticated operators.

Despite the above advantages, chemical precipitation of metals in water still has the following disadvantages:

- The precipitates are in the form of light tiny flocks requiring extra coagulation/ flocculation.
- Large volumes of sludge are generated, inducing additional waste-disposal costs. The addition of treatment chemicals may increase the waste sludge by up to 50% (EPA, 2000).
- Regulation requirements are not always met using hydroxide and carbonate precipitation alone. Each dissolved metal has its own distinct pH level for maximum hydroxide precipitation.
- Because metal hydroxides are increasingly soluble above or below their individual maximum precipitation point, even a slight pH adjustment to precipitate one metal may put another back into solution.
- It requires working with corrosive chemicals, thereby increasing safety concerns (EPA, 2000; METALSORB, 2004).

The main drawbacks are: the use of a large amount of chemicals to reduce metals to an acceptable level of discharge (Jüttner *et al*. 2000), the generation of large sludge volumes that are usually hazardous or unstable in terms of heavy metal mobilization and require either safe land filling or disposal, further treatment of sludge to meet the disposal criteria, and the valuable metal losses (Yang *et al*., 2001; Bose *et al*., 2002; Wingenfelder *et al*., 2005).

b. Coagulation–Flocculation

Principally, the coagulation process destabilizes colloidal particles by adding a coagulant and results in sedimentation (Shammas *et al*., 2004). To increase the particle size, coagulation is followed by the flocculation of the unstable particles into bulky floccules (Semerjian and Ayoub, 2003). The general approach of this technique includes pH adjustment and involves the addition of ferric/alum salts as the coagulant to overcome the repulsive forces between particles (Licskó *et al*., 1997).

In spite of its advantages, coagulation -flocculation has limitations such as high operational cost due to chemical consumption. The increased volume of sludge generated from coagulation-flocculation may hinder its adoption as a global strategy for wastewater treatment. This can be attributed to the fact that the toxic sludge must be converted into a stabilized product to prevent heavy metals from leaking into the environment (Ayoub *et al*., 2001)**.** To overcome such problems, electro-coagulation may be a better alternative than the conventional coagulation as it can remove the smallest colloidal particles and produce just a small amount of sludge (Vik, 1984; Elimelech and O'Melia, 1990). However, this technique also creates a floc of metallic hydroxides, which requires further purification, making the recovery of valuable heavy metals impossible (Persin and Rumeau, 1989).

c. Electrodialysis

In the electrodialysis process, ionic components of a solution are separated through the use of semipermeable ion-selective membranes (Ahalya *et al*., 2003). This process may be operated in either a continuous or a batch mode. The disadvantage of the electrodialysis process is the formation of metal hydroxides which clog the membrane. To reduce the membrane fouling, activated carbon pre-treatment, possibly preceded by chemical precipitation and some form of multimedia filtration may be necessary (Metcalf and Eddy, 2003). The electrolytic process has not been widely utilized in full-scale treatment of metal wastes.

d. Flotation

Flotation is employed to separate solids or dispersed liquids from a liquid phase using bubble attachment (Wang *et al*., 2004). The attached particles are separated from the suspension of heavy metal by the bubble rise. Flotation can be classified as: (i) dispersed-air flotation, (ii) dissolved-air flotation (DAF), (iii) vacuum air flotation, (iv) electro-flotation, and (v)

biological flotation. Among the various types of flotation, DAF is the most commonly used for the treatment of metal-contaminated wastewater (Zabel *et al*., 1984). Adsorptive bubble separation employs foaming to separate the metal impurities. The target floated substances are separated from bulk water in a foaming phase. Although it is only a kind of physical separation process, heavy metal removal by flotation has the potential for industrial application (Jokela and Keskitalo, 1999).

Flotation can be employed to treat inorganic effluent with a metal concentration of less than 50 mg L^{-1} or higher than 150 mg L^{-1}. Other advantages, such as, a better removal of small particles, shorter hydraulic retention times and low cost make flotation one of the most promising alternatives for the treatment of metal-contaminated wastewater (Matis *et al*., 2003).

e. Ion exchange

Ion exchange is a unit process in which ions of a given species are displaced from an insoluble exchange material by ions of a different species in solution. Materials used for the exchange of metals include zeolites, weak and strong anion and cation resins, chelating resins. Ion exchange processes are highly pH dependent. Solution pH has a significant impact on the metal species present and the interaction between exchanging ions and the resin (Eckenfelder *et al*., 2000). The disadvantages of this process include high cost and partial removal of certain ions (Ahalya *et al*., 2003).

f. Reverse osmosis

Reverse osmosis is used for the removal of dissolved constituents from wastewater remaining after advanced treatment. When two solutions having different solute concentrations are separated by a semi-permeable membrane, a difference in chemical potential will exist across the membrane. Water will tend to diffuse through the membrane from the lower concentration side to the higher concentration side (Akpor and Muchie, 2010; Grampton, 1982; Stiason, 1979). Reverse osmosis has been proposed for treatment for recovery of heavy metals. To protect the reverse osmosis membranes, feed solution pH must be adjusted. Reverse osmosis alone will not achieve complete recovery and reuse of the solutions.

Pre-treatment required prior to the reverse osmosis unit includes equalization, media filtration, pH adjustment and anti-precipitant additions. The process is expensive.

g. Ultrafiltration

Ultrafiltration technologies can be used in a variety of ways in wastewater treatment and water reuse systems. Ultrafiltration can reduce the amount of treatment chemicals, has smaller space requirements, and reduce labour requirements. On the contrary, this method uses more electricity, may need pre-treatment and requires replacement of membranes. The generation of sludge is another disadvantage of this process (Eckenfelder *et al*., 2000).

h. Adsorption

Adsorption process has been, and actually is, the most frequently applied method in the remediation of mine wastewaters, and consequently the most extensively studied. Basically, adsorption is a mass transfer process by which a substance is transferred from the liquid phase to the surface of a solid, and becomes bound by physical and/or chemical interactions (Kurniawan *et al*., 2006).

The term adsorption is used also to describe two kinds of forces of interaction between the adsorbate and the adsorbent. These interaction forces are broadly described as physisorption (physical adsorption) and chemisorption (chemical adsorption) (Rouquerol, 1999). Their basic characteristics are given below in Table 2.2.

Table 2.2 Properties of physisorption and chemisorption (Atkins, 1994)

Physisorption	**Chemisorption**
Multilayer adsorption	Monolayer adsorption
Low degree of specificity	Depends on the reactivity of adsorbent and adsorbate substance
Desorption is possible (adsorbed molecule keeps its identity)	Desorption is impossible (adsorbed molecule loses its identity)
Always exothermic (energy involved is < - 40kJ mol^{-1})	Exothermic or endothermic, chemical bond forms (energy involved can reach several hundreds of kJ mol^{-1})
System generally reaches thermodynamic equilibrium rapidly	Activation energy is involved and at low temperatures, system may not reach equilibrium

Physical adsorption (physisorption) is relatively non-specific and is due to the operation of weak forces between molecules. In this process, the adsorbed molecule is not fixed to a particular site on the solid surface; it is free to move over the surface (Sawyer *et al*., 1994).

The physical interactions among molecules, based on electrostatic forces, include dipole-dipole interactions, dispersion interactions and hydrogen bonding.

Chemical adsorption (chemisorption) is also based on electrostatic forces, but much stronger forces are at play in this process (Sawyer *et al*., 1994). In chemisorption, the attraction between adsorbent and adsorbate is a covalent or electrostatic chemical bond between atoms, with shorter bond length and higher bond energy (Montgomery, 1985).

The enthalpy of chemisorption is very much greater than that for physisorption, and typical values are in the region of 200 kJ mol^{-1}, whereas the value for physisorption is about 20 kJ mol^{-1}. Except in special cases, chemisorption is exothermic.

A spontaneous process requires a negative free energy (ΔG^o) value. Because, the translational freedom of the adsorbate is reduced when it is adsorbed, entropy (ΔS^o) is usually negative.

Therefore, in order for $\Delta G^o = \Delta H^o - T\Delta S^o$ to be negative, ΔH^o is expected to be negative, and the process is exothermic. If the enthalpy values less negative than -25 kJ mol^{-1}, system is physisorption and if the values more negative than -40 kJ mol^{-1} it is signified as chemisorption (Atkins 1994). The adsorption type as well as the values of enthalpy associated is given in table 2.3.

Table 2.3 The bond energies of various mechanisms for adsorption (Atkins, 1994)

Interaction between adsorbent and adsorbate	**Enthalpy (kJ mol^{-1})**		**Adsorption type**
	-ΔH	**+ΔH**	
Electrostatic chemical bonding	> 40	> 200	Chemisorption
Dispersion interactions and hydrogen bonding	8 - 40		Physisorption
Dipole-dipole interaction	< 8	< 20	Physisorption

The liquid –solid interface

The adsorption process, as illustrated in Figure 2.2, takes place in four steps: (1) bulk solution transport, (2) film diffusion transport, (3) pore transport and (4) adsorption.

The bulk solution transport involves the movement of the adsorbate through the bulk liquid to the boundary layer of fixed film of liquid surrounding the adsorbent, typically by advection

and dispersion. The film diffusion transport is the transport by diffusion of the material through the stagnant liquid film to the entrance of the pores of the adsorbent (Figure 2.1).
Pore transport involves the transport of the adsorbate through the pores by a combination of molecular diffusion through the pore liquid and/or by diffusion along the surface of the adsorbent. Adsorption involves the attachment of adsorbate to adsorbent at an available adsorption site (Metcalf and Eddy, 2003). Adsorption can occur on the outer surface of the adsorbent and in the macropores, mesopores, micropores, and sub-micropores. The surface area of the macropores and mesopores is small compared with the surface area of the micropores and sub-micropores, so the amount of material adsorbed there is usually considered negligible.

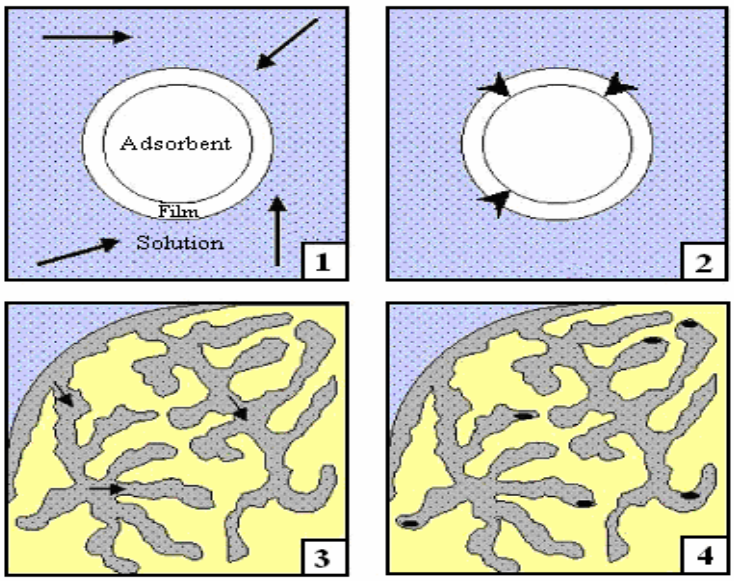


Figure 2.1 Schematic illustrations of adsorption steps

When an adsorption process mechanism is studied, the main goals are to find and explain the order of selectivity for different heavy metals and to quantitatively compare the effects of the influence of factors towards the adsorption capacity. For these purposes, the experimental data can be analysed by adsorption isotherms, thermodynamic (for equilibrium condition) and kinetics parameters (evolution with time) (Cozmuta *et al.*, 2012; Violante *et al.*, 2010).

In mine water treatment, some of the most common adsorbents used for heavy metal removal are zeolite and bentonite.

(i) Zeolite

Zeolites are crystalline, hydrated aluminosilicate of alkali and alkaline earth cations having an infinite, open, three-dimensional structure. It is able to lose and gain water reversibly and exchange extra-framework cations, both without change of crystal structure (Mumpton, 1999). The primary building block of the zeolite framework is the tetrahedron, the centre of which is occupied by a silicon or aluminium atom, with four atoms of oxygen at the vertices. Each oxygen atom is shared between two tetrahedrons and the tetrahedrons form a continuous framework. Substitution of Si^{4+} by Al^{3+} defines the negative charge of the framework, which is compensated by monovalent or divalent cations located together with water therefore they are termed as exchange or extra-framework cations, whereas Si^{4+} and Al^{3+} are not exchanged under ordinary conditions and are termed as tetrahedral or framework cations (Tsitsishvili *et al*., 1992).

The typical formula for natural zeolite is:

$(Me^{+}, 1.5Me^{2+})x(Al_xSi_yO_{2(x-y)}).zH_2O$

Me^{+} = Na, K, Li; Me^{2+}= Ca, Mg, Ba, Sr.

The chemical composition is usually variable and depends and with the report between $Si^{4+}$and Al^{3+}, and the type and concentration of the counterbalance cations.

The zeolite structure is mainly composed of three components (Tsitsishvili *et al*., 1992):

1. Alumino-silicate framework
2. Exchangeable cations
3. Water

The aluminosilicate framework is the most conserved and stable component of zeolite. The topology of the framework, the numbers and distribution of charges (Al^{3+} sites) are basically formed at the crystal growth stage and define a series of technologically important properties of zeolites (Tsitsishvili *et al*., 1992). Both Si/Al ratio and cation contents determine the properties of most zeolites (Vaughan, 1978). Zeolites may be classified in three groups according to Al/Si ratio in their frameworks (Ribeiro *et al*., 1984):

- Low-silica or aluminium rich zeolites A and X (ratio Si/Al≈1)
- Intermediate silica zeolites: zeolite Y, mordenite, zeolite L, natural zeolites (ratio Si/Al = 2 : 5)
- High silica zeolites: zeolite beta, ZSM-5 (ratio Si/Al ≥ 10)

Most researchers in their work have observed that the pre-treatment of natural zeolites improves ion exchange capacity (Gunaya *et al*., 2007; Inglezakis *et al*., 2004; Han *et al*., 2006). The selectivity of the zeolites for metal ions has also been studied by authors such as Semmens *et al.* (1978) and Inglezakis *et al*. (2004).

The cationic exchange capacity CEC of zeolites is basically the amount of Al^{3+} ions that substitute the Si^{4+} ions in the tetrahedral zeolite framework (Mumpton, 1999; Ouki and Kavannagh, 1999); the Si/Al ratio. The greater the aluminium content, the more incoming ions are needed to balance the charge, thus the higher the exchange capacity. Other factors that determine the adsorption capacity of zeolites by heavy metals are:

- The hydration diameters; of ions sitting in the framework and those incoming into the zeolite.
- Hydration enthalpies
- Solubility of cations

The selectivity order of zeolites for metal ions is usually brought about by the various factors that influence adsorption and ion exchange behaviour in zeolites (Zamzow *et al.*, 1990). This brings about effects such as the sieving effect for metal ions or the availability of the specific exchange sites in the zeolite. Depending on the arrangement of the zeolite crystal lattice or pore volumes, the incoming ions will be affected, and may diffuse through the structure or fail to move through the pores.

Most researchers have found different cation exchange capacities and interestingly, it was noted that clinoptilolite exhibits different selectivity series for different metal ions.

The reversible nature of ion exchange makes the regeneration process of clinoptilolite an important step in ion exchange. It also makes the processes economical as the zeolite samples can be reused for a couple of cycles before the structures are exhausted. The adsorbed metal ions can be recovered and re-used.

In South Africa, up to 75% of pure zeolite beds (mainly consisting of heulandite and mordenite) are located in the Heildelberg-Riversdale area. It occurs in altered tuff beds overlying bentonite-rich horizons (Wipplinger and Horn, 1998). Clinoptilolite has been found in two principal areas of South Africa namely:

- Western Cape Province, in the Heildelberg-Riversdale area

- Northern KwaZulu - Natal: in the Nxwala Estate near the Mkuze Game Reserve of the Lebombo Mountains (Wipplinger and Horn, 1998).

(ii) Bentonite

Bentonite is clay generated frequently from the alteration of volcanic ash, consisting predominantly of smectite minerals, usually montmorillonite (70-90%). In montmorillonite, tetrahedral layers consisting of [SiO_4] - tetrahedrons enclose the [$Me(O_5,OH)$]-octahedron layer (Me is mainly Al, Mg, but Fe is also often found). The silicate layers have a slight negative charge that is compensated by exchangeable ions in the inter-crystallite region. The charge is so weak that the cations (in natural form, predominantly Ca^{2+}, Mg^{2+} or Na^{+} ions) can be adsorbed in this region with their hydrate shell. The extent of hydration produces inter-crystalline swelling. Depending on the nature of their genesis, bentonites contain a variety of accessory minerals in addition to montmorillonite. These minerals may include quartz, cristobalite, feldspar, calcite and gypsum. The presence of these minerals can impact on the industrial value of a deposit, reducing or increasing its value depending on the application. Bentonite presents strong colloidal properties and its volume increases several times when coming into contact with water, creating a gelatinous and viscous fluid (Permien and Lagaly, 1994).

The non-stoichiometric formula is $2[(Al_{1.67}Mg_{0.33})(Si_{3.5}Al_{0.5})O_{10}(OH)_2]$. Mg^{2+} ions often substitute Al^{3+} ions, resulting in a net negative charge. It is made up of 3- layers clay with one aluminum oxide sheet surrounded by two silicon oxide sheets (Figure 2.2).

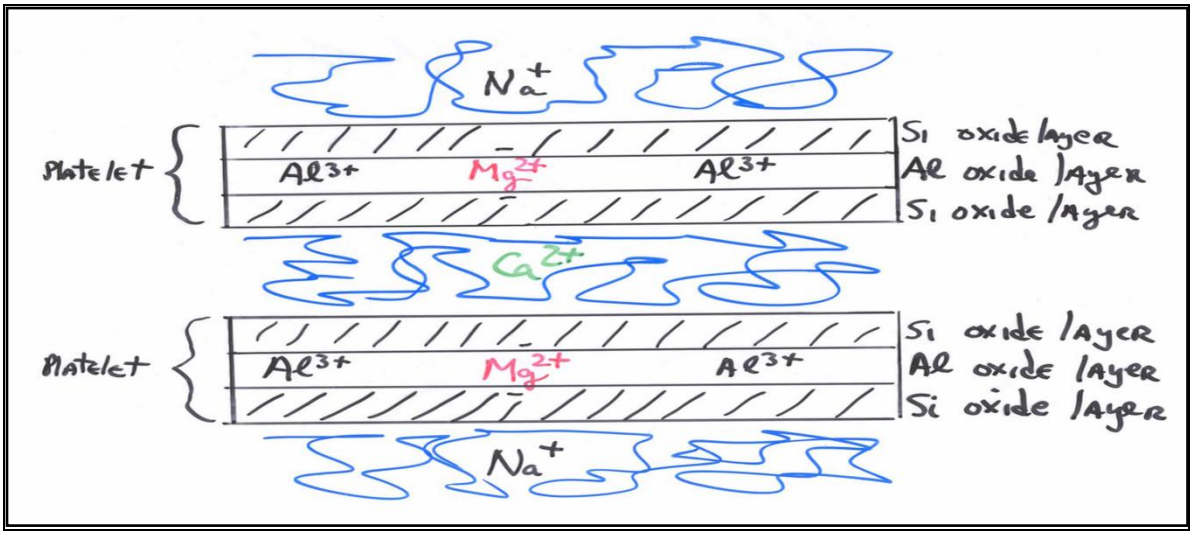


Figure 2.2 Layer structure of bentonite (www.scribd.com, April 2010)

The internal aluminium oxide sheet and external silicon oxide sheet both share oxygen atoms. Such an arrangement would be electrically neutral, but Mg^{2+} ions often substitute Al^{3+} ions, resulting in a net negative charge. The interlayer space an essential characteristic of clay minerals from this group is easily accessible to other polar solvents and water. Smectite group minerals have a good cation exchange capacity due to the presence of hydrated cations in their interlayer surfaces. These cations can be easily exchanged by heavy metals, compensating the negative charge generated on the aluminium oxide layered when an Mg^{2+} replaces an Al^{3+} ion. The hydrated cations commonly present are the Ca^{2+} and Na^{+} cations (La Grega *et al*., 1994). The compensation of the negative charge is as follows (Siguin, 1994):

$$2\text{Na-smectite} + M^{2+} \rightarrow \text{M-smectite} + 2Na^{+} \qquad (2.20)$$

The special properties of bentonite include: hydration, swelling, water absorption, viscosity, thixotropy, which make it a valuable material for a wide range of uses and applications. The cation exchange process is reversible and stoichiometric, which varies depending on the concentration of the metal ions, pH of the solution and the nature of the metal ion. The cation exchange capacity for Ca and Na bentonite are 80 and 150 milliequivalents (by 100g of material), respectively (Calarge *et al*., 2006; La Grega *et al*., 1994).

Most industrial applications involve the swelling property of bentonite to form viscous water suspensions. Depending upon the relative proportions of clay and water, these mixtures are used as bonding, plasticizing, and suspending agents. Bentonites disperse into colloidal particles and, accordingly, provide large surface areas per unit weight of clay. This large surface area is a major reason why bentonite functions so well in stabilizing emulsions, or as a medium to carry other chemicals. Bentonites react chemically with many organic materials to form compounds which are used as gelling agents in a variety of organic liquids (Clem and Doehler, 1961).

Bentonites are selected for each industrial need on the basis of type and quality. This selection is based principally on physical properties, and chemistry of the bentonite becomes involved only to the extent that it influences the physical properties.

In the world, South Africa was rated as the 21st producer of bentonite in 2009 with over 40340 Metric tons of bentonite exported (USGS, Mineral Resources Program, 2012).

2.2.2 Phytoremediation

Phytoremediation is a remediation process that entails the use of plants to partially or substantially remediate selected substances in contaminated soil, sludge, sediment, groundwater, surface water and wastewater. It is also referred to as green remediation, botano-remediation, agro-remediation or vegetative remediation (Pivetz, 2001). The removal of metal contaminants from water through phytoremediation occurs by any of three mechanisms: phytoextraction, rhizofiltration and phytostabilisation (Lasat, 2000; UNEP, 2010).

As it is with any technology, phytoremediation has several advantages and disadvantages. When compared to conventional remediation processes, the advantages of phytoremediation include:

- Economical and low cost technology.
- Less disruptive to the environment and does not involve waiting for new plant communities to decolonize the site.
- No need for disposal sites, hence reducing risk of spread of contaminants.
- More aesthetically pleasing than traditional methods.
- Potential to treat sites polluted with more than one type of pollutant.

Despite the above advantages, some of the disadvantages include:

- Dependent on the growing conditions (climate, geology, altitude, temperature) required by the plant, hence success depends on tolerance of the plant to the pollutant.
- Requires access to agricultural equipment and knowledge to operate at large scale.
- Risk of release of contaminants collected in senescing tissues being released back into the environment.
- Contaminants may be collected in woody tissues used as fuel.
- Since it is dependent on plant growth, when compared to other technologies, remediation time is long.
- Possibility for environmental damage due to leaching of soluble contaminants.
- Because of shallowness of plant roots, there is the problem of depth limitation; hence effectiveness can only be achieved within zone of influence of plant roots (Hinchman and Negri, 1997; Pivetz, 2001; Gardea- Torresdey *et al*., 2005).

Several species of *Thlaspi, B. juncea*, *Salix* spp., and *Populus* species have been tested for remediation ability in pilot studies or are currently in commercial application.

Researchers have also realized that phytoextraction can be used for the recovery of precious metals such as gold, silver, platinum, and palladium, which indicates the wide possibilities of the phytoremediation technology with regards to mining (Gardea -Torresdey *et al*., 2005).

Presently, over 400 species of plants are identified to have potential for remediation of water sources (Lone *et al*., 2008). The ability of water hyacinth (*Eichhornia crassipes*) to absorb and translocate cadmium, lead, copper, zinc, and nickel in wetlands has been investigated by Liao and Chang (2004). They defined translocation ability as the quantity of copper, lead, cadmium, nickel, and zinc translocated in the plant's tissues, which was expressed as a root/shoot ratio. The ratio results they obtained were in the order of copper > lead > cadmium > nickel > zinc. In their investigation, water hyacinth plants had a high bio-concentration of these trace elements when grown in water environments with low concentrations of the five elements. Their results revealed that, the concentrations of these five elements in the roots were 3 to15 times higher than those in the shoots.

In the Witwatersrand Basin, some phytoremediation programmes have been undertaken by AngloGold Ashanti through the Ecological Engineering Programme with the University of the Witwatersrand. Some successes have been reported (Angus, 2005; Weiersbye, 2007;

Weiersbye and Witkowski, 1998; 2002; 2003; Witkowski and Weiersbye, 1998; 2005; Weiersbye *et al*., 2005; Straker *et al.*, 2004a, b).

2.2.3 Microbial remediation process

Microbial bioremediation is defined as the process by which micro-organisms are stimulated to rapidly degrade hazardous organic contaminants to environmentally safe levels in soils, subsurface materials, water, sludge, and residues. Microbes deal with poisonous chemicals by applying enzymes to convert one chemical into another form and taking energy or utilizable matter from this process. The chemical transformations generally involve breaking of large molecules into several small molecules in simpler form. In view of the interest in water and wastewater treatment, the response of micro-organisms towards toxic heavy metals is of importance. In some cases the by-products of microbial remediation are not only harmLess but may prove useful (Gupta *et al*., 2003).

The manner in which micro-organisms interact with heavy metal ions depends partly on whether they are eukaryotes or prokaryotes. Procaryotic cells have a much simpler and smaller structure than eukaryotic cells and lack a true membrane-delimited nucleus (Ehrlich, 1997; Gadd, 2010). It generally lacks extensive, complex, internal membrane systems although with a plasma membrane. In contrast, eukaryotic cell have a membrane-enclosed nucleus and many membranous organelles. They are more complex morphologically and are usually larger than procaryotes. Algae, fungi, protozoa, higher plants, and animals are eukaryotic (Prescott *et al*., 2002).

Eukaryotes (fungi, protists) are more sensitive to metal toxicity than bacteria. In the presence of toxic concentrations, several resistance mechanisms are activated, for example: the production of peptides of the family of metal binding proteins, such as metallothioneins (MTs); the regulation of the intracellular concentration of metals, with expression of protein transporters of ligand-metal complexes from the cytoplasm to the inside of vacuoles and efflux of metal ions by ion channels present in the cell wall (Valls and Lorenzo, 2002). Several studies have shown that many organisms, prokaryotes and eukaryotes, have different natural capacities to adsorb toxic heavy metal ions, giving them different degrees of intrinsic resistance, particularly in diluted solutions (between 10 to 20 mg L^{-1}), due to their mobility, as well as the solubility and bioavailability capacities of these metal ions (Malik, 2004; Tabak

et al., 2005; Kim *et al*., 2007; Chen and Wang, 2008). For the bioremediation of heavy metals on an industrial scale, it is important to use low-cost biomaterial, which can be a by product or waste material with high removal capacity, since the low cost of this biomass is crucial for the process to be economically viable (Volesky and Holan, 1995; Zouboulis *et al*., 2001).

Several studies have been conducted with the purpose of improving the resistance and/or the ability of micro-organisms to accumulate heavy metal ions, including the studies of the following parameters: pH (Naeem *et al.,* 2006); temperature; different metal concentrations and biomass (Soares *et al.,* 2003; Kim *et al.,* 2005), competitiveness of ions of different elements; metal contact time (Kotrba and RumL, 2000), composition of the culture medium (Ghosh *et al*., 2006); bioaugmentation/biostimulation (Roane and Pepper, 2001; Silva *et al*., 2004), resistance to toxicity of heavy metals of Gram positive/Gram-negative bacteria (Samuelson *et al*., 2002); intracellular/extracellular bioaccumulation; viable /non-viable cells; free /immobilized cells and biological processes by aerobic/anaerobic micro-organisms (Dias *et al*., 2002; Liu *et al*., 2005; Tabak *et al*., 2005; Wang and Chen, 2006; Silva *et al*., 2004). The search for new technologies for the removal of toxic metals from contaminated sites has focused on biosorption, which is based on the metal binding capacities of various biological materials.

Biosorption can be defined as the ability of biological materials to accumulate heavy metals from wastewater through metabolically-mediated or physicochemical uptake pathways (Fourest and Roux, 1992). Algae, bacteria, fungi and yeasts have all proven to be potential metal biosorbents (Volesky, 1990). Many indigenous organisms isolated from sites contaminated with heavy metals have tolerance to heavy metal toxicity and these microbial activities have always been the natural starting point for all biotechnological applications. It is therefore necessary to isolate bacterial strains with novel metabolic capabilities and to establish degradation pathways both biochemically and genetically. Potent metal biosorbents in the bacteria class include the genus Bacillus (Nakajima and Tsuruta, 2004; Tunali *et al*., 2006), Pseudomonas (Chang *et al*., 1997; Uslu and Tanyol, 2006) and Streptomyces (Mameri *et al*., 1999; Selatnia *et al*., 2004a). The biosorption process involves a solid phase (sorbent or biosorbent; biological material) and a liquid phase (solvent, normally water) containing a dissolved species to be sorbed (sorbate, metal ions).

Biosorption is based on passive (metabolism-independent) or active (metabolism-dependent) accumulation processes (Wang and Chen, 2006), in combinations that differ qualitatively and

quantitatively, depending on the type of biomass, its origin, feasibility, and type of processing (Veglio and Beolchini, 1997). A classification of the mechanisms of metal accumulation can be made based on the dependence of cellular metabolism or according to the location of the metal within the cell.

Biosorption mechanisms

There are many ways for the metal to be taken up by the microbial cell due to the complex structure of micro-organisms. Biosorption mechanisms may be classified according to various criteria (Figure 2.3), although most of them are not yet fully understood.

The transportation of metal across the cell membrane yields intracellular accumulation, which is dependent on the metabolism of the cell. This means that this kind of biosorption may only take place within viable cells (Costa and Leite, 1991; Gadd *et. al.*, 1988).

It is often associated with an active defense system of the micro-organism, which reacts in the presence of a toxic metal. During non-metabolism dependent biosorption, metal uptake occurs by means of physicochemical interaction between the metal and the functional groups present on the microbial cell surface (Kuyucak and Volesky, 1988).

This is based on physical adsorption, ion exchange and chemical sorption, which is not dependent on cell metabolism. Cell walls of microbial biomass, which consists mostly of polysaccharides, proteins and lipids, have abundant metal binding groups such as carboxyl, sulphate, phosphate and amino groups. This type of biosorption, i.e., non-metabolism dependent, is relatively rapid and can be reversible (Kuyucak and Volesky, 1988).

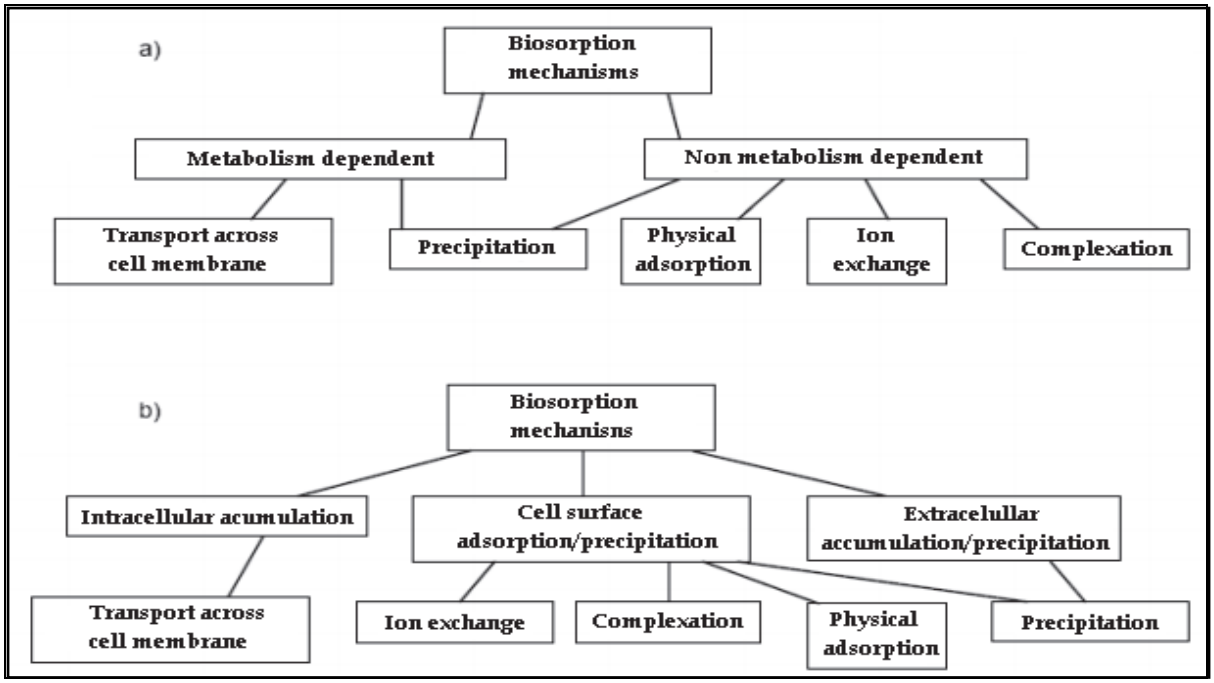


Figure 2.3 Mechanisms of biosorption, a) classification according to dependence on cell metabolism, b) classification according to the location within the cell and the metal removed (Veglio and Beolchini, 1997).

In the case of precipitation, metal uptake may take place both in the solution and on the cell surface (Ercole *et al*., 1994). Furthermore, it may be dependent on cell metabolism if, in the presence of toxic metals, the micro-organism produces compounds that favour the precipitation process. Precipitation may not be dependent on cell metabolism, if it occurs after a chemical interaction between the metal and the cell surface (Perpetuo *et al*, 2011).

Due to the complexity of biomaterial, it is possible for several of these mechanisms to occur simultaneously, in degrees that depend on the biosorbent and environmental conditions (Kefala *et al*., 1999; Volesky, 2001; Gavrilescu, 2004).

Biosorption capacity is affected mainly by three factors:

(i) Characteristics of the metal ion (atomic weight, ionic ray, valence).

(ii) Environmental conditions (pH, temperature, ionic strength, contact time, biomass concentration).

(iii) The nature of the biosorbent, which may determine differences in selectivity and affinity to metal ions, since the type and species of micro-organisms, conditions of growth, physiological state and cell age may all affect the binding mechanism to heavy metals (Wang & Chen, 2006; Chen & Wang, 2008).

The following items are the main biosorption mechanisms, which can also be considered mechanisms of resistance or tolerance to heavy metals developed by micro-organisms:

I .Transport across cell membranes: Heavy metal transportation across microbial cell membranes may be mediated by the same mechanism used to convey metabolically important ions such as potassium, magnesium and sodium. The metal transport systems may become complicated by the presence of heavy metal ions of the same charge and ionic radius associated with essential ions. This kind of mechanism is not associated with metabolic activity. Basically, biosorption by living organisms comprises of two steps: first, an independent binding metabolism where metals are bound to the cell walls; and second, metabolism-dependent intracellular uptake, whereby metal ions are transported across the cell membrane (Costa *et al*., 1991; Gadd *et al*., 1988; Huang *et al*., 1990; Nourbaksh *et al*., 1994).

II. Ion exchange: Cell walls of micro-organisms contain polysaccharides and bivalent metal ions exchange with the counter ions of the polysaccharides. For example, the alginates of marine algae occur as salts of K^+, Na^+, Ca^{2+}, and Mg^{2+}. These ions can exchange with counter ions such as Cu^{2+}, Cd^{2+} (Kuyucak and Volesky, 1989).

III. Complexation: The electrostatic attraction between a metallic ion/ chelating agent and a polymer (excreted by a viable or non viable micro-organism) result in the formation of an extracellular complex. It can be caused by: biosurfactants, polysaccharides, proteins and nucleic acids. These chelating agents contain pairs of electrons that present electrostatic attraction and if they cling to the metallic ions, there is no electron transfer. The final structure has the electric charge of the sum of individual charges of the participants of the complex (Veglio and Beolchini, 1997; Davis *et al*., 2003).When this detoxification/ complexation system is overloaded, "oxidative stress" of the cell occurs (Gavrilescu, 2004).
Metal removal from the solution may also take place by complex formation on the cell surface after interaction between the metal and the active groups. Aksu *et al*. (1992) hypothesized that biosorption of copper by C. vulgaris and Z. ramigera takes place through both adsorption and the formation of coordination bonds between metals and amino and carboxyl groups of cell wall polysaccharides. Complexation was found to be the only mechanism responsible for the accumulation of calcium, magnesium, cadmium, zinc, copper and mercury by Pseudomonas syringae. Micro-organisms may also produce organic acids

(e.g., citric, oxalic, gluconic, fumaric, lactic and malic acids), which may chelate toxic metals, thus resulting in the formation of metallo-organic molecules. These organic acids help in the solubilization of metal compounds and leaching from their surfaces. Metals may be biosorbed or complexed by carboxyl groups found in microbial polysaccharides and other polymers.

IV. Precipitation: Precipitation may be either dependent on the cellular metabolism or independent of it. In the former case, metal removal from solutions is often associated with the active defense system of the micro-organisms. They react in the presence of toxic metal producing compounds, which favour the precipitation process. In the case of precipitation that is not dependent on cellular metabolism, it may be a consequence of the chemical interaction between the metal and the cell surface. The various biosorption mechanisms mentioned above can take place simultaneously (Perpetuo *et al*, 2011).

V. Adsorption: Physical adsorption is a process where the metal ion in solutions binds onto polyelectrolytes present in microbial cell wall through electrostatic interactions, Van der Waals forces, covalent bonding, redox interaction and bio-mineralization to achieve electro neutrality. This process is independent of metabolism, and it is reversible and very promising, as it presents many advantages, especially for treating large volumes of wastewater with low concentrations of contaminants (Ahluwalia and Goyal, 2007; Kuroda and Ueda, 2010; Nishitani *et al*., 2010).

In physical adsorption, the metal ions are attracted by the potential negative of the cell wall, and both are dependent on pH. The influence of pH on metal accumulation by yeasts, algae and bacteria are very similar; for example, in yeast, at pH < 2 the accumulation of metals is practically zero, because at low pH the active sites of the cell wall are associated with protons, restricting the approach of metal cations, and thus resulting in a repulsive force. Therefore, as the pH increases, an increasing number of sites (acetamide chitin, structural polysaccharides of fungi, phosphate and amino groups of nucleic acids, amino and carboxyl groups of proteins and hydroxyl groups of polysaccharides) are replaced by negative charges, increasing the attraction of metallic cations and adsorption on the cell surface (Perpetuo *et al.*, 2011).

Accordingly, the solubility of metallic ions decreases and, consequently, their bioavailability is reduced, and precipitation occurs (Esposito *et al*., 2002; Chen & Wang, 2008; Nishitani *et al*., 2010; Kuroda and Ueda, 2011). Thus, a pH range of between 4 and 8 is generally accepted as "good" for the biosorption of heavy metals for almost all types of biomass (Borro and Fein, 2005; Wang and Chen, 2006; Machado *et al*., 2008).

VI. Oxidation-reduction (redox): Micro-organisms can mobilize or immobilize metal ions, metalloid and organo-metal compounds, thus promoting redox processes. Only prokaryotes are capable of oxidizing metals such as Mn^{2} , Fe^{2+}, Co^{2+} , Cu, AsO^{2-}, Se^{0}/SeO_3^{2-}, or reducing Mn^{4+}, Fe^{3+}, Co^{3+}, AsO_4^{2-}, SeO_4^{2-}/SeO_3^{2}, whilst obtaining energy from these reactions (Gavrilescu, 2004). When, for example, the Fe^{3+} ion is reduced to Fe^{2+}, or the Mn^{4+} ion is reduced to Mn^{2+}, there is an increase in the solubility of these metals. Microbial species can efficiently immobilize heavy metals through their ability to reduce heavy metal ions, reducing them to a lower oxidation state, and giving rise to metallic elements which are less bioactive (Valls and Lorenzo, 2002; Gadd, 2004).

VII. Bio-methylation: Micro-organisms can transform metal ions through the bio-methylation mechanism. Hg, As, Cd, Se, Sn, Te and Pb ions can be methylated by a variety of bacteria, filamentous fungi and yeasts, under both aerobic and anaerobic conditions, which may result in increased mobility. This enzymatic mechanism involves a transfer from the methyl group (CH_3) to metals and metalloids. The methylated compounds formed differ in their solubility, volatility and toxicity (Roane and Pepper, 2000; Gadd, 2000). For example, methyl and dimethyl mercury are more toxic than inorganic Hg ions, however, these are intermediate forms of processing for Hg^{0}. Inorganic forms of As are more toxic than the methylated species (acids and methyl-As dimethyl-As), the methylated and inorganic forms of Se and Cd are highly toxic (Roane and Pepper, 2001; Tabak, 2005).

VIII. Siderophores: When micro-organisms are grown in an iron deficient medium, they produce specific iron chelators, so called siderophores. They play an important role in the complexation of toxic metals and radionuclides, by increasing their solubility. Siderophores have low molecular weights, and have compounds such as catecholate, phenolate or hydroxamate as their binding groups. Many bacteria, such as Actinomycetes

Azotobacter and those of the genus Pseudomonas, synthesize these substances to capture the iron ions they require for their metabolic activity, or for biosorption (Pattus and Abdallah, 2000; Gazsó, 2001).

IX. Bio-surfactants: Bio-surfactants are natural surfactants synthesized by plants: (saponins), micro-organisms (glycolipids) and the bodies of organisms (bile salts), and they have several advantages over industrially-produced surfactants, such as lower toxicity to degrading micro-organisms and less recalcitrance in the environment, greater diversity of chemical structures; performance over a broader range of conditions at different temperatures and pHs (Bognolo, 1999). Bio-surfactants of microbial origin (mainly aerobic) are the result of the metabolic by-products of bacteria, fungi and yeasts, which are released into the medium. The hydrophilic portion may consist of amino acids, peptides or saccharides, and the hydrophobic portion is usually formed by saturated or unsaturated fatty acids (Champion *et al*., 1995; Mulligan, 2005; Li and Li, 2011).

X. Metal-binding cysteine-rich peptides: When cells are exposed to heavy metals in toxic concentrations, an induction of expression of peptides rich in cysteine residues, metallothioneins (MTs), glutathione (GSH) or phytochelatin (PCs) occurs. These are non enzymatic molecules, with low molecular weight, which are resistant to thermo-coagulation and acid precipitation. The main feature of these peptides is to form complexes with divalent metals and metal-thiols. (Bae *et al*., 2000; 2001).

- ***Metallothioneins (MTs):*** Metallothioneins (MTs) are a group of well preserved structures of proteins that act as antioxidants, and they are distributed among all living organisms. They have low molecular weight and they are rich in cysteine residues. The presence of thiol groups (R-SH) in the cysteine chemical structure enables the capture of metal ions such as Cd^{2+}, Fe^{2+}, Hg^{2+}, Cu^{2+} and Zn^{2+}. MTs are composed of two separate domains, namely the β domain in the N-terminal region, and α domain in the C-terminal region. The β domain possesses nine cysteine residues linking three divalent ions, the α domain already has eleven cysteine residues and binds four ions, thus a total of seven ions per molecule are bound (Cobbett and Goldsbrough, 2002; Thirumoorthy *et al*., 2007). The MTs have several functions, including the detoxification of heavy metals and protection against the presence of ROS. Thus, MTs are responsible for reducing the effect of oxidative stress caused by these ions, but they are also responsible for maintaining homeostatic cellular redox

balance. According to these characteristics, protein synthesis is only induced by metals. (Cobbett and Goldsbrough, 2002; Smith *et al*., 2007).

- ***Glutathione (GSH):*** Glutathione (GSH), L-Glutamyl-L-cysteinyl-glycine (Figure 2.4), is a soluble antioxidant, recognized as the most important non-protein thiol present in all living organisms. It consists of three amino acids (Glu-Cys-Gly), and it is the cysteine thiol group of the active site that is responsible for its biochemical properties (Bae and Mehra, 1997; Penninckx, 2000; Mendonza-cózatl *et al*., 2005).

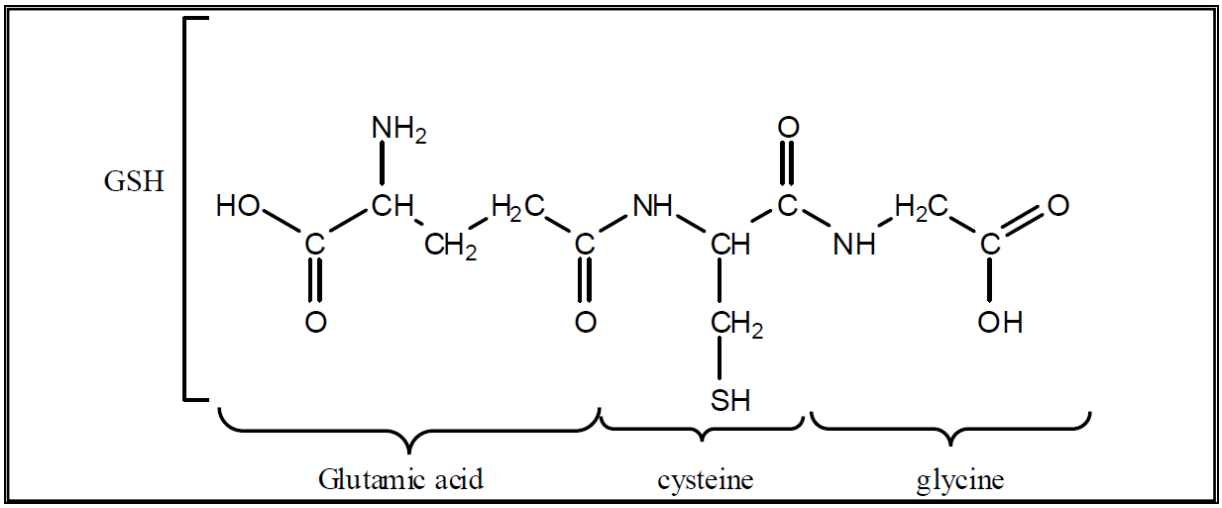


Figure 2.4 Chemical structure of glutathione (GSH) (Bae & Mehra, 1997)

- ***Natural phytochelatins (PCs) and synthetic phytochelatin (EC20):*** PCs are small cysteine rich peptides with the general structure (Glu-Cys) nGly (n = 2-11) (Figure 2.5-A) (Grill *et al*., 1985; Cobbett, 2000). PCs are synthesized from glutathione (GSH) in steps catalyzed by PC synthase (Grill *et al*., 1985; Gupta *et al*., 2004). They enable ions to bind to various heavy metal ions through thiol residues and carboxyl (Kobayashi *et al*., 2005; Inouhe, 2005). These PCs are present in plants, fungi, nematodes, parasites and algae, including cyanobacteria. Despite being classified as MT-III, the PCs have a greater capacity for binding heavy metal ions (1 atom per cysteine basis) than MTs. The pioneering work that targeted the expression of recombinant PCs in *E.coli* were faced with the difficulty imposed by the chemical bonds of type γ present between Glu-Cys units, which are the result of multi-enzyme processes. These bindings are different for type α among the present amino acid chains of all proteins (Bae *et al*., 2001; Cobbett, 2000; Penninckx, 2000; Gupta *et al*., 2004; Inouhe, 2005; Hirata, 2005; Mendoza-Cózatl, 2005; Wu *et al*., 2006).

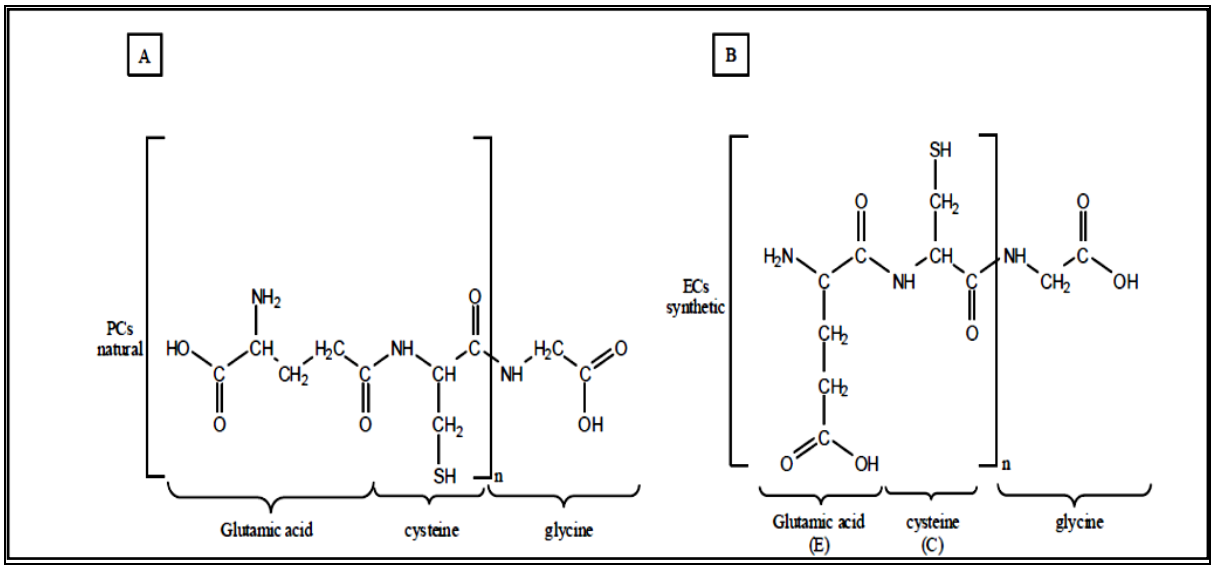


Figure 2.5 Chemical structures of molecules binding heavy metals:
A) Natural phytochelatin (PC) and B) Synthetic phytochelatin (EC) - glutamic acid (glu-E) and cysteine (Cys-C) (Bae *et al.*, 2000).

XI) The "cell-surface display" system: Cell surface proteins constitute an important class of bio-molecules because they are situated at the interface between the cell and the environment. The cells have systems for anchoring specific proteins to the surface and confining them to certain areas (Kondo and Ueda, 2004). The expression of heterologous peptides on the cell surface ("cell-surface display ") is a powerful technique widely used in the biotechnology area in the following processes: production of recombinant vaccines, antigens, antibodies, enzymes and library peptides (Kuroda *et al.*, 2001; Chen and Georgiou, 2002; Samuelson *et al.*, 2002; Rutherford and Mourez, 2006; Wang *et al.*, 2007; Kuroda and Ueda, 2010; Nishitani *et al.*, 2010; Kuroda and Ueda, 2011).

Further investigation has been done on the effect of some organic compounds produced by fungal such as histidine, cysteine, sorbitol and mannitol in their capacity of metal uptake in various conditions. This is presented in the later sections of this work.

In this work, *Penicillium simplicissimum* (fungi) and *Oedogonium sp* (algae) were used for the biosorption of heavy metals from synthetic aqueous solutions and from mine wastewater. A brief description of these species is given in the following paragraph.

2.2.4 Fungi in bioremediation

Bioremediation involves the use of plants or micro-organisms, viable or not, natural or genetically engineered to treat environments contaminated with organic molecules that are difficult to break down (xenobiotics) and to mitigate toxic heavy metals, by transforming them into substances with little or no toxicity, hence forming innocuous products (Dobson and Burgess, 2007; Li and Li, 2011).

Bioremediation is a versatile process that can be applied *in-situ*, at the contaminated site, or *ex-situ*, involving removal of contaminated material to be treated elsewhere. *In-situ* bioremediation technologies are more economical and release fewer pollutants into the environment; however, they may require longer treatment timeframes than the *ex-situ* techniques (Vidali, 2001; Tabak *et al.*, 2005; Costa *et al.*, 1991). Currently, there is wide variety of micro-organisms (bacteria, fungi, yeasts and algae) that are being studied for use in bioremediation processes, and some of these have already been employed as biosorbents of heavy metals (Roane and Pepper, 2000; Machado *et al.*, 2008; Bogacka, 2011). The main advantages of biosorption over conventional treatment methods include: low cost, high efficiency, minimization of chemical and biological sludge, selectivity to specific metals, no additional nutrient requirement, regeneration of the biosorbent, and the possibility of metal recovery (Kratochvil and Volesky, 1998). The major bioremediation studies conducted for heavy metals removal by fungal biomasses are presented in the Appendix A.

Desorption is a very important process in the success of the applicability of bioremediation for the treatment of wastewater, because it allows for the recovery of adsorbed metal ions, as well as the recycling and reuse of biomass for a new cycle of metal recovery. There is obviously great interest in the development of a procedure that enables the recovery of removed metal ions, as well as for the cellular integrity of the biosorbents to be maintained, thus allowing for their regeneration and reuse in successive cycles of sorption-desorption. This results in the simultaneous acquisition of two valuable products: treated water and low-cost recovery of metal (Aldor *et al*., 1995; Volesky, 2001; Yu and Kaewsarn, 2001).

Fungal treatment of wastes in nature has been known for centuries (Mohandrao *et al*., 1972). The ubiquitous presence of fungi has allowed acclimation to some if not most types of wastes. During the last decade, fungi have been used in the treatment of a wide variety of wastes, wastewaters, and the role of fungi in the bioremediation of various hazardous and

toxic compounds in soils and sediments has been established. Fungi have also demonstrated the ability to remove heavy metals and to degrade, in some cases mineralize, phenols, halogenated phenolic compounds, petroleum hydrocarbons, polycyclic aromatic compounds, and polychlorinated biphenyls (Sing, 2006).

Fungal cell walls can act as a cation exchanger due to their negative charge originating from the presence of different functional groups, e.g. carboxylic, phosphate, amine or sulfhydryl, in different wall components (hemicelluloses, pectin, lignin, etc.) (Fomina *et al*., 2007). The relative importance of each functional group is often difficult to resolve (Strandberg *et al*., 1981). Cell walls of fungi are rich in polysaccharides and glycoproteins such as glucans, chitin, mannans and phospho-mannans (Figure 2.6). These polymers provide abundant sources of metal binding ligands. The cell wall structures of fungi present a multi-laminate architecture where up to 90% of their dry mass consists of amino or non-amino polysaccharides (Farkas, 1980). In general, the fungal cell wall can be considered as a two-phase system consisting of a chitin skeleton framework embedded in an amorphous polysaccharide matrix (Farkas, 1980).

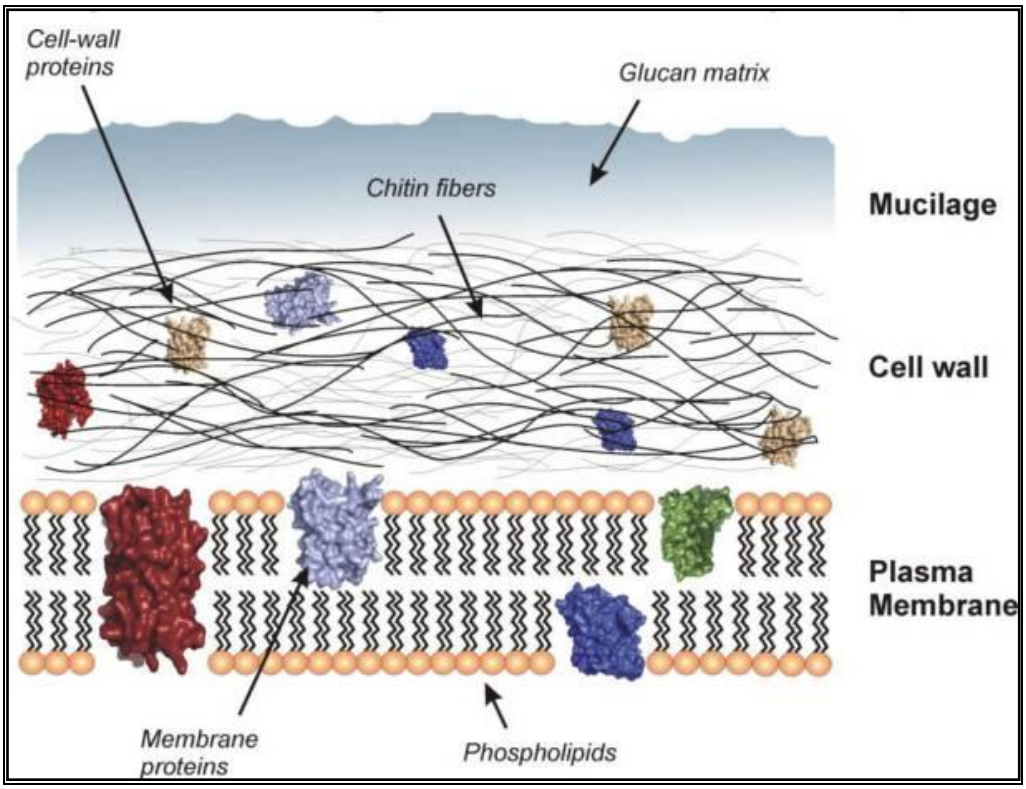


Figure 2.6 Schematic representations of the outer fungal cell layers (Farkas, 1980)

Pretreatment of fungal biomass in boiling water or with alcohols, dimethyl sulfoxide, or potassium hydroxide increased the uptake capability to about 10,000 parts per million (dry weight). Chitin, cellulose and cellulose derivatives from wall fungal interfered in metal ion uptake process (Galun *et al*., 1983).

Fungi have been harnessed by humans for several applications for thousands of years. They are well known to degrade, or cause deterioration to, a wide variety of materials and compounds, processes known as mycodegradation and mycodeterioration, respectively (Sing, 2006). Polyethylene degradation is a good example of mycodegradation. *Penicillium simplicissimum* YK is able to degrade polyethylene, with a molecular weight of 400 to 28,000 (Yamada *et al*., 2001).

Fungi are present in aquatic sediments, terrestrial habitats and water surfaces and play a significant part in natural remediation of metal and aromatic compounds. Fungi also have advantages over bacteria since fungal hyphae can penetrate contaminated soil, reaching not only heavy metals but also xenobiotic compounds. Despite of the abundance of such fungi in wastes, penicillia in particular have received little attention in bioremediation and biodegradation studies (Lúcia, 2009). Additionally, several studies conducted with different strains of imperfecta fungi, *Penicillium sp*. have demonstrated their ability to degrade different xenobiotic compounds with low co-substrate requirements, and could be potentially interesting for the development of economically feasible processes for pollutant transformation.

The ability of most fungi to produce extracellular enzymes for the assimilation of complex carbohydrates without prior hydrolysis makes possible the degradation of a wide range of pollutants. They also have the advantage of being relatively easy to grow in fermenters, thus being suited for large scale production (Leitão, 2009). Another advantage is the easy separation of fungal biomass by filtration due to its filamentous structure. In comparison to yeasts, filamentous fungi are less sensitive to variations in nutrients, aeration, pH, temperature and have a lower nucleic content in the biomass. In addition, several *Penicillium* strains have been shown to be able to live in saline environments, an advantage of these micro-organisms over the others in the bioremediation field (Leitão, 2009). *Penicillium* strains generally are halotolerant micro-organisms, able to grow either in the presence or in the absence of salt; those halotolerants that are able to grow, above approximately 15% (w/v) NaCl are considered extremely halotolerant. Hypersaline wastes are generated in several

industrial activities, such as chemical manufacture, oil and gas production and waste minimization practices (Leitão, 2009). These wastes, commonly designated as produce waters, are constituted by water containing high concentration of salts, oil, organic acids, heavy metals, and radionuclides *(*Woolard, 1995) therefore, the ability of halotolerants to remediate pollutants in the presence of salt is useful for biological treatment without damage to the physically sensitive ecosystem.

Penicillium simplicissimum

Penicillium belongs to the *phylum Ascomycota*, however its taxonomic characterization is still a matter of discussion and the difficulties in identifying most *Penicillium* species requires multidisciplinary approaches. Clarification of species concepts in the genus *Penicillium* was supported mainly by morphological characteristics. Raper and Thom (1949), for example, based *Penicillium* taxonomy classification on the combination of macroscopical (such as colony texture and colour) with micro morphological features. In spite of the fact this feature was regarded as subjective by Pitt, Stolk and Samson, the colour of the conidial mass has been pointed out to be a species-specific characteristic that varies in concomitance with distinctive morphological features (Christensen, 1994; Pitt, 1979; Stolk, 1983). Dorge proposed a method for direct identification of pure *Penicillium* species using image analysis (Dorge *et al*., 2000).

The various species of *Penicillium* can colonise many different environments. They are common in soils, in foods, in drinks and in indoor air (Banke, 1997). There are several reasons why *Penicillium* remediation of heavy metal and xenobiotics is important to researchers and practitioners. Fungi are usually slow growing and often require substrates for co-metabolism. The morphology and growth characteristics of fungi are responsible for the rapid colonization of substrates. Structural heterogeneity is considered to be one of the most important characteristics of fungal pellets. This feature depends on density of packing and affects limitation of both nutrient and oxygen (Cox *et al*., 1998).

2.2.5 Algae in bioremediation

The term algae refer to a large and diverse assemblage of organisms that contain chlorophyll and carry out oxygenic photosynthesis. Although most algae are microscopic in size and are

thus considered to be micro-organisms, several forms are macroscopic in morphology. These colonial forms of algae occur as aggregates of cells (Davis *et al*., 2003). In turn, each of these cells shares common functions and properties, including the storage products they utilize as well as the structural properties of their cell walls. The algae are included in the plant kingdom and are distinguished from other chlorophyllous plants on the basis of sexual reproduction. The differences between reproduction in the algae and that of plants is as follows: (1) in unicellular algae, the organisms themselves can function as gametes; (2) in certain multicellular algae, the gametes may be produced in special unicellular containers or gametangia; or (3) in others, the gametangia are multicellular, whereby every gametangial cell is fertile and produces a gamete (Bold and Wynne, 1985).

Marine algae (popularly known as Seaweeds) are widely distributed throughout the world. The presence of functional groups such as carboxyl, sulfate, amino and hydroxyl groups in the algal cell wall makes it an ideal biosorbent for heavy metal removal. Brown algae (Phaeophyta), green algae (Chlorophyta) and red algae (Rhodophyta) are the few important divisions of algae. When comparing these divisions on metal sequestration characteristics, Phaeophyta comprises of alginate and Chlorophyta comprises of xylans and mannans in their respective cell walls. Rhodophyta comprises galactans in addition to xylans. These characteristics are absent in vascular plants and form the basis by which the algae are studied and classified (Bold and Wynne, 1985).

Several characteristics are used to classify algae, including the nature of the chlorophyll(s), the cell wall chemistry, and flagellation. One common characteristic is that all types of algae contain chlorophyll a. However, the presence of phytopigments other than chlorophyll a is characteristic of a particular algal division. The nature of the reserve polymer synthesized as a result of photosynthesis is also a key variable used in algal classification (Davis *et al*., 2003). It is important to point out, however, that there have been many classification schemes employed to date and the following discussion is based on the work of Bold and Wynne (1985). Accordingly, their divisions include Cyanophyta, Prochlorophyta, Phaeophyta, Chlorophyta, Charophyta, Euglenophyta, Chrysophyta, Pyrrhophyta, Cryptophyta and Rhodophyta.

Biosorption in algae has mainly been attributed to the cell wall properties where both electrostatic attraction and complexation can play a role. Cryptophyta, for example, does not

have a cell wall (Lee, 1989). Pyrrhophyta (dinoflagellates) can be ‘‘naked’’ or protected by cellulosic ‘‘thecal’’ plates (Bold and Wynne, 1985; Lee, 1989). The Chrysophyceae of the division Chrysophyta can be either ‘‘naked’’ or have scales, cellulosic walls or a cell envelope (Lee, 1989). None of these types of algae perform very well as heavy metal biosorbents. The Appendix B gives a summary of bioremediation studies conducted for heavy metals removal by algal biomasses.

Typical algal cell walls of Phaeophyta, Rhodophyta, and many Chlorophyta are comprised of a fibrillar skeleton and an amorphous embedding matrix. The most common fibrillar skeleton material is cellulose (Figure 2.7). It can be replaced by xylan in the Chlorophyta and Rhodophyta in addition to mannan in the Chlorophyta.

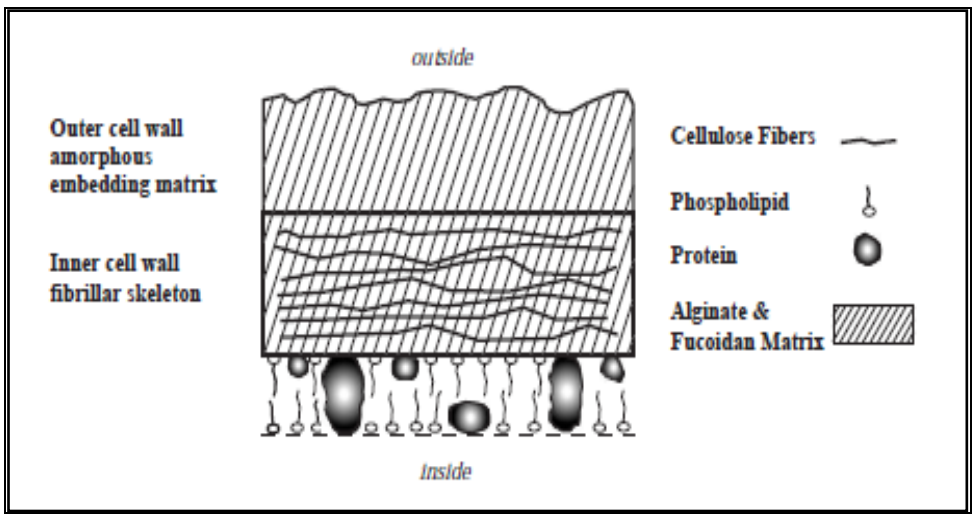


Figure 2.7 Cell wall structures in the brown algae (After Schiewer and Volesky, 2000)

The Phaeophyta algal embedding matrix is predominately alginic acid or alginate (the salt of alginic acid, Figure 2.8) with a smaller amount of sulfated polysaccharide (fucoidan); whereas the Rhodophyta contains a number of sulfated galactans (e.g. agar, porphyran, etc.) (Davis *et al*., 2003).

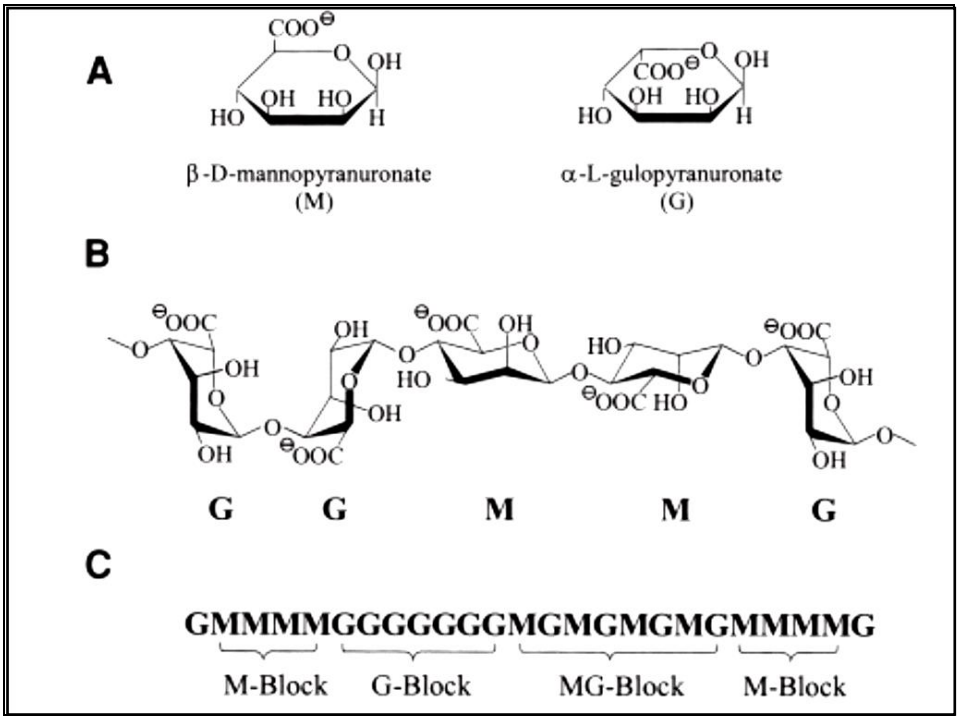


Figure 2.8 Alginate structural data: (A) alginate monomers (M versus G); (B) the alginate polymer; (C) chain sequences of the alginate polymer (After Smidsrød and Draget, 1996)

Both the Phaeophyta and Rhodophyta divisions contain the largest amount of amorphous embedding matrix polysaccharides. This characteristic, combined with their well known ability to bind metals, makes them potentially excellent heavy metal biosorbents (Mackie and Preston, 1974).

Extracellular polysaccharides

- ***Alginic acid***

Alginic acid may be present in both the cell wall matrix and in the mucilage or intercellular material and can constitute between 10% and 40% of the dry weight (untreated) of the algae (Percival and McDowell, 1967). Its abundance is dependent on the depth at which the algae are grown and it also displays seasonal variations (Mackie and Preston, 1974).

Alginic acid or alginate, the salt of alginic acid, is the common name given to a family of linear polysaccharides containing 1,4-linked β-D-mannuronic (M) and α-L-guluronic (G) acid residues arranged in a non-regular, blockwise order along the chain (Figure 2.5a-c) (Haug *et al*., 1966). The residues typically occur as (–M–)n, (–G–)n, and (–MG–)n sequences or

blocks. The carboxylic acid dissociation constants of M and G have been determined as pKa = 3.38 and pKa ¼ 3:65; respectively, with similar pKa values for the polymers (Haug, 1961), where:

pKa = - log Ka and Ka = $[-COO^-][H^+]/[-COOH]$

The salts of alginic acid with monovalent ions (alkali metals and ammonium) are soluble, whereas those with divalent or polyvalent metal ions (except Mg^{2+}) and the acid itself are insoluble (Percival and McDowell, 1967). M- and G-block sequences display significantly different structures and their proportions in the alginate determine the physical properties and reactivity of the polysaccharide (Haug *et al*., 1967). Polymannuronic acid is a flat ribbon-like chain; its molecular repeat is 10.35Å and it contains two diequatorially (1e → 4e) linked β-D-mannuronic acid residues in the chair conformation. In contrast, polyguluronic acid contains two diaxially (1a-4a) linked α-L-guluronic acid residues in the chair form which produces a rod-like polymer with a molecular repeat of 8.7 Å (Atkins *et al*, 1973). This key difference in molecular conformation between the two homopolymeric blocks is believed to be chiefly responsible for the variable affinity of alginates for heavy metals (Atkins *et al*., 1973).

- ***Alginate metal affinity and binding***

In the previous sections we have seen that not only is the polymer conformation of the two block residues (M and G) in alginate different, but also that the proportion of these two constituents changes depending on the genus of the algae and from which part of the plant the polysaccharide is extracted. Furthermore, variations in M:G ratio exist from species to species (Haug *et al*., 1974). Variation in the affinity of some divalent metals to alginates with different M:G ratio was demonstrated early on by Haug, 1974. He showed that the affinity of alginates for divalent cations such as Pb^{2+}, Cu^{2+}, Cd^{2+}, Zn^{2+}, Ca^{2+}, etc. increased with the guluronic acid content. The selectivity coefficients for the ion-exchange reaction between sodium and divalent metals were determined for two alginates (Haug *et al*., 1965) and confirmed the higher affinity of guluronic acid rich alginates for divalent metals.

The higher specificity of polyguluronic acid residues for divalent metals is explained by its ‘‘zigzag’’ structure which can accommodate the Ca^{2+} (and other divalent cations) ion more easily. The alginates are thought to adopt an ordered solution network, through inter-chain

dimerization of the polyguluronic sequences in the presence of calcium or other divalent cations of similar size (Figure 2.9). The rod-like shape of the poly-l-guluronic sections results in an alignment of two chain sections yielding an array of coordination sites, with cavities suitable for calcium and other divalent cations because they are lined with the carboxylate and other oxygen atoms of G residues. This description is known as the ‘‘egg-box’’ model (Morris *et al*., 1980; Rees, 1981).

The regions of dimerization are terminated by chain sequences of polymannuronic acid residues. As a result, several different chains may become interconnected and this promotes gel network formation. The viscosity depends on the degree of linkage, the higher the degree of linkage, the greater the resulting viscosity. The higher specificity of polyguluronic acid residues for divalent metals is explained by its ‘‘zigzag’’ structure which can accommodate the Ca^{2+} (and other divalent cations) ion more easily (Davis *et al*., 2003). The alginates are thought to adopt an ordered solution network, through inter-chain dimerization of the polyguluronic sequences in the presence of calcium or other divalent cations of similar size (Figure 2.9).

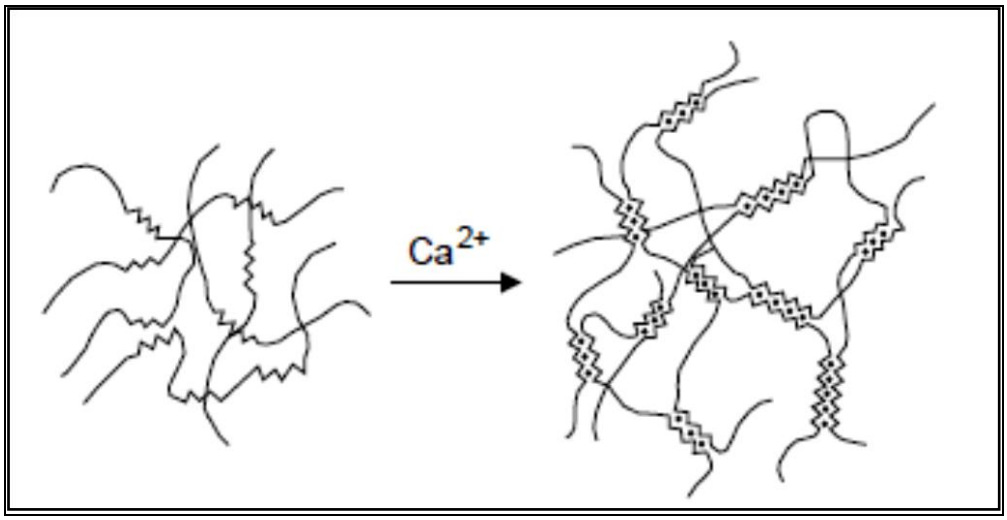


Figure 2.9 Schematic representation of the calcium-induced gelation of alginate in accordance with the ‘‘egg-box’’ structure (Christensen *et al*., 1990)

- ***Mechanisms of biosorption by algae***

I. Ion-exchange

It should be pointed out that the term ion-exchange does not explicitly identify the binding mechanism, rather it is used here as an umbrella term to describe the experimental observations. The precise binding mechanism (s) may range from physical (i.e. electrostatic or London-van der Waals forces) to chemical binding (i.e. ionic and covalent) (Myklestad, 1968).

II. Complexation

The preferential binding of heavier ions is explained by the stereochemical effects, since larger ions might better fit a binding site with two distant functional groups (Haug and Smidsrød, 1965). The ‘‘egg-box’’ model, in addition to other models with more accurate steric arrangements have been supported by X-ray diffraction (Mackie *et al*., 1983) and NMR spectroscopic analyses (Steginsky, 1992). Accordingly, metal sequestration can be viewed as the complexation (or coordination) of a central heavy metal to a multidentate ligand, the alginate. Regions of the alginate polymer rich in ‘G’ residues (G-blocks), which display a higher selectivity for divalent metal ions, provide a multi-dentate environment for complexation whereas in regions rich in mannuronic acid complexation would be predominantly monodentate and therefore weaker. More specifically, the key appears to be the orientation of the oxygen atoms with respect to $–COO^-$. In guluronic acid the ring oxygen and the axial O-1 form a spatially favourable environment with $–COO^-$, as opposed to the equatorial O-1 which occurs in mannuronic acid residues (Paskins *et al*., 1976).

***Oedogonium* sp.**

Oedogonium is a genus of filamentous green algae; filamentous means the colony is one cell thick. The green algae are the large group of algae from which the embryophytes (higher plants) emerged (Palmer *et al*., 2004). As such, they form a paraphyletic group, although the group including both green algae and embryophytes is monophyletic (and often just known as kingdom Plantae). The green algae include unicellular and colonial flagellates, most with two flagella per cell, as well as various colonial, coccoid, and filamentous forms, and macroscopic seaweeds. There are about 6,000 species of green algae (Thomas, 2002). Many

species live most of their lives as single cells, while other species form colonies, coenobia, long filaments, or highly differentiated macroscopic seaweeds.

All green algae have mitochondria with flat cristae. When present, flagella are typically anchored by a cross-shaped system of microtubules and fibrous strands, but these are absent among the higher plants and charophytes, which instead have a 'raft' of microtubules, the spline. Flagella are used to move the organism. Green algae usually have cell walls containing cellulose, and undergo open mitosis without centrioles (Hoek van den *et al*., 1995).

- ***Classification***

The taxonomy of the green algae, *Oedogonium* sp. is as follow (Guiry, 2009):

Super kingdom: *Eukaryotae*
Kingdom: *Plantae*
Subkingdom: *Viridiplantae*
Phylum: *Chlorophyta*
Subphylum: *Tetraphytina*
Class: *Chlorophyceae*
Order: *Oedogoniales*
Family: *Oedogoniaceae*

- ***Description***

The green algae *Oedogonium sp.* is an unbranched uniseriate filaments attached to substratum by basal holdfast cells, occasionally free-floating. They are filamentous green alga with cylindrical cells, which can form dense mats of coiled filaments. The vegetative cells are generally uniform in size and shape in each species; usually cylindrical, but sometimes undulate, nodulate, or even angulate in profile view; all cells in filament normally capable of division (Lopez-Bautista, 2011). They are uninucleate, highly vacuolate, and with a large reticulate, parietal chloroplast containing one to many (usually) pyrenoids. Pyrenoid matrix penetrated by numerous, branched, cytoplasmic channels. The shapes of basal holdfast cell and apical cell are often distinctive. They are abundant, renewable non-toxic algae which

could be obtained very economically on a large scale locally from a near by pond, ditches and other pools of water (Gupta and Rastogi, 2008).

Oedogonium prefers phanerogamic macrophytes, littoral zones and soft water rich in humic compounds and iron. In such conditions a relatively high number of species can cohabit without any indication of competition and with more or less synchronic reproduction (Cambra and Aboal, 1992). *Oedogonium* reproduces in two ways: sexually and asexually.
The cell walls of the *Oedogonium* consist of an inner cellulose membrane with a peripheral investvent of amyloid. Wurdack (1923) finds the cellulose inner layer to be bound eternally by a zone of pectose which is covered in turn by chitin. Recent unpublished work seems to confirm both the cellulose and the pectic compounds.

The plant cell wall is composed of polysaccharides and proteins. In addition, some cells have walls impregnated with lignin. In all cases, the polysaccharides constitute the major part of the wall. The wall polysaccharides are often classified into cellulose, hemicelluloses, and pectin and these three types are represented in almost all cell walls in varying proportions (Tiffany, 1936).

Cellulose is the main load-bearing structure and is composed of b-1, 4-linked glucan chains organized in more or less crystalline microfibrils. Hemicelluloses include several different polymers, chiefly xylans, xyloglucans, and (gluco) mannans, which are characterized by having a backbone of b-1, 4-linked sugars with an equatorial linkage configuration (Scheller and Ulvskov, 2010). Pectin is the third group of polysaccharides, characterized by relatively high extractability using acid or chelators and a high content of GalUA. Together, the hemicelluloses and pectins constitute the matrix in which cellulose microfibrils are embedded. The interactions between the different polysaccharides ensure the strong yet dynamic and flexible properties of the cell wall (Harholt, 2010).

Microbial remediation has several advantages and disadvantages. Some of the advantages are:

- It uses relatively low-cost, low-technology techniques, hence requires moderate capital investment. When compared to other remediation processes, it is fairly inexpensive.

- Since it is a natural process, it is environmentally safe, hence usually perceived by the public as an acceptable treatment process.
- It does not generate waste
- It is self-sustaining since the microbes are able to degrade the contaminant increase and decreases when the contaminant is degraded.
- The residues for the treatment are usually harmLess products and include carbon dioxide, water, and cell biomass.
- It can be used alongside other technologies.
- It can be carried out on site, often without causing a major disruption of normal activities.

Some of the disadvantages are:

- It is not always suitable, however, as the range of contaminants on which it is effective is limited, the time scales involved are relatively long, and the residual contaminant levels achievable may not always be appropriate.
- Bioremediation is limited to those compounds that are biodegradable. Not all compounds are susceptible to rapid and complete degradation.
- There are some concerns that the products of biodegradation may be more persistent or toxic than the parent compound.
- Biological processes are often highly specific, since success is dependent on the presence of metabolically capable microbial populations, suitable environmental growth conditions, and appropriate levels of nutrients and contaminants.
- It is difficult to extrapolate from bench and pilot-scale studies to full-scale field operations, for research is needed to develop and engineer bioremediation technologies that are appropriate for sites with complex mixtures of contaminants that are not evenly dispersed in the environment.
- Although the methodologies employed are not technically complex, considerable experience and expertise may be required to design and implement a successful bioremediation program, due to the need to thoroughly assess a site for suitability and to optimize conditions to achieve a satisfactory result, (Viladi, 2001; Humar and Pohleven, 2006; Golden Environmental Services, 2007).

As already indicated in Chapter 1, the most common methods of remediation used in the Witwatersrand Basin goldfields are chemical precipitation (liming) and, to a lesser extent, phytoremediation. There are no known applications of adsorbents such as zeolite and bentonite, while the use of microbial techniques has been limited to leaching for recovery of gold. As such, wide-scale application of these methods is still open for exploitation in the basin. This study, as highlighted earlier, explores the potential of a biofunctionalised system of zeolite/bentonite (using fungi and algae) as an adsorbent for the removal of heavy metals from gold mine wastewaters. This way, the study aims to bridge the gap created by the commonly used world-wide approaches in which these adsorbents are used as single systems. The proposed tandem intends to take advantage of the efficacies of each of those adsorbents in creating a biofunctionalised system that performs better than its individual components.

As noted earlier, there are abundant resources of zeolite and bentonite in South Africa. This, combined with the ubiquity of fungal and algal biomass in gold mining environments, makes the study potentially viable and cost-effective.

Chapter 3: Materials and methods

This chapter describes in detail the research approach, namely: modification of zeolite/bentonite with proxy-compounds (histidine, cysteine, mannitol and sorbitol); immobilisation of *Penicillium simplicissimum* on zeolite/bentonite; extraction of alginates from fresh algae as well as synthesis of the alginate complex impregnated with zeolite. The collection of green algae and mine water samples is also described. The methods used for the characterisation of the biosorbents as well as the experimental protocol followed for adsorption and desorption studies (in batch and column modes) are detailed. The methodology used in this work comprises two studies, namely:

- A comparative study: looking at differences and similarities, in terms of adsorption processes, between natural and modified zeolite/bentonite.
- A manipulative study: varying set point conditions and establishing their effect on the adsorption efficiencies.

It should be noted here that the notation zeolite/bentonite has been adopted and means a zeolite system and a bentonite system and not a system consisting of both zeolite and bentonite as one entity. Thus, natural zeolite/bentonite means a system of natural zeolite and another of natural bentonite while zeolite/bentonite-proxy compound means a system of zeolite modified with a proxy compound and another system of bentonite modified with a proxy compound.

3.1 Field studies

The sampling of green algae and mining water was done in two mining sites: the West Wits (WW) operations and the Central Rand gold field, respectively.

3.1.1 Collecting materials (algae samples)

The Mponeng, Savuka and TauTona mines are situated on the West Wits Line and are part of the West Wits (WW) operations (AGA, 2008). These mines are located approximately 75 km west of Johannesburg within the Gauteng Province in South Africa (Figure 3.1).

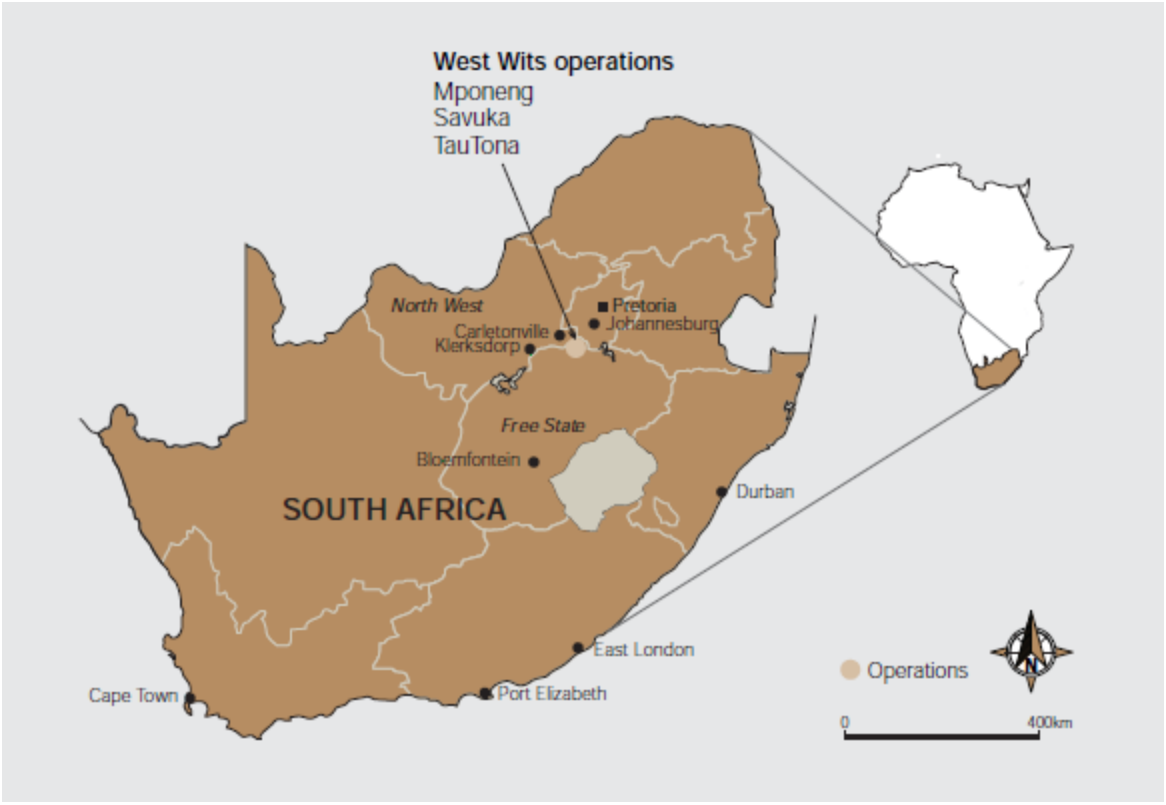


Figure 3.1 West Wits operations in the regional context (AGA, 2008b)

The algal strains used in this study were collected from the West Boundary Dam pond (26^{o} 34.693'S, 27^{o}34.694'E) (mat-forming alga) and the Varkenslaagte stream (26^{o} 34.693'S, 27^{o}34.694'E) (filamentous green alga) (Figures 3.2 and 3.3), located in the WW operations. The fresh algae from water bodies was harvested in plastic bags and kept in the deep freezer (-20^{o}C). In addition, water samples were also collected from the dams and the stream for metals analysis. The identification of the fresh algae was carried out in the School of Animal, Plant and Environmental Sciences, University of the Witwatersrand.



Figure 3.2 Mat- forming algae in the West Boundary Dam



Figure 3.3 Filamentous green algae in the Varkenslaagte stream

3.1.2 Collecting water samples

The developed biosorbents were applied for the removal of metal ions from mine water samples collected in the vicinity of gold mining activities in the Central Rand goldfield, Johannesburg. The Natalspruit (Figure 3.4) was selected for this study because its headwaters lie in an area in which gold tailings dumps abound. The stream is also impacted by leachates from abandoned tailings footprints.

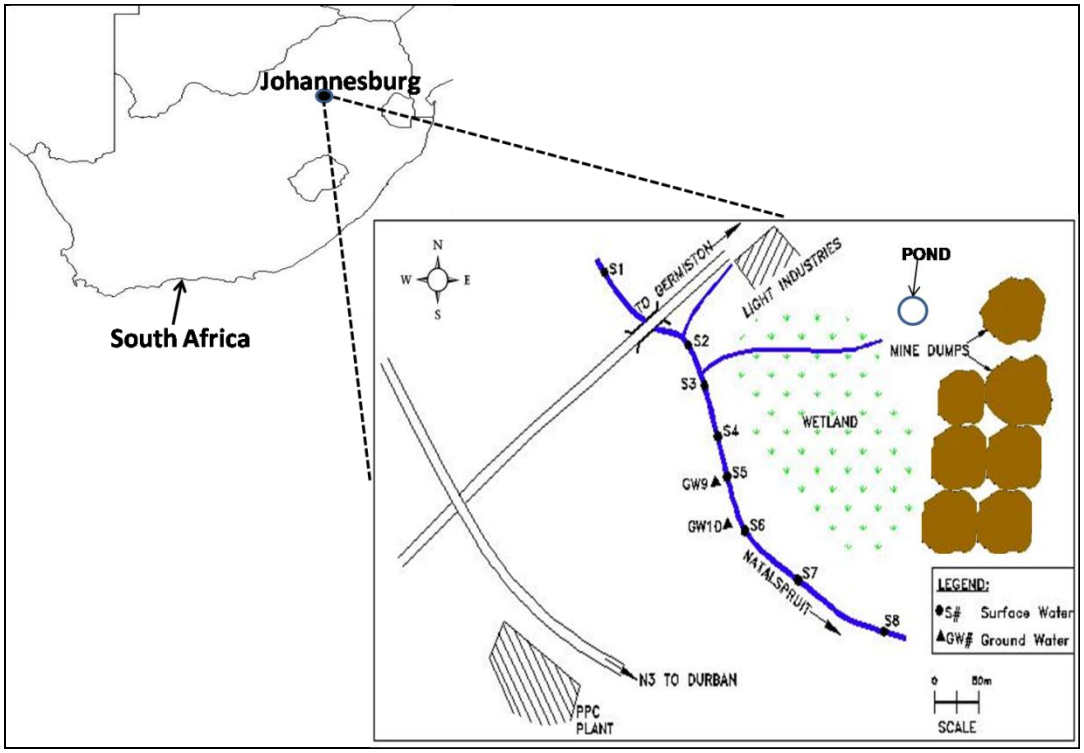


Figure 3.4 Map of study area and sampling points

Sampling was carried out along the Natalspruit, adjacent and downstream to the mining area. Five samples (one pit water and four surface water samples, S1 –S4) were collected using polypropylene containers according to commonly accepted sampling protocols (Hermond and Fechner-Levy 2000; Mugo and Orians, 1983). It should be noted that the other sampling points were not used in this study, but only in another study (Bakatula *et al.*, 2012).

The geochemical parameters (pH, redox potential and electrical conductivity) were recorded in the field using field meters. The field measurements were carried out with a portable kit Multi Line F/Set 3 of the Wissenschaftlich- Technische Werkstatten, Weilheim (WTW, Germany) equipped with a pH electrode, an integrated temperature probe (Sen Tix 41), a standard conductively cell (Tetra Con 375) and an oxidation-reduction potential probe (Sen Tix ORP). The pH electrode was calibrated according to IUPAC recommendations against two buffer solutions pH 4.0 and pH 7.0. Redox potentials were obtained from Pt electrodes versus Ag/AgCl. The electrodes were checked using a standard buffer solution and all reported potentials were corrected relative to the standard hydrogen electrode (SHE).

The samples were filtered in the laboratory prior to application in the adsorption experiments.

3.2 Laboratory investigations

3.2.1 Biomaterials development

3.2.1.1 Natural zeolite/bentonite

Natural zeolite

The natural zeolite used as adsorbent in this study, white fine powder (particle size < 2 mm) was supplied by Sigma-Aldrich (Pty.) Ltd. South Africa. No treatment has been performed prior to experiments.

Natural Bentonite

The natural bentonite used as adsorbent in the present study, a grey fine powder (particle size < 2 mm), was supplied by Sigma-Aldrich (Pty.) Ltd. South Africa. The adsorbent was oven dried for 24 h at 60^{o} C before the experiments.

3.2.1.2 Modification of zeolite/bentonite with the proxy-compounds

The proxy compounds released by *Penicillium simplicissimum* were used individually to modify zeolite as well as bentonite for the adsorption of heavy metals. These include: histidine, cysteine, sorbitol and mannitol. Alginate, an algal polysaccharide was immobilised on zeolite and the following sub-sections give detailed procedures for the modification process using the above-mentioned compounds.

Zeolite/Bentonite-L-Histidine

For the zeolite/bentonite-histidine adsorbent, 10.0 g of natural zeolite/bentonite interacted at 60^{o}C for 48 h at pH 8 with 100 mL of solution containing 1.55 g of L-Histidine hydrochloride. Then, the synthesized sorbent was washed several times with de-ionized water to remove the possible unreacted L-Histidine. The biosorbent was re-suspended in de-ionized water, stirred for about 1 hour at room temperature and separated by filtration. The suspension was dried in the oven for 24 h at 60^{o}C. L-Histidine was analysed before and after reaction to determine the exact amount that was adsorbed onto the support system e.g. bentonite. All dried samples were pulverised to fine particles and stored prior to subsequent studies.

Zeolite/Bentonite-cysteine

Natural bentonite (10 g) was suspended in a 100 mM solution of cysteine hydrochloride monohydrate (8.778 g L^{-1}) for which the pH had previously been adjusted to 4.0 with HNO_3 or NaOH. The obtained suspension was stirred at room temperature for 12 h. The solid phase (Zeol-Cyst/Ben-Cyst) was separated by centrifugation, washed with de-ionised water several times and then dried at room temperature. The dried sorbent was pulverised to fine particles and stored prior to subsequent studies.

Zeolite/Bentonite-sorbitol

Natural bentonite (10 g) was suspended in a 100 mM solution of sorbitol (18.217g L^{-1}) at pH = 7. The obtained suspension was stirred at room temperature for 12 h. The solid phase (Zeol-Sorb/Ben-Sorb) was separated by centrifugation, washed with de-ionised water several times and then dried in the oven at 60^{o}C and stored prior to subsequent studies.

Zeolite/Bentonite-Mannitol

Mannitol being an isomer of sorbitol, the same procedure (described above) was followed as for the zeolite/bentonite-sorbitol.

3.2.1.3 Preparation of Zeolite/Bentonite-Penicillium simplicissimum

A strain of commercially-available *Penicillium simplicissimum* was used for the synthesis of zeolite/bentonite-*Penicillium simplicissimum.* The same species grows in the gold tailings dams and may be used for the bioremediation of heavy metals.
The P*enicillium simplicissimum* was grown in a basal medium prepared as follows:

i) Preparation of basal medium in 1 L

- $(NH_4)_2SO_4$: 1.15 g
- KCl : 0.67 g
- $MgSO_4.7H_2O$: 0.5 g
- Fe-EDTA : 5 mg
- $ZnSO_4.7H_2O$: 4.4 mg
- $CaCl_2.2H_2O$: 44.5 mg
- Inorganic K_2HPO_4 (100 mg L^{-1} phosphorous) : 0.56 g

- Yeast extract : 50 mg
- Glucose : 10 g
- The pH was recorded
- The mixture was placed on a magnetic stirrer and heated to allow the contents to dissolve, and the pH was recorded
- The mixture was autoclaved at 121^{o}C at 1000 Pa for 15 minutes and the pH was adjusted between 4 and 7 using dilute HCl or NaOH
- The mixture was then distributed in 20 mL aliquots into 50 Schott bottles (making up 100 mL).
- Zeolite (1.0 g) was then added into the Schott bottles containing the medium

All chemicals used were from Merck Ltd (South Africa).

ii) Preparation of homogenate

Penicillium simplicissimum (originally isolated from gold mine tailings) was obtained from the School of School of Molecular and Cell Biology**.** The strain was maintained on the following solid media: 39 g L^{-1} Potato Dextrose Agar (PDA) and 50 g L^{-1} Malt Extract Agar (MEA) and stored at 4^{o}C. A homogenate was prepared using 0.05% of Tween 80. Tween is a diluent, essentially a hydrocarbon compound. For experimental purposes, the pH of the basal medium (prepared as indicated above) was adjusted between pH 4 and 7 using 1 mol L^{-1}NaOH or 1 mol L^{-1} HCl.

iii) Spore inoculum preparation

Homogenate was inoculated under a sterilised laminar flux into the Schott bottles containing 20 mL of autoclaved medium broth and 2.5 g of bentonite/zeolite. Two drops of homogenate were used. The fungus was cultivated on a rotary shaker at 120 rpm and 25^{o}C for 1 to 20 days. The harvested biomass was separated from the broth by filtration and washed with de-ionised water and then oven-dried at 60^{o}C for 24 h. The mass of the harvest was recorded and plotted on a growth curve versus the number of days. The experiments were done in triplicate.

iv) Fungal biomass preparation

For experimental purposes, 2 drops of *Penicillium simplicissimum* homogenate were inoculated in a 250 mL conical flask containing 100 mL of growth medium at pH 4 and 20 g of zeolite/bentonite. Incubation was performed on a rotary shaker at 120 rpm and 25^{o}C. The biomass was harvested after 2, 5, 10 and 20 days so as to further study and relate the efficiency of adsorption with growth over the number of days. The biomass was harvested by filtration and then washed thoroughly with de-ionised water to remove the excess nutrient broth. The living biomass was then used for adsorption experiments.

For the heat-killed biomass, the harvested biomass was oven-dried after washing with de-ionised water, at 60 ^{o}C for 24 h, and powdered in a mortar, then stored in a desiccator and used for the subsequent experiments.

v) Identification of Penicillium simplicissimum

The morphological identification was done as follow: a dissecting needle (2 mm length and 1 mm thick) was used to pick up a small piece of *P. simplicissimum* sporulating culture (grown on PDA at 25ºC). The material was placed on a microscope slide (76 x 26 mm, 1-1,2 mm thickness, B&C Germany) in a small drop of lactophenol-cotton blue stain, spread over the slide surface using a dissecting needle and covered with a cover slip (20 x 20 mm, Superior, Marienfeld, Germany). Spores were examined under a light microscope (Zeiss, Germany) using both the low power (10X) and high power (100X) objectives.

3.2.1.4 Preparation of algal biomass

The fresh algal was divided into two aliquots: one was unwashed and kept in the deep freezer, the other was washed with de-ionised water several times to remove dust and impurities, kept on a filter paper to reduce the water content and freeze-dried (in a Labconco freeze-dryer). A portion of biomass was dried in an oven at 50°C until constant weight, the water content or moisture of the algae was determined followed by the metals analysis.

With a view to enhance metal sorption capacity of the biomass, it was subjected to various pre-treatment, such as, with 0.1 mM CH_3COOH glacial, 0.1 mM $H_2C_2O_4$ 99.99%. Many of these chemicals are inexpensive and readily available, and have been tried with other biomass types for enhancing their metal sorption potential (Mehta and Gaur, 2005). For pre-treatment,

the fresh algal biomass was suspended in 10 mL of the treating agent for 1h at 25±2 ^{o}C, and agitated on a shaker. After various treatments, the algal biomass was separated and washed with Milli-Q water till the pH of the washings reached neutrality. For biosorption experiments, washed samples were freeze-dried and the biomasses ground with a mortar and sieved to select particles between 2–3mm in size for use.

3.2.1.5 Isolation of alginates from Oedogonium sp.

Alginates were extracted from the bulk samples of dried *Oedogonium* sp. according to the protocol described by Rosel and Srivastava (1984). The ground algal material (1 to 2 g) was extracted three times in 0.1 M HCl (50 mL) for 30 min at room temperature. The residue was allowed to settle and the acid removed by aspiration. Alginate was extracted from the residue by 2% Na_2CO_3 (50 mL) for 90 min at room temperature. The extraction was repeated twice. The extracts were centrifuged at 1200 rpm for 20 min at room temperature. The supernatants from the three extractions were pooled. If necessary, the pooled supernatants were neutralised with 0.5 M HCl for overnight storage and alginic acid was precipitated by lowering the pH to 1.8–2.0 using 0.5 M HCl. After standing for 20-30 min, the precipitate was separated by filtration through two layers of mesh. The precipitated alginic acid was washed with 0.5 M HCl (400 mL) and then with cold distilled water (4 x 400 mL). The alginic acid was suspended in distilled water and the pH adjusted to pH 7 with 0.5 M NaOH. The resulting sodium alginate solution was freeze-dried, and weighed.

The alginate yields of *Oedogonium* sp. (in weight percent) was defined as:

$$\text{Yield}(\%) = \frac{dried\ mass\ of\ final\ alginate\ product}{dried\ algal\ mass\ before\ acid\ extraction} \text{ x } 100 \qquad (3.1)$$

3.2.1.6 Preparation of alginate complex beads

The synthesis of the alginate complex was as follows (Chmielewska *et al*., 2011): sodium alginate solution 1% was prepared by dissolving and gentle warming 1 g of solid alginate salt in 100 mL of distilled water. This was mixed with 2 g of natural zeolite powder for a time interval of 1 hour. The resultant liquid suspension was then dropped through the tip of a 1 mL pipette into 500 mL of 0.1 M $CaCl_2$ solution, which caused the immediate formation of insoluble gel beads about 3 mm in diameter. The beads were allowed to cure in mother solution overnight, and then washed thoroughly with distilled water (about 3 h) to remove the

excess of chlorides. The beads were left in the laboratory to dry on filter paper to soak up the external water content or were dried for 2 h in a drying oven at 60ºC (Choi *et al.*, 2009; Li and Li, 2011). However, the weights between the slow and fast oven-drying procedures differed by approximately 20-fold, due to water content differences. It must be pointed out that, in all measurements, the weight of the prepared biosorbent was calculated on the basis of the oven-dried mass (external water minimized while simultaneously maintaining the original structure). The sodium alginate, natural zeolite and calcium chloride used were obtained from Sigma Aldrich (South Africa).

3.2.2 Characterisation of the raw materials and the developed biosorbents

3.2.2.1 Physical properties

1. Zeolite/Bentonite identity

X-ray diffraction (XRD) analysis was performed on natural zeolite/bentonite samples to verify the mineral identity. The analysis was carried out with Bruker D2 Phaser (Karlsruhe, Germany) Diffractometer using Ni-filtered Cu Kα radiation. Then the basal spacing of each sample was calculated using Bragg's law:

$$2d\sin\theta = n\lambda \tag{3.2}$$

Where d is the basal spacing (Å), θ the angle of diffraction (^{o}), λ the wavelength (nm), and n is the path differences between the reflected waves which equals an integral number of wavelengths (λ).

2. Porosity characterisation

The specific surface area and pore size distribution analysis of natural as well as modified zeolite/bentonite were determined by BET analysis.

0.2 g of samples were degassed in N_2 at 400 °C for 4 hours prior to analysis using a Micromeritics Flow Prep 060, sample degas system. The surface areas and pore size distributions were then obtained at -196 °C. The pore size distribution and specific surface areas of the samples were determined via N_2 adsorption/desorption according to the BET method using a Micromeritics Tristar surface area and porosity analyzer. In order to confirm

the accuracy of the results, the analysis was repeated three times for all samples and the measurements were in good agreement.

3. Thermal properties

The thermogravimetric analysis (TGA) measures the weight change of the material as a function of temperature and time in a controlled environment (Dinger, 2005). The increase, decrease, or constancy of mass of samples at each temperature in the firing program indicates the presence or absence of reactions and the nature of each reaction that takes place. The thermal stability of natural zeolite/bentonite was assessed with thermogravimetric analysis (TGA) carried out on a Perkin-Elmer Diamond DTG/TDA analyser. The temperature range was from 50 to 400^{o}C at a heating rate of 10^{o}C min^{-1} under nitrogen flow rate of about 20 mL min^{-1}.

3.2.2.2 Chemical properties

1. Chemical composition

Chemical composition was determined by the X-ray Fluorescence analysis in the School of Geosciences at Wits University. Elemental percentages of mainly Si, Al, Fe, Na, K, Ca and Mg were determined by means of this analysis. As a result of XRF analysis, chemical composition of zeolite/bentonite was determined and based on this composition; Si/Al ratio of zeolite/bentonite was estimated and the water content was determined.

2. Elemental analysis

The LECO CHNS-932 analyser was used to determine the amount of C, H, and N in the natural and modified zeolite/bentonite. This analysis permits to confirm the modification of the natural sorbent with compounds as histidine, cysteine, mannitol and sorbitol. In this case, 2 mg of sorbent was placed in a silver capsule and heated in the furnace where it was completely combusted at 1000°C. This instrument relies on infrared detection to measure the weight percent of carbon, hydrogen, and sulphur, while nitrogen was measured using thermal conductivity detection. A certified reference material was used for calibration and the results are given in Table 3.1 below. The data processing was simply performed by the software incorporated in the instrument and the results are given in percentage of carbon, nitrogen and hydrogen.

Table 3.1 CHNS calibration results with corn gluten (Leco)

	% C	% H	% N	% S
Certified value	52.29 ± 0.39	7.13 ± 0.07	11.35 ± 0.07	0.933 ± 0.04
Calibration	52.28 ± 0.22	7.26 ± 0.16	11.21 ± 0.09	1.076 ± 0.11

3. Cationic exchange capacity (CEC)

The cationic exchange capacity (CEC) was determined by the $BaCl_2$ Compulsive Exchange Method (Gillman and Sumpter, 1986). The CEC of a clay mineral is simply a measure of the quantity of sites on the clay surface that can retain positively-charged ions (cations) by electrostatic forces. Cations retained electrostatically are easily exchangeable with other cations in the solution and are thus readily available. It is also an index of the clay activity and mineralogy, which is important for calculating mineralization rates, leaching rates and interaction with pollutants.

In the procedure of determining CEC (Allen *et al*., 1974), the cations particularly Na^+, K^+, Ca^{2+} and Mg^{2+} are displaced from the exchange sites on the material colloids and replaced by a cation from the extractant. After the washing stage, the adsorbed cation is then displaced by a leaching solution in which it is subsequently determined. Almost all procedures in use for CEC have this sequence.

Two different, but numerically equivalent, sets of units can be used: meq/100 g (milliequivalents of charge per 100 g of dry material) or $cmol_c/kg$ (centimoles of charge per kilogram of dry material).

4. Surface charge characterisation

The surface cgarge was determined using the Zeta potential measurements measurements on natural and modified zeolite/bentonite were conducted on a Malvern Zetasizer Nano ZS model. The zeta potential was measured as a function of pH and the isoelectric point (point of zero charge pH_{PZC}) was determined. 0.1 wt% material suspensions were dissolved in hexane and pH adjustments made using HCl or NaOH. After the pH stabilized, the required amount of these solutions was transferred to the measuring cell and about 3 values of zeta potential were measured at room temperature.

5. Verification of surface property modification

Fourier Transform Infra-red (FTIR) analysis was performed to determine the different functional groups on the surface and to verify the functionalization of natural zeolite/bentonite. FTIR spectra were measured directly from natural and modified zeolite/bentonite using a Tensor 27 (Bruker, Germany) device in the range of 4 000 to 400 cm^{-1}.

6. ***Composition of the extracted alginates***

^{1}H-NMR Spectroscopy was used to determine the composition of the alginates extracted from the algal biomass collected in the gold mine dams.

The freeze-dried Na alginates (20 mg) were dissolved in 1 mL of deuterium oxide (D_2O, 99.9%) and analysed using a Bruker NMR Avance 500 MHz instrument. All the ^{1}H spectra were recorded without the suppression of the water signal using the purified alginate without any preliminary treatment. The Na-alginates extracted from the *Oedogonium* algae were subject to a partial hydrolysis (pH 2.85) with 0.5 M HCl for 30 min at 100^{o}C for the separation of the monomers (Abdel-Fattah and Edrees, 1972; Matsuhiro *et al*., 2007). The fraction soluble was enriched by the mannuronic acid (M) whereas the insoluble fraction constitutes the guluronic acid (G). Both fractions were dried and then dissolved with D_2O for the NMR analysis. The mole ratio of M:G ratios of the sodium alginate extracts was determined after peaks assignments using the MestRe Nova software.

3.2.3 Analytical procedures

3.2.3.1 Chemicals and reagents

Reagents used for the sorption studies were of analytical grade. Standards used for quantification were of high purity and were obtained from Sigma-Aldrich and Merck, South Africa.

3.2.3.2 Preparation of standard solutions

The synthetic metal ion solutions (Co^{2+}, Cu^{2+}, Fe^{3+}, Cr^{3+}, Hg^{2+}, Ni^{2+}, U^{6+} (as UO_2^{2+}) and Zn^{2+}) were prepared by weighing appropriate amounts of their nitrate salts: $Cu(NO_3)_2.3H_2O$, $Co(NO_3)_2.6H_2O$, $NiSO_4.7H_2O$, $Cr(NO_3)_3.9H_2O$, $Zn(NO_3)_2.6H_2O$, $UO_2(NO_3)_2.6H_2O$, $Fe(NO_3)_3.9H_2O$, $Hg(NO_3)_2.H_2O$) which were sufficiently dried to enable preparation of

standard solutions of 1000 mg L^{-1}. Appropriate aliquots were taken from these standards for subsequent dilution to the desired concentration level. A 1000 mg L^{-1} stock solution containing a mixture of each metal (multi-component solution) was also prepared in a similar way. The solutions were acidified using 1 mol L^{-1} HNO_3 to avoid the precipitation of the metals and stored in a refrigerator at 4^{o}C prior to the relevant experiments.

3.2.3.3 Metal analysis

Heavy metal (Co, Cu, Cr, Fe, Hg, Ni, Zn and U) concentrations were obtained using inductively coupled plasma-optical emission spectroscopy (ICP-OES) (Kleve, Germany) instrument with a coupled charge detection (CCD) system. The parameters in Table 3.2 were used and each element was determined at various wavelengths. The standards, supplied by Spectro at a concentration of 10 mg L^{-1} were used to make working standards of concentration 0.05, 0.1, 0.2, 0.5 and 1 mg L^{-1}. Calibration curves were then constructed after the analysis of these standards.

Table 3.2 Table of parameters of ICP-OES (Spectro, Kleve)

Parameter	Value
Plasma power	1400 W
Coolant flow	12 mL min^{-1}
Auxiliary flow	1 mL min^{-1}
Nebulizer flow	1 mL min^{-1}
Type of nebulizer	Cross-flow
Injector tube diameter	0.889 mm

The detection limit (mg L^{-1}) was: Cu – 0.001; Co – 0.002; Cr - 0.003; Fe - 0.002; Hg - 0.001; Ni - 0.007; Zn - 0.008; U - 0.035.

3.2.3.4 Sorption studies

Adsorption was done in batch mode; the column test was performed only for the natural zeolite/bentonite and zeolite/bentonite- *Penicillium simplicissimum*. The adsorption of Cu, Co, Cr, Fe, Zn, Hg, Ni and U onto natural sorbents and biosorbents was studied for single and

multi-component systems. The following parameters were assessed: effect of pH, contact time, metal concentration, temperature and mass of adsorbent.

❖ Batch experiments

In batch adsorption experiments, 1 g to 2 g of biosorbent samples were added to polypropylene containers containing 50 mL of known concentration of single or multi-component standard. The pH of the solution was adjusted by addition of dilute HNO_3 or NaOH solution.

The contents were shaken for a given period of time and temperature at 150 rpm. At equilibrium, the solutions were filtered using 0.45 μm Whatman filter paper and the equilibrium concentrations determined using ICP-OES. Data obtained from the batch adsorption tests was used to calculate the metal-binding capacity, q_e*(mg/g)* of the different sorbents using the following mass balance equation:

$$q_e = \frac{(C_o - C_t)V}{M} \tag{3.3}$$

where: q_e is the amount of metal ions adsorbed *(mg* g^{-1}*)*, C_o and C_t are metal ion concentrations in solution before and after adsorption *(mg* L^{-1}*)*, V the volume of the medium *(L)* and M the amount of the biosorbent used in the reaction mixture (g).

The distribution of coefficient, K_d *(L* mol^{-1}*)* was also calculated using the following relationship:

$$K_D = \frac{C_0 - C_e}{C_e} \cdot \frac{V}{M} \tag{3.4}$$

where: C_o and C_t are the initial and final metal ion concentration in solution *(mg* L^{-1}*)* respectively, V is the solution volume *(L)* and M is the mass of the sorbent used *(g)*.

Tests were carried out with varying conditions as follows: the effect of pH, metal concentrations, contact time, temperature and adsorbent mass.

i) Effect of pH

The influence of pH in the range of 2 to 12 was studied while the metal concentrations, shaking time and amount of sorbent were fixed at 100 mg L^{-1}, 12 h and 2.0 g, respectively. The experiments were done at room temperature. The pH of the solution was adjusted by using a dilute sodium hydroxide solution and nitric acid.

ii) Effect of metal concentration - Isotherm studies

Experiments were carried out to determine the effect of metal concentration on adsorption. The concentrations were varied at room temperature from 50 to 500 mg L^{-1} at a fixed pH (3), amount of bentonite (2.0 g) and shaking time (12 h).

iii) Effect of contact time - Kinetic studies

The adsorption of metals by different sorbents was studied as a function of time. 500 mL of solution containing 100 mg L^{-1} of metals were shaken at 150 rpm with 25.0 g of sorbent at room temperature for different intervals of time ranging from 10 min to 12 h. The pH of the metal solution was adjusted to 3. Samples (5 mL) were taken with time, the total volume drawn being < 10% of the total. This was to minimize the change in the ratio between the metal concentration and the sorbent mass (Mihaly-Cozmuta, personal communication).

iv) Effect of temperature - Thermodynamic studies

Experiments were carried out to determine the effect of temperature on metal adsorption on different sorbents. 2.0 g of adsorbents were added to 100 mL of solution containing 100 mg L^{-1} of metals. The reaction mixture was shaken in a temperature-controlled room at 291.15 K, 295.15 K, 299.15 K and 303.15 K at 150 rpm for the equilibrium time. The shaking time and pH were fixed at 12 h and 3, respectively.

v) Effect of adsorbent mass

The effect of adsorbent dosage on adsorption was examined by operating various dosages (1, 2, 5 and 10 g) applied to 50 mL of a solution containing 100 mg L^{-1} metals at 298.15 K in order to assess the effect of adsorbent dosage for metal removal. The pH and contact time were fixed at 3 and 12 h, respectively.

vi) Desorption studies on batch mode

The regeneration of the biosorbent was conducted using 0.5 M HNO_3. The mixture was agitated in 250 mL bottles at 150 rpm for 12 h using a mechanical automated shaker. The solution was then filtered using a Whatman No. 41 filter paper. The concentration of the metal ions at equilibrium in the filtrate was measured using the ICP-OES. The desorption efficiency was calculated using the following equation:

Desorption efficiency: $\frac{Amount\ of\ metal\ ions\ desorbed\ (mg/L)}{Amount\ of\ metal\ ions\ adsorbed\ (mg/L)}$ X 100 % (3.5)

❖ Column experiments

Most industrial adsorption processes are carried out in column systems. The column sorption was performed:

- To investigate the efficiency of a laboratory fixed-bed sorption column for the adsorption of Cu, Co, Cr, Hg, Fe, Ni, Zn and U in single and multi-metals aqueous solutions.
- To investigate any interactions (i.e. synergistic/antagonistic effects) when combining different metals in the same metal aqueous solution.

The fixed bed column studies were carried out in laboratory scale using glass columns of 1.5 cm diameter and 12 cm length at isothermal conditions (T = 25 ± 1^{o}C). The column was packed with adsorbent between two supporting layers of equilibrated glass wool to prevent adsorbent particles from flowing out. The schematic diagram of the column is shown in Figure 3.5 with a bed depth of 3 cm and filling weight of 5.0 g.

i) Biosorption of heavy metals in column mode

The metals solution (100 mg L^{-1} at pH 3.0) was fed through the fixed-bed column in the down flow mode, the flow rate was kept at 2 mL min^{-1}. Before the operation, the bed was rinsed with distilled water and left overnight to ensure a closely packed arrangement of particles with no void, channels, or cracks. The effluent samples were collected at specified time intervals (10 min) and measured for the remaining metal ion by ICP-OES. The flow of the column was continued until the effluent concentration (C_t) approached the influent concentration (C_o), C_t/C_o = 0.98. A peristatic pump (MASTERFLEX L/S, Heidolph 5201 (Figure 3.5)) was used to control the flow rate at inlet and outlet for providing constant flow of metal (2 mL min^{-1}) and desorbing solution in a fixed bed column.

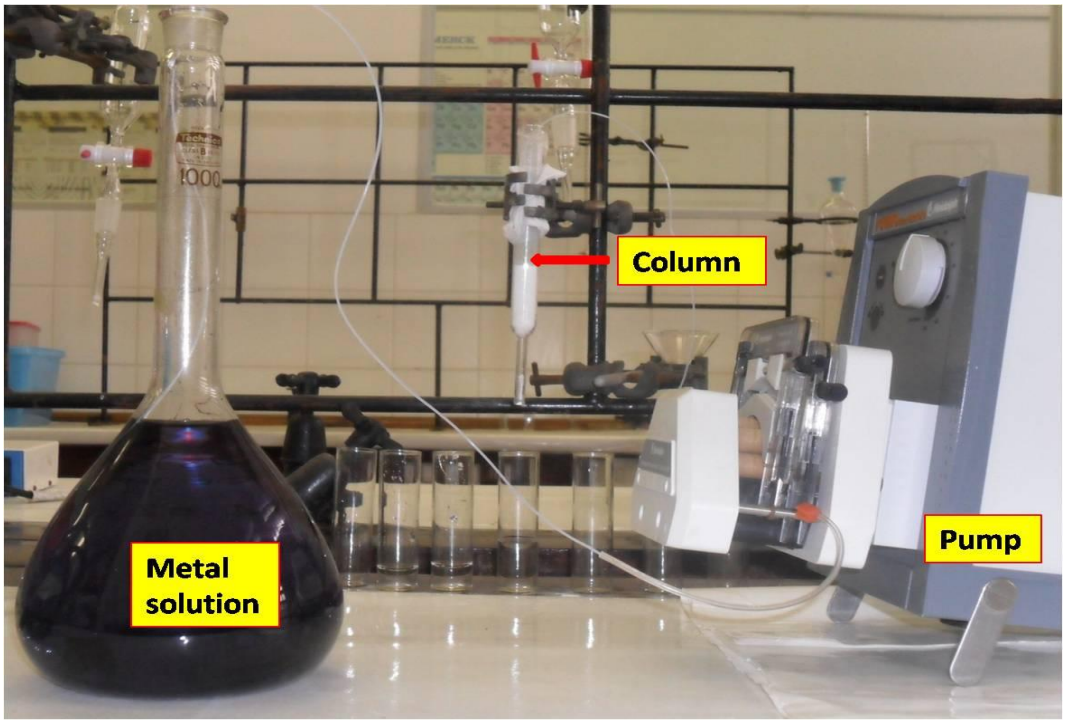


Figure 3.5 Photograph of the column experiment set-up (taken by the author)

ii) Regeneration of biosorbents in column mode

After every run, the column was regenerated using 0.5 M HNO_3 as stripping solution, which was being feed to the column in the same direction as the loading solution, down flow mode. This procedure is called co-flow regeneration. The elution stage was left to run for 90 min, and by this time, most of the ions would have been desorbed. After the stripping stage, the column was washed with de-ionised water that was also feed from the top at 4 mL/min for 10 min; after this the column was ready for use again. About 3 regeneration cycles were carried out for each experiment and the adsorption efficiencies determined.

3.2.3.5 Metal analysis in fresh algae (Oedogonium sp.)

Exact weights of each alga (500 mg dry weight) were placed into a beaker. 25 mL of concentrated analytical grade nitric acid (Merck) was added to the beaker and the contents were left at room temperature over night. The mixture was warmed for 2 h at 50^{o}C, then at 180^{o}C for 4 h. After cooling, 20 mL of de-ionized water was added to the beaker and the contents were filtered through Whatman filter paper 0.45 μm. The solutions were then

transferred to 25 mL volumetric flasks and the volumes were completed to 25 mL with de-ionised water.

The concentration of total metals was measured in the aliquots of algae using ICP-OES (Spectro, Kleve, Germany).

3.2.3.6 Biosorption studies on algal biomass

The use of *Oedogonium* sp. in the implementation of bioremediation strategies for toxic heavy metals was evaluated. The biosorption of Cu^{2+}, Co^{2+}, Fe^{2+}, Hg^{2+}, Ni^{2+}, Zn^{2+}, Cr^{3+} and UO^{2+} on the algal biomass *Oedogonium* sp. was investigated in batch experiments. The effect of pH, metals concentration (isotherms), contact time (kinetics) and temperature were studied. The procedures are described as follows:

i) Effect of pH

250 mg of dried biomass was added to 250 mL of metal ion solution of 100 mg L^{-1} concentration in single as well as in multi-components systems. The pH (2-7) was adjusted using 0.5 mol L^{-1} solution of NaOH or HNO_3, then mixture was shaken for 12h at room temperature at 150 rpm. The concentration of metal ions in the filtered supernatant solution was determined using ICP-OES (Spectro, Kleve, Germany).

ii) Effect of initial metal concentration

Adsorption isotherms were carried out at different initial concentration solution of single component as well as multi-component standard, varying from 50 to 500 mg L^{-1} while maintaining the adsorbent mass and pH at constant level. At equilibrium the solutions were filtered and the equilibrium concentrations determined using ICP-OES (Spectro, Kleve, Germany).

iii) Effect of contact time - Kinetic studies

Kinetic studies were carried out with 25 g of fresh algae/500 mL solution of 100 mg L^{-1} of metal ions. The mixture was shaken at 150 rpm at room temperature (25±2 ^{o}C) and the sampling times were 0, 10, 20, 30, 60, 90, 120, 150, 180 min. At each sampling, 5 mL of sample was drawn from the system and analysed in the liquid phase for Cu, Cr, Co, Fe, Hg,

Ni, U and Zn in single and multi-components system. The initial pH of solutions was adjusted to 3 as determined in the previous studies.

Total sampling volume throughout the kinetic studies was less than 10% of the total volume and change in solution volume with each sampling was taken into account during calculations. The metal content in the supernatant was determined after filtration by ICP-OES (Spectro, Kleve, Germany).

The amount of metal adsorbed by algae was calculated using the equation (3.3).

iv) Effect of temperature-Thermodynamic parameters

The experiments were carried out at two different temperatures, i.e. 20 and 40 ^{o}C. The initial metal concentration was fixed at 100 mg L^{-1} at pH 3. The thermodynamic parameters (ΔG^{o}, ΔH^{o} and ΔS^{o}) for the adsorption process were calculated using the equations 3.32.

v) Effect of algal mass

To determine the effect of biosorbent mass, different mass of biosorbent 0.2 – 1.2 g were varied and suspended in metal ions solutions of fixed initial concentration and pH. The adsorption procedure was the same as described earlier.

vi) Biosorption-desorption cycles

In order to determine the reusability of the *Oedogonium sp*. biomass, consecutive biosorption-desorption cycles were repeated five times by using the same biomass. Desorption of metal ions was done using 0.5 mol L^{-1} of HCl solution. The algal biomass loaded with heavy metal ions was placed in the desorbing medium at room temperature and was constantly stirred on a rotary shaker for 60 min at 150 rpm. After each cycle of adsorption and desorption, the algal biomass was washed with Milli-Q water and reconditioned for adsorption in the succeeding cycle. The biosorbent was removed and the supernatant was analysed for Cu^{2+}, Co^{2+}, Cr^{3+}, Hg^{2+}, Fe^{3+}, Ni^{2+}, Zn^{2+} and UO_2^{2+} released into the solution, by ICP-OES.

3.2.3.7 Biosorption studies on Na-Alginate-zeolite complex

In order to determine the adsorption capacity of the alginate complex, batch tests were conducted and different parameters were assessed. These include: metal concentration, pH,

contact time and adsorbent mass. The adsorption procedure is the same as described in paragraph 3.2.3.4.

3.2.3.8 Desorption studies on Na-Alginate-zeolite complex

The biosorption and desorption of heavy metals on immobilized alginates was investigated by conducting five cycles of sorption/desorption. This was achieved by shaking thebiosorbent in 20 mL of 0.1 mol L^{-1} HCl for 2 h. The biosorbent was then rinsed with deionized water to remove any residual acidity, filtered and dried prior to re-use.

3.3 Data analysis

3.3.1 Statistical analysis

The accuracy of the adsorption models was demonstrated using two statistical parameters, namely: the correlation coefficient (r) equation 3.6 and normalized standard deviation Δq(%) equation 3.7.

$$r(x,y) = \frac{\sum (x-\bar{x})\cdot(y-\bar{y})}{\sqrt{\sum (x-\bar{x})^2 \cdot \sum (y-\bar{y})^2}} \tag{3.6}$$

$$\Delta q(\%) = 100\sqrt{\frac{\sum_{i=1}^{n}\left[\frac{q_{\exp}-q_{calc}}{q_{\exp}}\right]^2}{n-1}} \tag{3.7}$$

where: q_{exp} is the experimental metal ion uptake, q_{calc} the calculated amount of metal ions adsorbed and *n* is the number of experimental data.

The Curve Expert 1.37 freeware program was used for modelling of the data with the confidence level set at 95%.

3.3.2 Analytical figures of merit

i) Limits of detection (LOD)

The limit of detection, expressed as the concentration or the quantity, is derived from the smallest measure that can be detected with reasonable certainty for a given analytical procedure. Formally, the limit of detection is defined as the concentration of analyte required

to give a signal equal to the background (blank) plus three times the standard deviation of the blank. The detection limits were calculated as three times the standard deviations of the reagent blank.

ii) Precision

Three measurements were used to assess the precision or the reproducibility of analyses. Reagents and materials were accurately weighed using a Precis 180 A balance (Precis Balance Ltd., Buckinghamshire).

iii) Quality control

The use of glassware or polyvinylchloride (PVC) containers was avoided to prevent reaction of metals on the glass surface or the chloride and metals from the PVC. Polypropylene (PP) containers were used throughout the study and these were cleaned with metal free non-ionic detergent solution, rinsed with tap water, soaked in 8% HNO_3 acid for 12 h and then rinsed with de-ionised water from Milli-Q-water purification system as recommended by Arienzo *et al.,* (2001).

3.4 Fitting data in equilibrium (isotherms), kinetic and thermodynamic models

3.4.1 Isotherm models

i) Langmuir model

The Langmuir model is valid for monolayer localized physical adsorption onto a homogeneous surface with a finite number of identical sites. In monolayer adsorption, there is no transmigration of adsorbed molecules at the maximum adsorption, meaning that the adsorbed molecules do not deposit on each other; they only adsorbed on the free surface of the adsorbent. Hence it assumes uniform surface (all adsorbent sites are equivalent), the adsorbed molecules do not interact and they all adsorbed through the same mechanism (Hamdaoui and Naffrechoux, 2007). The Langmuir isotherm is limited in its application to adsorption in monolayer (Brev, 1958).

The Langmuir model is given by the equation 3.8.

$$q_e = \frac{q_m b C_e}{1 + bC_e} \qquad (3.8)$$

where: q_e (mg g^{-1}) is the amount adsorbed per unit weight of adsorbent at equilibrium, C_e (mg L^{-1}) is the equilibrium concentration of the adsorbate, and qm (mg g^{-1}) is the maximum adsorption capacity, and b (L mg^{-1}) is the constant related to the free energy of adsorption.

The essential characteristics of Langmuir isotherm can be expressed in terms of a dimensionless constant separation factor, R_L (Gupta *et al*., 2001; Weber and Chakraborti 1974) which is defined as:

$$R_L = \frac{1}{1 + C_e \,.\, b} \tag{3.9}$$

Using values of R_L, it is possible to obtain information about the isotherms. Types of isotherms for different values of R_L are listed in Table 3.3 (Gunaya *et al*., 2007; Wang *et al*., 2008; Garcia-Mendieta *et al*., 2009; Roberto and Rubio, 2009).

Table 3.3 Effect of separation factor, R_L, on isotherm shape

R_L value	***Type of isotherm***
$R_L > 1$	Unfavourable
$R_L = 1$	Linear
$0 < R_L < 1$	Favourable
$R_L = 0$	Irreversible

The thermodynamic parameter, Gibbs free energy change ΔG^0 (kJ mol^{-1}) for the specific adsorption, was calculated on the basis of constant *b* in the Langmuir isotherm, as following:

$$\Delta G^0 = - R.T.\ ln\ b \tag{3.10}$$

Enthalpy ΔH^0 (kJ mol^{-1}) and entropy ΔS^0 (kJ $(mol \cdot K)^{-1}$) changes were also calculated using the next equation:

$$\Delta H^0 = -R\left(\frac{T_2 \,.\, T_1}{T_2 - T_1}\right) ln\ \frac{b1}{b_2} \tag{3.11}$$

The enthalpy change and entropy change cam be calculated from a plot of *ln(b)* versus *1/T* (Wang *et al*., 2006).

ii) Freundlich model

The Freundlich model is an empirical formula for heterogeneous adsorption given by the equation 3.12.

$$q_e = K_F C_e^{1/n} \quad (3.12)$$

where: K_F ($mg^{1-(1/n)}$ $L^{1/n}$ g^{-1}) is a constant correlated to the relative adsorption capacity of the adsorbent and *n* is a constant indicative of the intensity of the adsorption.

Since the Freundlich model is an exponential equation, it assumes that the adsorption capacity of the adsorbent increases with the increasing of the concentration of the adsorbate. The exponent *1/n* is an index of the diversity of free energies associated with the adsorption of the solute by multiple components of a heterogeneous adsorbent.

The values for *n* and K_f can be obtained from the slopes and intercept of the Freundlich plot, respectively. A value of *n* between 1 and 10 refers to a beneficial adsorption. They predict the steepness and curvature of the isotherm. When $\frac{1}{n} < 1$, the isotherm is linear and the system has a constant free energy at all adsorbate concentrations. When $\frac{1}{n} > 1$, the isotherm is concave and sorbates are bound with weaker and weaker free energies, finally, when $\frac{1}{n} > 1$, the isotherm is convex and more adsorbate presence in the adsorbent enhance the free energies of further adsorption (Schwarzenbach, 2003). The linearized form of Freundlich sorption isotherm is:

$$ln\ q_e = ln\ K_f + \frac{1}{n} ln\ C_e \quad (3.13)$$

The constants K_f and *n* are obtained from the slope and intercept of the plot of $ln(q_e)$ versus $ln(C_e)$.

iii) Dubinin-Radushkevich (D-R) isotherm

This D-R model is used to estimate the characteristic porosity of the biomass to evaluate the nature of sorption based on the Polanyi potential theory assuming heterogeneous surface energies. This model can be written in the following linear form (Gunaya *et al*., 2007).

$$ln\ q_e = ln\ X_m + \beta.\ F^2 \quad (3.14)$$

$$F = R.T.ln\ (1 + \frac{1}{Ce}) \quad (3.15)$$

Where: *Xm*: the maximum sorption capacity of sorbent (mol g^{-1})

β: constant (mol^2 $(kJ)^{-2}$) related to mean sorption energy

F: the Polanyi potential

R: the gas law constant (kJ $(mol\ K)^{-1}$)

T: the absolute temperature (K)

β and *Xm* are obtained from the slope and intercept of the plot of *ln(qe)* versus F^2.

The values of sorption energy (*Es*) (kJ mol^{-1}) can be correlated to β by using the following relationship:

$$E_s = \frac{1}{\sqrt{-2\ .\beta}} \quad (3.16)$$

If the magnitude of *Es* is between 8 and 16 kJ mol^{-1}, the adsorption process proceeds by ion exchange, while for values of *Es* < 8 kJ mol^{-1}, the adsorption process is of a physical nature. (El-Kamash *et al*., 2005; Wang *et al*., 2008).

iv) Elovich isotherm

The equation defining the Elovich model is based on a kinetic principle assuming that the adsorption sites increase exponentially with adsorption, which implies a multilayer adsorption (Hamdaoui and Naffrechoux, 2007). It is expressed by the relation:

$$\frac{q_e}{q_m} = K_E\, C_e\, exp\ (-\frac{q_e}{q_m}) \quad (3.17)$$

Where: K_E is the Elovich equilibrium constant (L mg^{-1}) and q_m is the Elovich maximum adsorption capacity (mg g^{-1}). If the adsorption obeys Elovich equation, Elovich maximum adsorption capacity and Elovich constant can be calculated from the slope and the intercept of the plot $ln\ (q_e/C_e)$ versus q_e.

3.4.2 Kinetic models

The prediction of batch adsorption kinetics is necessary for the design of industrial adsorption columns. The nature of the adsorption process will depend on physical or chemical characteristics of the adsorbent system and also on the system conditions. In this study, experimental data were fitted using different kinetic models such as Lagergren's pseudo first-

order, pseudo second-order, Elovich kinetic equation and diffusion model in order to predict the mechanism involved in the adsorption process.

i) Lagergren's pseudo first-order model

The pseudo first-order rate expression is generally described by the following equation (Lagergren, 1898):

$$\frac{dq}{dt} = k_1 (q_e - q_t) \tag{3.18}$$

Where: q_t : Amount of metal adsorbed at any time (mg g^{-1}), (mol g^{-1})

q_e : Amount of metal adsorbed at equilibrium time (mg g^{-1}), (mol g^{-1})

k_1 : Pseudo first order rate constant (min^{-1})

Integrating and applying boundary conditions, (t = 0 to t and qt = 0 to qe), Equation (3.18) becomes:

$$log(q_e - q_t) = log(q_e) - \frac{k_1.t}{2.303} \tag{3.19}$$

$$q_t = q_e(1- e^{-k_1.t}) \tag{3.20}$$

Where: qe and k_1 can be determined from the intercept and slope of the plot, respectively. Thus the rate constant k_1 (min^{-1}) can be calculated from the plot of $log(q_e - q_t)$ versus time.

ii) Ho pseudo second-order model

The adsorption kinetic data can be further analysed using Ho's pseudo second-order kinetic, which is represented by (Ho and McKay, 1998; Ho *et al*. 1996a, b, Ho, 1995):

$$\frac{dq}{dt} = k_2 (q_e - q_t)^2 \tag{3.21}$$

Where: k_2 (kg mol^{-1} min^{-1}) is the rate constant of second-order model. For boundary conditions (t=0 to t and q_t =0 to q_e), equation 3.21 becomes:

$$\frac{t}{qt} = \frac{1}{k_2 qe^2} + \frac{1}{qe}\, t \tag{3.22}$$

$$q_t = \frac{qe^2.\ k_2.\ t}{1+qe\ .k_2.\ t} \tag{3.23}$$

The plot of $\frac{t}{qt}$ versus t should give a straight line if pseudo-second-order kinetic model is Applicable; qe and k_2 can be determined from the slope and intercept of the plot, respectively. The constant k_2 is used to calculate the initial adsorption rate h, at $t \rightarrow 0$, as follows:

$$h = k_2 q_e^2 \quad (3.24)$$

iii) Elovich equation

In reactions involving chemisorption of adsorbate on a solid surface without desorption of products, adsorption rate decreases with time due to an increased surface coverage. One of the most useful models for describing such activated chemisorption is the Elovich equation (Gunaya *et al*., 2007; Teutli-Sequeira *et al*., 2009).

The Elovich equation can be written as:

$$\frac{dqt}{dt} = a \,.\, exp(-b.\, q_t) \quad (3.25)$$

where: a is the initial adsorption rate (mol (kg min)$^{-1}$) because (dq_t/d_t)→ a when $q_t \rightarrow 0$.

Given that q_t =0 at t = 0, the integrated form of equation become:

$$q_t = \frac{1}{b} ln(t + t_0) + \frac{1}{b} ln\, t_0 \quad (3.26)$$

where: $t_0 = 1/(ab)$; if t is much larger than t_0 ($t » t_0$), equation can be simplified as:

$$q_t = \frac{1}{b} ln(a.b) + \frac{1}{b} ln\, t \quad (3.27)$$

a and b can be determined from the intercept and slope of the plot q_t against $ln(t)$.

The constant a is related to the rate of chemisorption and the constant b is related to the surface coverage (Teng and Hsieh, 1999).

iv) Intraparticle diffusion Weber-Morris model

Previous studies by various researchers showed that the plot of q_t versus $t^{0.5}$ represents multi-linearity, which characterizes two or more steps involved in the adsorption process (Sun and Yang, 2003). The intraparticle diffusion model is characterized by a linear relationship between the amounts adsorbed (q_t) and the square root of the time and is expressed as:

$$q_t = K_p \cdot t^{0.5} + I_d \quad (3.28)$$

Where K_p is the initial rate of the intraparticle diffusion coefficient (mol kg^{-1} min$^{0.5}$) and I_d is a constant.

The two parameters can be obtained from the intercept of the plot of q_t versus $t^{0.5}$. The interception (I_d) is used to examine the relative significance of the two transport mechanisms of the solute, intraparticle diffusion and external mass transfer (film or surface diffusion

through the film surrounding a zeolitic particle). Should I = 0, the intraparticle diffusion is considered as the rate limiting step, while, at I > 0, both external mass transfer and intraparticle diffusion is considered as the rate limiting step. The increase of I results in higher resistance of the liquid layer that surrounds the zeolite particle over the ions diffusion. The Weber-Morris has a significant importance as the possibility to determine the diffusion coefficient of ions inside the adsorbent material (Apiratikul *et al*., 2004).

Crank (1956) proposed the calculation of diffusion coefficient expressed as:

$$D_e = \pi \left(\frac{d_p \,.\, k_p}{12\,.qe}\right)^2 \qquad (3.29)$$

where: D_e is the effective diffusion coefficient ($cm^2 \cdot min^{-1}$) and d_p is the mean diameter particles (cm^{-1}). Using I_d constant is possible to evaluate the contribution of external or internal diffusion:

$$RC\ (\%) = 100.\frac{I_d}{qe} \qquad (3.30)$$

where: *RC*(%) is the relative coefficient and *qe* is the equilibrium sorption capacity obtained from the best fitted kinetic model between pseudo-first and pseudo-second order kinetic models. The higher *RC* would indicate the external mass transfer step as a rate limiting step, whereas the lower *RC* indicated that the intraparticle diffusion step was the rate limiting step.

v) The film diffusion model

When the transport of the adsorbate from the liquid phase up to the solid phase boundary plays the most significant role in adsorption, the liquid film diffusion model can be applied (Gunaya *et al*., 2007):

$$\ln(1-F) = -K_F \cdot t + I_f \qquad (3.31)$$

where: F is the fractional attainment of equilibrium ($F = qt/qe$) and K_F is the adsorption rate constant. A linear plot of - *ln (1 - F)* versus *t* with zero intercept would suggests that the kinetics of the adsorption process is controlled by diffusion through the liquid film surrounding the solid adsorbent ($I_f = 0$).

3.4.3 Thermodynamic parameters

In the column or batch adsorption systems, the designer should be able to understand the changes in reaction that can be expected during the process require the brief idea of

thermodynamic parameters. The concept of thermodynamic assumes that in an isolated system where energy cannot be gained or lost, the entropy change is the driving force (Ho, 1995; Ho and Wang, 2004). The thermodynamic parameters that must be considered to determine the process are: enthalpy of adsorption (ΔH^o), Gibb's free energy change (ΔG^o) and entropy change (ΔS^o) due to transfer of unit mole of solute from solution onto the solid–liquid interface. The important thermodynamic function ΔH^o is very useful whenever there is a differential change occurs in the system.

The change in entropy ΔS^o is used to identify the spontaneity in the adsorption process. The value of ΔH^o and ΔS^o were calculated using the equation 3.32 (Vadivelan and Kumar, 2005).

$$ln\ K_d = \frac{\Delta S^O}{R} - \frac{\Delta H^O}{RT} \quad (3.32)$$

Where R: Universal gas constant (8.314 J (mol K)$^{-1}$)

T: Absolute solution temperature (K)

K_d: Distribution coefficient, can be calculated by the equation 3.4.

The value of ΔS^o and ΔH^o can be obtained from the slope and intercept of the plot between $ln\ (K_d)$ versus $1/T$.

Another most important thermodynamic parameter involved in the adsorption process is the Gibbs free energy change ΔG^o (kJ mol^{-1}) and can be calculated using the relation:

$$\Delta G^o = -RT\ ln\ K_d \quad (3.33)$$

The distribution coefficient (K_d) implicitly indicates the selectivity, capacity, and affinity of an ion for ion exchange.

Activation Energy

Activation energy refers to the minimum kinetic energy that must be supplied to the system in order for a chemical process to take place. In adsorption processes, the activation energy can be obtained using Arrhenius equation (Levine, 1988):

$$ln\ \frac{k(T_2)}{k(T_1)} = -\frac{Ea}{R}\left(\frac{1}{T2} - \frac{1}{T1}\right) \quad (3.34)$$

Where k : apparent rate constant

Ea : activation energy

R : universal gas constant (8.314 J mol^{-1} K^{-1})

T : temperature (K)

Chapter 4: Results and Discussion

This chapter presents the results for the physical and chemical properties of the natural as well as the functionalised zeolite/bentonite; the sorption studies of natural and modified with proxy-compounds (histidine, cysteine and sorbitol); the sorption studies on zeolite/bentonite modified with *Penicillium-simplicissimum*, and the sorption studies on the zeolite-alginate system. Comparisons of the performance of these systems were drawn. The results obtained in batch studies with respect to sorption capacities, kinetic and thermodynamic modelling of the adsorption process are presented and discussed for each case. In the column experiments, the breakthrough points, column efficiency and the number of theoretical plates were assessed. The bed depth service time (BDST) model was used to analyse the adsorption within the service time.

4.1 Bentonite

4.1.1 Mineral and chemical properties

The X-ray diffraction (XRD) pattern of bentonite used throughout the study is presented in Figure 4.1.

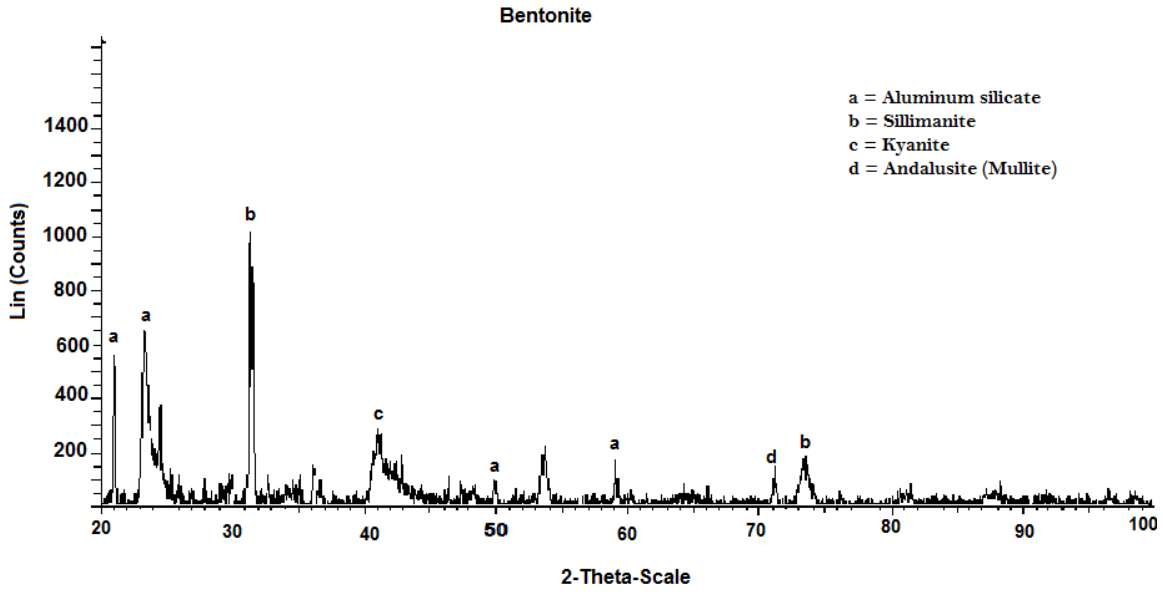


Figure 4.1 XRD spectrum of bentonite powder

Natural bentonite was found to be crystalline and mainly consisting of sillimanite, [$Al_2(SiO_4)O$], with the highest peak occurring at a 2θ value of 32. Most of the peaks are of aluminium silicate $(Al_xSi_{1-x})O_2$ occurring in different phases such as kyanite and andalusite.
The chemical composition analysis of the natural bentonite was performed using X-ray fluorescence (XRF) and the results are presented in Table 4.1. The Si/Al molar ratio of the sample was calculated as 2.67.

Table 4.1 Chemical composition of natural bentonite

Oxides	(%) (w/w)
Si O_2	52.26
Al_2O_3	17.25
Fe_2O_3	0.53
FeO	4.25
MnO	0.07
MgO	3.67
CaO	2.05
Na_2O	0.35
K_2O	1.38
TiO_2	0.4
P_2O_5	0.09
H_2O	17.72
Total	100.02

4.1.2 Physical surface characteristics

4.1.2.1 Surface area and pore volume analysis

Table 4.2 presents the values of the surface area and the pore volume of the natural and functionalised bentonite. The surface area of the natural bentonite was higher than that for the functionalised bentonite. The BET surface area significantly decreased after the modification due to the coverage of the pores of natural bentonite. The sequence followed the order: natural bentonite > bentonite-histidine > bentonite-mannitol > bentonite-sorbitol > bentonite-cysteine.

Table 4.2 Physical properties of natural and functionalised bentonite

	Bentonite-natural	*Bentonite-Histidine*	*Bentonite-Cysteine*	*Bentonite-Sorbitol*	*Bentonite-Mannitol*
Surface area ($m^2 g^{-1}$)	73.82	61.25	23.72	25.02	25
Pore volume ($cm^3 g^{-1}$)	0.103	0.009	0.054	0.061	0.059

4.1.2.2 Zeta potential measurements

The zeta potential of natural and modified bentonite as a function of suspension pH was studied in order to determine the surface charge of the biosorbents. The results are illustrated in Figure 4.2 (a) and (b).

Natural bentonite indicates a point of zero charge (pHpzc) at pH 4 and 8. Below pH 4, zeta potential of natural bentonite is negative. At pH values between 4 and 8, the zeta potential of natural bentonite exhibits positive values. The negative charge arises from the isomorphic substitution of Al^{3+} for Si^{4+} within the lattice; the broken bonds at the Si−O−Si generated at the particle surface during the grinding process and the lattice imperfections (Argun, 2007). It is well known that bentonite has a heterogeneous surface charge. The charge on the edges is due to the protonation/deprotonation of surface hydroxyl groups and therefore depends on the solution pH. Most of the negative surface charge on the bentonite is pH-dependent and is likely to be due to isomorphous substitution.

The electrical charge at the oxide-aqueous surface due to protonation or deprotonation of the surface hydroxyl can be described as (Laskowski, 1993):

$$M{-}OH + H^+ \leftrightarrow M{-}OH_2^+ \quad (4.1)$$

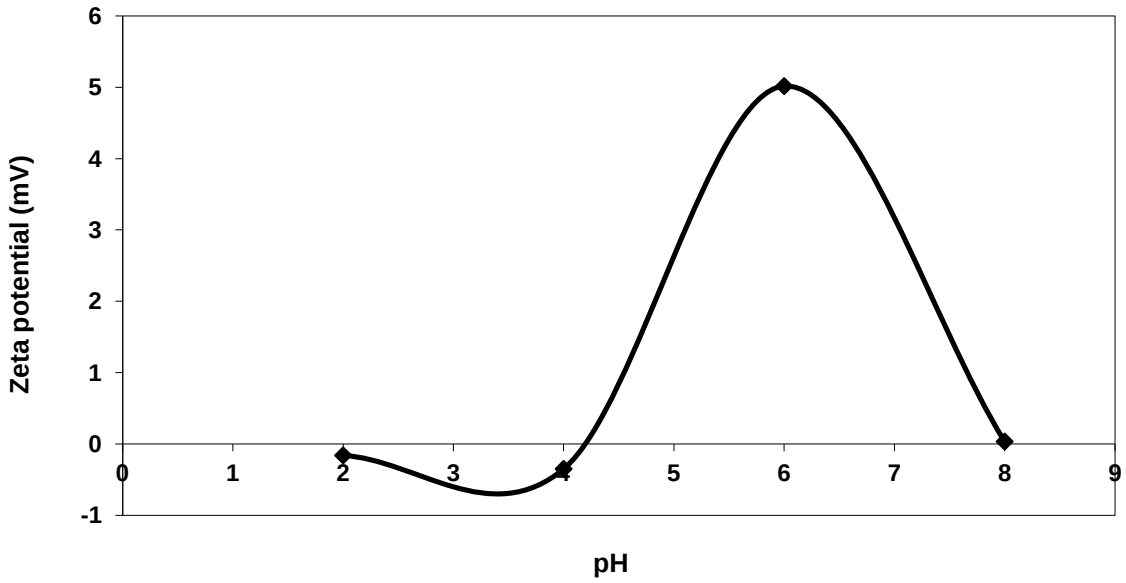
$$M{-}OH + OH{-} \leftrightarrow M{-}O^- + H_2O \quad (4.2)$$

where: M is the central metal ion (Si or Al) and at pHpzc,

$$[M{-}O^-] = [M{-}OH_2^+] \quad (4.3)$$

The point of zero charge is the point where the sorbent is least stable. In contrast, the modified bentonite exhibits negative zeta potential values at all studied pH values. Changes to the sign of the zeta potential of modified bentonite could be related to the presence of functional groups such as –NH, COO-, SH and OH on the surface of the sorbent.

(a)



(b)

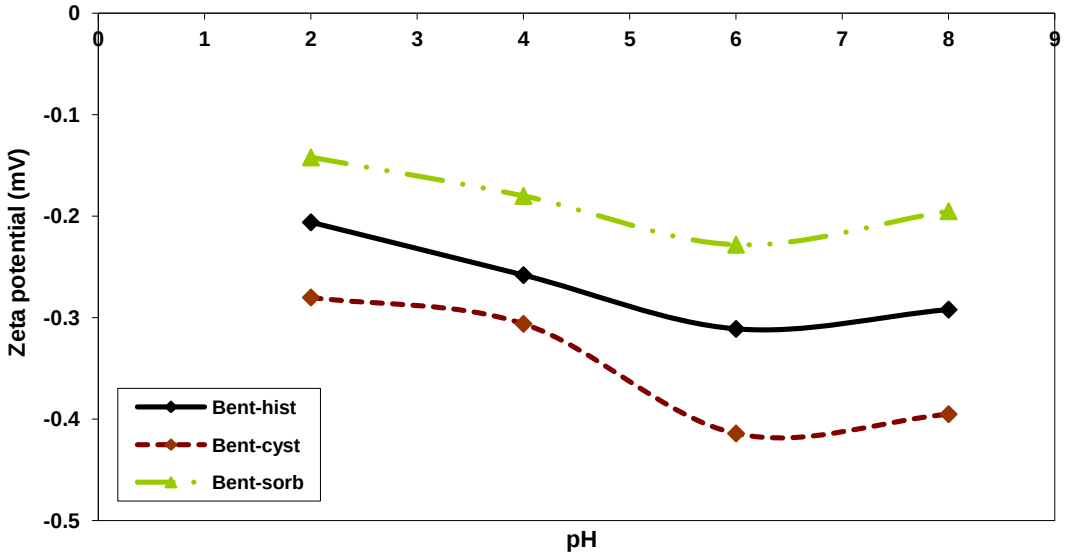


Figure 4.2 The zeta potential of: (a) natural bentonite (b) Bentonite-histidine, Bentonite-cysteine, Bentonite-sorbitol

In general, the zeta potential of the bentonite used in this study had very low values compared to those obtained in previous studies (Gök, 2007). The difference could be due to the origin of the sample as well as the solvent used in the experiment. The zeta potential of bentonite

depends not only on the pH, but also on ionic strength of the suspension, and the Al content of the framework.

4.1.2.3 Thermal analysis

The thermal analysis of the natural bentonite offered information about the thermal reactions and the stability of the bentonite. The thermal analysis curve of natural bentonite is illustrated in Figure 4.3.

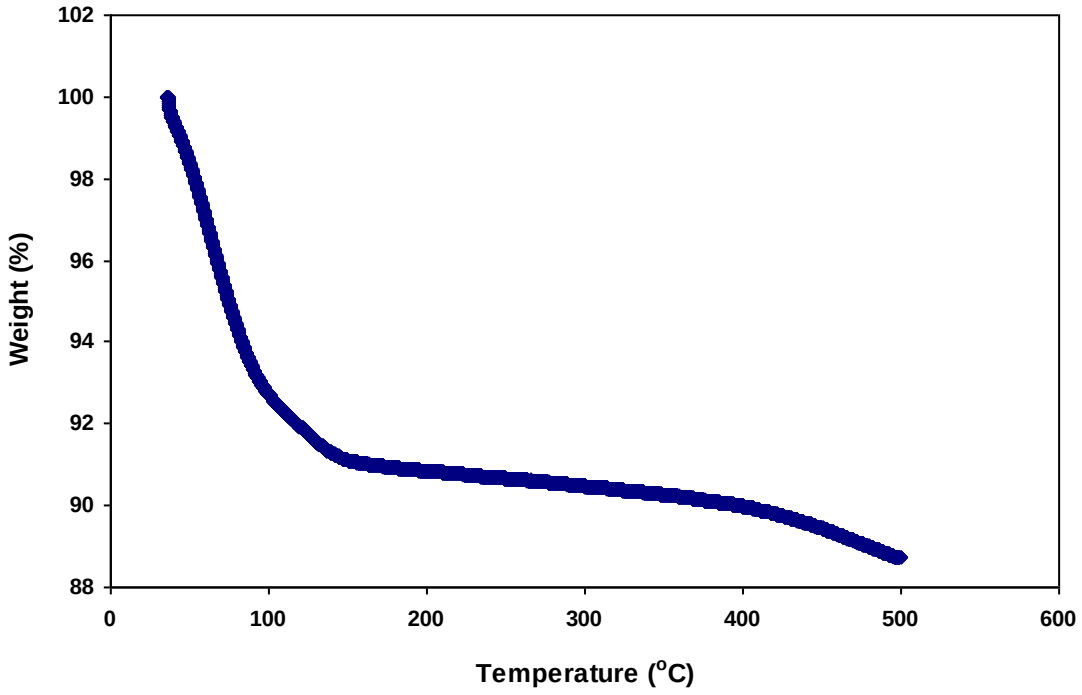


Figure 4.3 Thermogravimetric curve of natural bentonite

The TG/DTG curve (obtained under N_2 atmosphere, 20 mL min^{-1}, 5^oC min^{-1}) of natural bentonite shows a weight loss between 25-150^{o}C, corresponding to the desorption of internal and external water of hydration (100 - 91%). However, less thermally-induced changes were visible in the curves when the temperature was increased from 150°C to 400°C (91 – 90%), thereby suggesting that bentonite did not undergo any further thermally-induced changes over 400^{o}C. Less weight loss was observed above 500^{o}C, proving that bentonite is thermally stable over a temperature of 500^{o}C.

4.1.3 Chemical properties of the surface

4.1.3.1 Cationic exchange capacity and elemental analysis

The results for the cationic exchange capacity and elemental composition of the natural and modified bentonite are presented in Table 4.3. The elemental composition of the biomasses measured using the CHNS-analyser is also presented in Table 4.3. The CEC was obtained according to the $BaCl_2$ method with Na^+, K^+, Ca^{2+} and Mg^{2+} being the exchangeable cations in the bentonite cavities (Gillman and Sumpter, 1986; Chapman, 1965).

The results showed an increase in the amount of carbon (0.742%), hydrogen (0.258%) and nitrogen (0.744%) which was observed in the bentonite-histidine compared to the natural bentonite. An increase was also observed for the bentonite-cysteine with 0.466% carbon, 1.465% hydrogen, 0.678% nitrogen and 0.457% sulphur being recorded. The bentonite-sorbitol system had higher amounts of carbon (1.697%) and hydrogen (0.709%) whereas the amount of carbon and hydrogen in the bentonite-mannitol rose by 1.695% and 0.608%, respectively. These results, in addition to the FTIR spectra (Figure 4.4), prove that the modification of the natural bentonite was successful.

Table 4.3 Chemical properties of natural and functionalised bentonite

Sample	CEC (meq $100g^{-1}$)	H %	C %	N %	S %
Natural Bentonite	64.42	0.555	1.748	n.d	n.d
Bentonite-Histidine	42.54	0.813	2.490	0.744	n.d
Bentonite-Cysteine	45.21	2.015	2.214	0.678	0.457
Bentonite-Sorbitol	52.01	2.252	2.457	n.d	n.d
Bentonite-Mannitol	51.07	2.250	2.356	n.d	n.d

n.d: not detected

4.1.3.2 FTIR spectral analysis

According to Wieczorek *et al.* (2003), the sorption of an organic material onto a negatively-charged surface is a complex process involving both cationic exchange and hydrophobic bonding. The modification of their sorbent material was verified by the FTIR spectra.

The infrared spectrum for natural bentonite is shown in Figure 4.4, while the spectra for the modified bentonite are given in APPENDIX C. The wavenumbers for different adsorbents are given in Table 4.4.

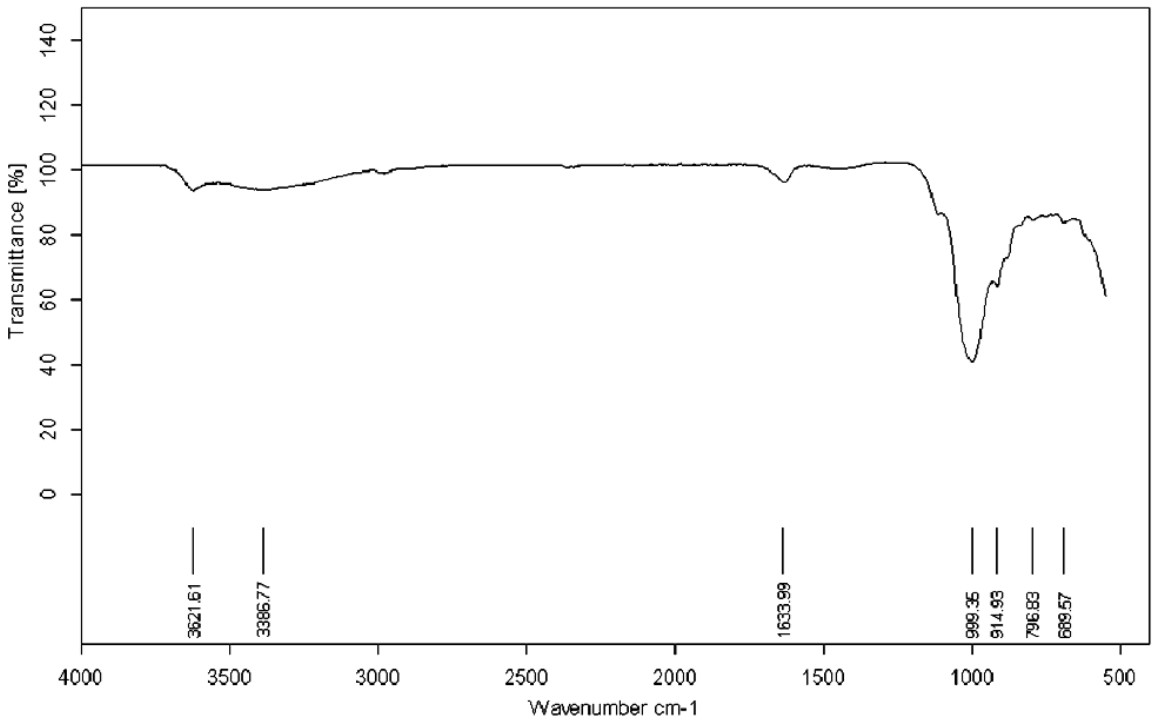


Figure 4.4 FTIR spectrum of the natural bentonite

The wavenumbers and vibration types associated with the IR spectra of natural bentonite, bentonite-histidine, bentonite-cysteine, bentonite-sorbitol and bentonite-mannitol are given in Table 4.4a, b, c, d, e.

Table 4.4a IR vibrations of natural bentonite

Wavenumber, cm^{-1}	***Vibration type***
3621	H stretching (Mg, Al)-OH
3386	O-H stretching H-OH
1633	O-H deformation
1150	Si-O stretching
999	Si-O-Si stretching
914	Al^{3+} binding, OH deformation
689	Si-O-Si

Table 4.4b IR vibrations of bentonite-histidine

Wavenumber, cm^{-1}	***Vibration type***
3734-3902	O-H, N-H
3689	O-H, N-H (H bonded)
2980	COO-
2850	C-H
1457	C=N, C-OH bending
1688	C=O amide I
1002	Si-O-Si stretching
915	Al^{3+} binding OH deformation
796	N-H wagging
687	C-H
592	Al-O-Si deformation

Table 4.4c IR vibrations of bentonite-cysteine

Wavenumber, cm^{-1}	***Vibration type***
3689	O-H, N-H
2981	S-H
2395	
1733	C=O
1635	H-OH deformation
1473	
999	Si-O-Si stretching
914	Al^{3+} binding OH deformation
796	COO-, C-H
675	C=C
578	O-H (bend out of plane)

Table 4.4d IR vibrations of bentonite-sorbitol

Wavenumber, cm^{-1}	***Vibration type***
3628	O-H stretching
3566	H-OH
3391	C-H
1635	H-OH
991	Si-O-Si stretching
914	Al^{3+} binding OH deformation
796	Si-O stretching

Table 4.4e IR vibrations of bentonite-mannitol

Wavenumber, cm^{-1}	*Vibration type*
3902-3617	OH (H-bonded)
2960	C-H
1740-1521	H-OH
992	Si-O-Si stretching
798	Si-O
616-563	O-H (bend out of plane)

In relation to the covalent binding between bentonite and histidine, the peaks at 3902 and 3734 cm^{-1} are likely to be N−H stretching caused by NH_2. The wide O−H band (approximately 3446 cm^{-1}) belonging to the carboxyl is invisible in the structure because it fits into the O−H stretching of histidine. The band at 1507 to 1489 cm^{-1} is for N−H bending and the band at 1457 cm^{-1} is a C=N stretching band. It can be seen that the C=O carbonyl band expected at 1630–1640 cm^{-1} fitted into the O−H bending of water in bentonite. As a result of this, the O−H bending of bentonite appears different, which can be seen from the spectra. The C−O stretching band is hidden by the peak of H-OH. From these results, it seems that bentonite interacts with the NH_2 groups of histidine. In addition, the band at 1507 cm^{-1} represents protonated NH_2, that is, NH_3 bending. Probably, this means that the bentonite surface protonated the histidine. Consequently, it can be concluded that the bentonite structure interacted with the NH_2 group of histidine.

With respect to the interaction between bentonite and cysteine, the peaks at 3500–2500 cm^{-1} are probably for the N–SH stretching vibrations. The broad O–H band (≈ 3500 cm^{-1}) belonging to the carboxyl in the structure is invisible because it is masked by the O–H stretching of the amino acid and water in the bentonite. The spectrum of bentonite-cysteine showed that the bands at 1396 (symmetric deformation of the NH_3 group), 1521 (deformation of the N–H group), 1733 (stretching of C=O), 675 (stretching of C–S) and 2450 cm^{-1} (stretching of S–H) decreased in intensity. All these results may be caused by the interaction between bentonite and the NH_2 group of cysteine.

The FTIR spectrum of sorbitol and mannitol demonstrates the obvious difference at the band between 1700 and 1500 cm^{-1} (C-H deformation); the difference can be seen also in the region of 3600 3900 cm^{-1} (O-H stretching).

4.1.4 Sorption studies

4.1.4.1 Sorption capacities, pH and isotherms of adsorption

i) Effect of pH

pH is one of the important parameters affecting heavy metal adsorption. Thus, the effect of pH on heavy metal adsorption was evaluated in the pH range 2 to 12. As shown in Fig. 4.5 (a) and (b), the maximum adsorption capacity for the metal studied, in the conditions described below, was 5 mg g^{-1} and this was reached at pH 5 for U, Ni, Cu and at pH 7 for Zn and Co. The maximum adsorption capacity of Fe was found to be constant for the whole pH range.

The adsorption rate of U, Ni, Zn, Cr, Co and Cu on natural bentonite was low at low pH and the rate increased with the pH. The adsorption rate of Hg decreased below pH 5 and then increased above this pH. This may be a result of disproportionation of Hg in solution, that is, Hg tends to be distributed as Hg^{+} and Hg^{2+}. The pH of hydrolysis for Hg^{+} is below 5 while that for Hg^{2+} is around 7.3 (there is enhanced adsorption at and beyond this pH). However, further work would be required to substantiate this possibility. The dependence of metal adsorption on pH is related to both the surface functional groups present on the biomass and the metal chemistry in solution. The low adsorption rate observed at low pH in natural bentonite can be attributed to the fact that low pH implies high H^{+} concentration, which tends to compete with the metal ions for the adsorption sites. Although the PZC of natural bentonite was obtained at pH 4 as seen in Figure 4.2 (a), the bentonite surface has negative charges at low pH, an attraction of metal ions is predicted which might be inhibited by the protons (Chrishan and Anirudhan, 2003).

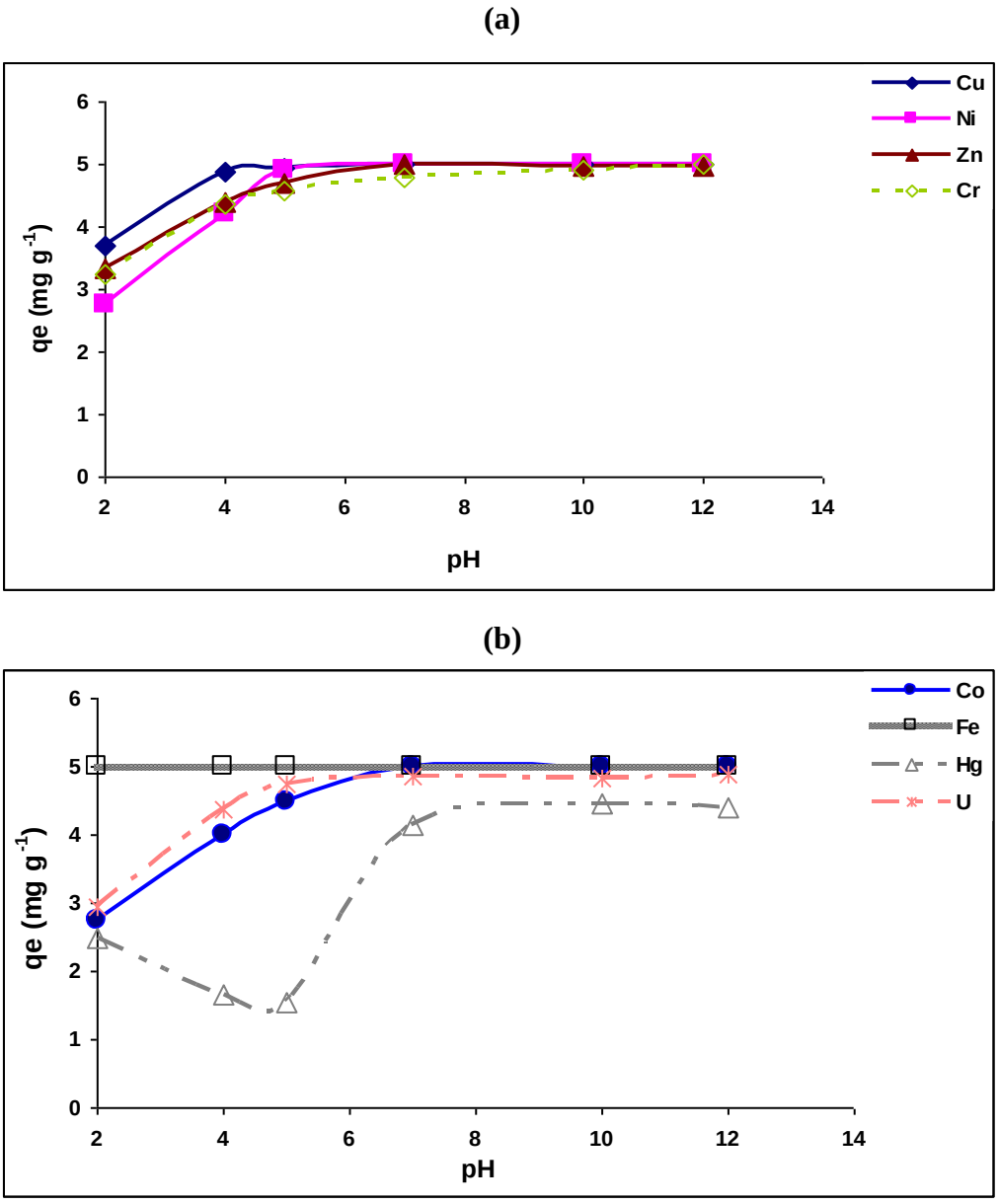


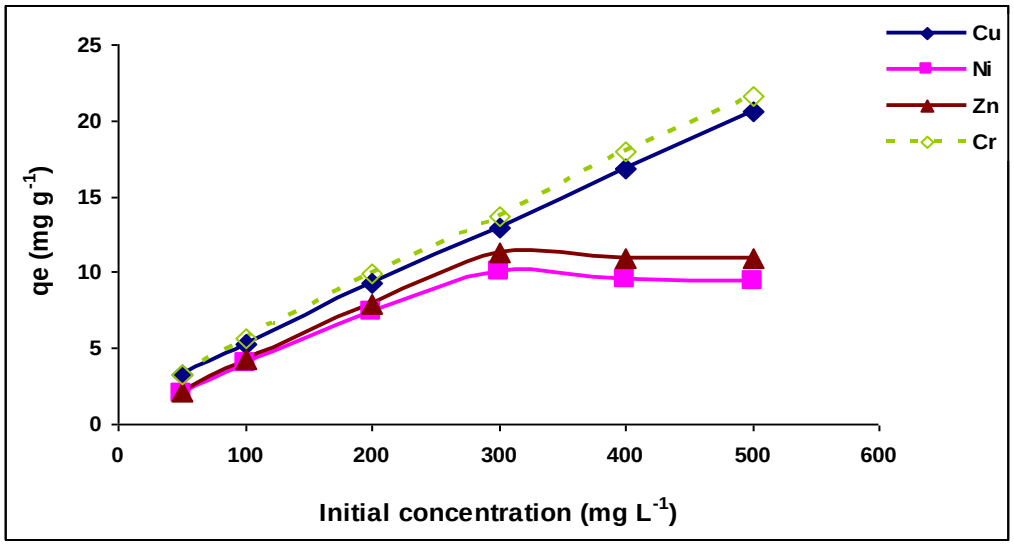
Figure 4.5 Effect of initial pH on adsorption of (a) Cu, Ni, Zn, Cr and (b) Co, Fe, Hg and U onto natural bentonite in single component solutions (C_i = 100 mg L^{-1}, Temp = 298.15±1^{o}K, agitation rate = 150 rpm, agitation time = 12 h).

Also, hydrolysis of the aluminium oxide sites at very low pH on the natural bentonite results in the loss of the crystallographic structure of the former and consequently its adsorbent capacity. The maximum adsorption capacity obtained at the pH range 5 to 7 for all the metals studied is due to the contribution of adsorption as well as precipitation since most of the metals hydrolyze at this pH range. A maximum and constant adsorption rate was observed at pH 7.

ii) Effect of concentration

The results for the dependence of adsorption on metal ion concentrations are shown in Figure 4.6 (a) and (b).

(a)



(b)

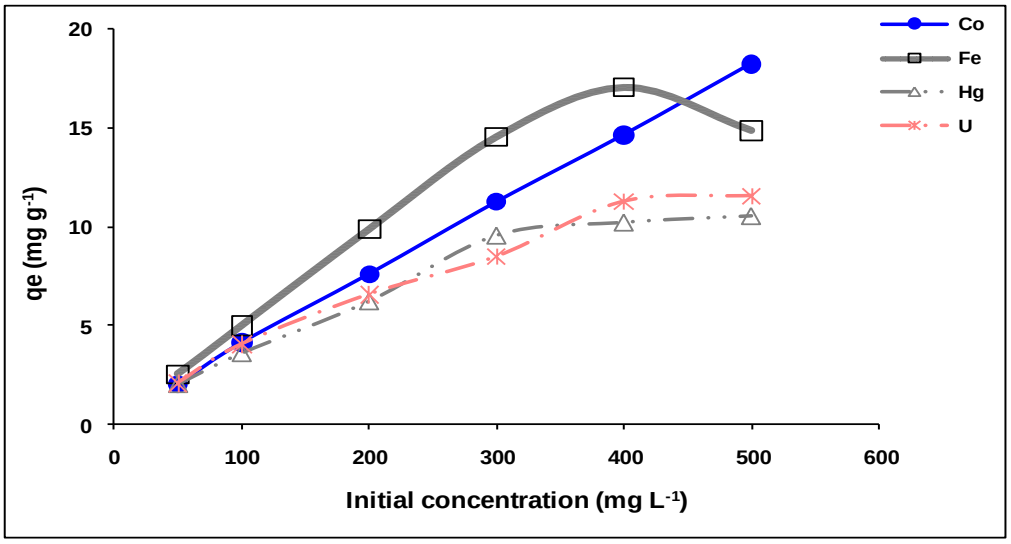


Figure 4.6 Effect of concentration on the adsorption of (a) Cu, Ni, Zn, Cr and (b) Co, Fe, Hg and U) onto natural bentonite in single-component solutions at pH 3 (Temp = 298.15±1^{o}K, agitation rate= 150 rpm, agitation time= 12 h)

Adsorption capacity increased linearly with increasing concentration. The saturation concentration was not reached for Cu, Cr and Co up to 500 mg L^{-1}. For the rest of the metals studied, a similar trend was observed as the adsorption capacity increased

with increasing concentration up to 300 mg L^{-1}. Equilibrium was reached at this concentration and the adsorption capacity was constant. The adsorption capacity of Hg and U decreased with concentration above 400 mg L^{-1}.

iii) Isotherms of adsorption for natural bentonite

In order to understand the adsorption mechanisms of metal ions onto the natural bentonite, three adsorption isotherm models, Langmuir, Freundlich and Dubinin-Radushkevich (D-R) were used to fit the experimental data obtained from the adsorption equilibrium experiments. Using the distribution coefficient (K_d) (calculated as the ratio of the metal ion concentration in the solid phase to the concentration in the liquid phase at equilibrium), the strength of the metal-bentonite bonds and the free adsorption energy were calculated. The different parameters calculated using the expressions given in section 3.4.1 from the experimental data and the correlation coefficient obtained are given in Table 4.5.

Based on the correlation coefficient, all the metals studied have a correlation > 0.950 for the Langmuir isotherm, suggesting that the adsorption occurs through a monolayer coverage.

The low coefficient of correlation values obtained for the Freundlich linear expression suggest that this model does not best describe the adsorption mechanism based on single-component solutions. Except for Cu, Cr, Co and U with correlation coefficient values greater than 0.950, the values of *n* range between 1.873 – 8.324, implying a beneficial process (favorable). The values of 1/*n* for all the metals studied are < 1, assuming that metals are bound with weak free energies (Özer *et al.*, 1997**).**

The adsorption mechanism is also well described by the D-R model for Cu, Co, Ni and U with high correlation coefficients values (> 950). The modeling results of the experimental data of the adsorption equilibrium experiments suggest that the adsorption of metal ions occurs by monolayer coverage on a heterogeneous surface.

Table 4.5 Parameters of the Langmuir, Freundlich and D-R models for the adsorption of metals on natural bentonite

Langmuir isotherm	***Fe***	***Cu***	***Cr***	***Co***	***Hg***	***Ni***	***Zn***	***U***
A	0.048	0.068	0.071	0.336	0.319	0.049	0.043	0.403
B	4.765	3.349	4.023	4.376	19.32	5.289	5.247	23.06
b	99.96	494.6	405.5	13.04	60.46	108.6	122.7	57.29
q_m (mol/kg)	0.209	0.299	0.213	0.228	0.052	0.189	0.190	0.043
ΔGo (kJ/mol)	-11.41	-15.38	-14.23	-6.366	-10.17	-11.62	-11.92	-10.03
Δq (%)	79.21	66.82	65.21	84.66	82.24	72.62	72.23	82.93
r	0.999	0.984	0.981	0.998	0.976	0.995	0.991	0.979
Freundlich isotherm	***Fe***	***Cu***	***Cr***	***Co***	***Hg***	***Ni***	***Zn***	***U***
A	0.295	0.202	0.254	0.169	0.255	0.244	0.451	0.002
B	0.121	0.276	0.287	0.332	0.534	0.387	0.457	0.474
K_f	0.507	1.592	1.498	1.478	1.799	1.754	2.820	1.004
n	8.324	3.622	3.602	3.012	1.873	2.580	2.186	2.109
ΔGo (kJ/mol)	-20.63	-8.978	-7.896	-7.465	-4.643	-6.396	-5.419	-5.228
Δq (%)	22.12	5.234	6.023	7.021	21.29	18.73	22.35	14.07
r	0.899	0.996	0.998	0.991	0.914	0.929	0.910	0.954
D-R isotherm	***Fe***	***Cu***	***Cr***	***Co***	***Hg***	***Ni***	***Zn***	***U***
A	-1.209	-0.809	-0.875	-0.886	-1.458	-0.767	-0.536	-1.919
B	-0.001	-0.002	-0.004	-0.003	-0.006	-0.004	-0.005	-0.005
Xm (mol/kg)	0.298	0.445	0.412	0.412	0.233	0.465	0.585	0.147
Es (kJ/mol)	23.49	14.94	15.22	12.28	9.479	10.64	9.769	10.36
Δq (%)	16.09	10.43	11.03	7.256	18.64	15.38	18.96	13.20
r	0.946	0.986	0.989	0.991	0.933	0.951	0.935	0.960
K_d	***Fe***	***Cu***	***Cr***	***Co***	***Hg***	***Ni***	***Zn***	***U***
A	11.01	8.302	8.201	6.428	4.869	5.751	5.649	4.923
B	-1782	-2130	-2036	-696.4	-987.7	-479.7	-485.9	-1276
ΔGo (kJ/mol)	-27.30	-20.58	-15.69	-15.93	-12.07	-14.25	-14.04	-12.20
K_{do}	60745	4031	3895	619.1	130.2	314.3	284.1	137.4
Δq (%)	163	113.8	124.2	48.56	8.099	23.73	11.85	19.56
r	0.810	0.797	0.785	0.859	0.984	0.957	0.985	0.933

Based on the normalized standard deviation, the experimental adsorption isotherms are best fitted with Freundlich models (Δq= 5.234 – 22.12 %) as well as on D-R models (Δq= 7.256 – 18.96 %). The maximum adsorption capacities (mol kg^{-1}) obtained on Langmuir isotherm are as follows: Cu (0.299) > Co (0.228) > Cr (0.213) > Fe (0.209) > Zn (0.190) > Ni (0.189) > Hg (0.052) > U (0.043). The variations of Gibbs free energy determined based on the distribution coefficient had values range of -12.20 to - 27.30 kJ mol^{-1}, meaning that the adsorption process occurred spontaneously.

The selectivity obtained based on distribution coefficient K_{do} (L kg^{-1}) is: Fe (60745) > Cu (4031) > Cr (3895) > Co (619.1) > Ni (314.3) > Zn (284.1) > U (137.4) > Hg (130.2). The values of the distribution coefficients are high for Fe and Cu which indicate the presence of stronger bonds.

The Dubinin-Radushkevich correlation coefficients were > 0.950, except for Fe, Hg and Zn, demonstrating the heterogeneous character of the adsorption surface of the bentonite. However, the Langmuir isotherm shows large errors (Δq) in assessing the maximum adsorption capacity (Table 4.5). The values of the mean free energy Es of sorption (D-R isotherm) in all cases were found to be in the range of 8–16 kJ mol^{-1}, which are within the energy ranges of ion exchange reaction mechanism, except for Fe with a value of 23 kJ mol^{-1}.

4.1.4.2 Effect of contact time and kinetics of adsorption

i) Effect of contact time

The study of sorption kinetics describes the adsorbate uptake rate and evidently, this rate controls the residence time of the adsorbate at the solid-liquid interface. The adsorption kinetics is important to predict the minimum contact time required for the maximum adsorption of heavy metals by the sorbent. This also provides information on the minimum time required for considerable adsorption to take place and the possible diffusion control mechanism between the metal ion as it moves from the bulk solution towards the adsorbent surface. The time-dependent behaviour of metal adsorption on natural bentonite is illustrated in Figure 4.7.

The results reveal that adsorption of all metals was rapid in the first 30 min and then slowed down considerably as the reaction approached equilibrium. The adsorption of metal ions on natural bentonite occurred following the sequence: Fe > Cu > Zn, Ni > Co > U > Hg. The initial fast rate may be due to the availability of the uncovered surface area of the bentonite since adsorption kinetics depends on the surface area of the adsorbent. In addition, the variation in the amount of metal ions adsorbed could be related to the nature and the concentration of the surface groups (active sites) responsible for the interaction with different metal ions.

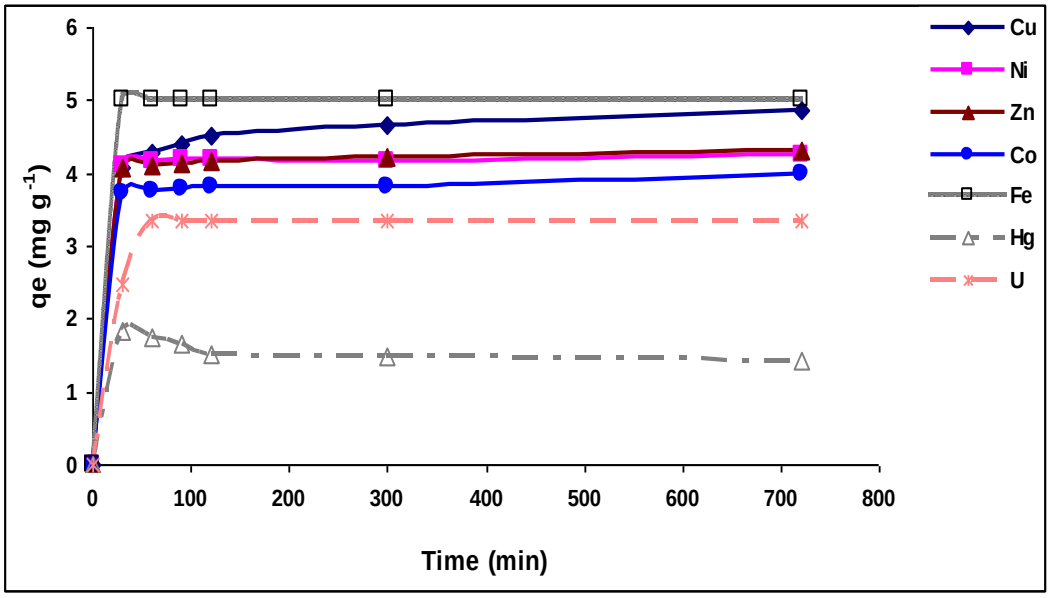


Figure 4.7 Effect of contact time on adsorption of Cu, Ni, Zn, Co, Fe, Hg and U onto natural bentonite in single-component solutions (C_i = 100 mg L^{-1}, Temp = 298.15±1^{o}K, agitation rate = 150 rpm)

The natural bentonite contains OH^- functional groups that take part in metal ion binding (Kumar *et al.*, 2011). This indicates that with passage of time, a higher fraction of the metal ions migrates from the bulk solution through the adsorbent boundary layer onto the active sites of the adsorbent and is adsorbed. This enhanced sorption of the metal ion with increase in agitation time may be due to the decrease in boundary layer resistance to mass transfer in the bulk solution and an increase in kinetic energy of the hydrated metal ion (Augustine *et al.*, 2007.

ii) Kinetic modelling of metal ion adsorption on natural bentonite

Modelling of kinetic data is fundamental for the industrial application of sorption since it gives information for comparison among different biomaterials under different operational conditions for designing and optimizing operational conditions for pollutant removal from wastewater. In order to investigate the mechanism of sorption of metal ions by natural bentonite and the potential rate-controlling steps, different kinetic models were used, namely: pseudo first-order, pseudo second-order, Elovich, intraparticle diffusion and film diffusion models. The parameters and constants obtained from the experimental data are presented in Table 4.6 below:

Table 4.6 Kinetic constants for the adsorption of metal ions on natural bentonite

Pseudo-first order							
	Fe	***Cu***	***Co***	***Hg***	***Ni***	***Zn***	***U***
A	-3.691	-1.952	-2.227	-2.937	-2.582	-2.342	-3.688
B	-0.010	-0.004	-0.006	-0.004	-0.005	-0.004	-0.013
qe (mol/kg)	0.015	0.011	0.006	0.001	0.003	0.005	0.001
K_1	0.023	0.009	0.015	0.009	0.010	0.010	0.030
Δq (%)	92.40	83.34	86.37	84.56	90.32	88.29	91.33
r	0.623	0.778	0.822	0.804	0.516	0.658	0.725
Pseudo – second order							
	Fe	***Cu***	***Co***	***Hg***	***Ni***	***Zn***	***U***
A	0.296	105.3	45.05	1266	22.71	53.66	177.9
B	11.17	13.05	14.76	109.3	13.81	15.15	71.03
qe (mol/kg)	0.089	0.077	0.062	0.009	0.072	0.066	0.0141
K_2	421.1	1.617	4.839	9.412	8.399	4.274	28.36
Δq (%)	0.008	2.452	1.352	2.979	0.851	1.974	9.459
r	1.000	0.999	1.000	0.999	1.000	1.000	0.999
Elovich model							
	Fe	***Cu***	***Co***	***Hg***	***Ni***	***Zn***	***U***
A	0.010	0.006	0.007	0.001	0.008	0.009	0.001
B	0.016	0.013	0.012	0.002	0.013	0.011	0.002
b	64.15	77.95	86.13	661.7	79.99	88.65	405.9
a	0.031	0.021	0.022	0.025	0.024	0.022	0.005
Δq (%)	17.17	12.89	15.46	10.94	16.45	15.11	13.45
r	0.961	0.991	0.983	0.975	0.959	0.981	0.621
Intraparticle diffusion model							
	Fe	***Cu***	***Co***	***Hg***	***Ni***	***Zn***	***U***
A	0.089	0.020	0.063	0.007	0.028	0.024	0.004
B	0.001	0.003	0.001	0.002	0.004	0.003	0.001
I_d	0.089	0.020	0.063	0.007	0.028	0.024	0.004
K_p	0.001	0.003	0.001	0.002	0.004	0.003	0.001
Δq (%)	0.010	28.13	0.658	3.197	29.54	29.81	30.77
r	0.721	0.672	0.752	0.817	0.730	0.743	0.802
Film diffusion							
	Fe	***Cu***	***Co***	***Hg***	***Ni***	***Zn***	***U***
A	-2.006	1.138	-1.138	-0.693	-0.923	-0.834	-2.335
B	-0.022	0.001	-0.008	-0.005	-0.011	-0.008	-0.014
I_f	-2.006	1.138	-1.137	-0.693	-0.923	-0.834	-2.335
K_f	0.022	0.002	0.008	0.005	0.011	0.008	0.014
Δq (%)	52.33	40.42	45.75	49.22	55.84	52.79	41.75
r	0.623	0.777	0.822	0.804	0.576	0.658	0.725

The experimental data obtained in the case of kinetic experiments fit best the pseudo-second order model (Δq = 0.008 - 9.459%) followed by the Elovich model which indicates the chemical nature of the adsorption. The adsorption of U on natural bentonite was only described by the pseudo-second order model.

Overall, the pseudo second-order was found to give the best fit and therefore, it could be used to predict the kinetics of adsorption of metal ions onto natural bentonite. This confirms chemisorption, since the rate limiting step is a chemical sorption. So the rate of occupation of

adsorption sites is proportional to the square of the number of unoccupied sites (Antures *et al.*, 2003).

In order to determine the ion-exchange kinetics of Cu, Co, Fe, Hg, Zn, Ni and U, the pseudo first-order and pseudo second-order kinetic models were examined. The calculated values of q_e from the pseudo first-order kinetic model, using equation 3.20 were noticeably lower than those calculated for the pseudo second-order kinetic model using equation 3.23. Additionally, the correlation coefficients (r) obtained from the pseudo second-order model were higher than those calculated for the pseudo first-order kinetic model. As a result, the adsorption of metal ions onto natural bentonite followed pseudo second-order reaction kinetics. The rate constants of pseudo second-order (k_2) were found to be in the ranges of 1.617 and 421.1 (mg min^{-1}) and a higher rate constant k_2 was obtained for Fe.

The Elovich equation parameters *a, b* and correlation coefficients, calculated from equation 3.27, are also presented in Table 4.6. The values of the correlation coefficients are in the range 0.959 and 0.991 (except for uranium which had a lower correlation coefficient of 0.621). Teng and Hsieh (1999) commented that the Elovich constant *a* and *b* are related to the chemisorption rate and the surface coverage, respectively. If we assume a chemisorptions process and the fact that the constant *a* is related to the chemisorption rate, the constant *a* should increase with the rate constant (k_2) of the pseudo-second order model. This means that, if the k_2 values decrease in the order: Fe > U > Hg > Ni > Co > Zn > Cu, the values of the Elovich parameter *a* decrease approximately in the same order. This correlation is available for the metals studied except for uranium. The adsorption process of U could be of a mixed chemical and physical process. To elucidate this problem, supplementary experiments are necessary.

The Elovich constant *b* was found to be higher for Hg (661.7 g mg^{-1}) and U (405.9 g mg^{-1}) compared to the ones obtained for the other metals (64 – 88 g mg^{-1}), suggesting that the coverage of bentonite particles with Hg ions was higher than that achieved by the other ions.

For the intraparticle diffusion model, the values of the initial rate K_p are in the range 1.10^{-3} and 4.10^{-3} mol kg^{-1} $min^{0.5}$. The initial rate decreased in the sequence: Ni > Zn, Cu > Hg > Fe, Co, U. Besides, there is an inverse relationship between the initial sorption rate (K_p) and the boundary layer thickness (I_p). Thus, it can be said that there is a decrease in boundary layer thickness between the bulk solution and the adsorbent particle as the initial adsorption rate of metal ions increases.

4.1.4.3 Effect of temperature and thermodynamic parameters

i) Effect of temperature

The adsorption isotherms of Cu, Zn, Ni, Co, Fe, U and Hg sorption on natural bentonite were obtained at four different temperatures while keeping all other parameters (i.e. metal concentration, shaking time and pH) constant. The results obtained are given in Figure 4.8:

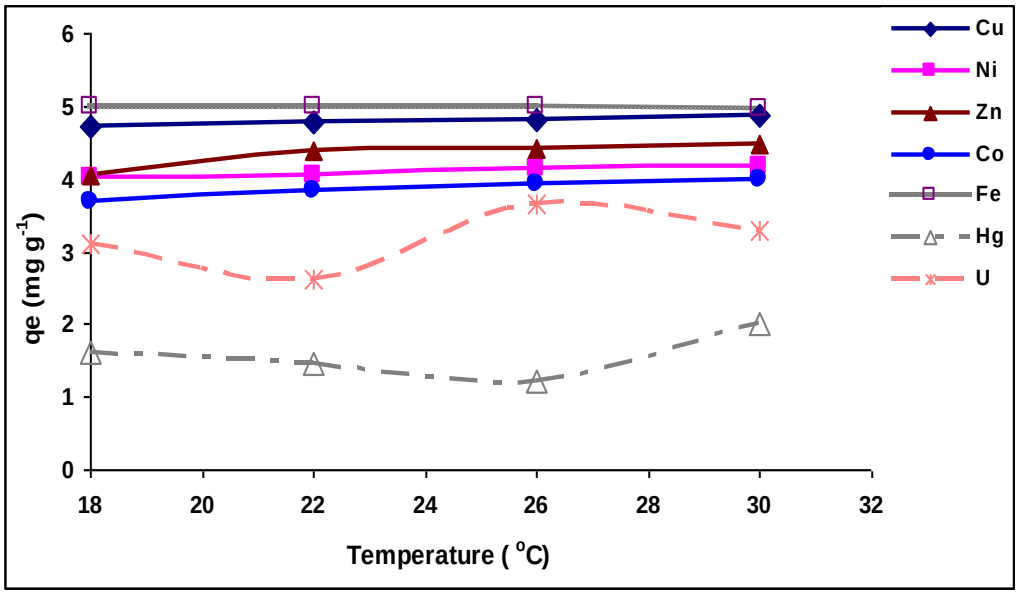


Figure 4.8 Effect of temperature on adsorption of Cu, Ni, Zn, Co, Fe, Hg and U onto natural bentonite in single component solutions (Ci = 100 mg L^{-1}, pH 3, agitation rate = 150 rpm, contact time = 12 h)

In general, the temperature did not affect much the adsorption of Cu, Co, Ni and Fe on natural bentonite. A slight increase of adsorption capacity was observed with Zn, Hg and U.

ii) Thermodynamic parameters

Thermodynamic parameters, i.e. enthalpy (ΔH^{o}), Gibbs free energy (ΔG^{o}) entropy change (ΔS^{o}), activation energy (Ea) for the sorption of Cu, Zn, Ni, Co, Fe, U and Hg on natural bentonite were calculated and the results are listed in Table 4.7.

Table 4.7 Thermodynamic parameters of metal ions adsorption on natural bentonite

	Ea	ΔH^o	ΔS	ΔG^o			
	kJ mol^{-1}	kJ mol^{-1}	J (K^{-1} mol)$^{-1}$	kJ mol^{-1}			
				291.15 ^oK	**295.15** ^oK	**299.15** ^oK	**303.15** ^oK
Cu	58.66	135.1	486.9	-6.797	-7.672	-8.185	-9.492
Ni	12.62	29.06	113.1	-3.437	-3.687	-3.957	-4.098
Zn	41.97	96.64	349.8	-3.464	-4.778	-5.031	-5.334
Co	20.80	47.89	176.1	-2.465	-2.937	-3.219	-3.422
Fe	-130.7	-283.6	-926.9	-25.55	-18.01	-13.73	-13.69
Hg	20.92	48.17	161.9	1.770	2.165	2.874	0.982
U	10.29	23.69	87.08	-1.200	-0.227	-1.878	-1.673

The values of activation energy E_a listed in Table 4.7, calculated from the Arrhenius equation (3.34), were higher (> 40 kJ mol^{-1}) for Cu and Zn implying chemisorption. This is completely consistent with the results obtained from kinetic modelling where the pseudo second-order model better fits the experimental data confirming chemisorption as the rate limiting step.

E_a values range from 10 to 20 kJ mol^{-1} for Ni, Co, Hg and U and as such, physisorption should be the limiting step of the adsorption process. However, this has to be confirmed by kinetic modelling since the process was described by the pseudo second-order as well as Elovich models. It means that these metals tend to bind to binding sites of low energy.

The positive values of ΔH^o showed that sorption of metals onto bentonite is an endothermic process, meaning that the increase of temperature favours the adsorption process. Thus, the enthalpy increases with the temperature. The values of ΔG^o were negative for the metals, indicating the feasibility of the adsorption process and the spontaneous nature of the adsorption. ΔG^o becomes more negative with increasing temperature which further shows that the sorption is favoured at higher temperature.

As shown in the Table 4.7, ΔS^o values are found in the range of 87 to 486.9 J mol^{-1} K^{-1} except for Fe with a negative value. The positive value of ΔS^o shows the increasing randomness at the solid-liquid interface during the sorption of metal ions onto natural bentonite and this increases slightly with temperature. Moreover, the negative value of ΔS^o corresponds to a decrease in degrees of freedom of the adsorbed species.

It was observed that the rate of adsorption (Table 4.8) for the metal ions increases with increasing temperature except for Fe and Hg metal ions for which the rate decreases with the increases of the temperature.

Table 4.8 The reaction rate of the adsorption of metal ions on natural bentonite

Rx rate(h^{-1})				
	291.15 ^{o}K	**295.15** ^{o}K	**299.15** ^{o}K	**303.15** ^{o}K
Cu	0.239	0.264	0.277	0.316
Ni	0.136	0.137	0.148	0.151
Zn	0.137	0.174	0.179	0.186
Co	0.111	0.122	0.128	0.132
Fe	0.601	0.485	0.461	0.453
Hg	0.043	0.039	0.033	0.029
U	0.062	0.081	0.089	0.109

4.2 Bentonite functionalised with proxy-compounds

4.2.1 Bentonite-Histidine

4.2.1.1 Sorption capacities, pH and isotherms

i) Effect of pH

The effect of pH on the adsorption of heavy metals onto bentonite-histidine is illustrated in Figure 4.9. The results for adsorption of metals onto bentonite-histidine showed high adsorption rate at low pH (< 4) for Co, Zn, Fe, Hg and U. An increase of adsorption capacity with pH was observed for Ni whilst the adsorption rate was constant at the all pH regimes for Cu. The formation of complexes between the metal ions and the bentonite-histidine system depends on the amine groups present on the adsorbent. The rate of adsorption increases with the increase in the amine group on the structure (Bajpai and Sachdeva, 2002). A decrease in adsorption rate was observed at very low pH due to the protonation of the amine group to form the ammonium ion.

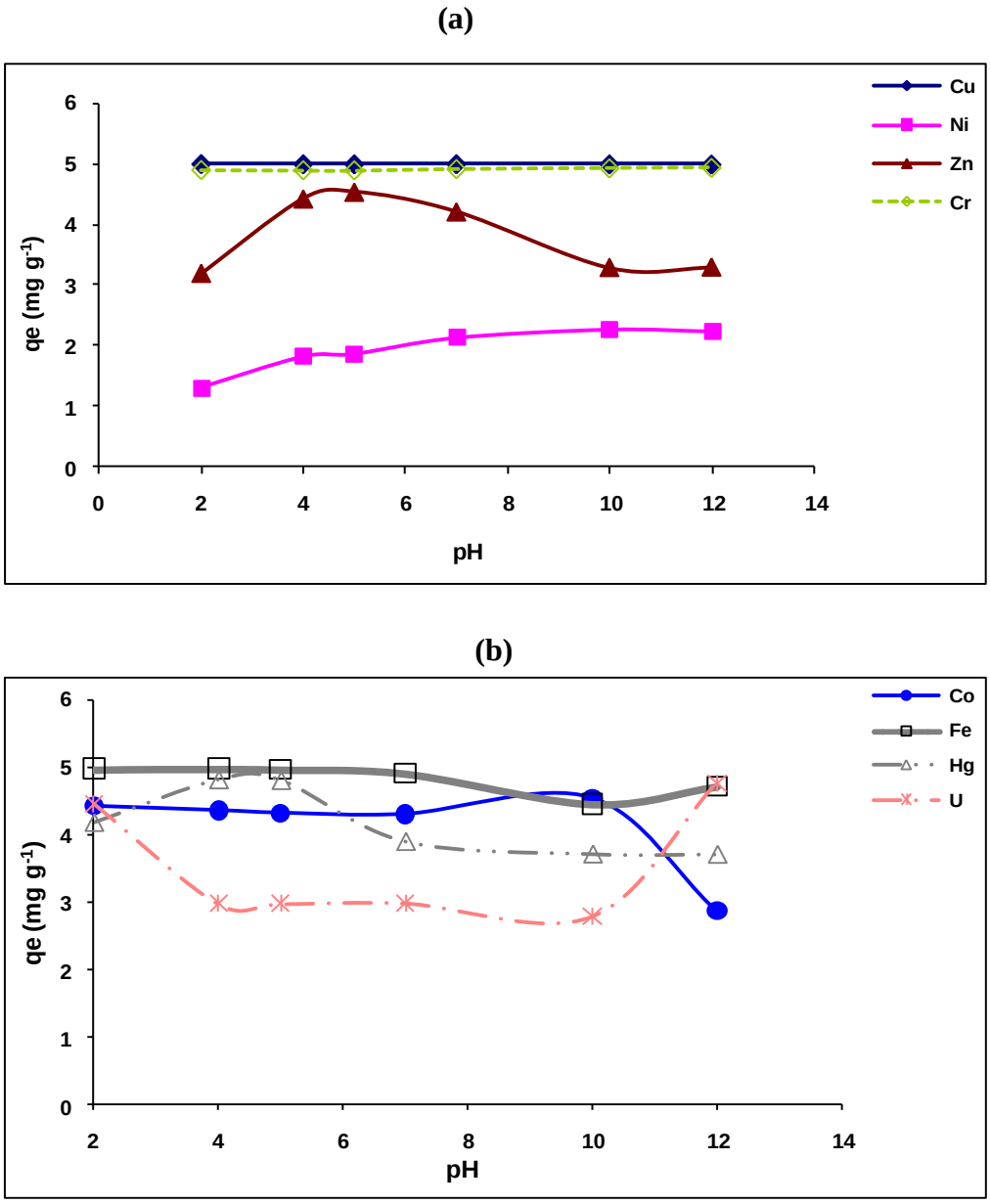


Figure 4.9 Effect of initial pH on adsorption of (a) Cu, Ni, Zn, Cr and (b) Co, Fe, Hg and U onto bentonite-histidine in single component solutions (Ci = 100 mg L^{-1}, Temp = 298.15±1^{o}K, agitation rate = 150 rpm, agitation time = 12 h)

Also, hydrolysis of the aluminium oxide sites at very low pH on the natural bentonite results in the loss of the crystallographic structure of natural bentonite and consequently the ligand's competition for the active sites of the bentonite-histidine. There is also destruction of the bentonite-histidine structure that results in low porosity and low adsorption rate. At very high pH values, the precipitation of the metal hydroxide out-weighs the adsorption of metals on bentonite-histidine and hence the destruction of the bentonite-histidine structure tends to decrease the rate of adsorption on the bentonite-histidine.

Histidine is an amino acid produced by micro-organisms. The structure of histidine (Figure 4.10), carries carboxylic and amine groups which are hard Lewis bases (which will attack hard Lewis acids e.g. Ni, Cu, Zn, Co). The imidazole side chain of histidine is a common coordinating ligand in metalloproteins and is a part of catalytic sites in certain enzymes (IUPAC-IUBMB, 2007; http://e.wikipedia.org/wiki/histidine, accessed, June 2009). L-histidine has an isoelectronic point at pH 7.47. The imidazole side chain of histidine has a pKa of approximately 6, and overall, the amino acid has a pH of 7.6. This means that relatively small shifts in pH will change its average charge. Below pH 6, the imidazole ring is mostly protonated as described by the Henderson-Hasselbach equation ($pH = pK_a + \log([A^-]/[HA])$. When protonated, the imidazole ring bears two NH bonds and has a positive charge. The positive charge is equally distributed between both nitrogens and can be represented with two equally important resonance structures. At low pH, L-histidine acts as a proton "shuttle". The amine group is protonated and, in the presence of the silicon oxide, zwitterions are formed which are less subjected to leaching compared to metal ions (Öztürk *et al.,* 1997).

The adsorption capacity of Ni was the lowest and increased with pH. Nickel in solution has about 21 H_2O molecules in its primary and secondary coordination spheres, almost twice higher than other transition metals. Complex formation (associative or dissociative) could be slow and could likely be through the outer sphere complexes as illustrated in Figure 4.10:

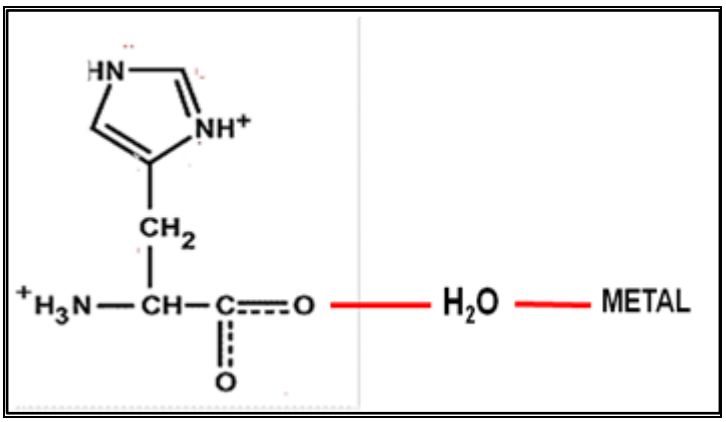


Figure 4.10 Illustration of the histidine-metal complex

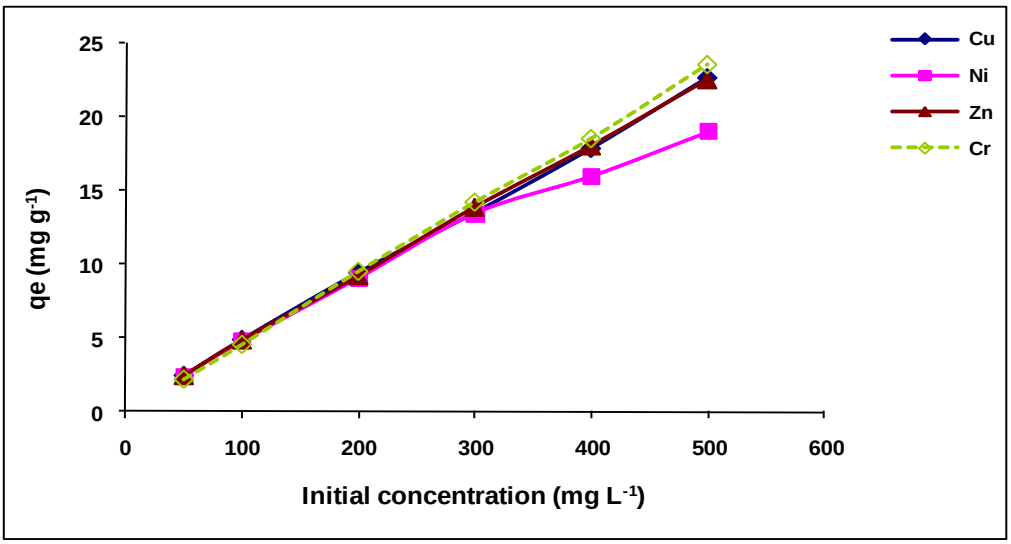
It is accepted that covalent bonds are formed between the amino groups of the L-histidine and the Al^{3+} cations in the center of the octahedral layer of bentonite structures (Laglay *et al.,* 2006).

ii) Effect of metal ion concentration

The effect of initial concentration on the biosorption of metal ions by bentonite-histidine at concentration levels ranging from 50 to 500 mg L^{-1} is shown in Figures 4.11(a) and (b). The results show that the adsorption capacity of Cu, Zn and Co increased with an increase in initial metal concentration and remained constant up to a concentration of 500 mg L^{-1}.

An increase followed by a decrease of the adsorption capacity was observed for Ni at 300 mg L^{-1} and at 400 mg L^{-1} for Fe, Hg and U. This could be attributed to the exhaustion of adsorption at higher concentrations of metals. Complexation and ion exchange in bentonite-histidine contribute to improve the adsorption capacity.

(a)



(b)

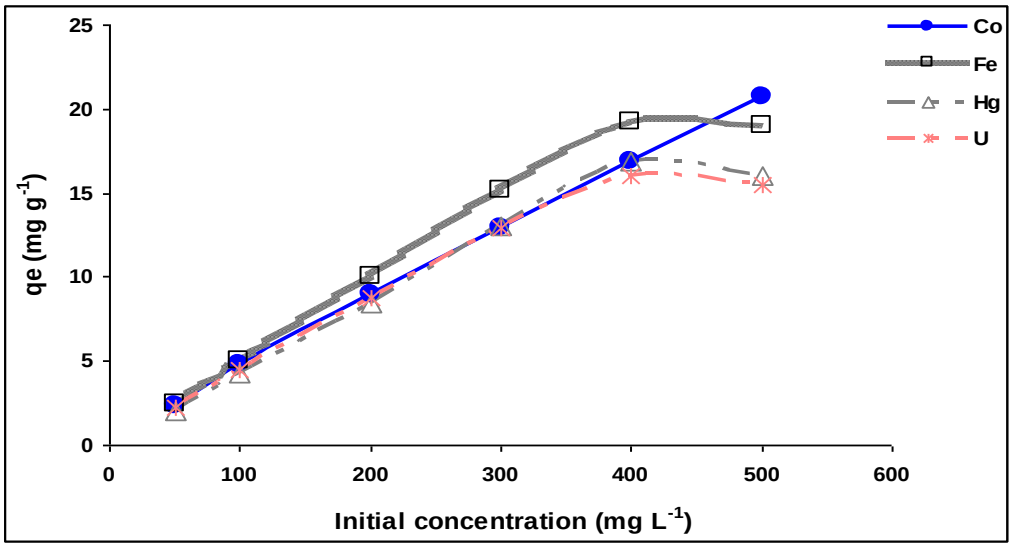


Figure 4.11 Effect of concentration on the adsorption of (a) Cr, Cu, Ni, Zn and (b) Co, Fe, Hg, U (in single-component solutions at pH 3) onto bentonite-histidine (Temp = 298.15±1^{o}K, agitation rate = 150 rpm, agitation time = 12 h)

iii) Isotherms of adsorption for bentonite-histidine

The biosorption data of metal ions were correlated with the isotherm models and the results of the parameters as well as constants are presented in Table 4.9.

Table 4.8 Parameters of the Langmuir, Freundlich and D-R models for the adsorption of metals on the bentonite-histidine system

Langmuir isotherm	***Fe***	***Cu***	***Co***	***Hg***	***Ni***	***Zn***	***U***
A	0.008	0.003	0.004	0.100	0.005	0.002	0.048
B	3.729	2.578	2.333	15.56	2.639	2.175	11.60
b	461.5	892.1	525.4	155.7	493.1	878.2	243.5
qm (mol/kg)	0.268	0.387	0.428	0.064	0.379	0.459	0.086
ΔGo (kJ/mol)	-15.21	-16.84	-15.52	-12.51	-15.37	-16.80	-13.62
Δq (%)	74.55	56.76	53.11	81.50	58.19	49.61	79.47
r	0.999	0.941	0.967	0.976	0.984	0.931	0.988
Freundlich Isotherm	***Fe***	***Cu***	***Co***	***Hg***	***Ni***	***Zn***	***U***
A	0.079	1.154	1.119	0.524	0.971	1.424	0.873
B	0.208	0.533	0.557	0.524	0.514	0.609	0.602
K_f	1.200	14.25	13.17	3.345	9.350	26.53	7.471
n	4.800	1.886	1.797	1.918	1.944	1.641	1.666
ΔGo (kJ/mol)	-11.92	-4.674	-4.453	-4.754	-4.819	-4.067	-4.13
Δq (%)	24.65	11.07	7.204	43.71	10.70	10.03	21.62
r	0.927	0.986	0.994	0.784	0.986	0.989	0.948
D-R isotherm	***Fe***	***Cu***	***Co***	***Hg***	***Ni***	***Zn***	***U***
A	-0.726	0.335	0.313	-0.806	0.178	0.616	-0.595
B	-0.002	-0.005	-0.005	-0.005	-0.005	-0.006	-0.006
Xm (mol/kg)	0.484	1.398	1.367	0.447	1.194	1.851	0.552
Es (kJ/mol)	16.95	10.21	9.611	9.667	9.928	9.487	9.511
Δq (%)	18.32	10.68	6.767	39.74	7.886	10.57	17.79
r	0.958	0.987	0.994	0.824	0.992	0.988	0.965
K_d	***Fe***	***Cu***	***Co***	***Hg***	***Ni***	***Zn***	***U***
A	6.098	7.482	6.796	5.846	6.835	7.196	4.063
B	-1510	-2159	-1069	-1499	-1031	-1714	-2156
ΔGo (kJ/mol)	-15.12	-18.55	-16.85	-14.49	-16.94	-17.84	-10.07
Kdo	9388	1776	894.3	345.9	930.2	1333	58.15
Δq (%)	77.62	25.38	22.13	16.68	20.96	21.85	75.23
r	0.802	0.919	0.915	0.963	0.943	0.889	0.993

The regression values presented in Table 4.9 indicate that the adsorption data for the metal-ions studied fit well the Langmuir, Freundlich and D-R isotherms with r > 0.950 except for Hg for which the process was described only by the Langmuir isotherm. With respect to the constant *b* (mmol g^{-1}, represents the maximum amount that can be sorbed), the biosorption on bentonite-histidine is followed the sequence: Cu> Zn > Co > Ni > Fe > U > Hg.

The low coefficient of correlation values obtained for the Freundlich linear expression suggest that this model does not best describe the adsorption mechanism based on single-component solutions except for Cu, Co and U which had coefficient of correlation values greater than 0.950. The values of *n* range between 1.641 – 4.8, implying a beneficial process and the values of 1/*n* for all the metals studied were < 1, assuming that metals were bound

with weak free energies. The adsorption mechanism is also well described by the D-R model for Cu, Co, Ni and U with high correlation coefficients values (> 0.950) except for Hg.

The modelling results of the experimental data of the adsorption equilibrium experiments suggest that the adsorption of metal ions occurs by monolayer coverage on heterogeneous surface energies. Based on normalized standard deviation, the experimental adsorption isotherms best fitted on D-R models (Δq = 6.767 – 18.32 %) then Freundlich models (Δq= 7.204 – 24.65 %), except for Hg.

The maximum adsorption capacities (mol kg^{-1}) obtained from the Langmuir isotherm are as follows: Zn (0.459) > Co (0.428) > Cu (0.0.387) > Ni (0.379)> Fe (0.268) > U (0.086) > Hg (0.064). The same trend was observed for the D-R isotherm. However, large errors (Δq) were obtained for the Langmuir isotherm in the assessment of the maximum adsorption capacity (Table 4.9).

The variations of Gibbs free energy values determined based on the distribution coefficient are negative with the value ranging from -10.07 to - 18.55 kJ mol^{-1}. This indicates that the process occurs spontaneously. The selectivity obtained for the distribution coefficient (L kg^{-1}) is as follows: Fe (9388) > Cu (1776) > Zn (1333) > Ni (930.2) > Co (894.3) > Hg (345.9) > U (58.15). The values of the distribution coefficients are high for Fe and Cu which indicate the presence of stronger bonds. This trend was also observed for the adsorption on natural bentonite.

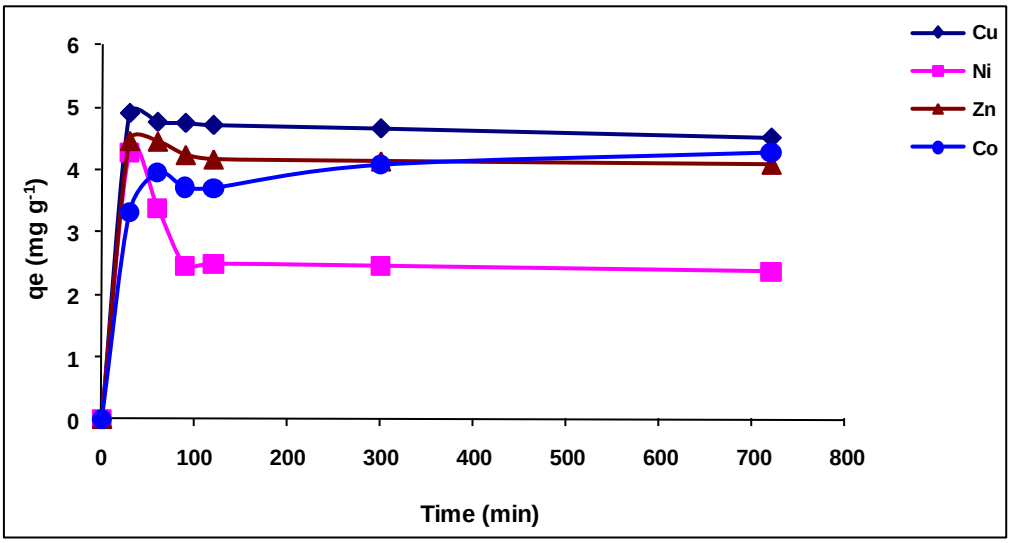
The Dubinin-Radushkevich correlation coefficients were also high, demonstrating the heterogeneous character of the adsorption surface of the bentonite-histidine. The values of the mean free energy Es of sorption (D-R isotherm) in all cases were found to be in the range of 8–16 kJ mol^{-1}, which are within the energy ranges of ion exchange reaction mechanism (physisorption).

4.2.1.2 Effect of contact time and kinetics of adsorption

i) Effect of contact time

Figure 4.12 shows the change in the adsorption capacity Cu, Co, Fe, Ni, Zn, Hg and U ions as a function of time.

(a)



(b)

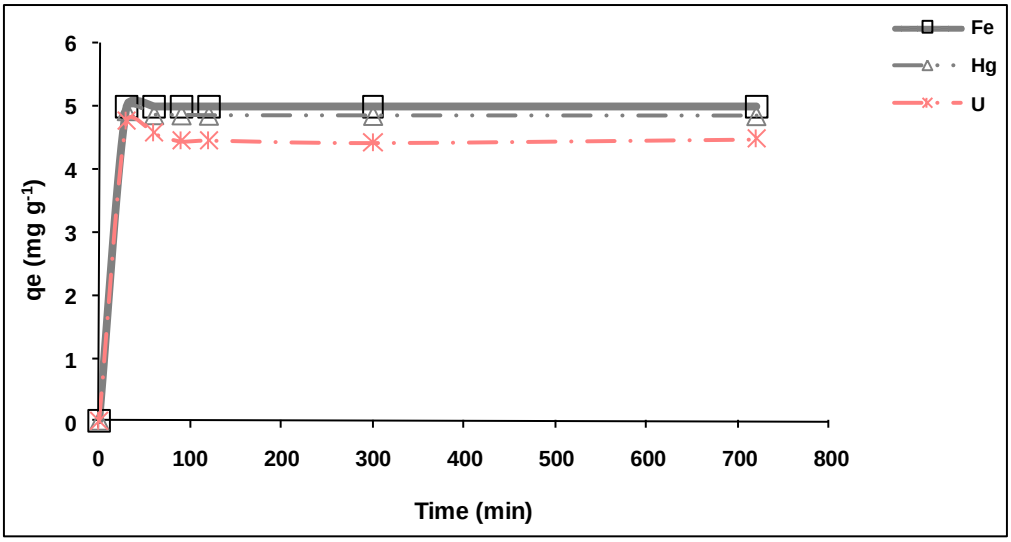


Figure 4.12 **Effect** of contact time on adsorption of (a) Cu, Co, Ni, Zn and (b) Fe, Hg and U onto bentonite-histidine in single component solutions (C_i = 100 mg L^{-1}, Temp = 298.15±1°K, agitation rate = 150 rpm)

Two steps were observed, namely: a rapid adsorption process which occurred within 30 minutes and a slow adsorption process as the reaction approached equilibrium (up to 12 h). The same trend was observed for the natural bentonite. The adsorption capacity of U and Hg increased drastically in the modified bentonite. The sorption of metals on natural bentonite followed the sequence: Fe > Cu > Zn, Ni > Co > U > Hg whilst for bentonite-histidine, the sequence was: Fe > Hg> Cu > U > Co, Zn > Ni.

The bentonite-histidine contains COO^-, OH^- and $-NH-$ functional groups that take part in metal ion binding. The adsorption capacity of Ni increased and reached a maximum after the

first 30 minutes but then decreased gradually and remained constant up to 720 minutes. This could be the effect of desorption, meaning that Ni is weakly bound to the biosorbent.

ii) Kinetic modelling of metal adsorption on bentonite-histidine

The parameters of the kinetic models with their correspondent coefficients of determination are summarized in Table 4.10.

Table 4.10 Kinetic constants for the adsorption of metal ions on bentonite-histidine

Pseudo-first order							
	Fe	***Cu***	***Co***	***Hg***	***Ni***	***Zn***	***U***
A	-4.410	-2.258	-1.894	-3.308	-1.562	-1.945	-2.877
B	-0.013	0.004	-0.004	-0.004	-0.002	-0.009	-0.003
qe (mol/kg)	0.001	0.006	0.013	0.001	0.027	0.011	0.001
K_1	0.029	0.009	0.010	0.009	0.005	0.020	0.008
Δq (%)	92.55	88.24	81.24	91.38	69.97	79.49	88.77
r	0.605	0.628	0.811	0.493	0.875	0.940	0.602
Pseudo – second order							
	Fe	***Cu***	***Co***	***Hg***	***Ni***	***Zn***	***U***
A	0.032	47.87	139.2	52.54	728.7	63.29	273.6
B	11.17	12.91	13.72	40.70	13.53	14.59	49.89
qe (mol/kg)	0.089	0.077	0.073	0.0246	0.0753	0.068	0.020
K_2	3847	3.483	1.353	31.53	0.251	3.365	9.099
Δq (%)	0.002	1.433	2.196	1.070	16.28	0.999	3.635
r	1.000	0.999	0.999	1.000	0.994	1.000	0.999
Elovich model							
	Fe	***Cu***	***Co***	***Hg***	***Ni***	***Zn***	***U***
A	0.014	0.010	0.007	0.004	0.001	0.009	0.003
B	0.016	0.013	0.012	0.004	0.010	0.012	0.003
b	64.14	75.53	82.56	235.4	97.16	85.67	295.5
a	0.038	0.029	0.021	0.010	0.010	0.024	0.007
Δq (%)	16.80	14.89	10.83	16.38	9.141	14.07	14.74
r	0.795	0.952	0.964	0.848	0.928	0.962	0.936
Intraparticle diffusion model							
	Fe	***Cu***	***Co***	***Hg***	***Ni***	***Zn***	***U***
A	0.036	0.028	0.022	0.010	0.012	0.024	0.007
B	0.005	0.004	0.004	0.001	0.003	0.004	0.001
Id	0.036	0.028	0.022	0.010	0.012	0.024	0.007
Kp	0.005	0.004	0.004	0.001	0.003	0.004	0.001
Δq (%)	29.27	29.93	31.05	29.44	34.50	29.98	29.99
r	0.721	0.747	0.814	0.723	0.895	0.770	0.740
Film diffusion							
	Fe	**Cu**	**Co**	**Hg**	**Ni**	**Zn**	**U**
A	-2.513	-0.794	-0.747	-0.883	-0.369	-1.482	-0.678
B	-0.028	-0.008	-0.005	-0.012	-0.002	-0.006	-0.008
I_f	-2.513	-0.794	-0.747	-0.883	-0.368	-1.482	-0.678
K_f	0.027	0.008	0.005	0.0120	0.002	0.006	0.007
Δq (%)	53.77	53.65	47.82	60.96	56.92	40.59	55.55
r	0.605	0.628	0.811	0.493	0.875	0.939	0.621

For natural bentonite, five kinetic models were used to fit the experimental data. The degree of goodness of fit of these kinetic models can be judged from the value of the correlation

coefficient, which can also be regarded as a criterion in the determination of the adequacy of the kinetic model. From the correlation coefficient values, adsorption of metal ions on bentonite-histidine is regarded as pseudo second-order ($\Delta q = 0.002 – 16.28\%$).

Overall, the pseudo second-order model was found to give the best fit and therefore, it could be used to predict the kinetics of adsorption of metals onto bentonite-histidine. The adsorption of Cu, Co and Zn is also described by the Elovich model with a correlation coefficient $r > 0.950$. Chemisorption could be the rate limiting step of the process. The calculated values of q_e from the pseudo-second order kinetics model were noticeably higher than those calculated from the pseudo first-order kinetic model.

Besides, the rate constants of pseudo second-order (k_2) were found to be in the range 0.251 - 3847 g (mg min) $^{-1}$. A higher rate constant k_2 was obtained for Fe in this case as it was for natural bentonite. The initial rate (K_p) values calculated from the intraparticle diffusion model ranged from $1*10^{-3}$ to $5*10^{-3}$ mol kg^{-1} $min^{0.5}$.

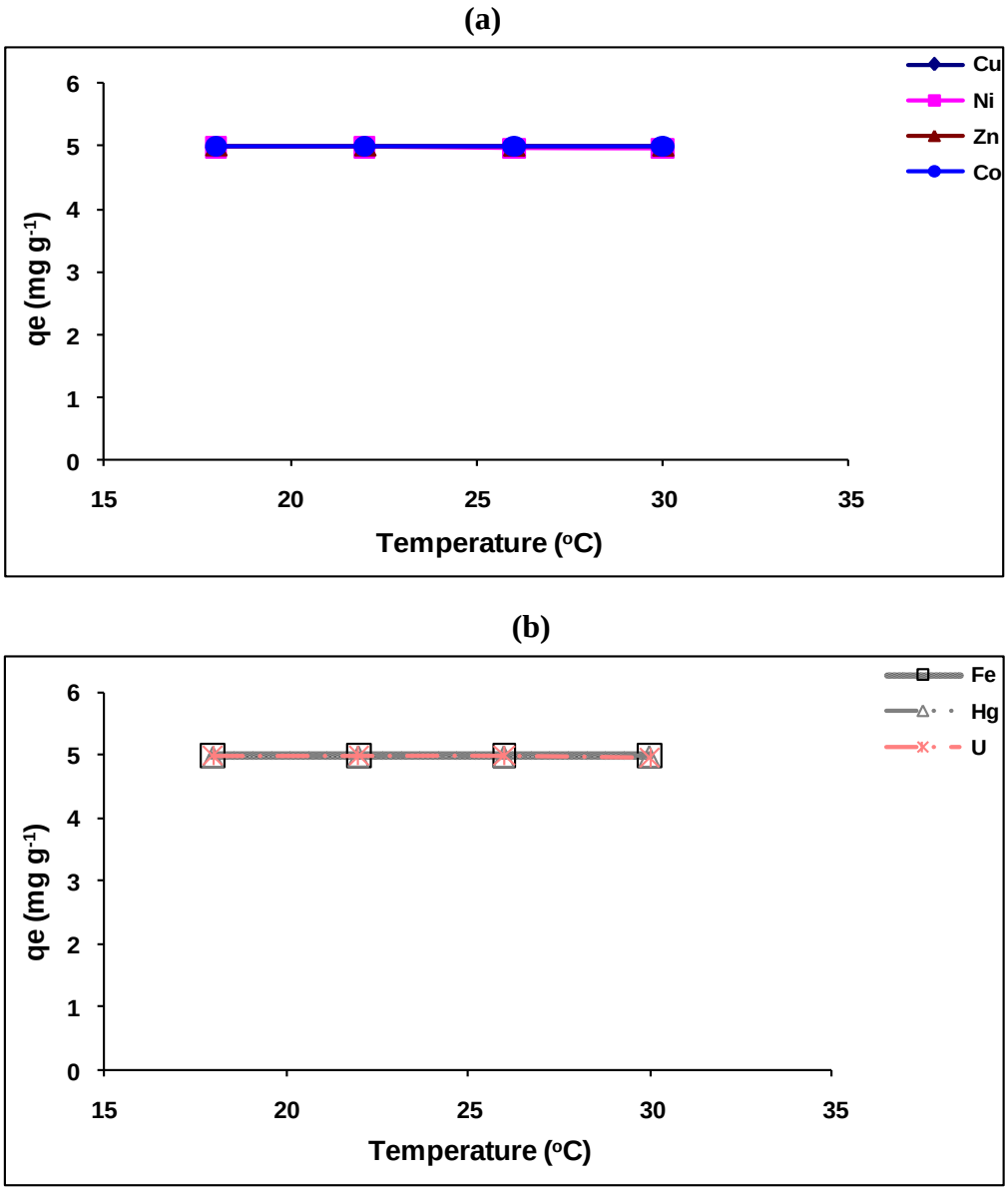
4.2.1.3 Effect of temperature and thermodynamic parameters

i) Effect of contact time

Figure 4.13 illustrates the equilibrium adsorption of metal ions as a function of temperature.

The adsorption isotherms for Cu, Zn, Ni, Co, Fe, U and Hg sorption on modified bentonite with histidine were obtained at four different temperatures while keeping all other parameters, i.e. metal concentration, shaking time and pH constant. In general, the temperature did not affect the adsorption efficiency of the metals studied. The maximum adsorption capacity was attained even at low temperature as shown in Figure 4.13.

This behaviour may be due to the weakness of adsorptive forces between the active sites of the adsorbents and the adsorbate species and also between the adjacent molecules of the adsorbed phase**.**



Figures 4.13 Effect of temperature on adsorption of (a) Cu, Co, Ni, Zn and (b) Fe, Hg and U onto bentonite-histidine in single component solutions (C_i = 100 mg L^{-1}, pH 3, agitation rate = 150 rpm, contact time = 12 h)

ii) Thermodynamic parameters

The thermodynamic parameters calculated from the experimental data are summarized in Table 4.11. The values of activation energies E_a calculated from the Arrhenius equation 3.34, were higher (> 40 kJ mol^{-1}) for Cu, Zn, Ni, Co and U implying a chemisorption process. This is consistent with the results obtained from kinetic modelling where the pseudo second-order best fits the experimental data, confirming chemisorption as the rate-limiting step.

E_a values range from 10 to 33 kJ mol^{-1} for Fe and Hg, suggesting that physisorption should be the limiting step of the adsorption process. These metals are likely to be bound to sites with low energy. The positive values of ΔH^o showed that the sorption of metals on bentonite-histidine is an endothermic process, thus the enthalpy increases with temperature. The negative values of ΔG^o indicate the feasibility and the spontaneity of the adsorption process.

Table 4.11 Thermodynamic parameters for the adsorption of heavy metals on the bentonite-histidine system

	Ea	Δ ***H°***	Δ ***S°***	Δ***G°***			
	kJ mol^{-1}	kJ mol^{-1}	J $(mol\ K)^{-1}$	kJ mol^{-1}			
				291.15 ^oK	**295.15** ^oK	**299.15** ^oK	**303.15** ^oK
Cu	52.49	122.4	479.1	-14.52	-14.99	-15.63	-17.31
Ni	57.46	132.3	496.2	-14.18	14.28	-12.53	-12.39
Zn	74.68	176.1	662.5	-14.18	-18.3	-16.61	-16.79
Co	63.42	146.1	557.7	-19.15	-19.56	-16.07	-16.30
Hg	33.72	77.7	315.4	-16.01	-15.75	-14.95	-14.15
U	104.4	239.6	892.3	-13.22	-19.263	-20.27	-20.29
Fe	10.82	350.4	1257	-18.16	-16.74	-16.34	-16.12

The results in Table 4.11 show that ΔG^o becomes more negative with increasing temperature meaning that sorption is favoured at higher temperature. The values of activation energy, enthalpy change and free energy for the adsorption of heavy metals on bentonite-histidine at each temperature were greater than those obtained at the same temperature for the natural bentonite. This could be due to complex formation between the metal ions and the amine groups attached on the bentonite structure.

As shown in the Table 4.11, ΔS^o values are positive for all the metal ions studied implying their randomness at the interface of the sorbent. Fe and U showed very high entropy values of 1257 and 892.3 J mol K^{-1}, respectively. It was observed that the rate of adsorption (Table 4.12) for the metal ions increases with increasing temperature with Fe being the least affected while mercury was the most affected.

Table 4.12 Rate of metal ions adsorption on bentonite-histidine

Rx rate (h^{-1})				
	291.15 ^{o}K	**295.15** ^{o}K	**299.15** ^{o}K	**303.15** ^{o}K
Cu	0.217	0.221	0.227	0.248
Ni	0.212	0.211	0.183	0.178
Zn	0.286	0.269	0.242	0.241
Co	0.272	0.288	0.234	0.234
Hg	0.198	0.232	0.217	0.217
Fe	0.239	0.241	0.243	0.245
U	0.281	0.284	0.295	0.219

4.2.2 Bentonite-Cysteine

L-Cysteine, an amino acid with the chemical formula $HO_2CCH(NH_2)CH_2SH$, can be synthesized by fungi such as *Saccharomyces cerevisiae* (Takagi *et al.,* 2002). Bentonite-cysteine contains the following functional groups: OH−, −SH− and COO−. The L-Cysteine offers several advantages over protein ligands in terms of economy, ease of immobilization and high adsorption capacity. It interacts with several proteins through its carboxyl, amino and −SH groups at near their isoelectric points (Figure 4.14).

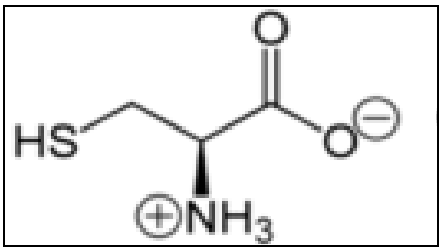


Figure 4.14 Structure of (R)-Cysteine in zwitterionic form at neutral pH.

The isoelectric point of L-cysteine at isoelectric point (pI) = 5.07, with pK(–COOH) = 1.96; pK(–SH) = 8.18 and pK($–NH_3^+$) = 10.28. Due to its *β*-thiol group, L-cysteine is the essential amino acid with the highest affinity to soft metal ions (Sillen and Martell, 1971; Berthon, 1995). L-cysteine molecules are immobilized covalently to the bentonite sorbents. It is specifically sorbed onto the surface sites of bentonite probably via its -NH_3^+ moiety while the thiol group remains free. It is accepted that covalent bonds are formed between the amino groups of the L-cysteine and the Al^{3+} cations at the center of the octahedral layer of the

bentonite structures (Faghihian and Nejati, 2009). Adsorption studies were performed for the bentonite-cysteine system and the results are presented in the following paragraphs.

4.2.2.1 Sorption capacities, pH, isotherms

i) Effect of pH

The pH on adsorption is presented in Figure 4.15. The adsorption capacity of metal ions was constant for the range of the pH range studied (2 to 12). The adsorption capacity for U was observed to increase as the pH rose from 2 to 5. Similar adsorption trends were observed for bentonite-histidine. In fact, the presence of functional groups like –NH–,–SH– and COO^- provided by the cysteine molecule, contribute in enhancing the adsorption capacity of natural bentonite. At low pH, $-NH_3^+$ or $-SH^{2+}$ are protonated simultaneously and compete with the protons for the negative charge. Also, HS (a soft base) has an affinity with soft metals such as Hg while NH_2 and COO^- (hard bases) will preferably bind to hard metals. Metals like Zn, Fe prefer the binding via S and N free binding sites. Studies performed on the metal complexes of cysteine indicate that the preferred binding mode of Cu, Fe and Zn with cysteine is bidentate (sulphur and nitrogens atoms). The maximum adsorption capacity observed at low pH is probably due to the presence of the functional groups which act as binding sites for metals ions.

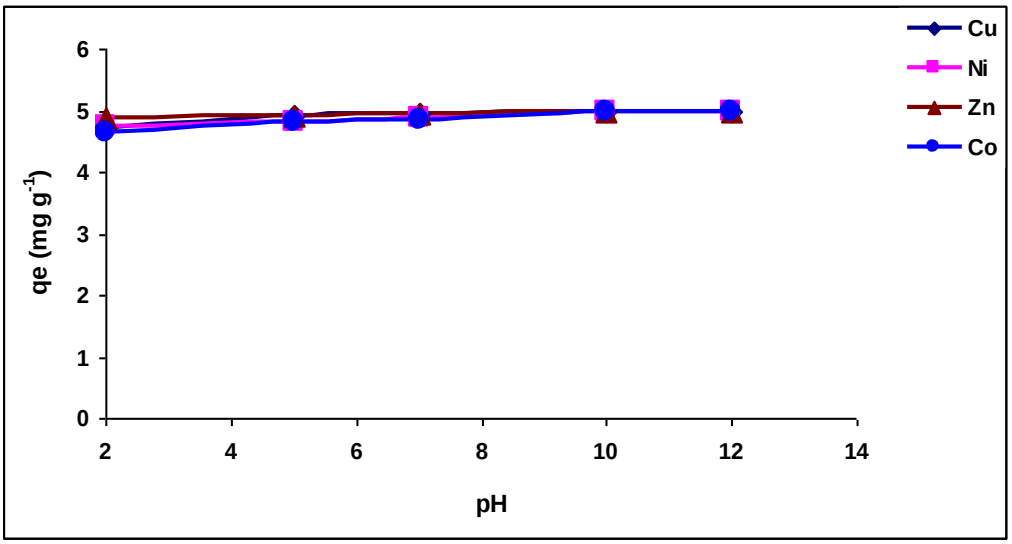
At lower pH, an excess of hydrogen ions can compete effectively with metal ions for binding sites but in this case the thiol and amino groups constitute a shuttle for protons, resulting in an enhancement of adsorption efficiency at low pH. The maximum adsorption capacity for U was reached at pH 5 which is its hydrolysis pH.

Moreover the formation of sparingly soluble polymeric coordination compounds of the sulphur-containing amino acids has to be taken into account. The precipitation of metal-cys complexes is mentioned by Kozlowski *et al.* (1990).

Furthermore, the persistence of Cr in solution depends on the amino acid concentration. Cu(II)-cys complexes are very unstable. They are very rapidly converted to polymeric Cu(I) complexes (Stricks and Kolthoff, 1951). With proceeding oxidation of L-cysteine, the formation of Cu(II)-cystine complexes can occur alternatively.

Due to their ‘soft’ character, thiol group-containing amino acids prefer to coordinate to ‘soft’ metal ions such as Hg(II).

(a)



(b)

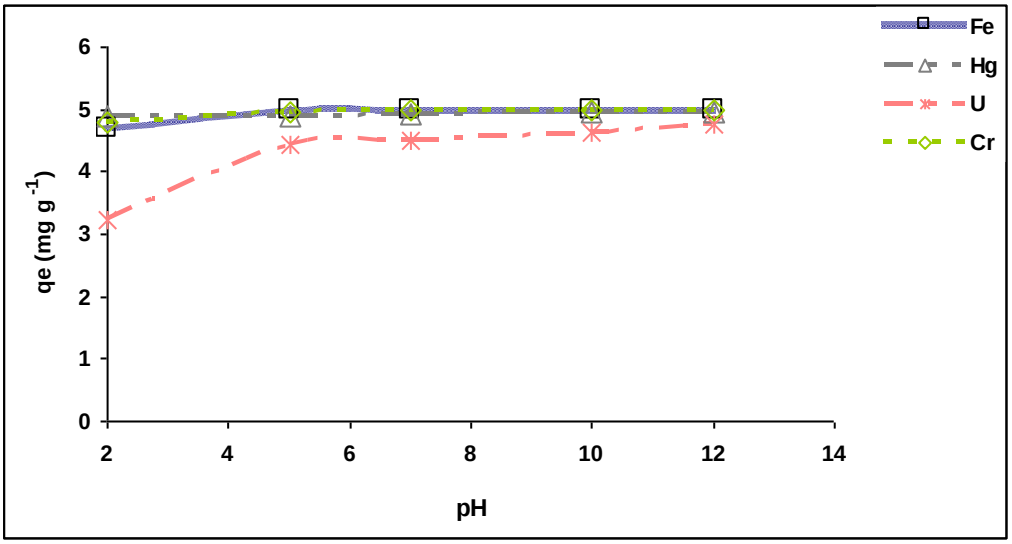
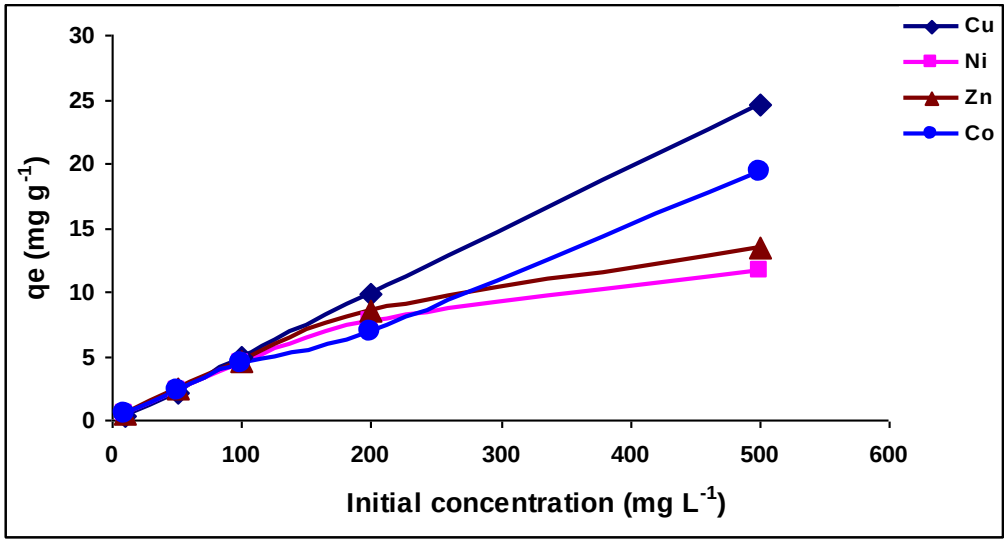


Figure 4.15 Effect of initial pH on adsorption of (a) Cu, Co, Ni, Zn and (b) Cr, Fe, Hg and U onto bentonite-cysteine in single component solutions (C_i = 100 mg L^{-1}, Temp = 298.15±1^oK, agitation rate = 150 rpm, agitation time = 12 h)

ii) Effect of concentration

The effect of different initial concentrations of metal ions on adsorption is shown in Figure 4.16.

(a)



(b)

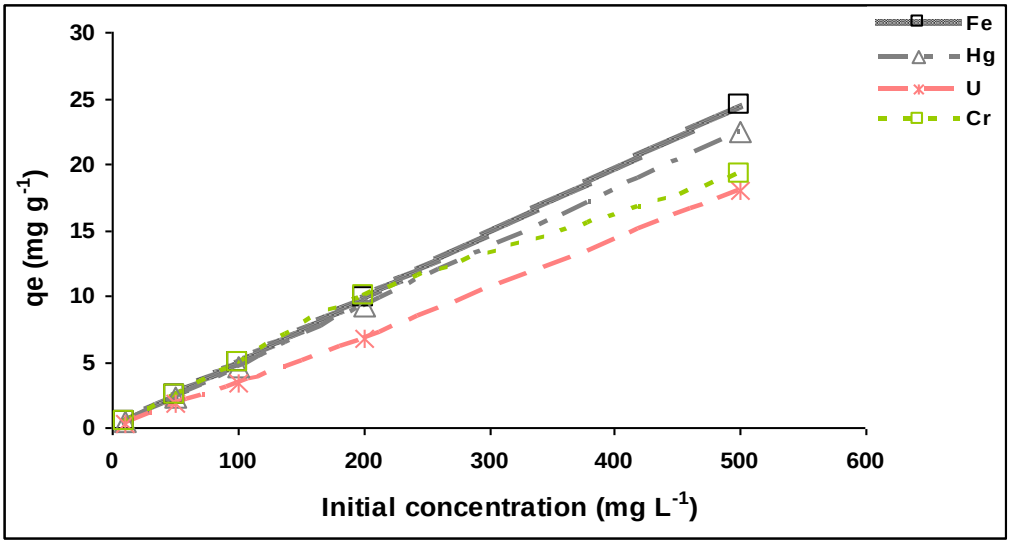


Figure 4.16 Effect of concentration on the adsorption of (a) Cu, Ni, Zn, Co (b) Cr, Fe, Hg and U onto bentonite-cysteine in single-component solutions at pH 3, Temp = 298.15±1^{o}K, agitation rate= 150 rpm, agitation time = 12 h)

The results showed that the adsorption capacity of metals increased with increasing initial concentration. The increase was constant for all the metal ions studied except for Zn and Ni with a slight decrease of the adsorption efficiency at 200 mg L^{-1}. Compared to the adsorption capacity of natural bentonite, the adsorption capacity of metals on bentonite-cysteine was enhanced, likely due to the presence of different functional groups which constitute binding sites for metals. The differences in the uptake level of the metals can be explained in terms of

the difference in the ionic sizes of the metal ions, the nature and distribution of active groups on the substrate and the mode of interaction between the metal ions and the substrate. Such behaviour can be attributed to the maintenance of the fixed number of binding sites in the biosorbent, while increasing the concentration of the metals.

iii) Adsorption isotherms for bentonite-cysteine

Table 4.13 shows the isotherms parameters and correlation coefficients obtained for the isotherms models used to fit the experimental data (non-linear fitting analysis).

Table 4.13 Parameters of the Langmuir, Freundlich and D-R models for the adsorption of metals on the bentonite-cysteine system

Langmuir Isotherms	***Fe***	***Cu***	***Co***	***Hg***	***Ni***	***Zn***	***U***	***Cr***
A	0.002	0.009	0.039	0.048	0.029	0.015	0.239	0.005
B	2.288	0.342	3.582	2.946	4.907	4.749	1.652	2.694
B	1237	38.26	92.08	61.38	166.9	308.4	6.911	4899
qm (mol/kg)	0.439	2.920	0.279	0.339	0.204	0.211	0.605	0.371
ΔGo (kJ/mol)	-17.65	-9.034	-11.21	-10.21	-12.68	-14.21	-4.792	-21.06
Δq (%)	73.33	72.92	72.08	75.49	68.08	67.29	75.78	66.95
R	0.923	0.555	0.753	0.466	0.998	0.997	0.547	0.999
Freundlich Isotherms	***Fe***	***Cu***	***Co***	***Hg***	***Ni***	***Zn***	***U***	***Cr***
A	0.257	0.221	0.182	0.206	0.126	0.068	0.207	0.174
B	0.261	0.331	0.369	0.446	0.368	0.312	0.551	0.245
K_f	1.809	1.661	1.520	1.606	1.338	1.169	1.610	1.495
N	3.839	3.022	2.709	2.239	2.714	3.202	1.818	4.074
ΔGo (kJ/mol)	-9.517	-7.491	-6.714	-5.550	-6.727	-7.938	-4.507	-10.09
Δq (%)	0.100	0.010	27.99	90.59	29.64	10.38	82.56	42.30
R	0.994	0.971	0.980	0.992	0.977	0.997	0.994	0.942
D-R Isotherms	***Fe***	***Cu***	***Co***	***Hg***	***Ni***	***Zn***	***U***	***Cr***
A	-0.017	0.586	-0.314	0.329	-0.377	-0.729	0.179	-0.152
B	-0.004	-0.005	-0.005	-0.007	-0.005	-0.003	-0.009	-0.002
Xm (mol/kg)	0.983	1.797	0.730	1.390	0.686	0.482	1.197	0.859
Es (kJ/mol)	14.27	9.580	10.41	8.556	10.18	12.86	7.442	14.68
Δq (%)	14.85	0.937	28.60	23.61	17.88	24.81	14.66	25.25
R	0.990	0.968	0.973	0.997	0.996	0.995	0.995	0.974
K_d	***Fe***	***Cu***	***Co***	***Hg***	***Ni***	***Zn***	***U***	***Cr***
A	10.20	4.570	6.119	5.422	6.135	7.457	3.818	10.48
B	-4073	2707	-28.78	8832	-274.1	-613.9	3799	-1627
ΔGo (kJ/mol)	-25.07	-11.33	-15.17	-13.44	-15.21	-18.49	-9.464	-25.97
K_{do}	26984	96.58	454.7	226.4	462.1	1732	45.51	35585
Δq (%)	55.83	0.002	126.4	150.4	90.22	165.7	87.81	176.85
R	0.737	0.572	0.749	0.122	0.872	0.711	0.557	0.893

From the Table 4.13, the obtained correlation coefficients are satisfactory ($r > 0.950$) for the Freundlich and the D-R isotherms. The adsorption of Ni, Zn and Cr is also described by the

Langmuir isotherm, assuming the monolayer coverage of the surface. The lowest Δq (0.937 – 28.60%) was obtained with the D-R isotherm.

Based on the correlation coefficient, all the metals studied have a correlation > 0.950 for the Freundlich and the D-R isotherms, suggesting that the adsorption occurs on a heterogeneous surface where the energy is not constant for all the binding sites. The maximum amount adsorbed calculated from the Langmuir isotherm is in the following sequence: Cu > U > Fe > Cr > Hg > Co > Zn > Ni. The selectivity of the metal ions depends on the functional groups which constitute the binding site. A low proportion of Ni was loaded, indicating lower stabilities of the Ni-amino acid complexes formed in solution or expressing a less effective competition of the amino acids with the metal-binding groups of the bentonite-cysteine.

The high correlation coefficient obtained with the Dubinin-Radushkevich isotherm demonstrates the heterogeneity character of the process. The values of the mean free energy Es of sorption (D-R isotherm) in all cases were found to be in the range of 8–16 kJ mol^{-1}, which are within the energy ranges of ion exchange reaction mechanism. The values of *n* obtained from the Freundlich isotherm were in the range of 1.818 to 4.074, 1/n < 1 confirming a beneficial adsorption.

The maximum adsorption capacities (mol Kg^{-1}) obtained for the Langmuir isotherm are as follows: Cu (2.920) > U (0.605) >Fe (0.439) > Cr (0.371) > Hg (0.339) > Co (0.279) > Zn (0.211) > Ni (0.204). The variations of Gibbs free energy determined based on the distribution coefficient have values ranging from -9.464 to -25.97 kJ mol^{-1}, showing that the adsorption process occurred spontaneously.

The selectivity obtained based on the distribution coefficient (L Kg^{-1}) is: Cr (35585) > Fe (26984) > Zn (1732) > Ni (462.1) > Co (454.7) > Hg (226.4) > Cu (96.58) > U (45.51). The values of the distribution coefficients were high for Cr, Fe and Zn, indicating the presence of stronger bonds.

4.2.2.2 Effect of contact time and kinetics of adsorption

i) Effect of contact time

The kinetic results obtained from batch experiments were analysed using different kinetic models. Figure 4.17 shows the change in the adsorption capacity of metal ions on bentonite-cysteine as a function of time using 1 g of biosorbent. The initial concentration, temperature and agitation speed were fixed at 100 mg L^{-1}, 25ºC and 150 rpm, respectively. The initial pH

was adjusted to 3. Two stages of the different sorption rate could be marked out in the sorption kinetics of the metal ions onto bentonite-cysteine.

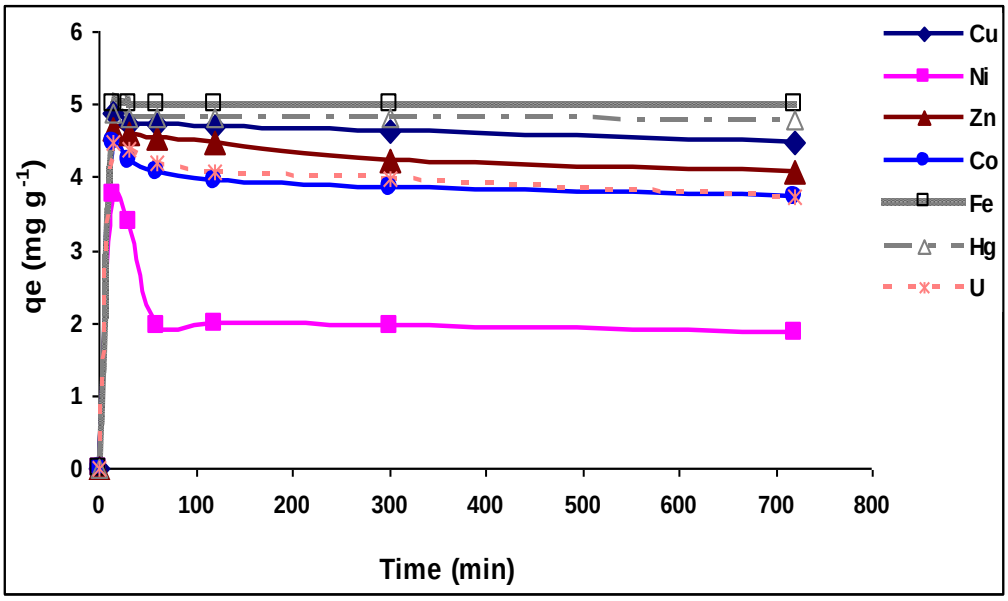


Figure 4.17 Effect of contact time on adsorption of Cu, Ni, Zn, Co, Cr, Fe, Hg and U onto bentonite-cysteine in single component solutions (C_i = 100 mg L^{-1}, Temp = 298.15±1^{o}K, agitation rate = 150 rpm).

The first one corresponds to the period of fast adsorption occurring during the first 30 minutes when 99% of the metal ions are being sorbed. The second stage includes a slow adsorption period with a low sorption rate. It was observed that the concentration of metal ions in the aqueous solution decreased rapidly at the incipient stage of adsorption and then reached almost equilibrium in about 30 minutes. This indicates that with passage of time, a higher fraction of metal ions migrates from the bulk solution through the adsorbent boundary layer onto the active sites of the adsorbent and is adsorbed. This enhanced sorption of the metal ion with increase in agitation time may be due to a decrease in boundary layer resistance to mass transfer in the bulk solution and an increase in kinetic energy of the hydrated metal ion. Thereafter, the reaction proceeded at a slower rate until equilibrium was reached and then almost stayed constant. A similar trend was observed for Ni as was observed in the bentonite-histidine system.

The parameters of the kinetic models with their corresponding coefficients of determination are calculated and summarized in Table 4.14. The results indicate that the pseudo second-order kinetic model gives somewhat a better fit to the data. It may attest to the complicated

and heterogeneous nature of interaction between the modified bentonite surface and the metals.

ii) Kinetic modelling of adsorption onto bentonite-cysteine

In order to investigate the kinetics of adsorption of metal ions on bentonite-cysteine, different models were used as for the previous cases. The kinetic models, the values of the parameters, and the correlation coefficients obtained using non-linear regression are listed in Table 4.14.

It was found that the pseudo-second-order model gave the highest values of correlation coefficients and predicted *q*e more accurately than the other four models investigated. Therefore, the pseudo-second order model could be used for the prediction of the kinetics of adsorption of metal ions on bentonite-cysteine with Δq (0.002-18.31%).

From the correlation coefficient values above, the adsorption of Ni ions on the bentonite-cysteine can be described by the pseudo first and second-order as well as by the film diffusion models whereas the adsorption of Cu, Co and U followed the pseudo second-order and Elovich kinetics.

The calculated values of q_e from the pseudo-second order kinetics model were higher than those calculated from the pseudo-first order kinetics model. Besides, the rate constants of pseudo-second order (k_2) were found to be in the range of 0.237 - 3847 g (mg min) $^{-1}$ and a higher rate constant k_2 was obtained for Fe. A similar trend was observed for natural bentonite.

The adsorption kinetics of Ni on bentonite-cysteine can be described by the film diffusion model with a correlation coefficient of 0.961. In this case, the film and pore diffusion equations (Eq. 4.4 and 4.5, respectively) were used to check whether the diffusion step controlled the ion exchange process or not (Argun, 2008).

$$D_f = 0.23\, r_0\, \delta\, q_e / t_{½} \quad (4.4)$$

$$D_p = 0.03\, r_0^2 / t_{½} \quad (4.5)$$

where: D_f is the film diffusion coefficient (cm^2/s), D_p the pore diffusion coefficient (cm^2/s), r_0 the radius of zeolite (0,001 cm), δ the film thickness (0,001 cm, assuming geometry of the spherical particles) and $t_{½}$ is the half time for the ion-exchange process (min). The half time ($t_{½}$) was calculated from the time requested for the ion-exchange process, which was determined from the quadratic equation $t = A + B\, q_e + C\, q_e^2$, by ploting t versus q_e (using Curve Expert 32 software).

Table 4.14 Kinetic constants for the adsorption of metal ions on bentonite-cysteine

Pseudo-first order							
	Fe	***Cu***	***Co***	***Hg***	***Ni***	***Zn***	***U***
A	-4.477	-2.259	-1.923	-3.310	-1.505	-2.090	-2.632
B	-0.011	-0.004	-0.004	-0.004	-0.004	-0.006	-0.005
qe (mol/kg)	0.002	0.006	0.012	0.001	0.031	0.008	0.002
K_1	0.026	0.009	0.008	0.009	0.008	0.014	0.012
Δq (%)	92.55	88.21	83.01	91.37	53.49	84.54	84.02
R	0.557	0.629	0.758	0.493	0.961	0.828	0.862
Pseudo – second order							
	Fe	***Cu***	***Co***	***Hg***	***Ni***	***Zn***	***U***
A	0.036	48.91	131.5	53.62	943.6	58.62	373.7
B	11.17	13.04	13.13	41.12	14.94	13.98	53.01
q_e (mol/kg)	0.089	0.077	0.076	0.024	0.067	0.072	0.018
K_2	3480	3.479	1.311	31.52	0.237	3.335	7.517
Δq (%)	0.002	1.447	3.992	1.084	18.31	1.234	1.464
R	1.000	0.999	0.999	1.000	0.992	1.000	1.000
Elovich model							
	Fe	***Cu***	***Co***	***Hg***	***Ni***	***Zn***	***U***
A	0.014	0.010	0.008	0.004	-0.002	0.008	0.002
B	0.016	0.013	0.013	0.004	0.009	0.012	0.003
B	64.13	76.32	79.34	237.9	108.4	81.69	314.4
A	0.038	0.029	0.023	0.010	0.007	0.024	0.006
Δq (%)	16.80	14.86	11.96	16.37	13.51	13.53	12.94
R	0.775	0.953	0.997	0.848	0.920	0.916	0.976
Intraparticle diffusion model							
	Fe	***Cu***	***Co***	***Hg***	***Ni***	***Zn***	***U***
A	0.036	0.028	0.024	0.010	0.006	0.024	0.006
B	0.005	0.004	0.004	0.001	0.003	0.004	0.001
Id	0.036	0.028	0.024	0.010	0.006	0.024	0.006
Kp	0.005	0.004	0.004	0.001	0.003	0.004	0.001
Δq (%)	29.27	29.93	30.76	29.44	36.87	30.22	30.57
R	0.721	0.747	0.788	0.723	0.948	0.782	0.799
Film diffusion							
	Fe	***Cu***	***Co***	***Hg***	***Ni***	***Zn***	***U***
A	-2.341	-0.792	-0.670	-0.881	-0.568	-1.075	-0.931
B	-0.028	-0.008	-0.005	-0.012	-0.001	-0.007	-0.006
If	-2.341	-0.792	-0.670	-0.881	-0.568	-1.075	-0.931
Kf	0.028	0.008	0.005	0.012	0.001	0.007	0.006
Δq (%)	59.88	53.63	50.79	60.95	53.23	45.36	45.58
R	0.557	0.629	0.758	0.493	0.961	0.828	0.862

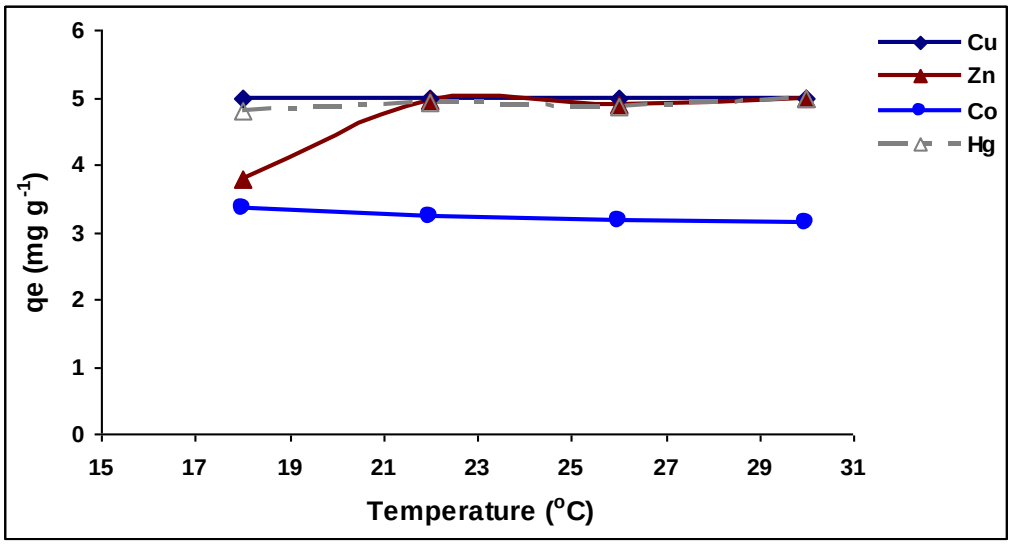
The calculated values of film diffusion coefficient (D_f) and pore diffusion coefficient for the adsorption of Ni were $5.179 * 10^{-7}$ cm^2 s^{-1} and $9.999 * 10^{-1}$ cm^2 s^{-1}, respectively. According to Michelson *et al*. (1975), D_f values should be in the range of 10^{-6} to 10^{-8} cm^2 s^{-1} for film diffusion to be the rate-limiting factor and D_p values should be in the range of 10^{-11} to 10^{-13} cm^2 s^{-1} for pore diffusion to be the rate-limiting factor. From these results it can be concluded that Ni diffusion through the film from the bentonite-cysteine surface is the rate-limiting step.

4.2.2.3 Effect of temperature and thermodynamic parameters

i) Effect of temperature

Figure 4.18 shows the equilibrium adsorption of metal ions as a function of the temperature. The initial concentration was fixed at 100 mg L^{-1} and initial pH was adjusted to 3. The amount of metals adsorbed on the bentonite-cysteine was constant at different temperatures (18 to 30^{o}C), except for Zn. This behaviour may be due to the weakness of adsorptive forces between the active sites of the adsorbents and the adsorbate species and also between the adjacent molecules of the adsorbed phase. This will be confirmed later by assessing the activation energy obtained from the process. The maximum adsorption capacity for Zn and U was reached at 22^{o}C and this remained constant up to 30^{o}C. Co and Ni had the lowest adsorption capacity compared to other metal ions.

(a)



(b)

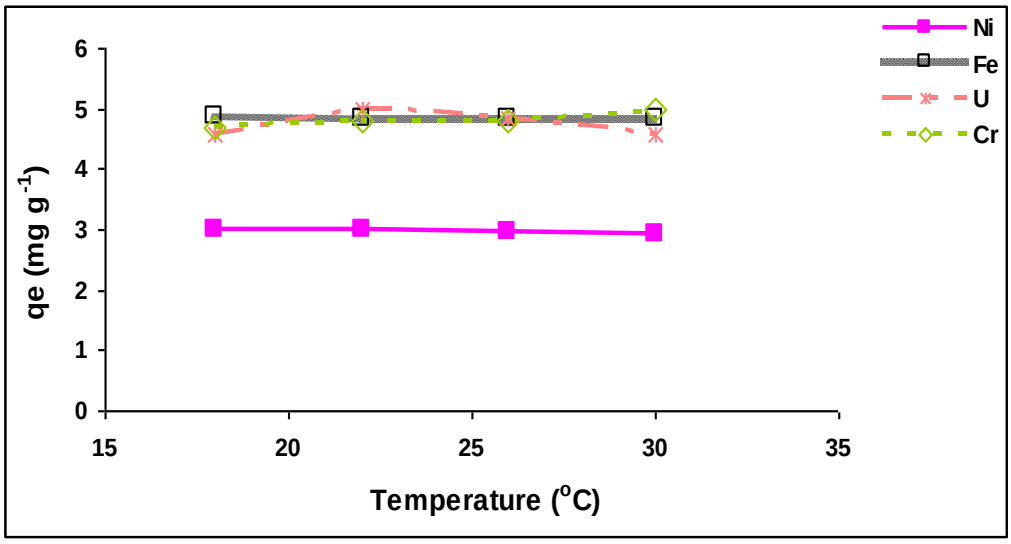


Figure 4.18 Effect of temperature on adsorption of (a) Cu, Zn, Hg, Co and (b) Cr, Ni, Fe, and U onto bentonite-cysteine in single component solutions (C_i = 100 mg L^{-1}, pH 3, agitation rate = 150 rpm, contact time = 12 h)

ii) Thermodynamic parameters of metal adsorption onto bentonite-cysteine

Thermodynamic parameters such as activation energy change in free energy (ΔG°) kJ mol^{-1}, enthalpy (ΔH°) kJ $mol^{-1}$and entropy (ΔS°) J K^{-1} mol^{-1} were determined and presented in Table 4.15.

Table 4.15 Thermodynamic parameters for the adsorption of metal ions on bentonite-cysteine

	Ea kJ mol^{-1}	ΔH^o kJ mol^{-1}	ΔS^o J(K $mol)^{-1}$	ΔG^o kJ mol^{-1}			
				291.15 ^oK	**295.15** ^oK	**299.15** ^oK	**303.15** ^oK
Cu	5.998	13.81	92.81	-14.92	-13.16	-12.96	-12.21
Ni	4.454	10.26	72.53	-1.014	-0.955	-0.941	-0.872
Zn	-4.208	-9.690	22.81	-2.771	-11.05	-13.38	-14.06
Co	10.23	23.57	85.59	-1.702	-1.485	-1.302	-1.350
Fe	2.384	5.489	49.04	-8.541	-8.415	-8.416	-8.294
Hg	-20.49	-47.19	-131.2	-7.635	-8.177	-10.57	-15.79
U	3.778	8.710	9.719	-10.78	-8.850	-8.523	-5.870
Cr	-25.73	-59.27	-176.3	-6.624	-7.834	-7.958	-13.44

The values of activation energy were positive and in the range of 4 to 10 kJ mol^{-1}, indicating the favourability of physisorption. Negative values of activation energy were obtained for Zn, Hg and Cr. The positive values of ΔH° show the endothermic nature of adsorption for Cu, Ni, Co, Fe and U. The adsorption of Zn, Hg and Cr was exothermic. In the case of physical adsorption, while increasing the temperature of the system, the extent of metal ion adsorption increases, thus ruling out the possibility of chemisorption. However, the low ΔH° value depicts that metal ions are physisorbed onto the adsorbent. The values of ΔG^o were negative for the metals, indicating the feasibility of the adsorption process and the spontaneous nature of the adsorption. In general, the Gibbs free energy decreases slightly with the increases of temperature, except for the adsorption of Zn, Hg and Cr where the free energy increases with the temperature.

As shown in Table 4.15, the change of entropy (ΔSº) was found low and positive for most of the metals, implying an increase of randomness at the solid-liquid interface during the adsorption process. A decrease of degrees of freedom was observed for Hg and Cr with negative values of entropy. The rate of adsorption of metal ions on bentonite-cysteine decreases with an increase in temperature. The calculated values are given in Table 4.16.

Table 4.16 Rate of the adsorption of metal ions on bentonite-cysteine

Rx rate (h^{-1})				
	291.15 ^{o}K	**295.15** ^{o}K	**299.15** ^{o}K	**303.15** ^{o}K
Cu	0.445	0.441	0.437	0.435
Ni	0.077	0.076	0.075	0.074
Zn	0.118	0.376	0.422	0.483
Co	0.092	0.087	0.082	0.083
Fe	0.296	0.288	0.285	0.283
Hg	0.266	0.536	0.355	0.293
U	0.207	0.640	0.288	0.202
Cr	0.269	0.267	0.251	0.233

4.2.3 Bentonite-Sorbitol

Sorbitol is a (2*S*, 3*R*, 4*R*, 5*R*)-hexane-1, 2, 3, 4, 5, 6-hexol with the following structure (Figure 4.19):

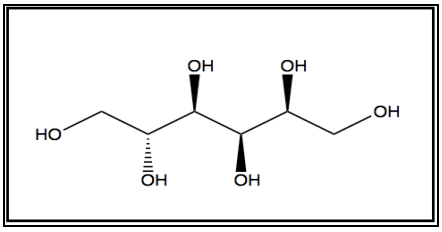


Figure 4.19 Structure of sorbitol

Sorbitol can be synthetised by fungi and the presence of OH^{-} functional groups can be used to bind metal ions by electrostatic attraction. Sorbitol was also used in this study to modify the bentonite. Adsorption of heavy metals was performed on the synthetised biosorbent and different parameters were investigated as for the previous studies. The results are given in the coming paragraphs.

4.2.3.1 Sorption capacities, pH, isotherms

i) Effect of pH

Figure 4.20 illustrates the effect of pH on the adsorption of heavy metal ions on bentonite-sorbitol. The pH values of the investigated solutions ranged from 2 to 12.

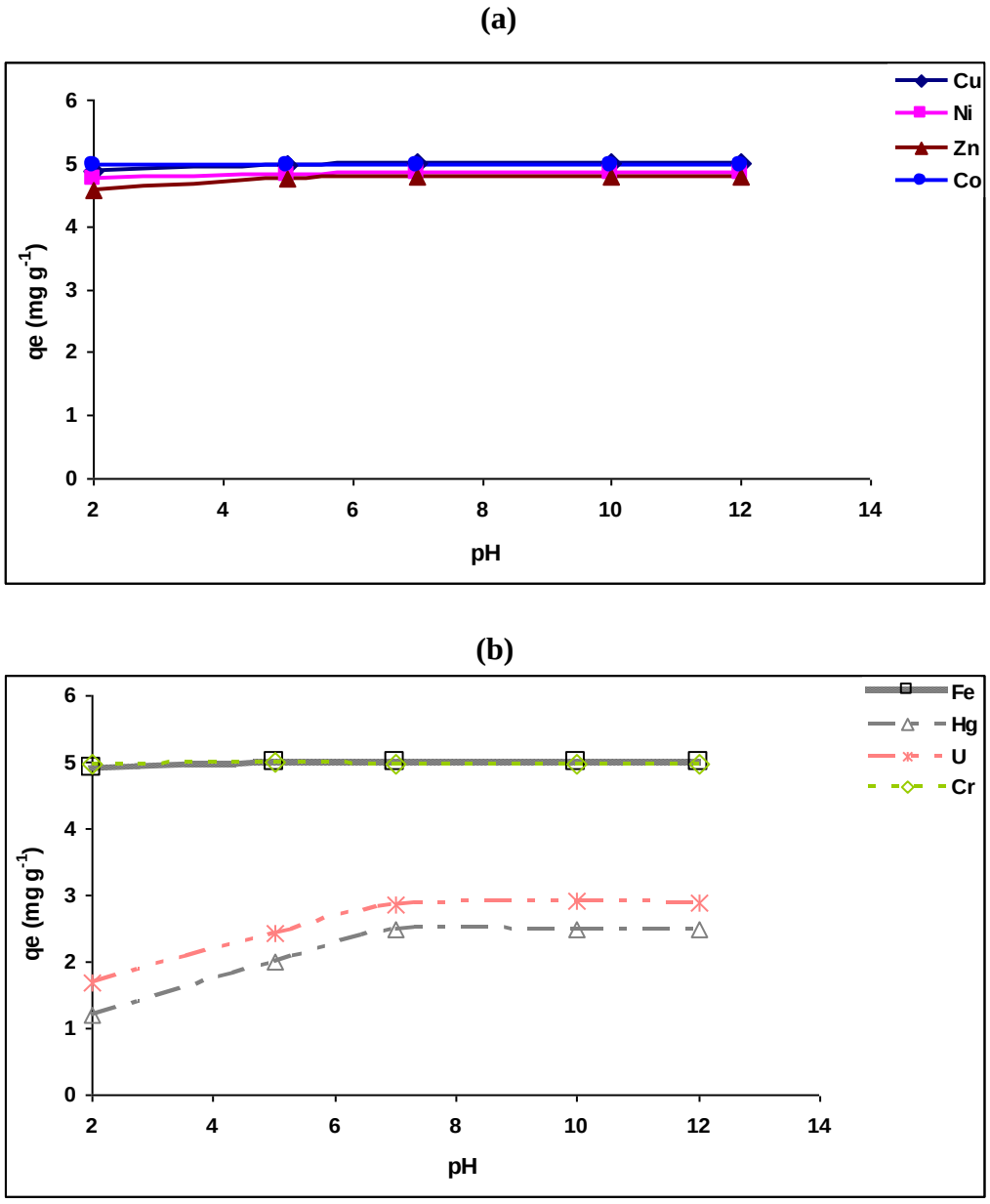


Figure 4.20 Effect of initial pH on adsorption of (a) Cu, Ni, Zn, Co and (b) Fe, Cr, Hg and U onto bentonite-sorbitol in single component solutions (Ci = 100 mg L^{-1}, Temp = 298.15±1^{o}K, agitation rate = 150 rpm, agitation time = 12 h)

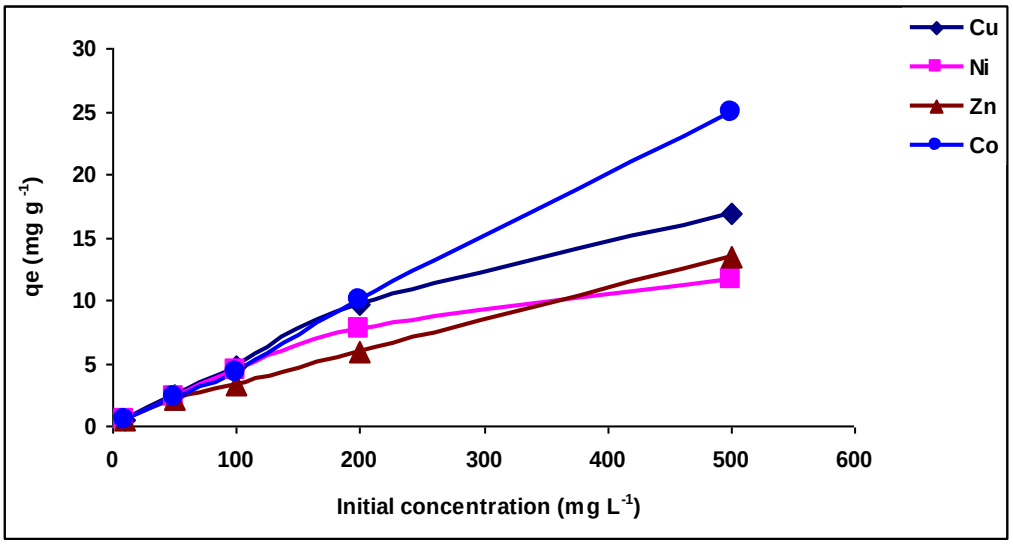
Figure 4.20 (a) and (b) shows that the adsorption capacities of Ni, Zn, Cu Cr, Fe and Co were almost constant for the pH range 2 to 12. U and Hg, with a low adsorption capacity, reached maximum adsorption at pH 7. Low uptake was observed for these ions at low pH due to competition of the protons for the binding sites. Also, –OH being a hard base prefers to bind with hard acids such as Co, Cr and Fe. This justifies the high adsorption capacity of these metal ions even at low pH. Hg, being a soft metal, does not have high affinity for this

functional group. The high amount adsorbed at high pH is a combination of adsorption and precipitation since at high pH; there is formation of metal-hydroxyl species.

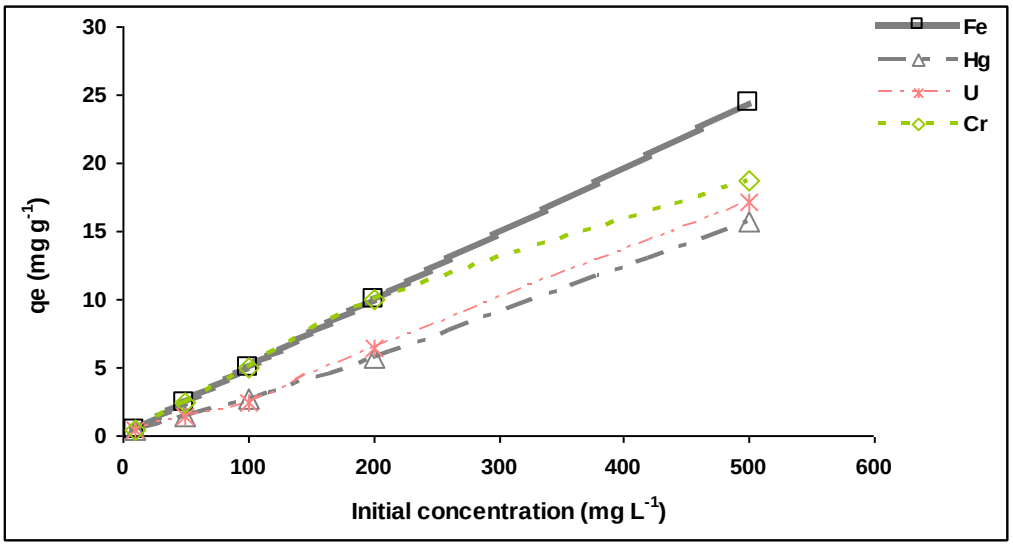
ii) Effect of concentration

It is evident from Figure 4.21 (a) and (b) that the amount of metal ions adsorbed increases constantly with the concentration of metals. A slight decrease in adsorption capacity was observed for Ni, Cu and Cr at 200 mg L^{-1}.

(a)



(b)



Figures 4.21 Effect of concentration on the adsorption of (a) Cu, Ni, Zn, Co and (b) Fe, Cr, Hg and U onto bentonite-sorbitol in single component solutions (at pH 3, Temp = 298.15±1^{o}K, agitation rate= 150 rpm, agitation time= 12 h)

iii) Isothermic modelling of the adsorption of metal ions on bentonite-sorbitol

The results obtained for the initial concentration were used for isothermic modelling. Three adsorption isotherm models were used: Langmuir, Freundlich and Dubinin- Radushkevich. The parameters and correlation coefficients are listed in Table 4.17.

The adsorption data were found to be in accordance with the Langmuir, the Freundlich and the D-R models. Detailed analysis of the regression coefficients showed that the Langmuir described the process with r > 0.975 except for Zn and U with a regression coefficient below 0.900. The Langmuir isotherm model suggests that the uptake occurs on a homogeneous surface by monolayer sorption without interaction between adsorbed ions.

The Freundlich isotherm model fitted well the process except for Hg, U and Cr with r < 0.950. The Freundlich model is a case for heterogeneous surface energies and it gives an exponential distribution of active sites. The Freundlich constants K_f and n, which respectively indicate the adsorption capacity and the adsorption intensity, were calculated and the values are presented in Table 4.17.

K_f values range from 1.812 to 1.038, the difference in magnitude is not significant. The value of $1/n$ less than unity is an indication that significant adsorption takes place at low concentration but the increase in the amount adsorbed with concentration becomes less significant at higher concentrations and vice versa (Teng and Hsieh, 1998).

The adsorption mechanism is also well described by the D-R model for Cu, Co, Ni and U with high correlation coefficients values (> 0.950) except for Hg. The modeling results of the experimental data of the adsorption equilibrium experiments suggest that the adsorption of metal ions occurs by monolayer coverage on heterogeneous surface energies. The maximum adsorption capacities (mol kg^{-1}) obtained on Langmuir isotherm are as follows: Fe (0.478) > Co (0.443) > Cr (0.359) > Cu (0.276) > Zn (0.215) > Ni (0.204) > Hg (0.135) > U (0.102). A different trend was obtained with the D-R isotherm (X_m, maximum sorption capacity) , with the following sequence: Co (1.425) > Cr (1.008) > Fe (0.954) > Cu (0.850)> Ni(0.686) > Hg (0.676) > U (0.599) > Zn(0.373).

The variations of Gibbs free energy values determined based on the distribution coefficient were negative with the values ranging from -7.604 to -20.38 kJ mol^{-1}. This indicates that the process occurs spontaneously.

Based on normalized standard deviation, the experimental adsorption isotherms are best described by D-R models (Δq = 0.973 – 82.51 %) and, to a lesser extent, the Freundlich models (Δq= 23 – 86 %).

The values of the distribution coefficients were higher for Cr, Fe and Co, indicating the presence of strong bonds. Based on the distribution coefficient K_{do}(L kg^{-1}), the selectivity was as follows: Cr (4199) > Fe (3723) > Co (1540) > Cu (393.7) > Ni (166.2) > Zn (130.9) > U (21.49) > Hg (19.55). These results confirm the weak bonds between the sorbent and metal ions like Hg and U.

Table 4.17 Isothermic modelling for the adsorption of metal ions on bentonite-sorbitol

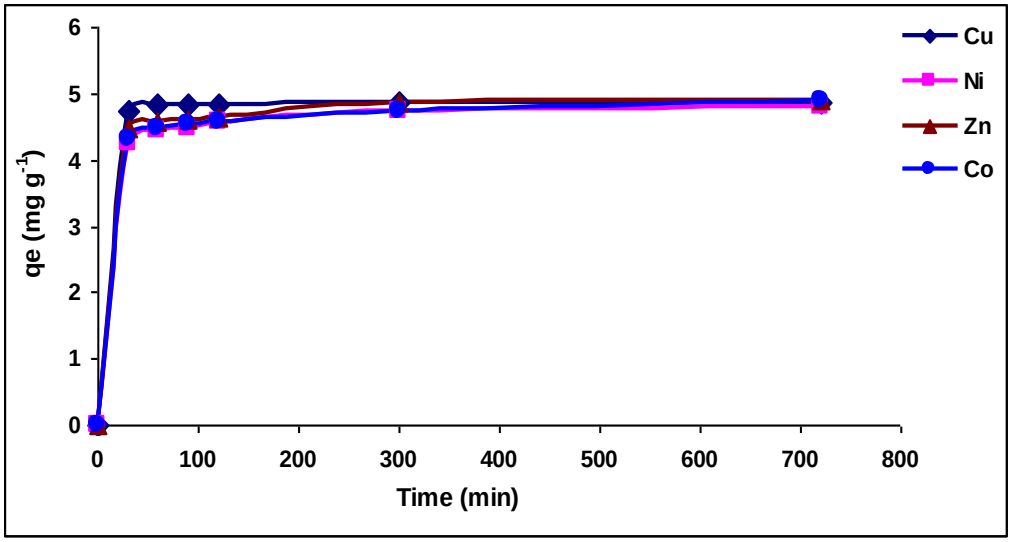
Langmuir Isotherms	***Fe***	***Cu***	***Co***	***Hg***	***Ni***	***Zn***	***U***	***Cr***
A	0.004	0.063	0.007	0.399	0.167	0.225	0.352	0.047
B	2.089	3.619	2.255	7.401	4.908	4.649	9.783	2.780
b	604.9	58.03	394.7	18.52	29.42	20.69	27.79	80.04
qm (mol/kg)	0.478	0.276	0.443	0.135	0.204	0.215	0.102	0.359
ΔGo (kJ/mol)	-15.88	-10.07	-14.82	-7.236	-8.383	-7.511	-8.241	-10.86
Δq (%)	96.34	96.53	96.29	96.04	96.45	96.19	96.05	96.86
r	0.985	0.997	0.967	0.975	0.998	0.838	0.306	0.999
Freundlich Isotherms	***Fe***	***Cu***	***Co***	***Hg***	***Ni***	***Zn***	***U***	***Cr***
A	0.258	0.169	0.256	0.142	0.126	0.016	0.125	0.168
B	0.265	0.341	0.289	0.554	0.368	0.359	0.543	0.253
K_f	1.812	1.538	1.804	1.391	1.338	1.038	1.335	1.474
n	3.776	2.933	3.454	1.805	2.714	2.183	1.841	3.952
ΔGo (kJ/mol)	-9.360	-7.271	-8.563	-4.476	-6.727	-6.899	-4.565	-9.796
Δq (%)	53.04	51.017	55.3	47.53	37.49	23.99	49.51	86.76
r	0.978	0.958	0.953	0.948	0.977	0.975	0.927	0.887
D-R Isotherms	***Fe***	***Cu***	***Co***	***Hg***	***Ni***	***Zn***	***U***	***Cr***
A	-0.048	-0.169	0.354	-0.391	-0.377	-0.987	-0.512	0.007
B	-0.005	-0.004	-0.006	-0.008	-0.008	-0.007	-0.008	-0.003
Xm (mol/kg)	0.954	0.850	1.425	0.676	0.686	0.373	0.599	1.008
Es (kJ/mol)	14.09	10.88	11.74	7.765	10.18	11.67	8.063	13.52
Δq (%)	45.72	0.973	43.25	69.76	22.61	62.22	82.51	43.04
r	0.959	0.883	0.967	0.928	0.996	0.950	0.905	0.941
K_d	***Fe***	***Cu***	***Co***	***Hg***	***Ni***	***Zn***	***U***	***Cr***
A	8.222	5.976	7.339	2.973	5.113	4.874	3.067	8.343
B	-1.649	-482.5	943.5	1941	-274.1	-259.5	2794	-1368
ΔGo (kJ/mol)	-20.38	-14.81	-18.19	-7.371	-12.67	-12.08	-7.604	-20.68
Kdo	3723	393.7	1540	19.55	166.2	130.9	21.49	4199
Δq (%)	69.76	66.64	73.63	52.22	61.72	56.26	50.83	77.03
r	0.614	0.873	0.872	0.096	0.873	0.617	0.144	0.977

4.2.3.2 Effect of contact time kinetics of adsorption

i) Effect of contact time

The results of the effect of contact time on the adsorption of the metal ions on bentonite-sorbitol are illustrated in Figure 4.22. The adsorption of metal ions studied occurred in two stages, as observed in the previous cases. The first stage was the immediate solute uptake achieved within 30 minutes, followed by the second stage, i.e. the subsequent uptake of solute which continued for a long time period.

(a)



(b)

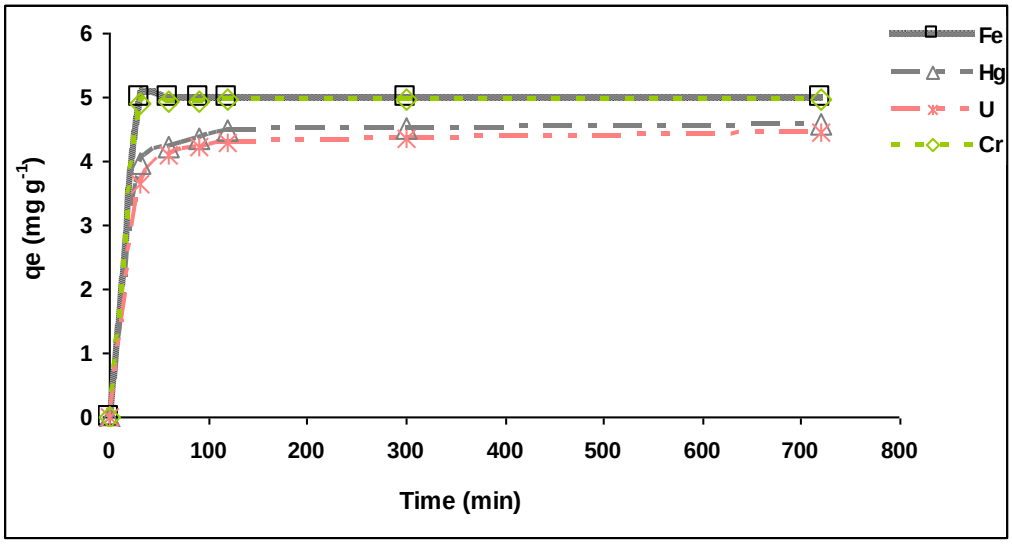


Figure 4.22 Effect of contact time on the adsorption of (a) Cu, Ni, Zn, Co and (b) Cr, Fe, Hg and U onto bentonite-sorbitol in single component solutions (C_i = 100 mg L^{-1}, Temp = 298.15±1^oK, agitation rate = 150 rpm)

The initial faster rate may be due to the availability of the uncovered surface area of the adsorbent initially, since adsorption kinetics depends on the surface area of the adsorbent. In addition, the variation in the amount of metal ion adsorbed by the adsorbent could be related to the nature and concentration of the surface groups (active sites) responsible for interaction with the metal ions.

ii) Kinetic modelling of adsorption onto bentonite-sorbitol

In order to investigate the mechanism of sorption of metal ions by the modified bentonite with sorbitol, different kinetic models were used, including: pseudo first-order, pseudo second-order, Elovich, intraparticle diffusion and film diffusion. The parameters and correlation coefficients are summarized in Table 4.18.

Table 4.18 Kinetic modelling of the adsorption of metal ions on bentonite-sorbitol

Pseudo-first order								
	Fe	***Cu***	***Co***	***Hg***	***Ni***	***Zn***	***U***	***Cr***
A	-2.331	-2.754	-2.004	-2.714	-1.960	-2.048	-2.752	-2.805
B	-0.008	-0.010	-0.004	-0.006	-0.006	-0.006	-0.005	-0.007
q_e (mol/kg)	0.005	0.002	0.010	0.002	0.011	0.009	0.002	0.002
K_1	0.018	0.023	0.012	0.014	0.014	0.014	0.011	0.015
Δq (%)	88.66	90.78	85.08	86.63	83.03	84.13	86.28	91.43
r	0.808	0.185	0.743	0.787	0.869	0.854	0.774	0.613
Pseudo – second order								
	Fe	***Cu***	***Co***	***Hg***	***Ni***	***Zn***	***U***	***Cr***
A	957.9	5.024	1092	3860	1088	1178	4779	879.9
B	6.973	13.071	7.411	27.02	7.533	8.202	32.77	6.475
q_e (mol/kg)	0.143	0.076	0.135	0.037	0.133	0.122	0.031	0.154
K_2	0.051	34.01	0.051	0.189	0.0521	0.057	0.225	0.047
Δq (%)	38.79	0.498	37.93	37.81	37.81	38.04	37.50	39.14
r	1.000	1.000	0.999	0.998	1.000	1.000	0.998	1.000
Elovich model								
	Fe	***Cu***	***Co***	***Hg***	***Ni***	***Zn***	***U***	***Cr***
A	0.082	0.012	2.280	0.017	0.063	0.061	0.013	0.094
B	0.001	0.013	0.063	0.001	0.003	0.002	0.001	0.005
b	884.6	75.11	330.5	1105	335.3	443.7	1078	2930
a	4512	0.032	3461	1819	4274	3265	1237	2861
Δq (%)	0.600	16.34	0.312	2.078	0.839	0.518	2.865	0.164
r	0.902	0.943	0.997	0.891	0.975	0.985	0.983	0.904
Intraparticle diffusion model								
	Fe	***Cu***	***Co***	***Hg***	***Ni***	***Zn***	***U***	***Cr***
A	0.034	0.030	0.028	0.008	0.028	0.026	0.006	0.038
B	0.005	0.004	0.004	0.001	0.004	0.004	0001	0.005
Id	0.034	0.030	0.028	0.008	0.028	0.026	0.006	0.038
Kp	0.005	0.004	0.004	0.001	0.004	0.004	0.001	0.005
Δq (%)	29.56	29.41	30.26	30.25	30.15	29.99	30.54	29.36
r	0.742	0.731	0.768	0.783	0.777	0.766	0.793	0.726
Film diffusion								
	Fe	***Cu***	***Co***	***Hg***	***Ni***	***Zn***	***U***	***Cr***
A	-1.426	-1.798	-0.780	-1.072	-1.079	-1.084	-0.901	-1.301
B	-0.010	-0.013	-0.007	-0.007	-0.006	-0.007	-0.007	-0.014
If	-1.425	-1.797	-0.780	-1.072	-1.078	-1.083	-0.901	-1.301
Kf	0.010	0.0132	0.006	0.007	0.0065	0.0068	-0.007	-0.014
Δq (%)	44.58	43.60	50.31	45.60	44.57	45.08	47.37	53.19
r	0.808	0.784	0.742	0.787	0.869	0.854	0.773	0.613

The experimental data showed good compliance with the pseudo second-order kinetic model ($r \geq 0.998$) for all the metal ions studied. The values of the rate constant, k_2, were found to be very high for Cu 34 L mg^{-1} min^{-1} compared to those for other metals, e.g 0.225 and 0.189 L mg^{-1} min^{-1} for U and Hg, respectively. The adsorption of Co, Ni, Zn and U can be also described by the Elovich kinetic model with a correlation coefficient ($r \geq 0.975$). It can be seen that the initial adsorption rate was in the sequence: Fe (4512) > Ni (4274) > Co (3461)> Zn (3265) > Cr (2861) > Hg (1819) > U (1237) > Cu (0.032).

4.2.3.3 Effect of temperature and thermodynamic parameters

i) Effect of temperature

The effect of temperature on the adsorption of heavy metals ions onto bentonite-sorbitol has been investigated and the results are illustrated in Figure 4.23. The initial concentration was fixed at 100 mg L^{-1} and initial pH was adjusted to 3. The adsorption efficiency increases with increase in temperature. The adsorption of Fe was constant and was not affected by the change of temperature. U and Hg showed a low adsorption capacity, probably due to the nature of functional group on the surface of the adsorbent.

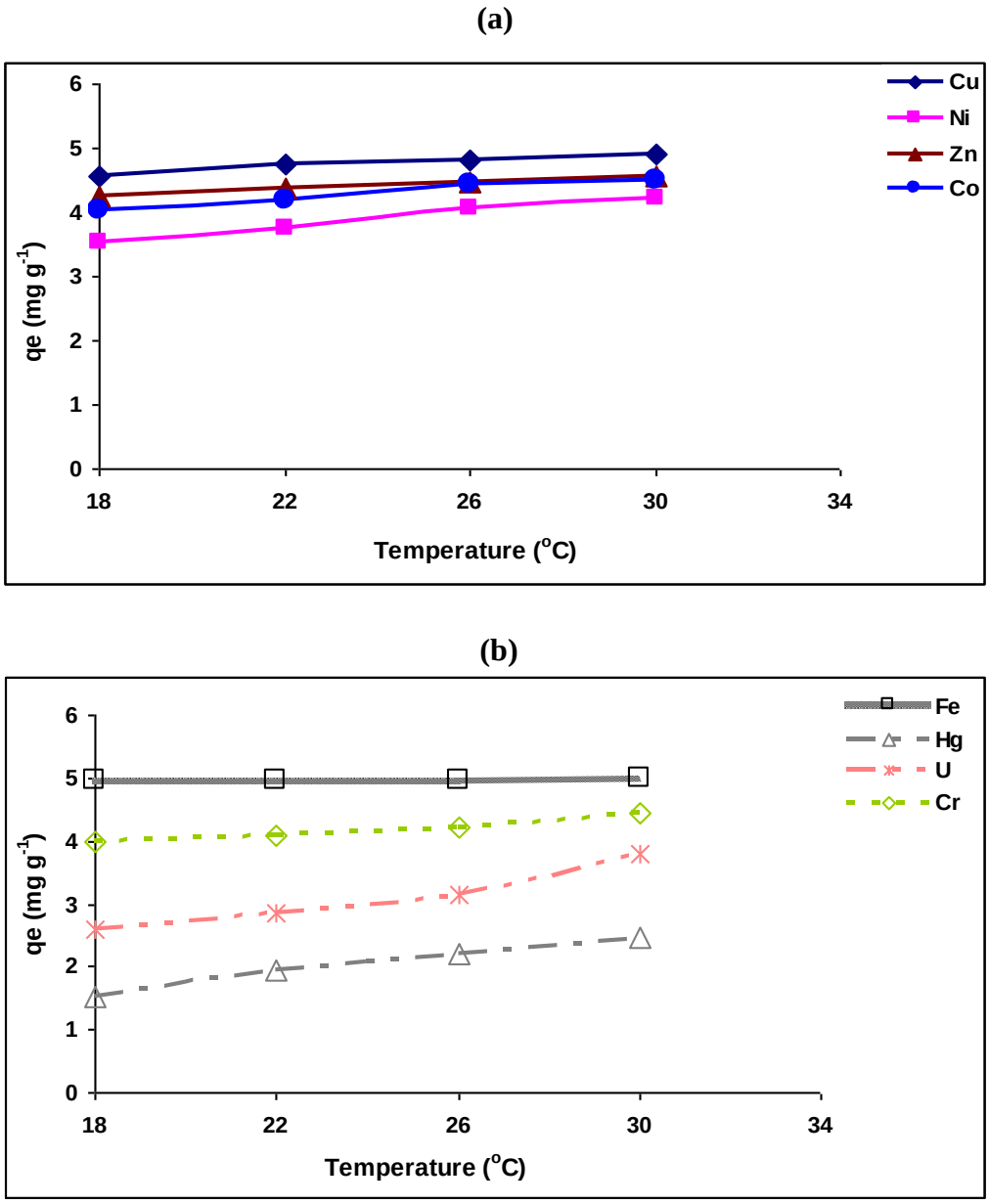


Figure 4.23 Effect of temperature on adsorption of (a) Cu, Ni, Zn, Co and (b) Cr, Fe, Hg and U onto bentonite-sorbitol in single component solutions (C_i = 100 mg L^{-1}, pH 3, agitation rate = 150 rpm, contact time = 12 h)

ii) Thermodynamic parameters for the adsorption of metal ions on bentonite-sorbitol

The thermodynamic parameters such as activation energy, standards Gibbs free energy ΔGº, enthalpy ΔHº and entropy ΔSº were calculated and the results obtained are presented in Table 4.19.

Table 4.19 Thermodynamic parameters for bentonite-sorbitol

	Ea kJ mol^{-1}	ΔH^o kJ mol^{-1}	ΔS^o J(K $mol)^{-1}$	ΔG^o kJ mol^{-1}			
				291.15 ^oK	**295.15** ^oK	**299.15** ^oK	**303.15** ^oK
Cu	93.19	-214.6	-0.703	-7.131	-7.131	-8.234	-9.776
Ni	50.19	-115.6	-0.382	-2.127	-2.670	-3.637	-4.284
Zn	40.18	-92.53	-0.297	-4.154	-4.741	-5.289	-5.981
Co	46.02	-105.9	-0.345	-3.430	-4.039	-5.086	-5.468
Fe	80.10	-184.5	-0.581	-11.50	-12.55	-13.19	-15.27
Hg	48.90	-112.6	-0.386	1.998	1.073	0.590	0.065
U	65.31	-150.4	-0.506	-0.210	-0.724	-1.344	-2.910
Cr	41.58	-95.76	-0.311	-3.280	-3.693	-4.222	-5.162

High activation energies (> 40 kJ mol^{-1}) were obtained for all the metals studied, implying a chemisorption process. This was consistent with the results obtained for the kinetic modelling where the pseudo-second order best fitted the experimental data, confirming chemisorption as the rate limiting step. The enthalpy was found to be negative for the metal ions studied, meaning that the process is exothermic. The negative values of ΔH^o showed that the sorption of metals on bentonite-zeolite is exothermic. The negative values of ΔG^o indicate the feasibility of the adsorption process and the spontaneous nature of the adsorption. ΔG^o for Hg was positive and increased with increasing temperature. As seen in the Table 4.19, ΔSº values were negative and were in the range 0.297 to 0.703 J mol^{-1} K^{-1}. The negative values of ΔSº correspond to a decrease in degrees of freedom of the adsorbed species. It was observed that the rate of adsorption (Table 4.20) for the metal ions increases with increasing temperature.

Table 4.20 Rate of the adsorption of metal ions on bentonite-sorbitol

Rx rate (h^{-1})	**291.15** ^{o}K	**295.15** ^{o}K	**299.15** ^{o}K	**303.15** ^{o}K
Cu	0.154	0.264	0.278	0.316
Ni	0.125	0.137	0.148	0.151
Zn	0.137	0.174	0.179	0.186
Co	0.111	0.122	0.128	0.132
Fe	0.428	0.454	0.461	0.485
Hg	0.023	0.029	0.035	0.043
U	0.061	0.062	0.110	0.119
Cr	0.124	0.191	0.206	0.243

The adsorption study was also done on the bentonite modified with mannitol. Mannitol and sorbitol are isomers, the only difference being the orientation of the hydroxyl group on carbon. The efficiency of the bentonite-mannitol for the adsorption of heavy metals is similar to that for bentonite-sorbitol. The adsorption of metals on bentonite-mannitol occurs on heterogenous surface following monolayer coverage. The experimental data fitted well the pseudo-second order as seen for the bentonite-sorbitol.

Mannitol is one of the most abundant energy and carbon storage molecules in nature, produced by a plethora of organisms, including bacteria, yeasts, fungi, algae, lichens, and many plants (Song and Vieille, 2009). D-Mannitol is the predominant carbon compound in conidiospores of the filamentous fungi and makes up to 10 - 15% of the dry weight. A number of physiological functions have been ascribed to mannitol, including serving as a reserve carbon source, as an antioxidant, and to store reducing power. Since mannitol supplied in the medium during sporulation repaired this deficiency, mannitol appears to be essential for the protection of fungal spores against cell damage under these stress conditions. Polyols or polyhydroxyalcohols are present in all organisms, from bacteria to animals. In particular, plants and fungi are known to accumulate high levels of polyols intracellularly, up to several hundred mmol L^{-1} (Witteveen and Visser, 1995).

4.3 Zeolite

The zeolite used in this study was commercially available and supplied by Sigma Aldrich. Adsorption studies were performed on natural zeolite as well as on modified zeolite. Histidine, cysteine, sorbitol and mannitol (proxy-compounds released by fungi) were used for this purpose. The characteristics of zeolite and the results obtained for the adsorption studies onto natural zeolite as well as on modified bentonite are given in the following paragraphs.

4.3.1 Mineral and chemical properties

The X-ray diffraction (XRD) results for the zeolite used throughout the studies is shown in Figure 4.24.

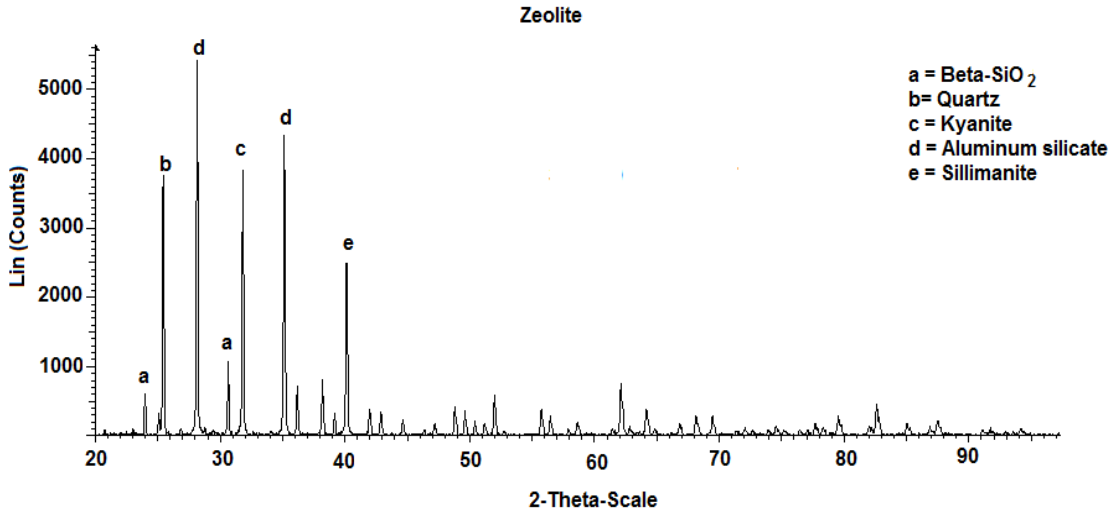


Figure 4.24 XRD pattern of natural zeolite

The crystallography of zeolite used in this study was monoclinic and the highest peak was at 2Θ value of 28, and the range of sharp peaks was 24 – 40. The zeolite sample mainly consisted of aluminium silicate in different phases, namely: beta-SiO_2, quartz, kyanite and sillimanite.

X-ray fluorescence (XRF) was used to determine the chemical composition of the natural zeolite. The results obtained are presented in Table 4.21. The Si/Al molar ratio of the sample has been calculated as 1.08. This is classified as “Low silica or aluminium-rich zeolites A and X”, the most common commercial adsorbents, which is considered as having a high

aluminium content possible in tetrahedral aluminosilicate frameworks. As a consequence, they contain the maximum number of cationic exchange sites balancing the framework aluminium, and thus the highest cationic contents and exchange capacities (Ribeiro *et al*., 1984).

Table 4.21 Chemical composition of natural zeolite

Oxides	(%) (w/w)
Si O_2	40.6
Al_2O_3	32.92
Fe_2O_3	0.01
FeO	0.08
MnO	0.01
MgO	0.06
CaO	0.03
Na_2O	19.92
K_2O	0.25
TiO_2	0.02
P_2O_5	0.01
H_2O	6.1
Total	100.01

4.3.2 Physical surface characteristics

4.3.2.1 Surface area and pore volume analysis

The results obtained for the surface area and the pore volume for the natural and functionalised zeolites are listed in Table 4.22a. As observed for the bentonite, the surface area of natural zeolite decreased with modification of the surface.

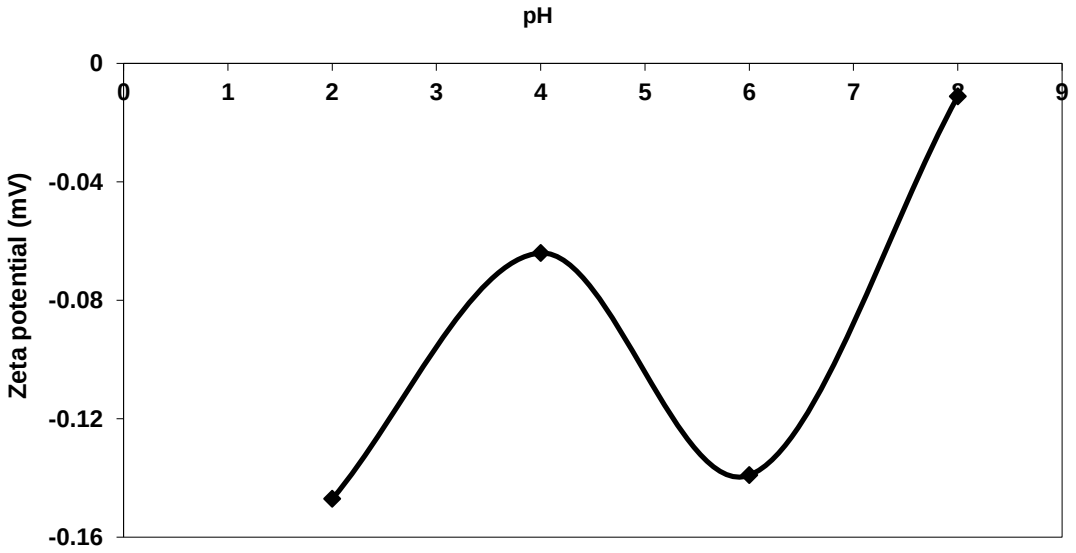
Table 4.22a Physical properties of natural and functionalised zeolite

	Zeolite-natural	**Zeolite - Histidine**	**Zeolite - Cysteine**	**Zeolite - Sorbitol**	**Zeolite - Mannitol**
Surface area (m^2 g^{-1})	0.692	0.545	0.423	0.555	0.520
Pore volume (cm^3 g^{-1})	19.52	28.56	18.39	15.42	16.58

4.3.2.2 Zeta potential analysis

The variation of the zeta potential for both natural zeolite and modified zeolite with respect to pH has been studied in order to determine the surface charge of the biosorbent and the results are shown in Figure 4.25.

(a)



(b)

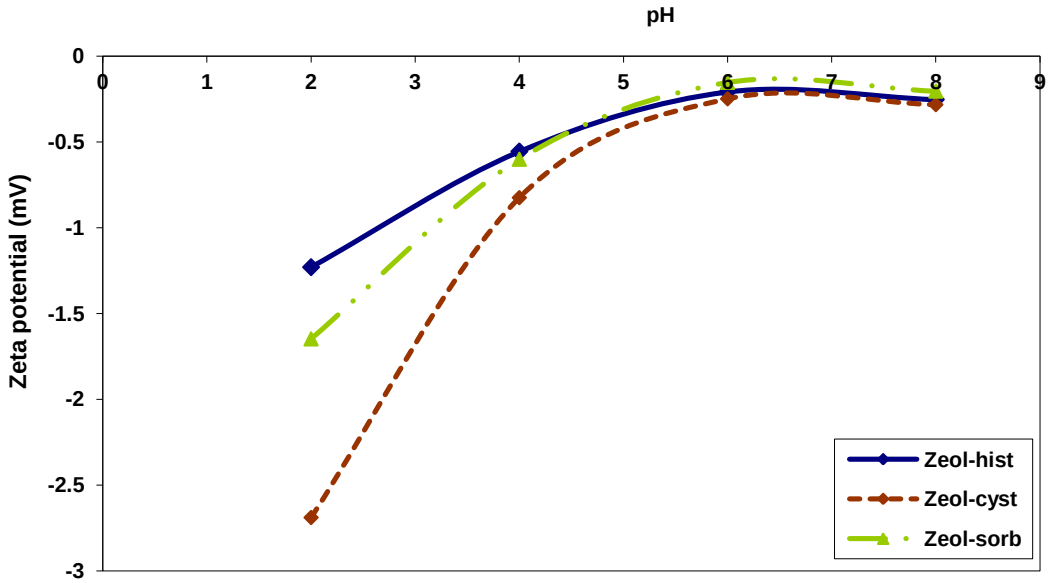
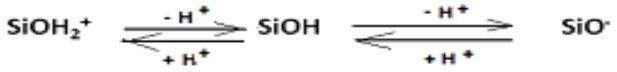


Figure 4.25 The zeta potential of: (a) natural zeolite (b) zeolite-histidine, zeolite-cysteine, zeolite-sorbitol

Natural zeolite did not exhibit the point of zero charge (PZC) over the pH range 2 to 8 as seen in Figure 4.25 (a). As explained for the bentonite, the surface charge of zeolites results from the protonation or dissociation of the hydroxyl groups, so that the pH controls the particle surface charge, and hence the zeta potential, through the following mechanisms (Kuzniatsova *et al.*, 2007).



(4.6)



(4.7)

Due to the abundant presence of terminal Si–OH and Al–OH at the surface, zeolite is classified as a weak electrolyte. The zeta potential of zeolites depends not only on the pH, but also on ionic strength of the suspension, and the Al content of the framework. The type of zeolite structure defines the number of silanol and aluminol groups existing at the crystal surfaces (Caratzoulas, 2005). Increasing concentrations of Al atoms shift the isoelectric point (IEP) to lower pH values, which is attributed to the higher acidic strength of Al atoms (Nikolakis, 2005). Another possible explanation of this effect is that bridging hydroxide groups (Si–OH–Al) at the zeolite surface can be easily deprotonated to form Si–O$^-$ at a wide range of pH making the surface more negatively charged (Yang *et al.*, 2002). When the Si/Al ratio in zeolite decreases, the protonation of silanol groups in acidic solutions is counteracted and in turn the IEP is shifted to lower pH values.

The zeolite surface remains negatively charged due to the dissociation of the hydroxyl groups (Eqs. (4.6) and (4.7)) and there is no isoelectric point in the pH range 2 to 8. Since no additional background electrolyte was used to enhance the ionic strength, the measured zeta potential closely follows the surface charge of zeolite crystals in the suspension. To maximize the colloidal stability of the suspensions, it is a pre-requisite to make the surface charge of the zeolite particles as negative as possible, a condition which is best fulfilled by the surface modification of the zeolite by organic molecules such as histidine, cysteine and sorbitol. In fact, zeta potentials of modified zeolites were more negative than for the natural one. This is evidence of the modification of the natural zeolite.

4.3.2.3 Thermal analysis

The TGA/DTG results obtained under N_2 atmosphere (20 mL/min, 5^oC/min) from room temperature to 500^oC are presented in Figure 4.26.

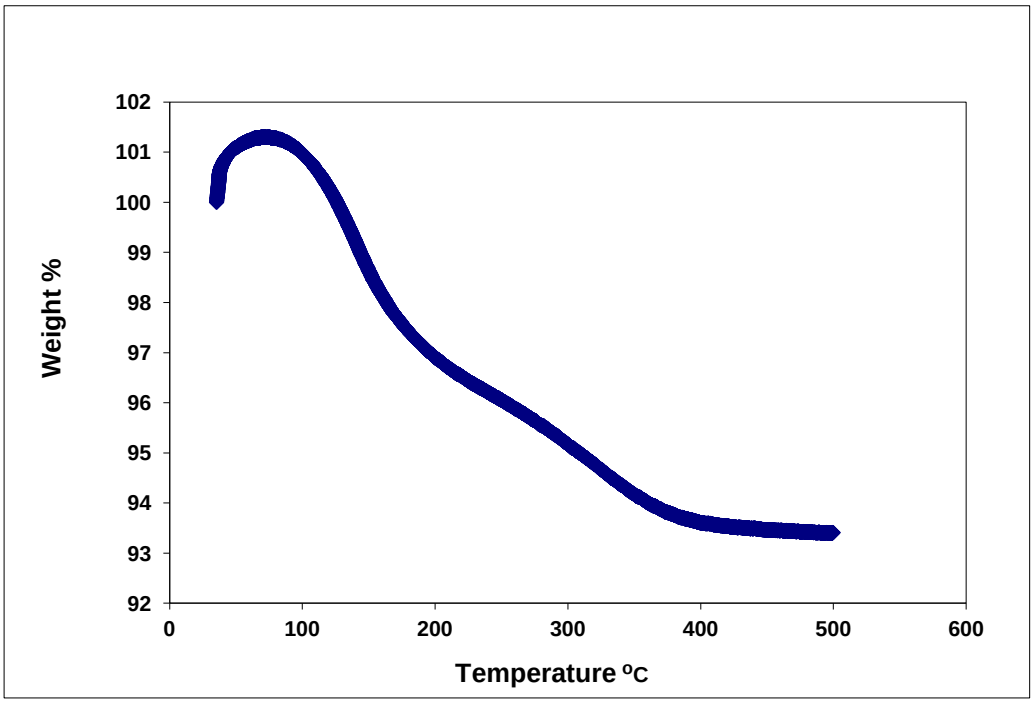


Figure 4.26 Thermogravimetric curve of natural zeolite

In the TGA/DTG curves, the weight loss observed below 200°C was associated with the loss of the free water in zeolite (101 – 96%). However, less thermally-induced changes were visible in the curves when the temperature was increased from 200°C to 400°C (96 – 93%), thereby suggesting that zeolite did not undergo any further thermally-induced changes over 400^oC. This proves that zeolite is thermally stable over a temperature of 500^oC.

4.3.3 Chemical properties of the surface

4.3.3.1 Cationic exchange capacity and elemental composition

The values for the cation exchange capacity and the elemental composition of natural zeolite as well as the functionalised zeolite are listed in Table 4.22b. The CEC was found to be higher in natural zeolite. The amount of C, H and N increased in the functionalised zeolite and S was analysed in the zeolite-cysteine, proving the modification of natural zeolite.

These results were confirmed by FTIR spectra (Figure 4.27).

Table 4.22b Chemical properties of natural and modified zeolite

Sample	CEC (meq $100g^{-1}$)	H %	C %	N %	S %
Natural Zeolite	61.06	2.209	0.219	n.d	n.d
Zeolite-Histidine	60.25	2.814	1.564	0.555	n.d
Zeolite-Cysteine	58.62	2.765	1.681	0.785	0.587
Zeolite-Sorbitol	54.22	2.980	1.874	n.d	n.d
Zeolite-Mannitol	55.26	2.892	1.775	n.d	n.d

n.d: not detected

4.3.3.2 FTIR spectral analysis

The infrared spectrum for natural zeolite is shown in Figure 4.27.

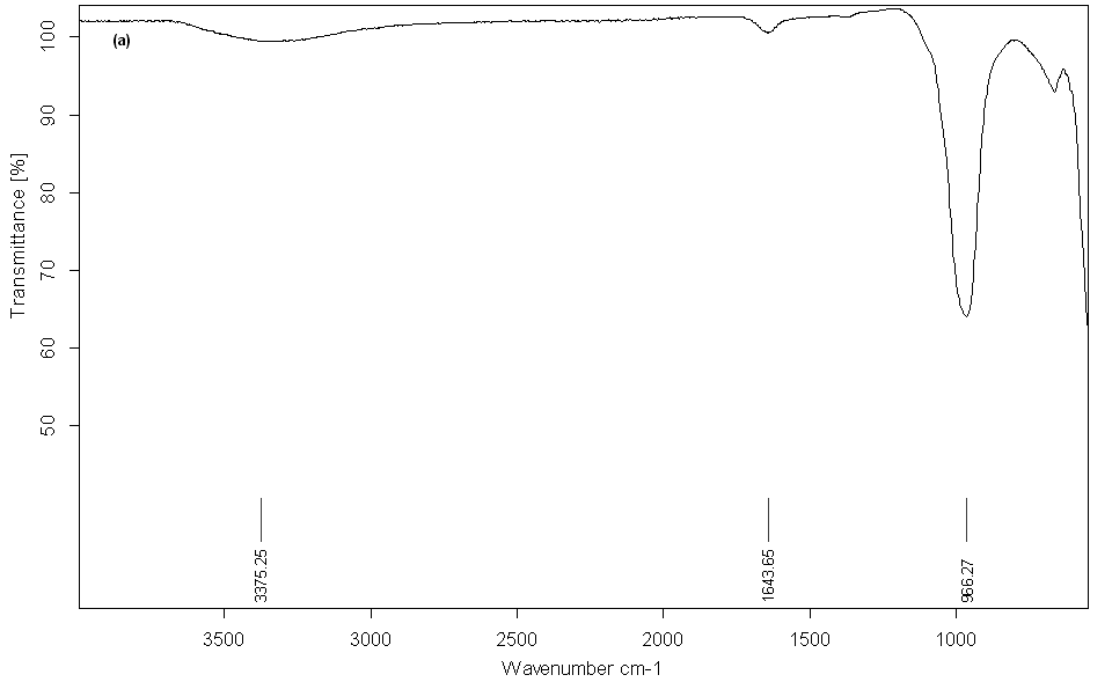


Figure 4.27 FTIR spectrum of natural zeolite

The spectra for zeolite-histidine, zeolite-cysteine, zeolite-sorbitol and zeolite-mannitol are given in the APPENDIX D. The wavenumbers and vibration types associated with the IR spectra for natural and modified zeolite are listed in Table 4.23a, b, c, d.

Table 4.23a IR vibrations of natural zeolite

Wavenumber, cm^{-1}	***Vibration type***
3337	O-H stretching H-OH
1643	O-H deformation
966	Si-O-Si stretching
689	Si-O-Si

Table 4.23b IR vibrations of Zeolite-Histidine

Wavenumber, cm^{-1}	***Vibration type***
3710-3953	O-H, N-H
3648	O-H, N-H (H bonded)
2980	COO-
2350	C-H
1507	C=N, C-OH bending
1683	C=O amide I
1002	Si-O-Si stretching
915	Al^{3+} binding OH deformation
796	N-H wagging
687	C-H
592	Al-O-Si deformation

Table 4.23c IR vibrations of Zeolite-Cysteine

Wavenumber, cm^{-1}	***Vibration type***
3666-3902	O-H, N-H
2980	S-H
2341-2360	C-H
1748	C=O
1635	H-OH deformation
1541	C=N
966	Si-O-Si stretching
668	C=C

Table 4.23d IR vibrations of Zeolite-Sorbitol & Zeolite-Mannitol

Wavenumber, cm^{-1}	***Vibration type***
Zeolite-Sorbitol	
3628	O-H stretching
3566	O-H stretching
3391	C-H
1635	H-OH
991	Si-O-Si stretching
914	Al^{3+} binding OH deformation
796	
Zeolite-Mannitol	
3902-3617	OH (H-bonded)
3587	
3391	
2980	C-H
2360	
1748-1473	H-OH
992	Si-O-Si stretching
798	Si-O
616-563	O-H (bend out of plane)

As seen for the bentonite, the spectra of zeolite-histidine, zeolite-cysteine, zeolite-sorbitol and zeolite-mannitol are dominated by bands of the host material, although peaks associated with the presence of the N-H, S-H, C=C, C=O and OH groups are also visible. For instance, the common, large and intense bands located at 3700 and 3000 cm^{-1} can be attributed to axial -OH and -NH group deformations, which are more evident in the zeolite-histidine and cysteine spectra.

4.3.4 Sorption studies

Various operational parameters were tested to determine adsorption characteristics of natural zeolite/bentonite as well as modified for heavy metal ions adsorption from aqueous solutions. These include pH, contact time, metal ion concentration and temperature.

4.3.4.1 Sorption capacities, pH and isotherms

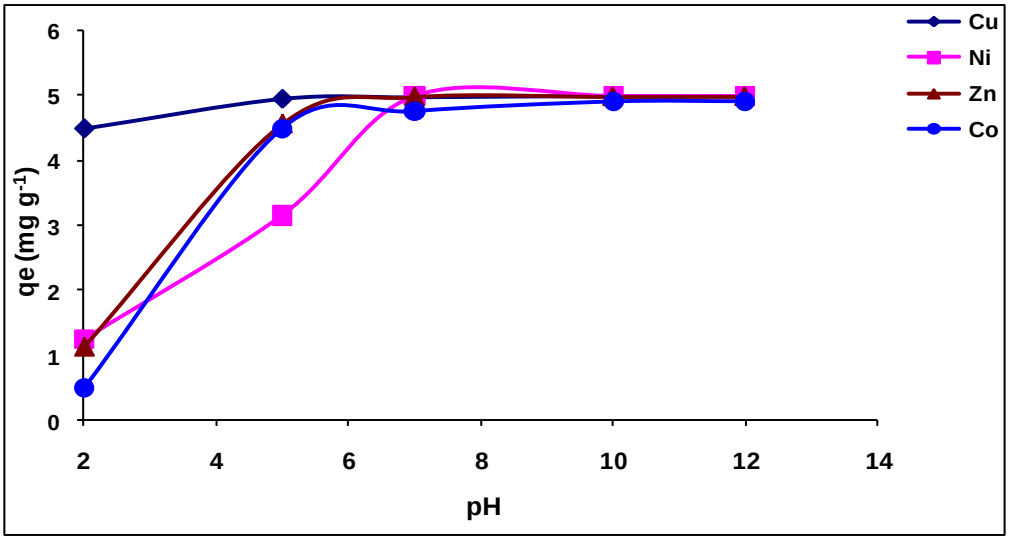
i) Effect of pH

The most important parameter influencing the adsorption is the pH of the adsorption medium. The effect of pH on the adsorption of metal ions on natural zeolite is illustrated in Figure 4.28.

Generally, the adsorption of metals increases with increase in pH. A maximum adsorption capacity of 5 mg g^{-1} was reached at pH 5-6 for Cu, Co, Cr, Hg, Ni, Zn and U. Adsorption capacity was constant for the whole range of pH studied for Fe. Low pH levels, especially below 4, are reported as undesirable in zeolite applications because this would adversely affect the chemical structure of the mineral (Ali and El-Bishtawi, 1997). The structure of zeolites, particularly with low Si/Al ratio may collapse in the presence of acids with pH lower than 4, but the severity will be more at pH below 3. The low adsorption of metal ions at low pH may be due to the collapse of the structure of zeolite.

The amount of metal ions adsorbed at lower pH values can also be explained by the competition between the protons and the metals for active sites in the zeolite particle. Although the measurement of the zeta potential (Figure 4.25 (a)) showed that the zeolite surface was negatively charged from pH 2 to 8. The hydroxylated surfaces of oxides develop a charge on the surface in aqueous solution through amphoteric dissociation. With increasing pH, the competition from the protons decreases and the positively charged ions can be exchanged with exchangeable cations and/or be adsorbed at the negatively charged sites. At pH higher than 6, the high adsorption observed is a combination of precipitation of metal hydroxide and adsorption. Therefore, the adsorption of metals ions on zeolite is difficult to quantify at pH values higher than 6.

(a)



(b)

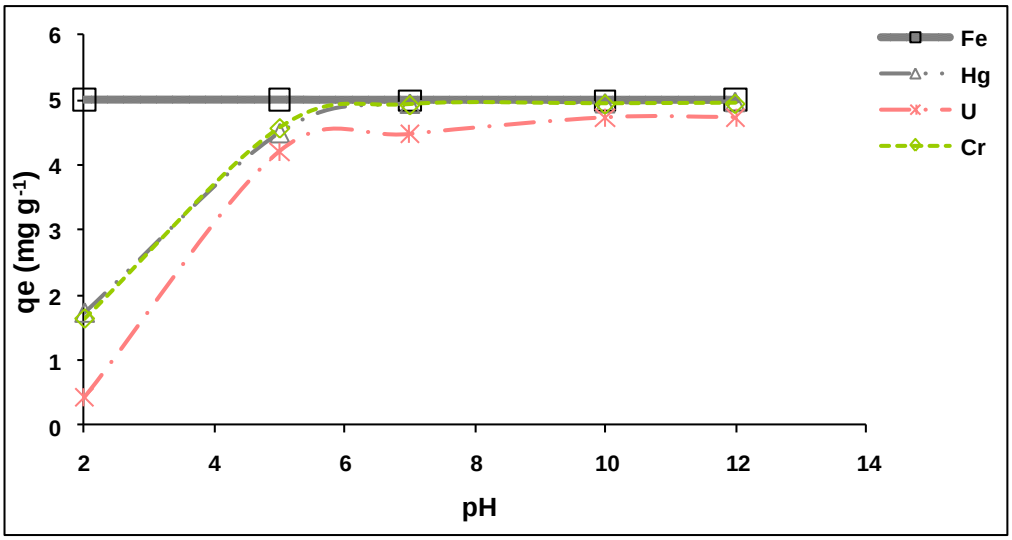


Figure 4.28 Effect of initial pH on adsorption of (a) Cu, Ni, Zn, Co and (b) Fe, Hg, Cr and U onto natural zeolite in single component solutions (C_i = 100 mg L^{-1}, Temp = 298.15±1^oK, agitation rate = 150 rpm, agitation time = 12 h)

ii) Effect of concentration

The effect of the initial concentration on the adsorption of metals at concentration levels ranging from 50 to 500 mg L^{-1} is shown in Figure 4.29.

The results show that the adsorption of heavy metal ions at different concentrations increased linearly until equilibrium was reached and then remained constant after that.

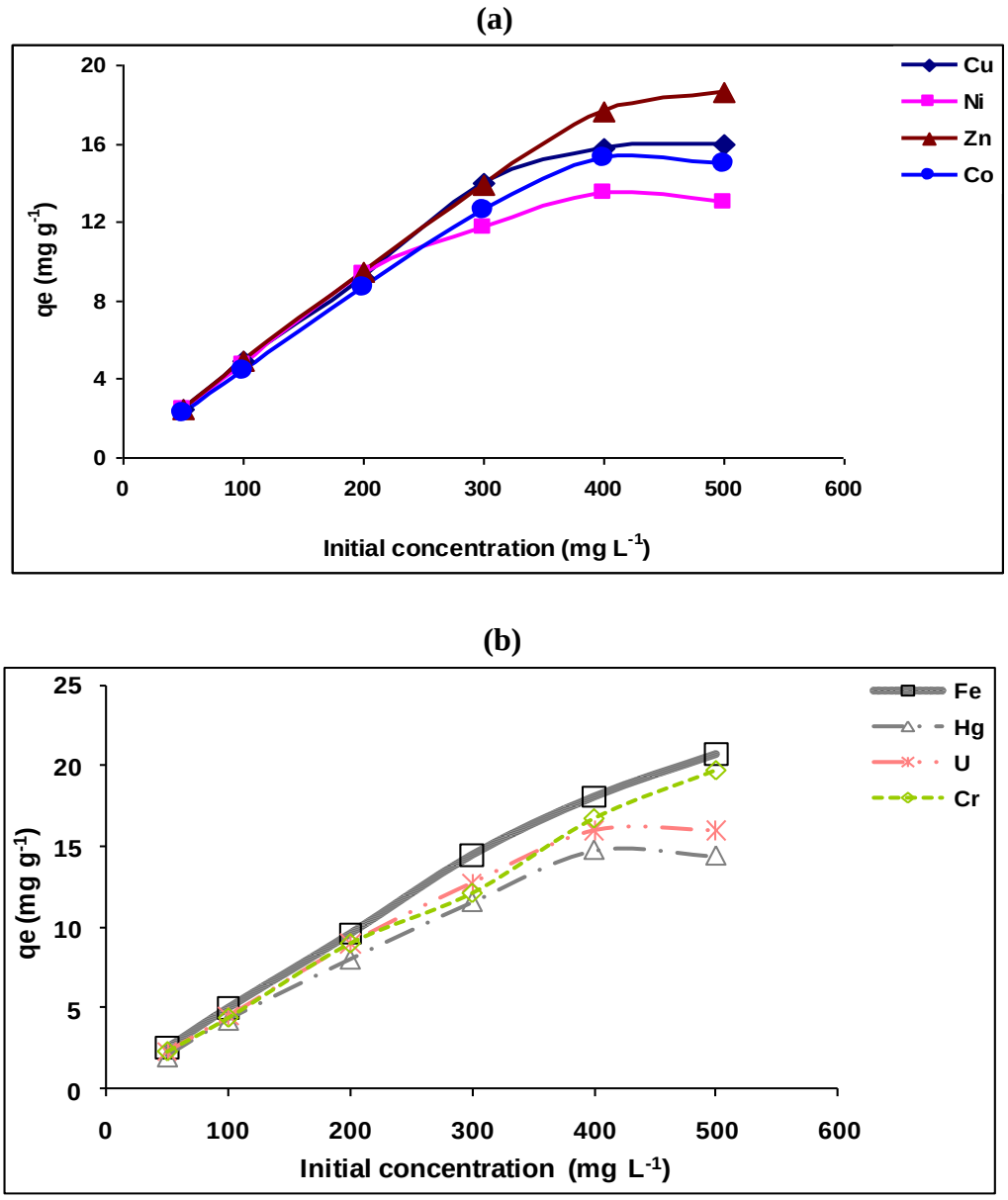


Figure 4.29 Effect of concentration on the adsorption of (a) Cu, Ni, Zn, Co and (b) Cr, Fe, Hg and U onto natural zeolite in single component solutions (pH 3, Temp = 298.15±1^{o}K, agitation rate = 150 rpm, agitation time = 12 h)

The adsorption capacity of metal ions on natural zeolite increases with metal concentration up to 300 mg L^{-1}. The decrease of the uptake was less for Fe and Cr. For U and Hg, the equilibrium was reached at 400 mg L^{-1}, assuming the saturation of the active sites. Percentage adsorption for metal ions decreases with increasing metal concentration in aqueous solutions. These results indicate that energetically less favourable sites become involved with increasing metal concentrations in the aqueous solution.

The heavy metal uptake is attributed to different mechanisms of ion-exchange processes as well as to the adsorption process. During the ion-exchange process, metal ions had to move through the pores of the zeolite mass and through channels of the lattice to replace exchangeable cations (mainly sodium and calcium).

iii) Isotherms of adsorption for natural zeolite

The sorption data of heavy metal ions have been modelled with the Langmuir, Freundlich and Dubinin-Radushkevich ***(***D-R) models. The adsorption isotherms for metal ions on natural zeolite were obtained at various bulk metal concentrations from 50 to 500 mg L^{-1}, while keeping all other parameters, i.e. agitation speed, pH and zeolite amount constant.
The distribution coefficient (K_d) was evaluated and the free energy calculated. The isothermic model parameters and statistical fits of the sorption data are summarised in Table 4.24.

Based on the correlation coefficient, the Langmuir model described the sorption data with r > 0.970, suggesting that the adsorption follows monolayer coverage. The data for Cr adsorption did not fit the Langmuir isotherm with r < 0.950. According to the *b* (mmol g^{-1}) parameter, sorption on natural zeolite followed the sequence: U > Hg > Fe > Zn > Cu > Co > Ni > Cr. The H^+ exchange capacity of zeolites and the strength of the hydration shells of cations are mainly responsible for the adsorption sequence.
The maximum adsorption capacities (mol kg^{-1}) obtained on the Langmuir isotherm are as follows: Cr (0.428) > Fe (0.380) > Zn (0.297) > Co (0.276) > Cu (0.259) > Ni (0.228) > Hg (0.081) > U (0.079). The maximum adsorption is observed when the sorbent surface is covered with a monolayer of metal ions. The adsorption was also described by the D-R model, except for Ni and U for which the sorption data did not fit the D-R isotherm. This implies the heterogenous character of the adsorption surface of zeolite.
The selectivity obtained based on the distribution coefficient (L kg^{-1}) was: Fe (8750) > Zn (1619) > Cu (1411) > Ni (982.7) > U (516.2) > Cr (479.5) > Co (433.3) > Hg (286.5). The values of the distribution coefficients are high for Fe, Zn and Cu which indicate the presence of stronger bonds. The variations of Gibbs free energy determined based on the distribution coefficient have values ranging from -14.02 to -22.50 kJ mol^{-1}, meaning that the adsorption process occurred spontaneously.

Table 4.24 Parameters of the Langmuir, Freundlich and D-R models for the adsorption of metals on natural zeolite

Langmuir Isotherms	***Fe***	***Cu***	***Co***	***Hg***	***Ni***	***Zn***	***U***	***Cr***
A	0.039	0.101	0.145	0.183	0.181	0.064	0.123	0.097
B	2.629	3.867	3.624	12.42	4.391	3.367	13.41	2.337
b	66.27	38.10	25.04	67.99	24.26	52.78	108.7	24.18
qm (mol/kg)	0.380	0.259	0.276	0.081	0.228	0.297	0.074	0.428
ΔGo (kJ/mol)	-10.39	-9.024	-7.983	-10.46	-7.905	-9.832	-11.62	-7.897
Δq (%)	76.14	76.16	76.07	76.04	76.14	76.13	76.07	75.99
r	0.993	0.998	0.995	0.971	0.999	0.999	0.977	0.927
Freundlich Isotherms	***Fe***	***Cu***	***Co***	***Hg***	***Ni***	***Zn***	***U***	***Cr***
A	0.134	0.136	0.581	0.542	-0.079	0.389	0.364	1.220
B	0.207	0.263	0.436	0.524	0.219	0.321	0.445	0.608
K_f	1.363	1.368	3.811	3.485	0.833	2.447	2.313	16.60
n	4.837	3.799	2.292	1.909	4.550	3.111	2.245	1.645
ΔGo (kJ/mol)	-11.99	-9.024	-5.681	-4.731	-11.28	-7.713	-5.565	-4.079
Δq (%)	14.53	15.54	17.56	17.59	19.44	12.37	26.88	16.09
r	0.972	0.946	0.946	0.920	0.910	0.973	0.787	0.968
D-R Isotherms	***Fe***	***Cu***	***Co***	***Hg***	***Ni***	***Zn***	***U***	***Cr***
A	-0.308	-0.269	-0.053	-0.184	-0.350	-0.114	-0.226	0.142
B	-0.002	-0.004	-0.005	0.007	-0.004	-0.004	-0.006	-0.005
Xm (mol/kg)	0.735	0.764	0.948	0.832	0.705	0.892	0.798	1.153
Es (kJ/mol)	14.73	11.68	9.686	8.484	11.05	11.43	9.012	9.605
Δq (%)	21.87	22.01	15.93	25.99	27.26	12.03	32.82	20.62
r	0.961	0.953	0.950	0.964	0.910	0.986	0.934	0.962
K_d	***Fe***	***Cu***	***Co***	***Hg***	***Ni***	***Zn***	***U***	***Cr***
A	9.078	7.252	6.071	5.658	6.890	7.389	6.246	6.173
B	-2828	-1098	-538.3	-1349	-817.1	-1373	-2354	-519.6
ΔGo (kJ/mol)	-22.50	-17.98	-15.05	-14.02	-17.08	-18.32	-15.48	-15.30
Kdo	8758	1411	433.3	286.5	982.7	1619	516.2	479.5
Δq (%)	84.25	59.39	8.275	6.133	61.39	47.97	12.71	17.62
r	0.752	0.903	0.991	0.984	0.908	0.897	0.948	0.899

4.3.4.2 Effect of contact time and kinetics of adsorption

i) Effect of contact time

Adsorption of Cu, Co, Cr, Fe, Hg, Ni, Zn and U onto zeolite was found to be time-dependent as seen in Figure 4.30. As seen in the Figures, the adsorption of all metals was quite rapid initially, but gradually slowed with passage of time reaching a maximum in 30 minutes. The initial faster rate may be due to the availability of the uncovered surface area of the adsorbent since adsorption kinetics depends on the surface area of the adsorbent.

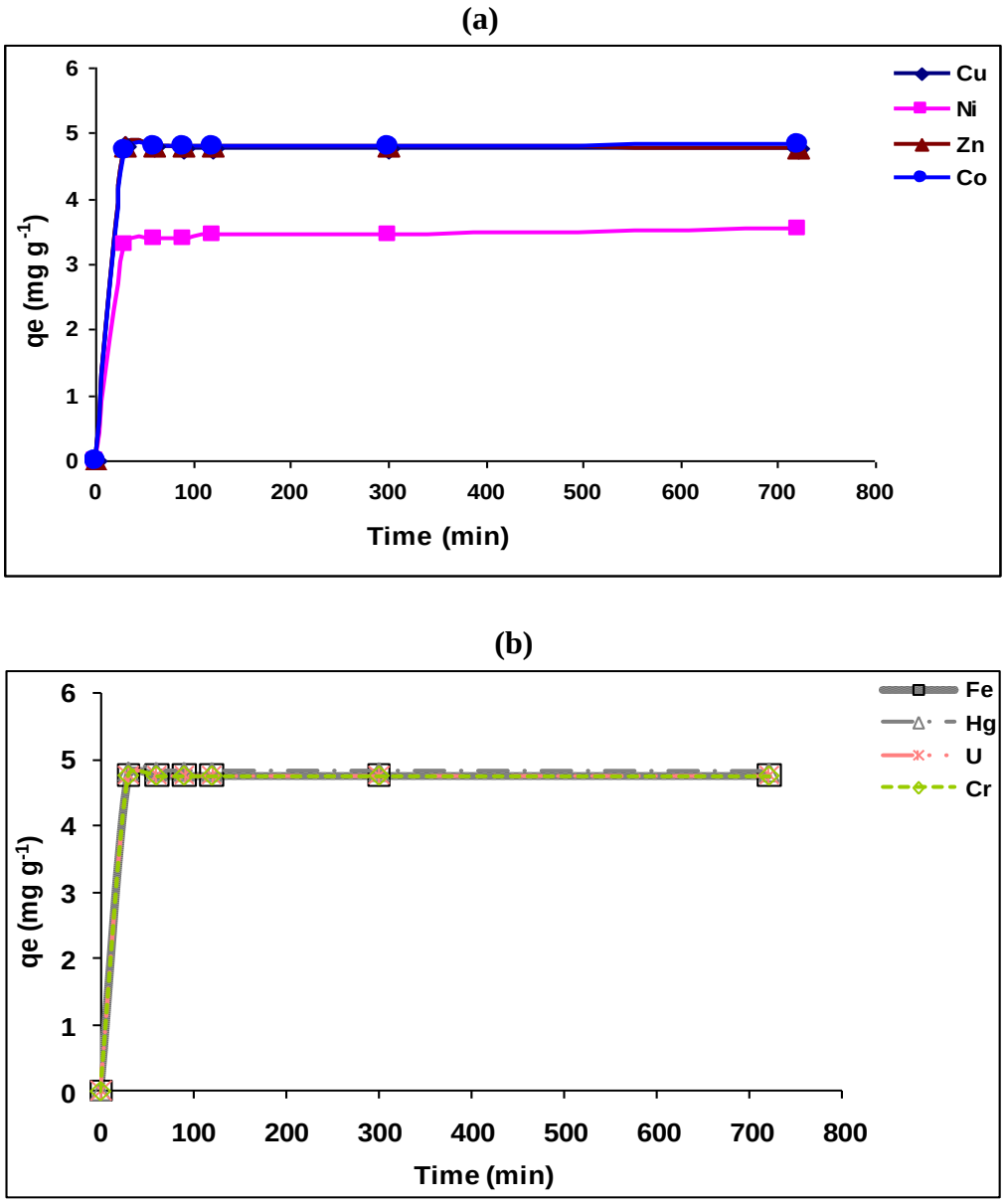


Figure 4.30 Effect of contact time on adsorption of (a) Cu, Ni, Zn, Co and (b) Cr, Fe, Hg and U onto natural zeolite in single component solutions (pH =3, C_i = 100 mg L^{-1}, Temp = 298.15±1^{o}K, agitation rate = 150 rpm)

ii) Kinetic modelling of metal ion adsorption on natural zeolite

The time-dependent experimental adsorption data were used for kinetic modelling. The model equations used for fitting the data are: pseudo first-order, pseudo second-order,

Elovich, intraparticle diffusion and film diffusion models. The parameters and constants obtained from the experimental data are reported in the Table 4.25.

Table 4.25 Kinetic constants for the adsorption of metal ions on natural zeolite

Pseudo-first order								
	Fe	***Cu***	***Co***	***Hg***	***Ni***	***Zn***	***U***	***Cr***
A	-2.804	-2.920	-2.934	-3.602	-2.438	-3.299	-3.100	-2.541
B	-0.004	-0.006	-0.007	-0.005	-0.004	-0.009	-0.004	-0.009
qe (mol/kg)	0.002	0.001	0.001	0.008	0.005	0.001	0.001	0.003
K_1	0.009	0.014	0.015	0.012	0.009	0.020	0.009	0.022
Δq (%)	91.48	91.50	91.58	90.91	88.89	92.07	85.84	89.89
r	0.460	0.584	0.596	0.649	0.615	0.643	0.771	0.822
Pseudo – second order								
	Fe	***Cu***	***Co***	***Hg***	***Ni***	***Zn***	***U***	***Cr***
A	11.07	6.676	4.815	138.9	53.74	1.638	143.2	7.241
B	11.64	13.23	12.21	100.9	16.59	13.62	137.1	12.09
qe (mol/kg)	0.086	0.076	0.082	0.009	0.061	0.073	0.007	0.083
K_2	12.23	26.22	30.96	73.24	5.124	113.3	13.12	20.21
Δq (%)	0.867	0.276	0.227	0.817	1.509	0.035	2.754	0.193
r	0.998	1.000	0.999	0.998	0.998	1.000	0.998	0.999
Elovich model								
	Fe	***Cu***	***Co***	***Hg***	***Ni***	***Zn***	***U***	***Cr***
A	0.013	0.012	0.012	0.004	0.008	0.011	0.001	0.012
B	0.015	0.013	0.014	0.002	0.010	0.013	0.001	0.014
b	67.21	76.16	70.21	583.7	96.89	78.26	826.9	69.65
a	0.036	0.032	0.034	0.014	0.023	0.031	0.002	0.034
Δq (%)	16.53	16.55	16.48	16.12	15.22	16.72	11.16	16.34
r	0.747	0.990	0.958	0.991	0.962	0.972	0.985	0.953
Intraparticle diffusion model								
	Fe	***Cu***	***Co***	***Hg***	***Ni***	***Zn***	***U***	***Cr***
A	0.034	0.030	0.032	0.024	0.022	0.029	0.002	0.032
B	0.004	0.004	0.005	0.001	0.003	0.004	0.001	0.004
Id	0.034	0.030	0.032	0.024	0.022	0.029	0.002	0.032
Kp	0.004	0.004	0.005	0.001	0.003	0.004	0.001	0.004
Δq (%)	29.39	29.35	29.38	29.47	29.81	29.29	30.98	29.39
r	0.721	0.724	0.727	0.730	0.741	0.722	0.803	0.730
Film diffusion								
	Fe	***Cu***	***Co***	***Hg***	***Ni***	***Zn***	***U***	***Cr***
A	-0.909	-1.204	-1.319	-1.061	-0.813	-1.669	-0.678	-1.700
B	-0.013	-0.014	-0.014	-0.011	-0.009	-0.017	-0.005	-0.012
If	-0.908	-1.204	-1.320	-1.061	-0.813	-1.669	-0.678	-1.699
Kf	0.013	0.014	0.014	0.011	0.009	0.017	0.005	0.012
Δq (%)	63.68	55.23	53.64	52.36	54.14	51.24	49.96	43.25
r	0.459	0.584	0.596	0.689	0.617	0.642	0.771	0.822

Based on linear regression ($r > 0.95$) values, the adsorption kinetics of the metals onto zeolite could be described well by both pseudo second-order and Elovich models. These imply that chemisorption could be the rate-limiting step. The adsorption of Fe is only described by the pseudo second-order model. As seen in Table 4.25, the calculated values of q_e from the

pseudo first-order model were lower compared to those for the pseudo second-order kinetic model. The rate constants for the pseudo second-order (k_2) range from 5.124 to 113.3 g (mg min^{-1}) and these values were found to be higher than the ones obtained for the pseudo first-order kinetic model with Zn exhibiting the higher rate. The Elovich constant *b* was found to be higher for U (826.9 g mg^{-1}) and lower for Fe (67.21 g mg^{-1}). This implies that the surface coverage was high for uranium.

4.3.4.3 Effect of temperature and thermodynamic parameters

i) Effect of temperature

The effect of temperature on metal adsorption was studied in the temperature range 18 to 30^{o}C and the results are presented in Figure 4.31. The results indicated that the amount of Fe, Cu, Co, Zn, Ni and Cr was constant for the range of temperature investigated. The adsorption of Hg and U increases with an increase in temperature. In general, heavy metal uptake is enhanced by increasing temperature due to activation of metal ions by enhancing adsorption at the coordination sites of zeolites (Babel and Kurniawan, 2003). Also, at higher temperatures, ions become smaller due to their reduced hydration radii and their movement becomes faster (Inglezakis *et al.*, 2004), resulting in higher adsorption efficiencies.

Some previous studies showed that the adsorption of some metal ions e.g. Pb^{2+} on zeolite was independent of temperature in the range 20^{o}C to 35^{o}C (Ali and El-Bishtawi, 1997).

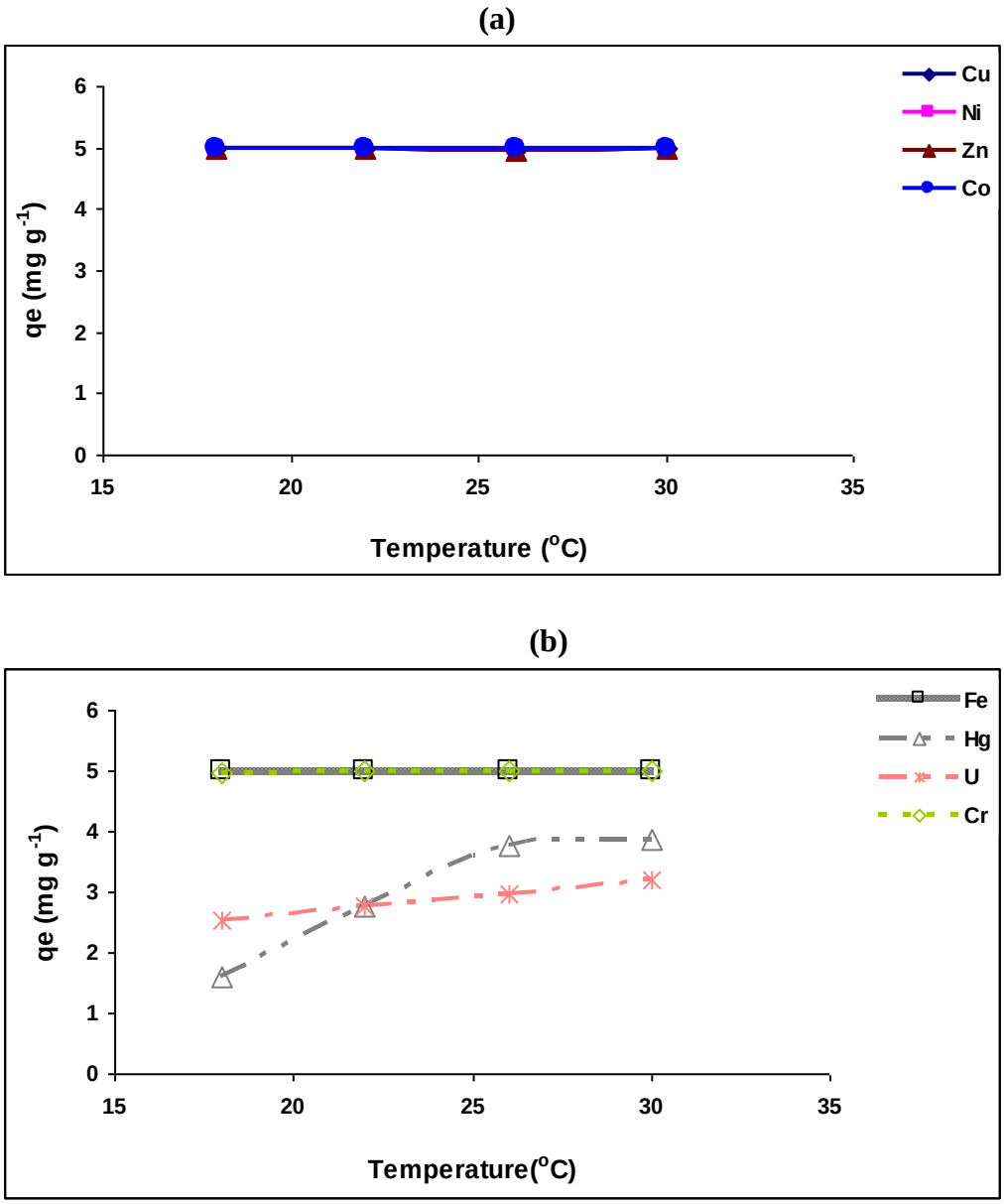


Figure 4.31 Effect of temperature on adsorption of (a) Cu, Ni, Zn, Co and (b) Cr, Fe, Hg and U onto natural zeolite in single component solutions (C_i = 100 mg L^{-1}, pH 3, agitation rate = 150 rpm, contact time = 12 h)

ii) Thermodynamic parameters

The thermodynamic constants, Gibbs free energy (ΔG^o), enthalpy change (ΔH^o) and entropy change (ΔS^o) were calculated to evaluate the thermodynamic feasibility of the process and to confirm the nature of the adsorption process. The Gibbs free energy change of the process is related to equilibrium constant (Kc) by the equation:

$$\Delta G^o = - RT \ln K_C \qquad (4.8)$$

The Gibbs free energy change is related to the enthalpy change (ΔHº) and entropy change (ΔSº) as:

$$\ln K_o = \Delta S^o / R - \Delta H^o / RT \quad (4.9)$$

The calculated parameters are presented in Table 4.26.

Table 4.26 Thermodynamic parameters for natural zeolite

	Ea	ΔH^o	ΔS	ΔG^o			
	kJ mol^{-1}	kJ mol^{-1}	J (K^{-1}mol)$^{-1}$	kJ mol^{-1}			
				291.15 ^oK	**295.15** ^oK	**299.15** ^oK	**303.15** ^oK
Cu	57.89	-133.3	-403.8	-6.638	-17.23	-12.86	-15.72
Ni	107.5	-247.6	-764.3	-19.80	-20.55	-21.89	-24.96
Zn	37.72	86.87	242.1	-22.83	-17.56	-12.01	-16.38
Co	7.820	-18.11	10.70	-6.809	-17.18	-22.45	-21.22
Fe	37.28	85.87	349.1	-14.95	-20.07	-20.17	-15.89
Hg	161.8	-372.6	-1263	-23.16	-0.517	-2.765	-4.795
U	12.59	29.01	-96.30	-1.420	-0.951	-13.45	-0.959
Cr	44.42	-102.3	-296.3	-13.63	-16.52	-15.58	-16.02

The activation energy values obtained from the Arrhenius equation (3.34) were > 40 kJ mol^{-1} for Cu, Ni, Hg and Cr, meaning that these metals are adsorbed through a chemisorption reaction. This was confirmed by the fitting to the pseudo second-order kinetic model. The metal ions as Cr, Zn, Fe and U, with activation energy ranging from 12 to 38 kJ mol^{-1}, prefer to bind to binding sites of low energy. The negative values of enthalpy change indicated the exothermic nature of the process. The enthalpy change was positive for the adsorption of Zn, Fe and U, for which the process was endothermic and an increase of temperature would increase the metal adsorption. The negative ΔGº value confirmed the feasibility of the sorption process and the spontaneous nature of adsorption. The positive ΔSº values indicated the affinity of the adsorbent for Zn, Co and Fe while negative values of entropy show a decrease of the degrees of freedom of the metal ions. The negative values of ΔG^o indicate the feasibility of the adsorption process and the spontaneous nature of the adsorption. Generally, ΔG^o increases with the increase of temperature, except for Zn. As shown in Table 4.27, the rate of adsorption increases with increasing temperature.

Table 4.27 Rate of adsorption of metals on natural zeolite

Rx rate (h^{-1})				
	291.15 ^{o}K	**295.15** ^{o}K	**299.15** ^{o}K	**303.15** ^{o}K
Cu	0.431	0.441	0.520	0.585
Ni	0.679	0.698	0.734	0.825
Zn	0.596	0.593	0.542	0.403
Co	0.584	0.691	0.702	0.752
Fe	0.526	0.576	0.676	0.682
Hg	0.032	0.067	0.116	0.170
U	0.075	0.086	0.451	0.750
Cr	0.470	0.522	0.530	0.561

In general, the metal uptake is favoured at higher temperature since higher temperature activates the metal ions for enhancing adsorption at the coordinating sites of the minerals. Also, it is mentioned that cations are moving faster with increasing temperature and likely explanations are that, retarding specific or electrostatic interactions become weaker and the ions become smaller because solvation is reduced.

4.4 Zeolite functionalised with proxy-compounds

4.4.1 Zeolite-Histidine

4.4.1.1 Sorption capacities, pH, isotherms of adsorption

i) Effect of pH

The influence of pH in the adsorption of Cu, Co, Cr, Hg, Fe, Ni, Zn and U was investigated and the results are reported in Figure 4.32.

The maximum adsorption capacity of Cu, Co, Cr, Fe, Ni and Zn was constant for the pH range 2 to 12. Since, the zeolite surface has been modified using the histidine, the formation of the metal ion-histidine-zeolite complex occurs as explained in 4.2.1.1. At low pH, histidine is protonated and a zwitterion form is obtained. The latter acts as a shuttle for protons and the competition between H^{+} and cations towards the active sites is reduced. This explained the high uptake of metal ions at low pH.

The uptake of Hg and U was higher compared to the ones obtained with the natural zeolite and maximum adsorption capacity was attained at pH 5. The selectivity of adsorption of metal ions on the immobilised surface will also depend on the nature of the functional group.

For instance, histidine contains the amino and carboxyl groups, which are hard bases. According to the hard-soft acid base (HSAB) theory, the –NH– being a hard base, will prefer to bind with a hard acid such as Cr, Fe, U as well as Pearson's borderline Lewis acids e.g. Co, Cu, Zn, Ni. This explains the high uptake of U at low pH compared to the results obtained for the non-modified zeolite. The low uptake of Ni could be due to the size and high energy required for the formation of the hydrated nickel complex.

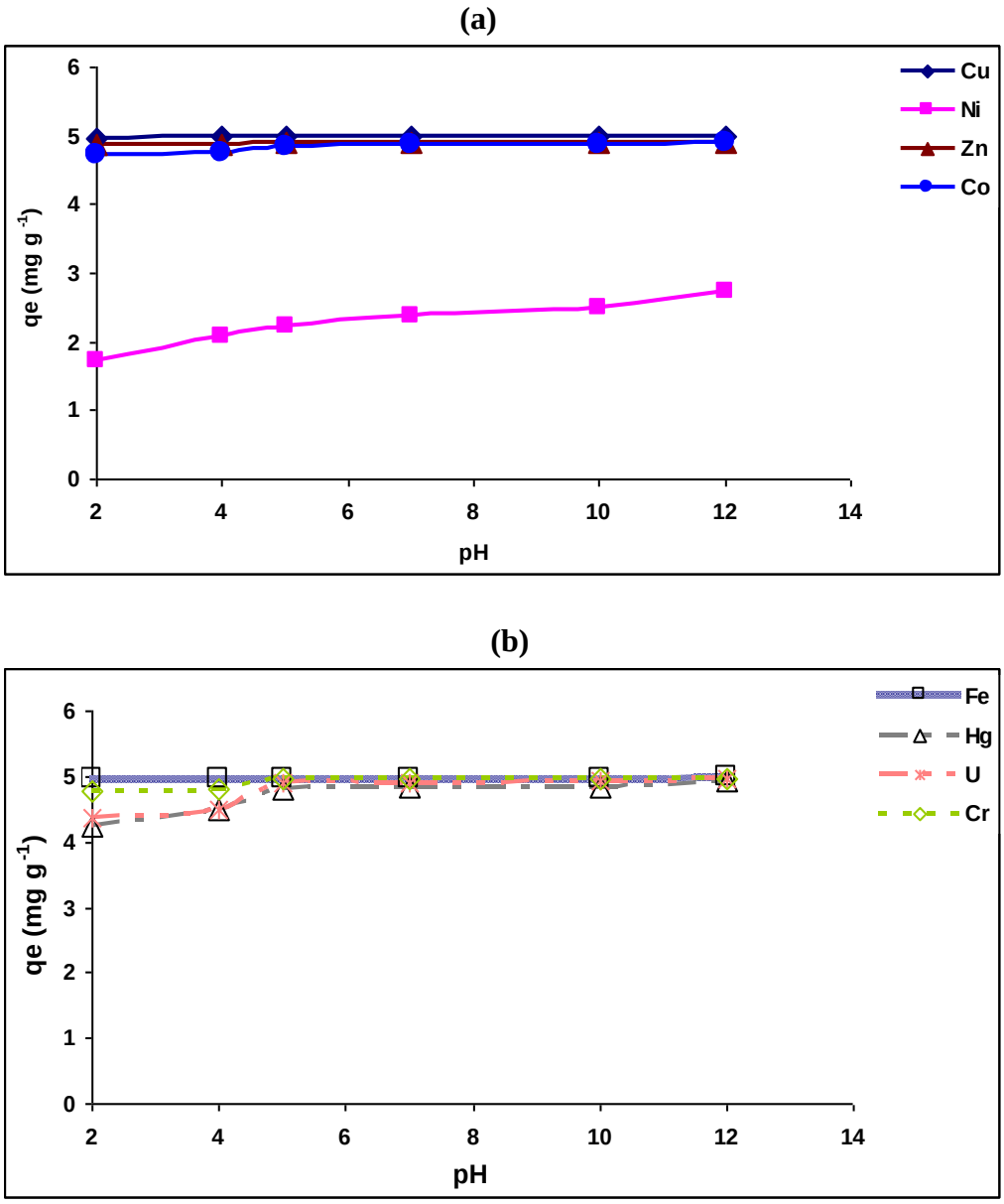


Figure 4.32 Effect of initial pH on adsorption of (a) Cu, Ni, Zn, Co and (b) Cr, Fe, Hg and U onto zeolite-histidine in single component solutions (C_i = 100 mg L^{-1}, Temp = 298.15±1^oK, agitation rate = 150 rpm, agitation time = 12 h)

i) Effect of metal ion concentration

Figure 4.33 illustrates the effect of the initial metal concentration on the adsorption of metal ions on zeolite-histidine. The initial metal concentration varied from 50 to 500 mg L^{-1}.

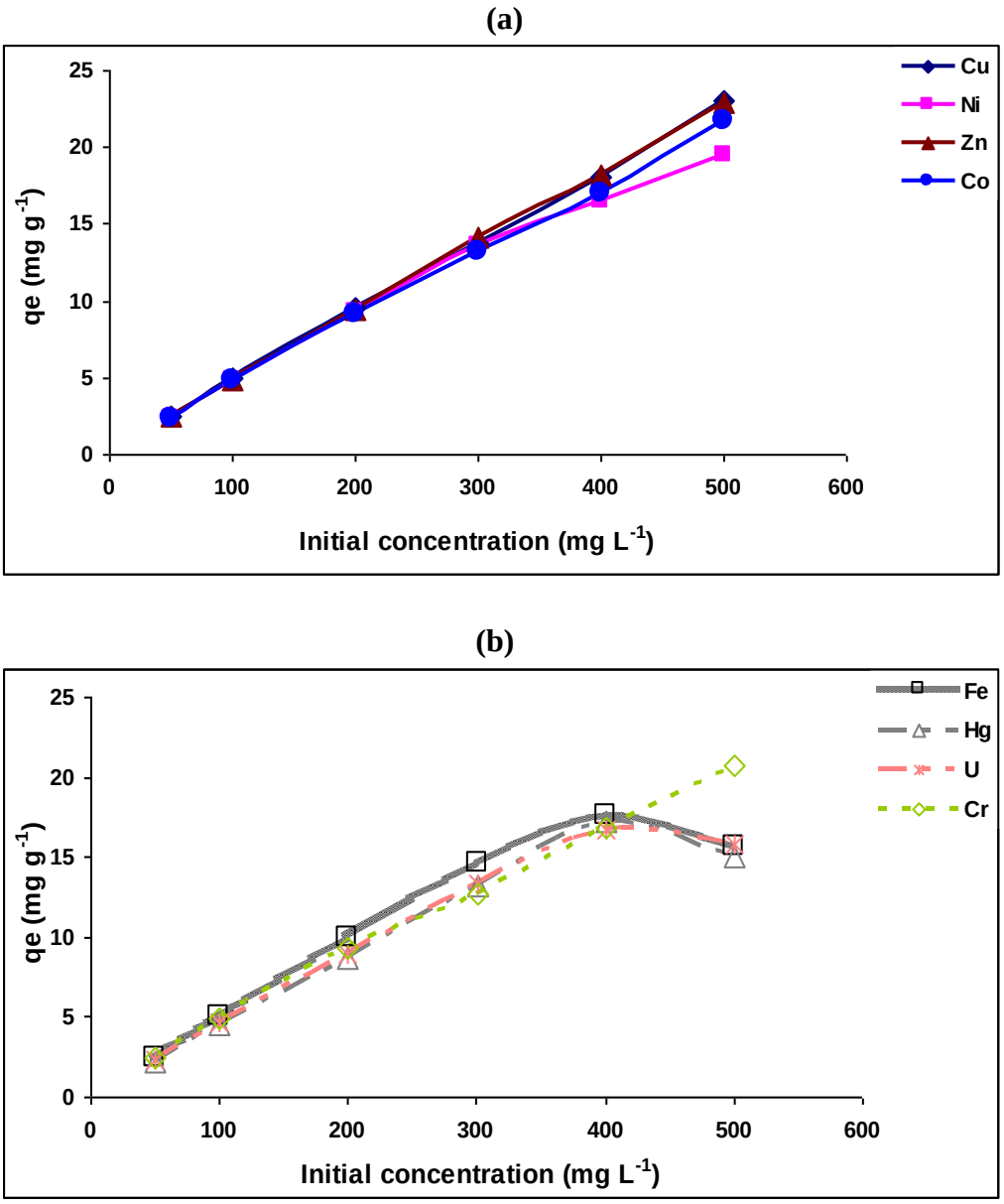


Figure 4.33 Effect of concentration on the adsorption of (a) Cu, Ni, Zn, Co and (b) Cr, Fe, Hg and U onto zeolite-histidine in single component solutions (pH=3, Temp = 298.15±1^{o}K, agitation rate= 150 rpm, agitation time= 12 h)

The results showed that the adsorption efficiency increases as the initial metal ion concentration increases. The increase was constant for the adsorption of Cu, Co, Ni, Zn and Cr up to 500 mg L^{-1}.The decrease of the adsorption capacity observed at 400 mg L^{-1} for Fe, Hg and U shows nearness to saturation of the available binding sites. Also, the uptake will depend on the amount of histidine immobilized on the surface of the zeolite.

ii) Isotherms of adsorption for zeolite-histidine

Sorption isotherms represent the distribution of metal ions between aqueous and solid phases (biosorbent) when the concentration increases and as long as binding sites are not saturated. These isotherms permit the calculation of the maximum adsorption capacities and different constants. The isothermic biosorption parameters are presented in Table 4.28.

Table 4.28 Parameters of the Langmuir, Freundlich and D-R models for the adsorption of metals on the zeolite-histidine

Langmuir Isotherms	***Fe***	***Cu***	***Co***	***Hg***	***Ni***	***Zn***	***U***	***Cr***
A	0.076	0.035	0.058	0.122	0.071	0.033	0.109	0.067
B	3.537	2.909	2.704	12.48	2.922	2.787	14.03	2.548
b	46.66	83.46	46.72	102.2	41.42	85.66	128.4	37.96
qm (mol/kg)	0.283	0.344	0.369	0.081	0.342	0.359	0.071	0.392
ΔGo (kJ/mol)	-9.526	-10.97	-9.529	-11.47	-9.231	-11.03	-12.03	-9.015
Δq (%)	76.35	76.02	76.01	76.12	76.07	76.01	76.11	76.04
r	0.999	0.959	0.954	0.983	0.994	0.958	0.987	0.960
Freundlich Isotherms	***Fe***	***Cu***	***Co***	***Hg***	***Ni***	***Zn***	***U***	***Cr***
A	-0.052	0.764	0.914	0.319	0.586	1.054	0.155	0.698
B	0.159	0.403	0.475	0.423	0.384	0.485	0.377	0.409
K_f	0.887	5.802	8.196	2.087	3.856	11.33	1.428	4.996
n	6.258	2.483	2.105	2.361	2.602	2.063	2.652	2.446
ΔGo (kJ/mol)	-15.51	-6.154	-5.219	-5.854	-6.450	-5.113	-6.573	-6.064
Δq (%)	17.02	11.55	7.412	32.46	5.475	7.433	30.17	8.402
r	0.952	0.979	0.991	0.789	0.994	0.992	0.728	0.989
D-R Isotherms	***Fe***	***Cu***	***Co***	***Hg***	***Ni***	***Zn***	***U***	***Cr***
A	-0.452	0.011	0.066	-0.206	-0.071	0.083	-0.274	-0.025
B	-0.002	-0.004	-0.004	-0.006	-0.004	-0.004	-0.006	-0.004
Xm (mol/kg)	0.636	1.011	1.069	0.814	0.932	1.087	0.760	0.975
Es (kJ/mol)	16.47	11.56	10.59	9.164	11.13	11.20	9.352	11.20
Δq (%)	26.46	12.83	9.185	42.18	6.080	10.71	40.86	10.05
r	0.967	0.979	0.987	0.850	0.996	0.986	0.916	0.982
K_d	***Fe***	***Cu***	***Co***	***Hg***	***Ni***	***Zn***	***U***	***Cr***
A	9.404	7.867	7.044	6.212	7.072	7.554	6.496	7.153
B	-1675	-2915	-1340	-1871	-1151	-2320	-2692	-1221
ΔGo (kJ/mol)	-23.31	-19.50	-17.46	-15.40	-17.53	-18.73	-16.10	-17.73
Kdo	1213	2610	1145	498.9	1178	1908	662.7	1278
Δq (%)	34.69	42.43	26.16	7.287	34.18	27.82	14.28	37.67
r	0.805	0.903	0.920	0.992	0.924	0.908	0.954	0.912

A good fit of the data was obtained with the Langmuir isotherm with a correlation coefficient > 0.950, except for Cu with r = 0.937. The good fit reflects monolayer adsorption on a homogenous surface (Teng and Hsieh, 1998). The maximum amount (mol kg^{-1}) of metal ions adsorbed was calculated and followed the sequence: Cr (0.392) > Co (0.369) > Zn (0.359) > Cu (0.344) > Ni (0.342) > Fe (0.283) > Hg (0.081) > U (0.071).

The Langmuir constant ($b/ L\ mol^{-1}$) related to the free energy was in the following order: U > Hg > Zn > Cu > Co > Fe > Ni > Cr. The adsorption process could be described by both the Freundlich and the D-R models as well for the metal ions of concern except Hg and U.

The correlation coefficient obtained for the Freundlich isotherm ranged from 0.952 to 0.994, assuming adsorption on a heterogenous surface. Hg and U presented a correlation coefficient below 0.900. The values of K_f, the binding constant and *n*, the exponent are given in Table 4.28. The intensity of adsorption is an indication of the bond energies between metal ions and adsorbent and the possibility of slight physisorption rather than chemisorption (Vadivelan and Vasanthkumar, 2005). The values of n range between 2.063 and 6.258, indicating that the adsorption is much favourable, and $1/n < 1$, meaning that the metal ions are bound with weak free energies.

The results presented are consistent with the D-R isotherm except for Hg and U. The correlation coefficients are between 0.967-0.996. The values of the apparent energy of adsorption (Es) depict a physisorption process.

Based on the normalized standard deviation, the experimental adsorption isotherms were best described by Freundlich models (Δq= 5.475 – 32.46 %) followed by the D-R models (Δq= 9.185 – 42.18 %) and then the Langmuir. However, this sequence was not respected when comparing the coefficient correlation. A comparison of correlation coefficient (average) for the three isotherms gives the following sequence: Langmuir (0.972) > D-R (0.958) > Freundlich (0.927).

Using the distribution coefficient K_{do} (L Kg^{-1}), the variations of Gibbs free energy were determined and the values ranged from -15.40 to -23.31 kJ mol^{-1}, implying a spontaneous process. The selectivity based on K_{do} was as follows: Cu (2610) > Zn (1908)> Cr (1278) > Fe (1213) > Ni (1178) > Co (1145) > U (662.7) > Hg (498.9). The values of K_{do} prove that U and Hg are bound with weak bonds while other metals are bound with strong bonds. As explained before, the nature of the functional groups on the surface of the adsorbent plays a major role in the adsorption process.

4.4.1.2 Effect of contact time and kinetics of adsorption

i) Effect of contact time

The effect of residence time of adsorption was investigated for 12 h and Figure 4.34 shows the results obtained.

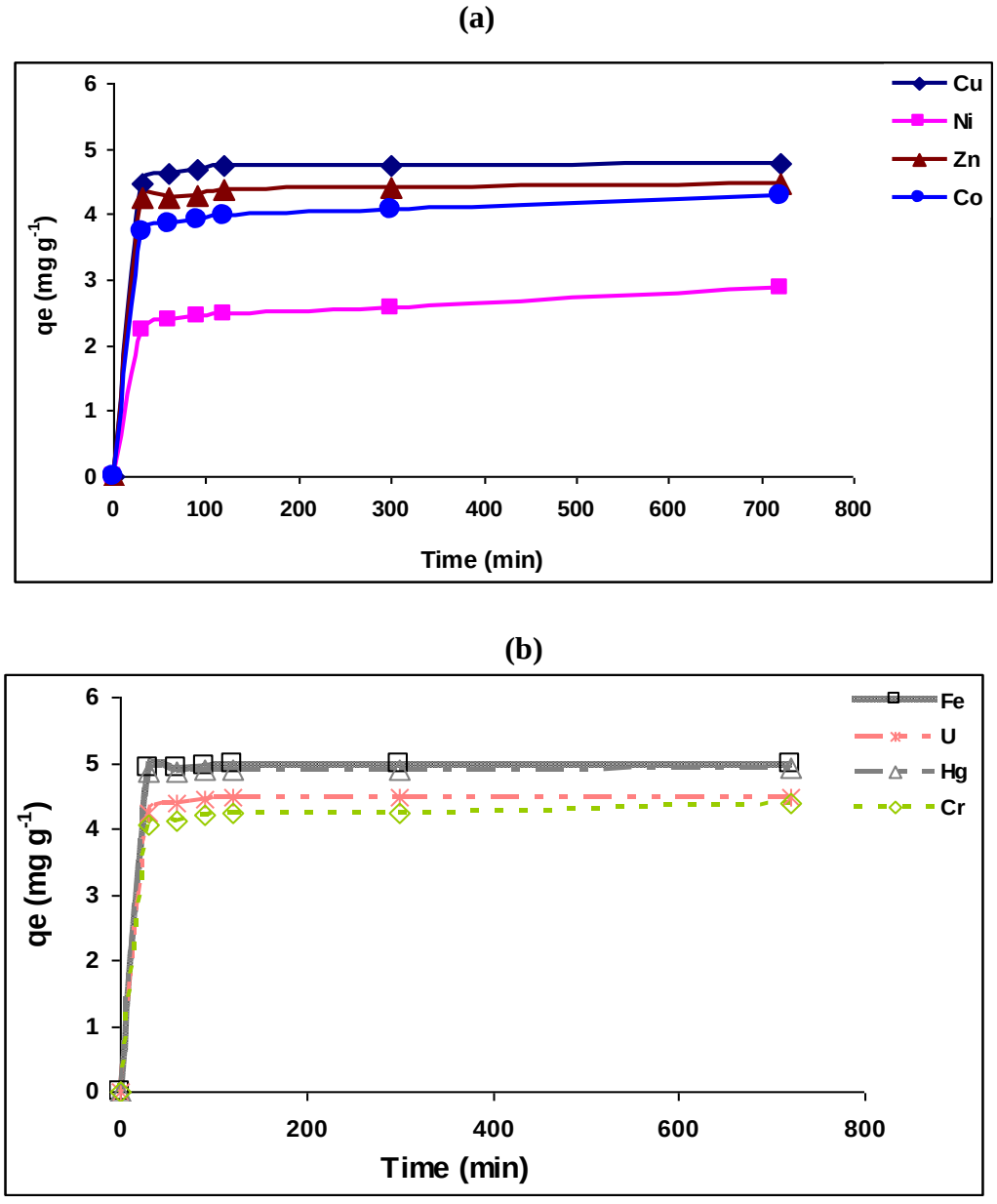


Figure 4.34 Effect of contact time on adsorption of (a) Cu, Ni, Zn, Co and (b) Cr, Fe, Hg and U onto zeolite-histidine in single component solutions (pH=2, C_i = 100 mg L^{-1}, Temp = 298.15±1^oK, agitation rate = 150 rpm)

The adsorption process occurs in two steps: the first occurring during the first 30 minutes of the adsorption and the second are slow and last for 12 h. This indicates that a higher fraction of metal ions migrates from the bulk solution through the adsorbent boundary layer onto the active sites of the adsorbent. The zeolite-histidine contains –NH–, COOH– and OH^- which are responsible for the metal ion binding. In this process, the Ni ion is less adsorbed due to its size and the high energy required for the formation of the zeolite-histidine-H_2O-Ni complex as explained previously.

ii) Kinetic modelling of metal adsorption onto zeolite-histidine

The kinetics of metal ions adsorption on zeolite-histidine was determined using pseudo first-order, pseudo second-order, Elovich, intraparticle diffusion and film diffusion kinetic models. The parameters of the kinetics models with their correspondent coefficients are listed in Table 4.29.

The experimental data gives a good fit with the pseudo-second order with a correlation coefficient of unity or nearly unity for all the metal ions. This confirms the chemisorption nature of the adsorption of metal ions on zeolite-histidine. The calculated values of q_e from the pseudo second-order model were 10 times higher in magnitude than those obtained from the pseudo first-order kinetic. The rate constants of pseudo second-order (k_2) range from 1.323 to 54.01 g (mg min^{-1}) and followed the sequence: U > Hg > Fe >> Cu > Zn > Cr > Co > Ni. These values were found higher than those obtained for the pseudo first-order kinetics.

The Elovich kinetic model could also described the adsorption process in such conditions except for U, Cu and Fe with r < 0.950. The constant *b* was found to be higher for U (305.2 g mg^{-1}) and lower for Fe (67.92 g mg^{-1}).

Table 4.29 Kinetic constants for the adsorption of metal ions on zeolite-histidine

Pseudo-first order								
	Fe	***Cu***	***Co***	***Hg***	***Ni***	***Zn***	***U***	***Cr***
A	-2.788	-2.371	-2.110	-3.437	-2.081	-2.366	-3.152	-2.199
B	-0.007	-0.006	-0.004	-0.005	-0.003	-0.005	-0.009	-0.004
qe (mol/kg)	0.002	0.004	0.008	0.001	0.008	0.004	0.001	0.006
K_1	0.016	0.013	0.008	0.011	0.006	0.011	0.021	0.009
Δq (%)	91.20	88.73	85.51	91.45	83.27	88.50	89.68	88.12
r	0.668	0.709	0.697	0.547	0.690	0.884	0.824	0.611
Pseudo – second order								
	Fe	***Cu***	***Co***	***Hg***	***Ni***	***Zn***	***U***	***Cr***
A	5.566	26.26	114.5	45.03	312.5	40.79	52.07	48.39
B	11.81	13.26	15.24	48.21	20.33	14.62	53.03	11.82
qe (mol/kg)	0.087	0.075	0.065	0.021	0.049	0.068	0.019	0.084
K_2	25.06	6.694	2.029	51.61	1.323	5.236	54.01	2.887
Δq (%)	0.226	0.328	3.403	0.641	6.408	1.456	1.024	2.013
r	1.000	1.000	0.999	1.000	0.990	0.998	1.000	0.999
Elovich model								
	Fe	***Cu***	***Co***	***Hg***	***Ni***	***Zn***	***U***	***Cr***
A	0.013	0.010	0.008	0.003	0.004	0.009	0.003	0.011
B	0.015	0.013	0.011	0.004	0.008	0.012	0.003	0.014
b	67.96	76.75	91.01	278.3	126.1	85.17	305.2	69.33
a	0.035	0.029	0.022	0.009	0.014	0.026	0.007	0.031
Δq (%)	16.50	15.29	13.30	16.41	10.78	15.30	15.65	14.87
r	0.945	0.894	0.994	0.956	0.976	0.960	0.806	0.955
Intraparticle diffusion model								
	Fe	***Cu***	***Co***	***Hg***	***Ni***	***Zn***	***U***	***Cr***
A	0.033	0.028	0.022	0.008	0.015	0.026	0.007	0.031
B	0.004	0.004	0.003	0.001	0.002	0.003	0.001	0.004
Id	0.033	0.028	0.022	0.008	00015	0.026	0.007	0.031
Kp	0.004	0.004	0.003	0.001	0.002	0.003	0.001	0.004
Δq (%)	29.36	29.73	30.39	29.41	31.32	29.72	26.61	29.95
r	0.726	0.749	0.766	0.745	0.790	0.743	0.746	0.745
Film diffusion								
	Fe	***Cu***	***Co***	***Hg***	***Ni***	***Zn***	***U***	***Cr***
A	-1.378	-1.080	-0.684	-1.013	-0.508	-0.934	-1.650	-0.755
B	-0.013	-0.009	-0.006	0.012	-0.005	-0.009	-0.011	-0.008
If	-1.378	-1.080	-0.684	-1.013	-0.508	-0.934	-1.649	-0.745
Kf	0.014	0.009	-0.006	0.012	-0.005	0.008	0.011	0.008
Δq (%)	50.28	48.98	52.33	57.76	54.02	51.18	42.63	54.51
r	0.668	0.709	0.697	0.547	0.689	0.683	0.824	0.611

4.4.1.3 Effect of temperature and thermodynamic parameters

i) Effect of temperature

Figure 4.35 shows the equilibrium adsorption of metal ions on zeolite-histidine as a function of temperature.

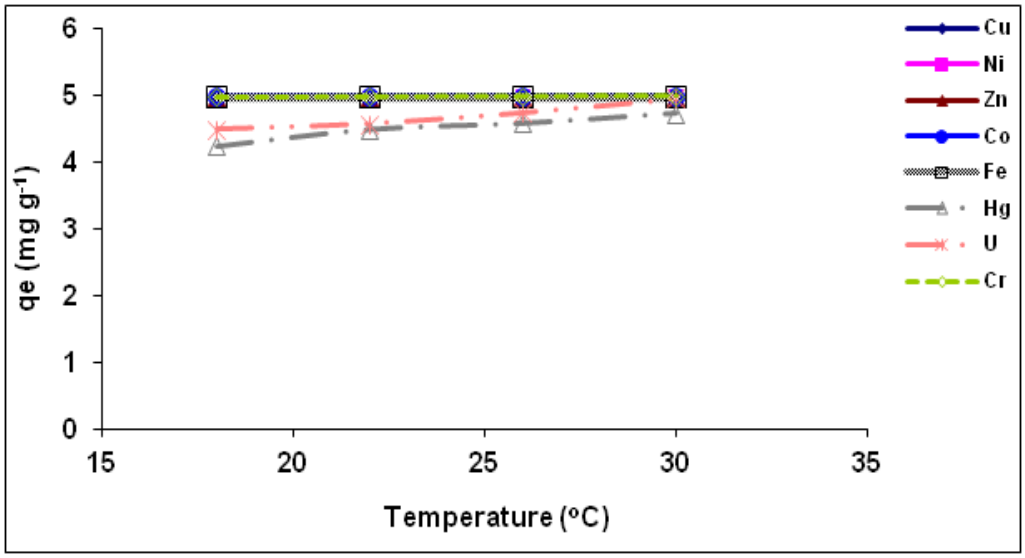


Figure 4.35 Effect of temperature on adsorption of Cu, Cr, Ni, Zn, Co, Fe, Hg and U onto zeolite-histidine in single component solutions (Ci = 100 mg L^{-1}, pH 3, agitation rate = 150 rpm, contact time = 12 h)

As for the previous studies, the uptake of metal ions on zeolite-histidine was not affected much by the change of temperature (18 to 30^{o}C). The adsorption capacity was constant for the temperature range investigated. A slight increase was observed for the adsorption of Hg and U.

ii) Thermodynamic parameters

Thermodynamic parameters such as activation energy, standards Gibbs free energy, ΔG^{o}, enthalpy, ΔH^{o} and entropy, ΔS^{o} changes were calculated from the experimental and are presented in Table 4.30.

Table 4.30 Thermodynamic parameters for the adsorption of heavy metals on zeolite-histidine

	Ea k.J/mol	ΔH^o k.J/mol	ΔS^o J (mol K^{-}1)	ΔG^o k.J/mol			
				291.15 ^{o}K	**295.15** ^{o}K	**299.15** ^{o}K	**303.15** ^{o}K
Cu	92.13	-212.2	-670.8	-12.59	-14.05	-15.65	-16.91
Ni	88.02	-202.7	-642.6	-11.49	-12.33	-13.24	-15.60
Zn	47.00	-108.2	-307.1	-16.18	-16.63	-17.23	-18.78
Co	29.73	-68.46	-174.9	-15.64	-16.40	-17.06	-17.51
Fe	46.51	-107.1	-303.3	-16.20	-16.83	-17.41	-18.78
Hg	71.71	-165.1	-542.1	-4.150	-5.354	-5.968	-7.276
U	149.1	-343.4	-1139	-5.257	-5.812	-7.215	-11.620
Cr	54.93	-126.5	-373.3	-14.45	-15.40	-16.14	-17.31

The values of activation energy, Ea, calculated from the Arrhenius equation were > 40 kJ mol^{-1} for Cu, Ni, Zn, Fe, Hg, U and Cr ions indicating adsorption through a chemisorption process. These results confirm those obtained for the kinetics with chemisorption as the rate-limiting step of the adsorption. The negative values of ΔH° show the exothermic nature of the adsorption and a decrease in temperature favours the adsorption process.

The negative values of ΔG° show that the adsorption is spontaneous and highly favourable for metal ions. The negative values of ΔS° indicate a decrease of the degrees of freedom of the metal ions at the interface of the sorbent.

The rate of reaction increases with an increase in temperature as seen in Table 4.31.

Table 4.31 Rate of metal ions adsorption on zeolite-histidine

Rx rate (h^{-1})				
	291.15 ^{o}K	**295.15** ^{o}K	**299.15** ^{o}K	**303.15** ^{o}K
Cu	0.434	0.477	0.524	0.559
Ni	0.396	0.419	0.444	0.516
Zn	0.557	0.565	0.577	0.621
Co	0.539	0.557	0.572	0.579
Fe	0.558	0.572	0.584	0.621
Hg	0.157	0.191	0.207	0.245
U	0.190	0.205	0.246	0.385
Cr	0.498	0.523	0.541	0.572

4.4.2 Zeolite-Cysteine

As explained in paragraph 4.2.2.1, L-cysteine is adsorbed onto the zeolite surface sites (silanolate groups = Si – O^-) via its -NH_3^+ moiety (Faghihian and Nejati-Yasdinejad, 2009). Sorption studies were performed on the immobilised zeolite. These include: effect of pH, temperature, metal concentration and contact time. The sorption mechanisms and the results obtained are given below.

4.4.2.1 Sorption capacities, pH and isotherms of adsorption

i) Effect of pH

The pH of the aqueous solution is one of the most important parameters playing a significant role in the interaction between solution and adsorbent, ions species in solution and species of functional groups of the adsorbent surface (Sprynskyy, 2011). The effect of pH was studied within the pH range 2 – 12. The results are shown in Figure 4.36 (a) and (b). The maximum adsorption capacity was reached at pH 6 for Ni and Cr ions while the adsorption capacity was at a constant maximum for all pH ranges studied for Cu, Co, Fe, Hg and Zn. A drastic increase of adsorption was observed with Hg and U compared to their adsorption on natural zeolite. This is probably due to the presence of functional groups on the surface of the biosorbent, such as: –NH–, –SH– and COO^- provided by the cysteine molecule. Further explanations were given in paragraph 4.2.2.1.

The results showed that above pH 5, Ni and Cr exist as hydroxy-complexes, meaning that a combination of adsorption and precipitation could have contributed to the increase of adsorption capacity observed beyond pH 5.

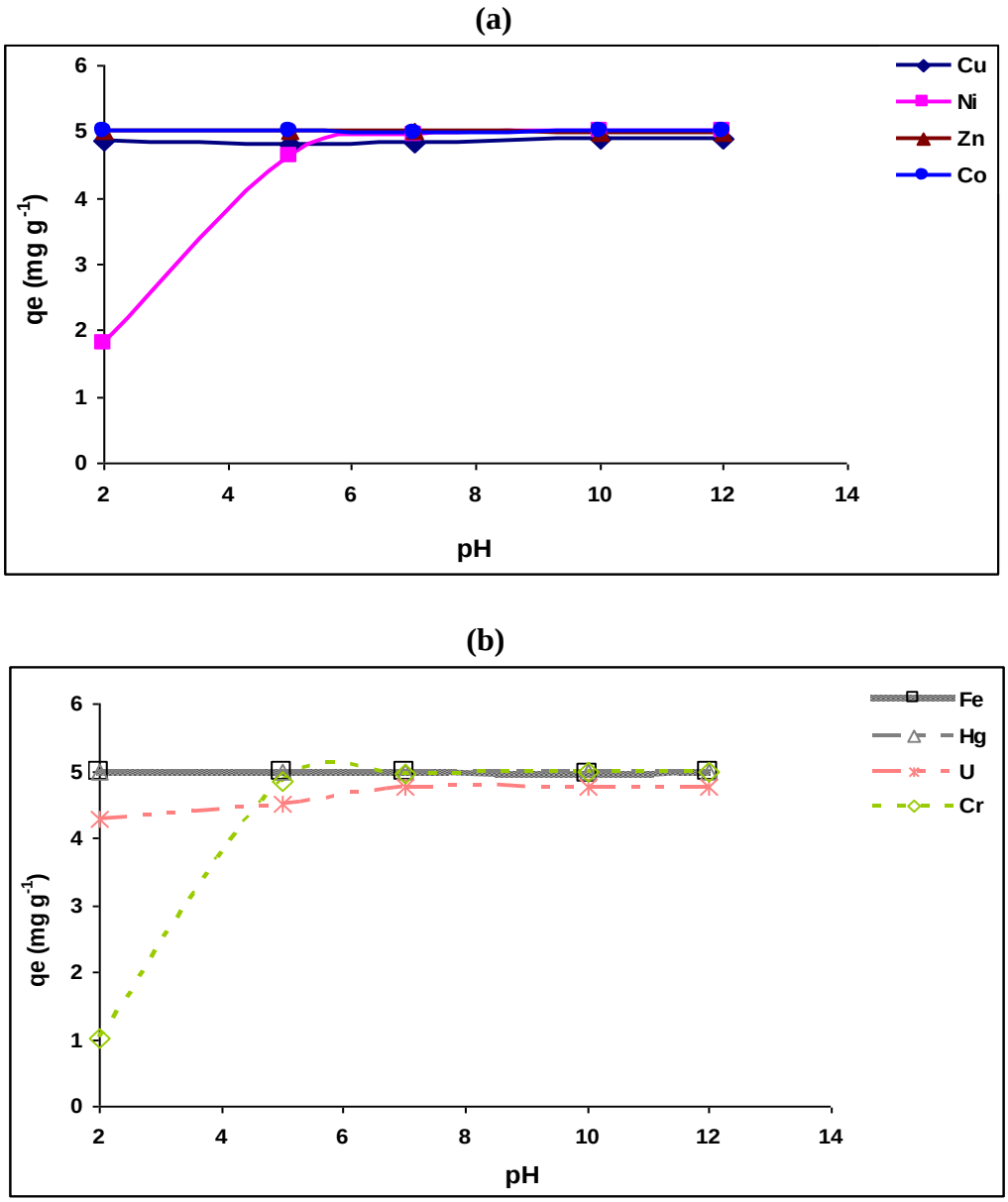


Figure 4.36 Effect of initial pH on adsorption of (a) Cu, Ni, Zn, Co and (b) Cr, Fe, Hg and U onto zeolite-cysteine in single component solutions (C_i = 100 mg L^{-1}, Temp = 298.15±1^{o}K, agitation rate = 150 rpm, agitation time = 12 h)

An illustration of the formation of Ni species as a function of pH is shown in Figure 4.37. The nickel species distribution or predominance diagram depicts the presence of insoluble $Ni(OH)_2$ species above pH 5. The latter can precipitate on the surface of the biosorbent, contributing to an increase of adsorption capacity since at this point it is difficult to distinguish adsorption from precipitation.

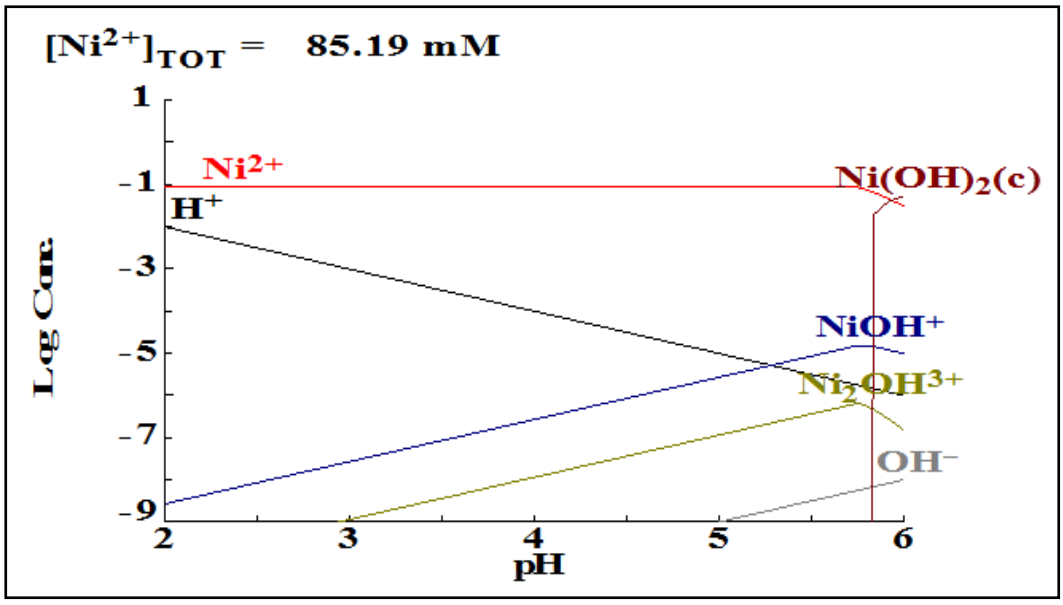
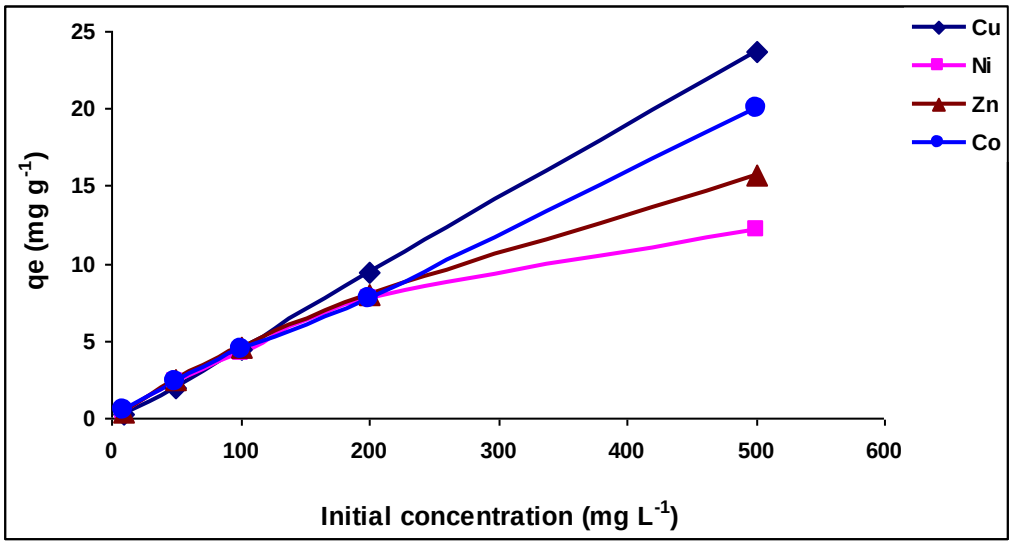


Figure 4.37 Nickel species distribution (using Medusa software)

ii) Effect of concentration

The effect of initial metal ions concentration was investigated in the range of 50 – 500 mg L^{-1}. The results are presented in Figure 4.38. The adsorption capacity firstly increased with increase of metal ions, reaching a saturation value at about 200 mg L^{-1} for Ni, Zn and Cr ions. A decrease in the rate of adsorption was observed for these metal ions beyond that concentration. The selectivity for a particular metal ion is subject to the ionic size of the ion and the nature of the functional group which constitutes the active sites. The rate of adsorption for Cu, Co, Fe, Hg and U ions was constant up to a concentration of 500 mg L^{-1}. The enhancement of the adsorption capacity may be due to the presence of functional groups (as described previously) on the surface of the biosorbent.

(a)



(b)

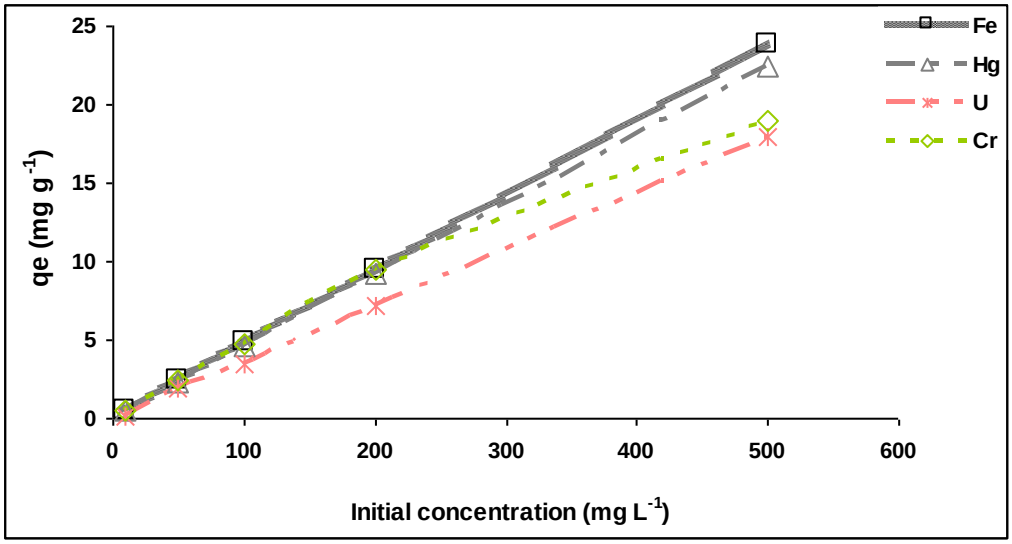


Figure 4.38 Effect of concentration on the adsorption of (a) Cu, Ni, Zn, Co and (b) Cr, Fe, Hg and U onto zeolite-cysteine in single component solutions (pH 3,Temp = 298.15±1^{o}K, agitation rate= 150 rpm, agitation time= 12 h)

iii) Adsorption isotherms for zeolite-cysteine

The adsorption data were analysed using the Langmuir, Freundlich and D-R models. The isothermic constants as well as the correlation coefficients are presented in Table 4.32.

Table 4.32 Parameters of the Langmuir, Freundlich and D-R models for the adsorption of metals on the zeolite-cysteine system

Langmuir Isotherms	***Fe***	***Cu***	***Co***	***Hg***	***Ni***	***Zn***	***U***	***Cr***
A	0.022	0.124	0.072	0.047	0.170	0.105	-0.018	0.048
B	1.290	-13.32	3.057	4.199	4.531	3.824	-53.79	2.544
b	59.57	107.6	42.51	89.97	26.61	36.27	14.57	52.60
qm (mol/kg)	0.774	0.075	0.327	0.238	0.220	0.261	0.019	0.393
ΔGo (kJ/mol)	-10.13	-7.421	-9.295	-11.15	-8.134	-8.901	-7.235	-9.823
Δq (%)	75.93	75.93	76.05	75.92	76.17	76.12	76.02	76.19
r	0.421	0.856	0.811	0.598	0.997	0.979	0.720	0.996
Freundlich Isotherms	***Fe***	***Cu***	***Co***	***Hg***	***Ni***	***Zn***	***U***	***Cr***
A	0.252	0.174	0.231	0.207	0.157	0.148	0.258	0.239
B	0.339	0.386	0.368	0.439	0.394	0.369	0.597	0.344
K_f	1.787	1.493	1.635	1.610	1.436	1.408	1.812	1.735
n	2.945	2.588	2.715	2.274	2.532	2.703	1.675	2.903
ΔGo (kJ/mol)	-7.301	-6.415	-6.731	-5.637	-6.278	-6.700	-4.153	-7.195
Δq (%)	14.56	32.89	51.44	1.007	61.35	112.2	52.67	58.27
r	0.973	0.971	0.981	0.995	0.956	0.876	0.887	0.985
D-R Isotherms	***Fe***	***Cu***	***Co***	***Hg***	***Ni***	***Zn***	***U***	***Cr***
A	0.554	0.642	-0.111	0.264	-0.179	-0.190	0.562	0.047
B	-0.005	-0.008	-0.005	-0.006	-0.006	-0.005	-0.011	-0.005
Xm (mol/kg)	1.740	1.901	0.896	1.302	0.836	0.827	1.755	1.048
Es (kJ/mol)	9.504	7.998	10.11	8.773	9.248	9.840	6.863	10.43
Δq (%)	57.96	19.24	26.56	22.72	25.73	72.27	22.51	14.89
r	0.982	0.976	0.981	0.997	0.978	0.878	0.899	0.992
K_d	***Fe***	***Cu***	***Co***	***Hg***	***Ni***	***Zn***	***U***	***Cr***
A	5.332	2.398	5.205	4.709	4.756	5.142	2.755	5.776
B	5016	1520	87.79	8247	-155.5	-199.1	4919	-237.6
ΔGo (kJ/mol)	-13.21	-5.946	-12.91	-11.67	-11.69	-12.74	-6.828	-14.32
Kdo	206.8	110.1	182.2	110.9	111.7	171.1	15.71	322.4
Δq (%)	76.73	16.95	62.68	79.12	61.89	60.59	94.69	67.25
r	0.443	0.816	0.783	0.564	0.917	0.766	0.406	0.873

The correlation coefficients presented in Table 4.32 indicate that the adsorption data for Fe, Cu, Co and Hg ions fit well the Freundlich as well as the D-R isotherms. The adsorption occurs on heterogeneous surface and according to *b* (mmol kg^{-1}), the maximum amount that can be adsorbed on zeolite-cysteine follows the sequence: Cu > Hg > Fe > Cr > Co > Zn > Ni > U.

The values of *n* obtained from the Freundlich isotherm range from 1 to 3 with *1/n* < 1, confirming a beneficial adsorption. The adsorption of Cr and Ni ions can be described by the three models with r > 0.950. This means that the adsorption of Cr and Ni on zeolite-cysteine may occur through monolayer coverage, on homogenous as well as heterogeneous surface. The values of adsorption energy were in the range of 6.863 to 10.43 kJ mol^{-1}, implying physisorption or an ion-exchange process.

Adsorption equilibrium isotherms of U ion onto zeolite-cysteine cannot be simulated by the above models, the correlation coefficient is less than 0.900. The distribution coefficient of U calculated was ten times less in magnitude compared to those for the other metal ions. This result was confirmed by the low value of the maximum amount obtained from the Langmuir isotherm. This value is far below compared to the values obtained for other metal ions. Further isotherm models could be used to fit the data. For instance, Sprynskyy *et al.* (2011) suggested the BET isotherm for the adsorption of uranium on talc. The Gibbs free energies calculated from the coefficients were negative for all the metal ions, suggesting a spontaneous and feasible process.

4.4.2.3 Effect of contact time and kinetics of adsorption

i) Effect of contact time

The adsorption of metal ions adsorption as a function of residence time was studied from 10 to 720 minutes. The results in Figure 4.39 show a two step process, namely: a fast one within the 30 first minutes followed by a slow down. At the initial stage, the rate of adsorption was higher due to the availability of more than the required number of active sites on the surface of the adsorbent and became lower at the latter stages of contact time due to a decrease in active sites. The adsorption capacity of Ni increased within the first 30 minutes, and then decreased gradually until equilibrium. Desorption could occur at this stage due to the weak bonds with the sorbent.

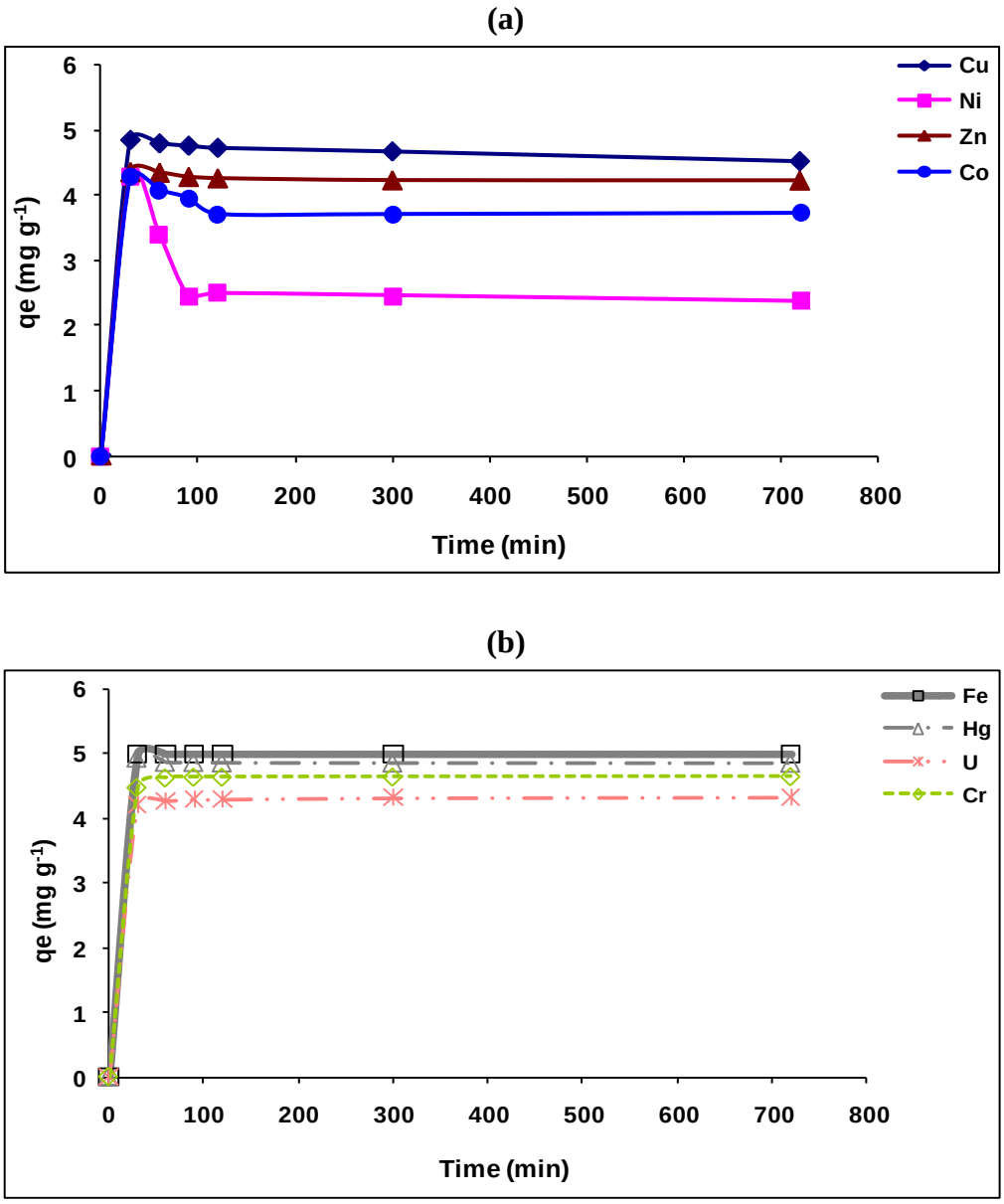


Figure 4.39 Effect of contact time on adsorption of (a) Cu, Ni, Zn, Co and (b) Cr, Fe, Hg and U onto zeolite-cysteine in single component solutions (pH=3, C_i = 100 mg L^{-1}, Temp = 298.15±1^oK, agitation rate = 150 rpm)

ii) Kinetic modelling of metal ions adsorption on zeolite-cysteine

The kinetics of sorption describes the solute uptake rate, which in turn governs the residence time of the sorption reaction. It is one of the important characteristics in defining the efficiency of sorption. Modelling of kinetic data is fundamental for the industrial application of sorption since it gives information for comparison among different biomaterials under different operational conditions for designing and optimizing operational conditions for

pollutant removal from wastewater systems (Benguella and Asissa, 2002). The time-dependent experimental adsorption data were used for kinetic modelling. The different kinetic models used were the pseudo first-order, pseudo second-order, Elovich, intraparticle diffusion and film diffusion. These kinetic models, the values of different parameters and the correlation coefficients obtained using non-linear regression are listed in Table 4.33.

Table 4.33 Kinetic constants for the adsorption of metal ions on zeolite-cysteine

Pseudo-first order								
	Fe	***Cu***	***Co***	***Hg***	***Ni***	***Zn***	***U***	***Cr***
A	-4.477	-2.318	-1.974	-3.308	-1.562	-2.356	-3.344	-2.778
B	-0.011	-0.006	-0.004	-0.004	-0.002	-0.008	-0.007	-0.009
qe (mol/kg)	0.002	0.005	0.011	0.004	0.027	0.004	0.008	0.002
K_1	0.026	0.013	0.009	0.009	0.005	0.018	0.017	0.020
Δq (%)	92.55	88.31	83.52	91.37	69.97	87.64	90.77	91.16
r	0.557	0.727	0.757	0.493	0.875	0.845	0.738	0.700
Pseudo-second order								
	Fe	***Cu***	***Co***	***Hg***	***Ni***	***Zn***	***U***	***Cr***
A	0.036	29.45	124.8	52.53	728.7	25.25	42.53	4.789
B	11.17	13.08	13.74	40.70	13.53	14.96	54.89	11.16
qe (mol/kg)	0.089	0.076	0.073	0.025	0.074	0.067	0.018	0.089
K_2	81.34	5.814	1.513	31.53	0.251	8.866	70.85	25.99
Δq (%)	0.002	0.217	4.675	1.073	16.28	0.894	0.088	0.896
r	1.000	1.000	0.999	1.000	0.993	0.995	0.997	1.000
Elovich model								
	Fe	***Cu***	***Co***	***Hg***	***Ni***	***Zn***	***U***	***Cr***
A	0.014	0.011	0.008	0.004	0.002	0.010	0.003	0.013
B	0.016	0.013	0.012	0.005	0.010	0.012	0.005	0.016
b	64.13	75.88	82.76	235.4	97.62	86.68	316.2	64.08
a	0.038	0.029	0.023	0.010	0.010	0.027	0.007	0.037
Δq (%)	16.80	15.21	12.63	16.39	9.141	15.72	16.19	16.19
r	0.775	0.928	0.950	0.848	0.928	0.954	0.922	0.686
Intraparticle diffusion model								
	Fe	***Cu***	***Co***	***Hg***	***Ni***	***Zn***	***U***	***Cr***
A	0.036	0.028	0.024	0.010	0.012	0.025	0.007	0.035
B	0.005	0.004	0.004	0.001	0.003	0.003	0.001	0.005
Id	0.036	0.028	0.024	0.010	0.012	0.025	0.007	0.035
Kp	0.005	0.004	0.004	0.001	0.003	0.003	0.001	0.005
Δq (%)	29.27	29.75	30.57	29.44	34.50	29.54	29.44	29.47
r	0.721	0.749	0.779	0.723	0.895	0.740	0.732	0.735
Film diffusion								
	Fe	***Cu***	***Co***	***Hg***	***Ni***	***Zn***	***U***	***Cr***
A	-2.341	-1.053	-0.709	-0.883	-0.369	-1.418	-1.377	-1.656
B	-0.028	-0.009	-0.006	-0.012	-0.002	-0.009	-0.012	-0.014
If	-2.341	-1.053	-0.709	-0.883	-0.369	-1.418	-1.377	-1.656
Kf	0.028	0.009	0.006	0.012	0.002	0.009	0.012	0.014
Δq (%)	59.88	48.86	50.39	60.96	56.93	43.64	47.23	46.02
r	0.557	0.727	0.757	0.493	0.875	0.845	0.824	0.699

Examination of Table 4.33 shows that pseudo second-order kinetic model gave the best fit for the description of the mechanism of adsorption of metal ions on zeolite-cysteine. The correlation coefficients obtained were higher than 0.990 for all the metals. The sorption

capacity q_e values obtained were ten times more than those calculated from the pseudo first-order kinetic model. The rate of adsorption was very high for Fe (3481 kg (mol min)$^{-1}$). Furthermore, the pseudo second-order is based on the assumption that sorption follows a second-order mechanism, with chemisorption as the rate-limiting step. So the rate of occupation of adsorption sites is proportional to the square of the number of unoccupied sites.

4.4.2.3 Effect of temperature and thermodynamic parameters

i) Effect of temperature

Adsorption experiments of metal ions on zeolite-cysteine were carried out at four different temperatures while keeping the other parameters constant (e.g. pH, initial concentration, contact time). Figure 4.40 illustrates the results obtained.

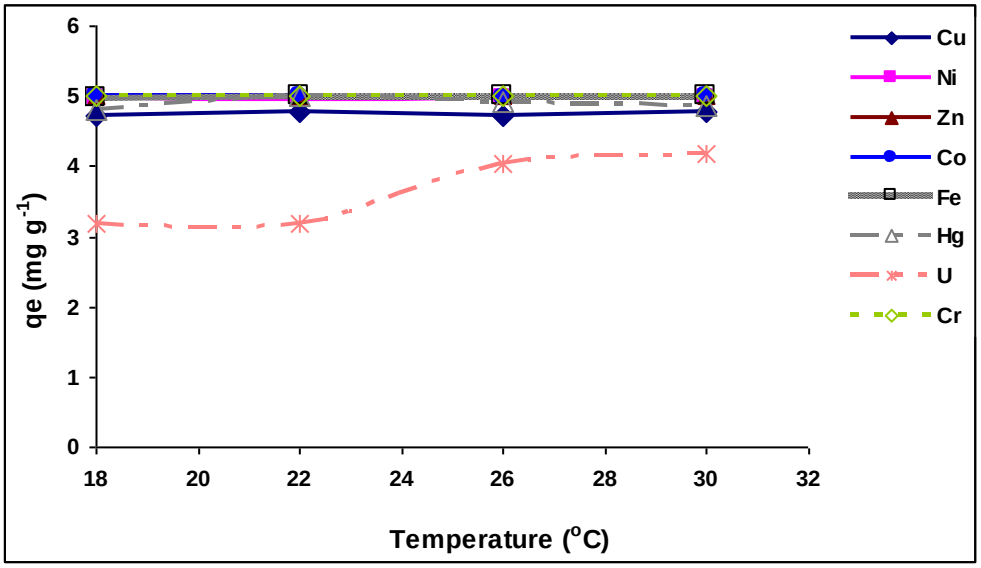


Figure 4.40 Effect of temperature on adsorption of Cu, Cr, Ni, Zn, Co, Fe, Hg and U onto zeolite-cysteine in single component solutions (C_i = 100 mg L^{-1}, pH 3, agitation rate = 150 rpm, contact time = 12 h)

It was found that adsorption capacity was not much affected by the change in temperature for the range of temperature studied. U was the only metal to be affected by the increase in temperature. This could result from two possible reasons, namely: the increase in chemical interaction between adsorbate and surface functionalities of adsorbent and also the increasing intraparticle diffusion rate of adsorbate molecules into the pores when temperature is increased.

ii) Thermodynamic parameters of adsorption of metal ions onto zeolite-cysteine

The thermodynamic parameters obtained are presented in Table 4.34. The rate of reaction as a function of temperature was calculated and the results are listed in Table 4.35.

Table 4.34 Thermodynamic parameters for the adsorption of metal ions onto zeolite-cysteine

	Ea kJ mol^{-1}	ΔH^o kJ mol^{-1}	ΔS^o J(K $mol)^{-1}$	ΔG^o kJ mol^{-1}			
				291.15 ^oK	**295.15** ^oK	**299.15** ^oK	**303.15** ^oK
Cu	18.81	-43.31	-121.7	-6.803	-7.422	-6.910	-7.859
Ni	13.06	-300.7	-987.3	-12.19	-11.20	-12.64	-13.24
Zn	17.19	-39.59	-73.51	-16.77	-16.21	-16.74	-18.17
Co	2.900	-6.679	-32.49	-15.39	-15.44	-15.15	-16.14
Fe	19.22	-44.25	-95.82	-14.94	-19.08	-17.10	-16.35
Hg	-110.2	-110.2	-322.8	-7.634	-8.561	-10.56	-16.20
U	63.82	-146.9	-490.5	-1.378	-1.393	-3.581	-4.064
Cr	34.23	-78.81	-193.8	-22.83	-21.96	-23.17	-22.36

As shown in Table 4.34, low values for activation energy were obtained for the metals studied, except U and Hg with Ea > 40 kJ mol^{-1} which implied a physisorption process. The values for ΔH^o were negative with higher values for Ni. The negative values of ΔH^o indicate that the sorption reaction is exothermic. An increase of temperature should decrease the adsorption capacity. The entropy values were negative ΔS^o, meaning a decrease of degrees of freedom for the metal ions at the sorbent-sorbate interface. The negative value of ΔG^o confirms the feasibility of the process and the spontaneous nature of sorption. The rate of adsorption increases with increasing temperature as seen in Table 4.34. The rate of the adsorption of metal ions onto zeolite-cysteine was favoured by temperature as seen in Table 4.35.

Table 4.35 Rate of the adsorption of metal ions on zeolite-cysteine

Rx rate (h^{-1})				
	291.15 ^oK	**295.15** ^oK	**299.15** ^oK	**303.15** ^oK
Cu	0.237	0.239	0.256	0.263
Ni	0.421	0.381	0.424	0.438
Zn	0.551	0.561	0.577	0.601
Co	0.508	0.524	0.530	0.534
Fe	0.515	0.541	0.573	0.648
Hg	0.266	0.293	0.355	0.522
U	0085	0.105	0.138	0.150
Cr	0.786	0.776	0.746	0.739

4.4.3 Zeolite-Sorbitol

4.4.3.1 Sorption capacities, pH and isotherms

i) Effect of pH

The binding of metals as a function of pH (for the range 2–12) is shown in Figure 4.41. Two trends were observed: (i) adsorption capacity was maximum and constant for the all ranges of pH studied for the metals: Cu, Ni, Zn, Co and Cr; and (ii) the second trend indicates that Fe, U and Hg are pH dependent with more metals bound at higher pH and the maximum uptake of metal ions taking place at pH 5.

According to the surface complexation theory, the increase in metal removal with increase in pH could be explained on the basis of a decrease in competition between proton and metal species for the surface sites and by a decrease in positive surface charge. Metal binding by substrate is reduced at low pH values due to increasing competition of protons for the same binding sites. Also, as explained before, the metal hydroxide complexes precipitate at high pH contributing to the increase of the metal uptake.

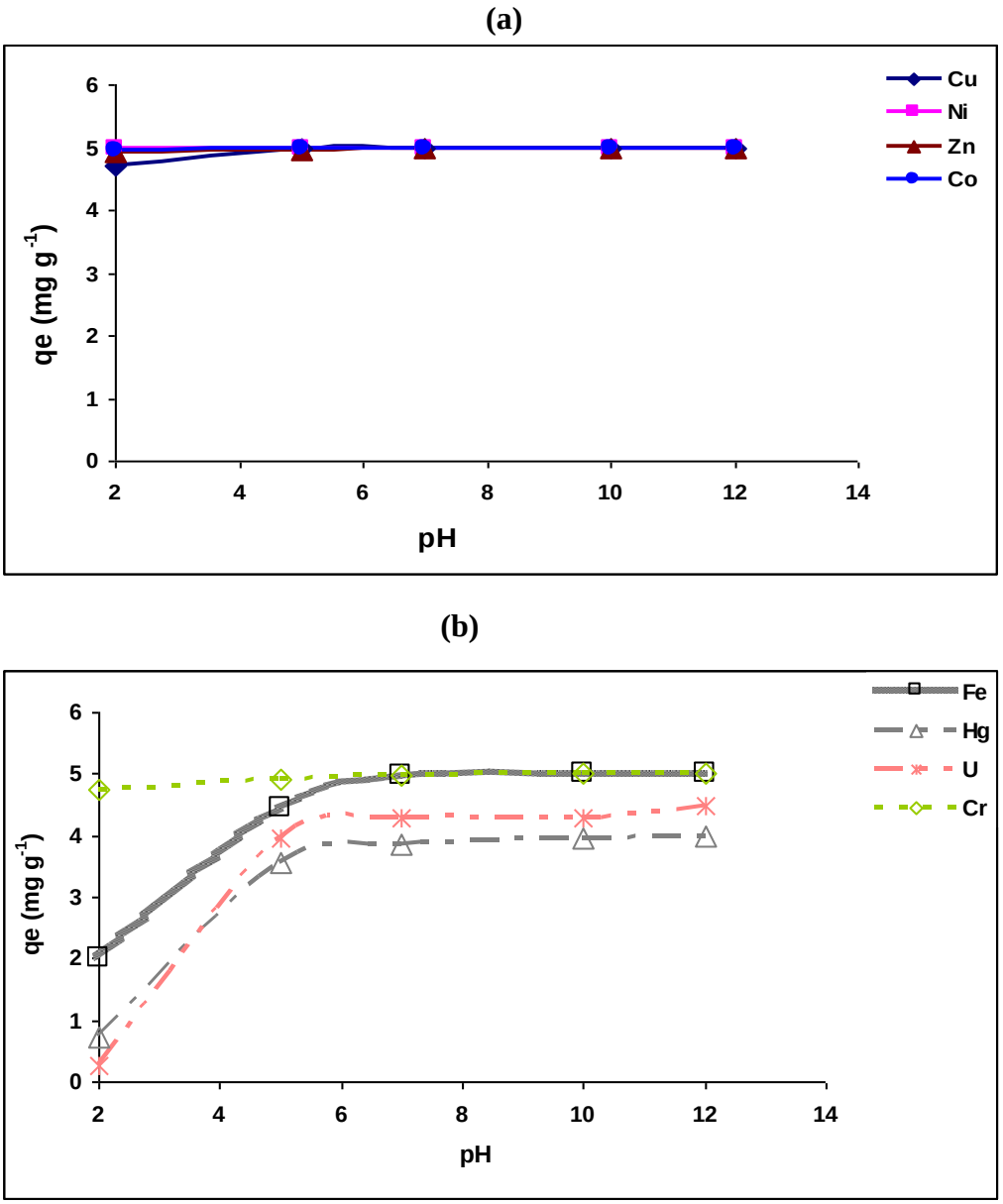
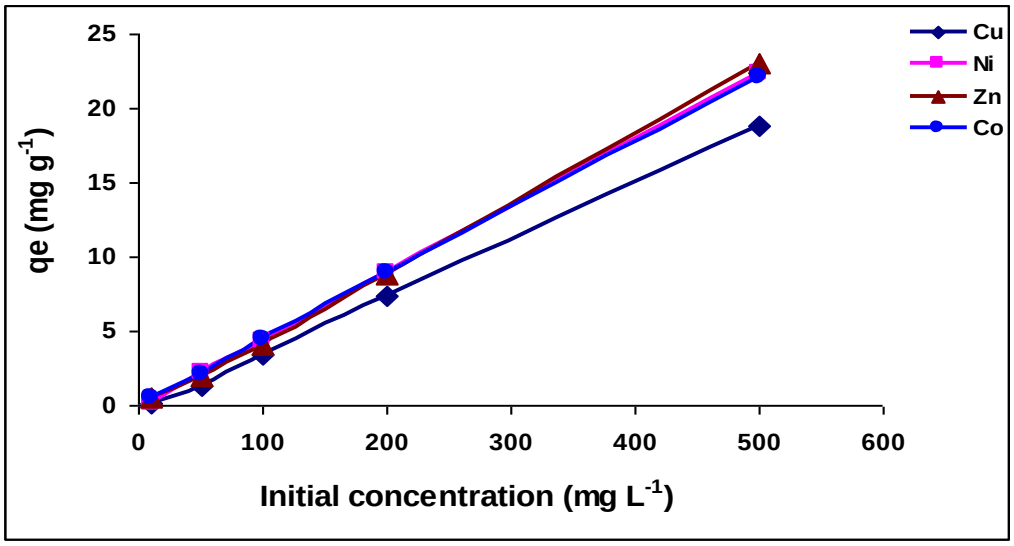


Figure 4.41 Effect of initial pH on adsorption of (a) Cu, Ni, Zn, Co and (b) Cr, Fe, Hg and U onto zeolite-sorbitol in single component solutions (C_i = 100 mg L^{-1}, Temp = 298.15±1^{o}K, agitation rate = 150 rpm, agitation time = 12 h)

ii) Effect of concentration

The effect of initial concentration on the adsorption of metal ions, at concentration levels ranging from 50 to 500 mg L^{-1} is shown in Figure 4.42.

(a)



(b)

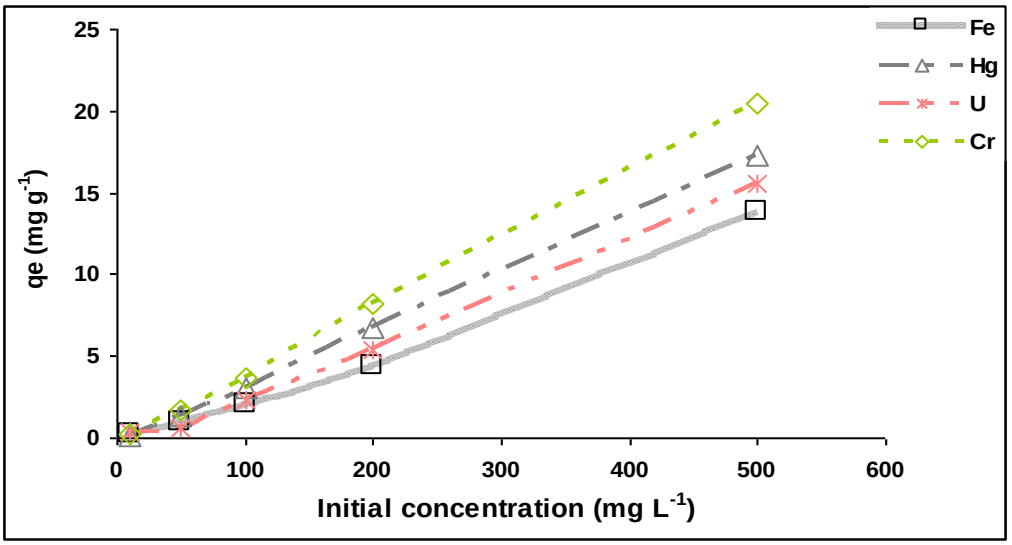


Figure 4.42 Effect of concentration on the adsorption of (a) Cu, Ni, Zn, Co and (b) Cr, Fe, Hg and U onto zeolite-sorbitol in single component solutions (pH 3, Temp = 298.15±1^{o}K, agitation rate= 150 rpm, agitation time= 12 h)

The figure shows that the adsorption of the metals at different concentrations increased linearly with increase in concentration. It can be seen that the saturation point was not reached up to 500 mg L^{-1}. The adsorption trend can be predicted to continue before saturation is reached. Sorption isotherms represent the distribution of metal ions between aqueous and solid phases (biosorbent) when the concentration increases and as long as binding sites are not saturated.

iii) Isotherms of adsorption for zeolite-sorbitol

The isothermic constants calculated from Langmuir, Freundlich and Dubinin-Radushkevich models are given in Table 4.36. The distribution coefficients as well as the Gibbs free energy calculated from the distribution coefficient are listed in Table 4.36.

Table 4.36 Parameters of the Langmuir, Freundlich and D-R models for the adsorption of metals on zeolite-sorbitol

Langmuir Isotherms	***Fe***	***Cu***	***Co***	***Hg***	***Ni***	***Zn***	***U***	***Cr***
A	0.605	0.626	0.062	0.428	0.194	0.074	0.585	0.258
B	0.717	15.03	1.314	11.88	-14.25	-0.180	-17.94	-9.106
b	1.186	24.01	21.25	27.78	73.25	2.432	30.66	35.21
qm (mol/kg)	1.394	0.066	0.761	0.084	0.071	5.544	0.557	0.109
ΔGo (kJ/mol)	-0.422	-6.693	-7.577	-6.244	-14.21	-5.203	-9.652	-10.22
Δq (%)	75.90	75.96	75.96	75.90	75.99	75.92	75.90	75.90
r	0.799	0.751	0.655	0.743	0.866	0.875	0.816	0.817
Freundlich Isotherms	***Fe***	***Cu***	***Co***	***Hg***	***Ni***	***Zn***	***U***	***Cr***
A	0.241	0.326	0.258	0.248	0.204	0.213	0.141	0.283
B	0.565	0.561	0.391	0.591	0.405	0.384	0.587	0.473
K_f	1.741	2.119	1.814	1.772	1.599	1.635	1.382	1.917
n	1.771	1.783	2.556	1.693	2.466	2.607	1.704	2.116
ΔGo (kJ/mol)	-4.390	-4.420	-6.335	-4.196	-6.114	-6.462	-4.225	-5.245
Δq (%)	6.045	36.37	85.79	16.62	46.34	65.89	9.329	24.96
r	0.984	0.978	0.979	0.996	0.784	0.904	0.993	0.983
D-R Isotherms	***Fe***	***Cu***	***Co***	***Hg***	***Ni***	***Zn***	***U***	***Cr***
A	0.066	0.881	0.312	0.431	0.536	0.127	0.424	0.771
B	-0.011	-0.012	0.006	-0.016	-0.008	-0.005	-0.008	-0.010
Xm (mol/kg)	1.069	2.413	1.366	1.539	1.710	0.880	0.654	2.163
Es (kJ/mol)	6.833	6.364	8.874	6.867	7.962	9.768	7.529	6.992
Δq (%)	33.41	11.97	41.58	38.78	33.29	79.79	12.47	95.04
r	0.968	0.988	0.966	0.999	0.779	0.982	0.966	0.992
K_d	***Fe***	***Cu***	***Co***	***Hg***	***Ni***	***Zn***	***U***	***Cr***
A	2.472	2.326	4.449	2.634	3.609	4.066	2.602	2.933
B	511.8	1886	2184	3688	4035	4304	2714	2012
ΔGo (kJ/mol)	-6.127	-5.765	-11.03	-6.530	-8.948	-10.08	-6.451	-7.271
K_{do}	11.84	10.23	85.58	13.93	36.95	58.34	13.49	18.79
Δq (%)	49.63	91.56	75.74	72.80	97.58	51.34	50.63	93.75
r	0.736	0.896	0.749	0.840	0.340	915	0.877	0.826

The values of statistical parameters show that the experimental data are described well by the models except for Zn and Ni with r < 0.900. The adsorption of Zn ion is described better by the D-R model (r > 0.982). Experimental data for Ni did not fit any of the models described above. Both models confirm the heterogeneous character of the adsorbent surface. The adsorption free energies E_s (kJ mol^{-1}) calculated from the D-R model predict a physical

process (Es < 8 kJ mol^{-1}) for the adsorption of Cu, Cr, Co, Fe, Hg, U and Ni whereas ion exchange process was predicted for Zn (Es > 8 kJ mol^{-1}).

The metal ions selectivity based on the distribution coefficients K_{do} (L kg^{-1}) was: Co (85.58) > Zn (58.34) > Ni (36.95) > Cr (18.74) > Hg (13.93) > U (13.49) > Fe (11.840 > Cu (10.23). These values are very low compared to those obtained for natural zeolite, suggesting weak bonds between the metal ions and the sorbent. Due to the modification using sorbitol, metal ions bind covalently with hydroxyl groups. ΔG^o values calculated from the distribution coefficient were negative ranging from -5.765 to -10.08 kJ mol^{-1}, confirming the feasibility and spontaneous nature of the process.

4.4.3.2 Effect of contact time and kinetics of adsorption

i) Effect of contact time

The adsorption of metal ions on zeolite-sorbitol was fast and occurred in 2 steps as seen in the Figure 4.43.

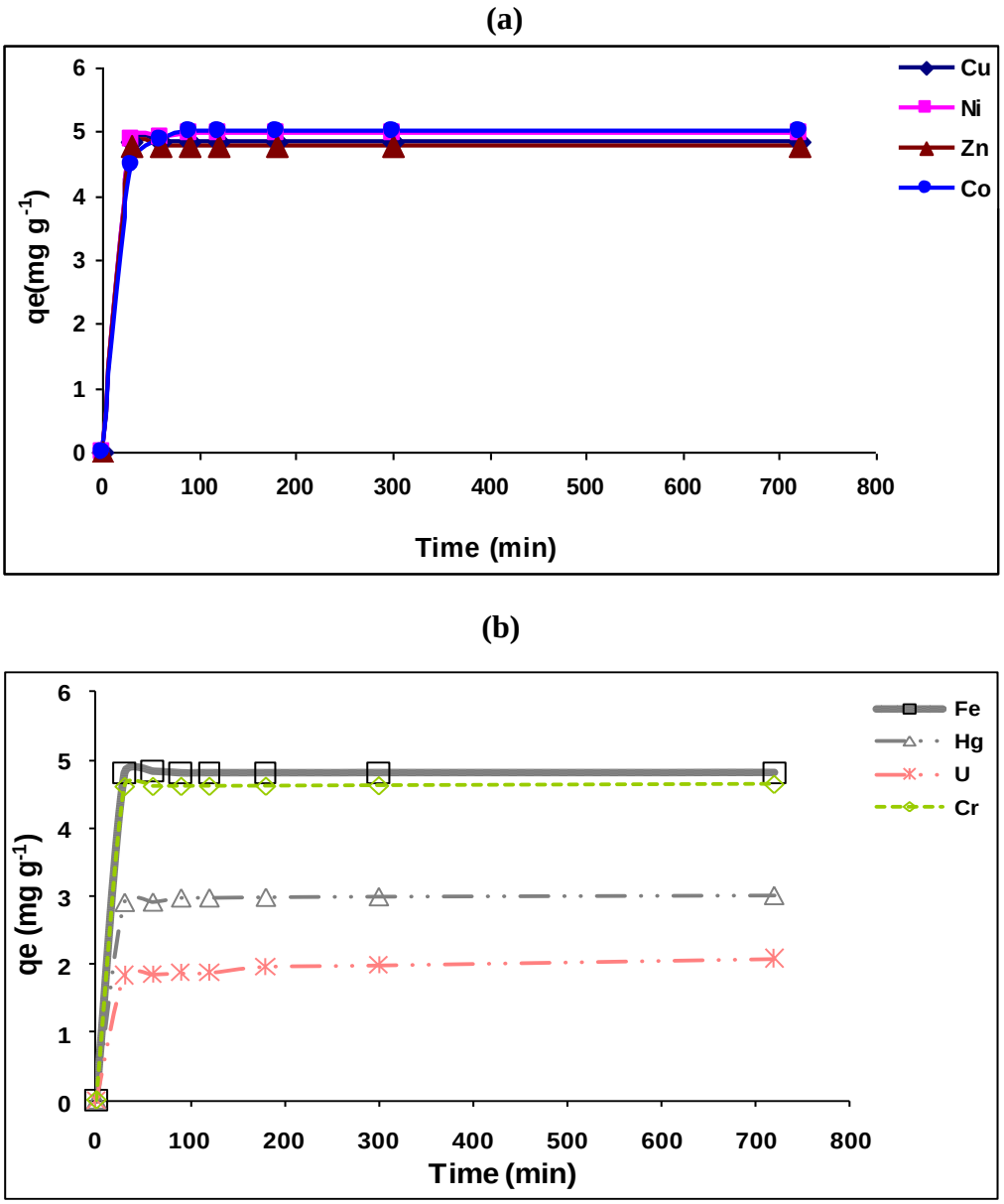


Figure 4.43 Effect of contact time on adsorption of (a) Cu, Ni, Zn, Co and (b) Cr, Fe, Hg and U onto zeolite-sorbitol in single component (pH 3, C_i = 100 mg L^{-1}, Temp = 298.15±1^{o}K, agitation rate = 150 rpm)

A similar trend was observed as in the previous study, namely: (i) initial rapid sorption extending over the first 30 minutes; (ii) step of slow down approaching equilibrium. Hg and U had the lowest adsorption capacities.

ii) Kinetic modelling of adsorption of metals onto zeolite-sorbitol

The experimental data on the adsorption of heavy metals on zeolite-sorbitol were modelled by the following: pseudo-first order, pseudo-second order, Elovich, intraparticle and film diffusion kinetic models. Table 4.37 presents different rate constants, the amount adsorbed and correlation coefficients.

Table 4.37 Kinetic constants for the adsorption of metal ions on zeolite-sorbitol

Pseudo-first order								
	Fe	***Cu***	***Co***	***Hg***	***Ni***	***Zn***	***U***	***Cr***
A	-3.474	-3.576	-2.457	-3.674	-3.112	-3.936	-3.454	-3.252
B	-0.009	-0.009	-0.018	-0.006	-0.010	-0.009	-0.004	-0.005
qe (mol/kg)	0.003	0.001	0.003	0.003	0.002	0.001	0.005	0.001
K_1	0.020	0.021	0.041	0.014	0.022	0.020	0.008	0.012
Δq (%)	92.93	92.32	88.97	90.61	91.16	92.34	87.71	91.76
r	0.601	0.623	0.844	0.714	0.731	0.596	0.728	0.527
Pseudo – second order								
	Fe	***Cu***	***Co***	***Hg***	***Ni***	***Zn***	***U***	***Cr***
A	0.743	0.662	13.48	180.2	10.31	1.660	1961	11.86
B	11.61	13.09	11.78	133.6	23.54	27.37	227.4	22.36
qe (mol kg^{-1})	0.086	0.076	0.085	0.007	0.042	0.036	0.004	0.045
K_2	181.2	259.1	10.28	99.11	53.74	451.4	26.36	42.17
Δq (%)	0.031	0.023	2.769	0.558	0.463	0.025	4.779	0.425
r	0.998	1.000	1.000	1.000	0.999	1.000	0.999	1.000
Elovich model								
	Fe	***Cu***	***Co***	***Hg***	***Ni***	***Zn***	***U***	***Cr***
A	0.013	0.012	0.011	0.002	0.006	0.006	0.001	0.007
B	0.015	0.013	0.015	0.001	0.007	0.006	0.003	0.008
b	66.65	75.20	67.60	772.3	135.3	157.2	136.7	128.8
a	0.037	0.033	0.032	0.003	0.018	0.016	0.001	0.019
Δq (%)	16.77	16.77	14.99	15.87	16.29	16.77	13.17	16.60
r	0.992	0.965	0.715	0.912	0.799	0.990	0.963	0.911
Intraparticle diffusion model								
	Fe	***Cu***	***Co***	***Hg***	***Ni***	***Zn***	***U***	***Cr***
A	0.034	0.031	0.031	0.003	0.017	0.015	0.001	0.018
B	0.004	0.004	0.004	0.002	0.002	0.002	0.001	0.002
Id	0.034	0.031	0.031	0.003	0.017	0.015	0.001	0.018
Kp	0.004	0.004	0.004	0.002	0.002	0.002	0.001	0.002
Δq (%)	29.28	29.28	29.84	29.54	29.42	29.28	30.41	29.34
r	0.721	0.721	0.764	0.737	0.732	0.721	0.767	0.722
Film diffusion								
	Fe	***Cu***	***Co***	***Hg***	***Ni***	***Zn***	***U***	***Cr***
A	-1.730	-1.844	-2.974	-1.187	-1.777	-1.729	-0.687	-1.114
B	-0.019	-0.020	-0.013	-0.010	-0.014	0.020	-0.006	-0.014
If	-1.729	-1.844	-2.974	-1.187	-1.777	-1.729	-0.687	-1.114
Kf	0.019	0.019	0.013	0.014	0.013	0.019	0.006	0.014
Δq (%)	54.39	52.49	38.85	48.76	44.24	54.83	51.60	59.53
r	0.601	0.623	0.844	0.714	0.731	0.596	0.728	0.527

The experimental data fit well the pseudo second-order model with a correlation coefficient close to unity, implying chemisorption. The rates (mg min^{-1}) of reaction obtained from the pseudo second-order have the following order: Zn > Cu > Fe >Hg > Ni > Cr >U > Co. The adsorption of Fe, Cu, Zn and U also followed the Elovich kinetic models with a correlation coefficient > 0.960, confirming a chemisorption process. The constant *a*, related to the rate of chemisorption, ranges from 0.001 for uranium to 0.037 for mercury. Besides, the values obtained for *b*, constant related to the extent of surface coverage, vary from 157.2 (Zn) to 67.60 (Co). These results are consistent with the rate of adsorption described by the pseudo second-order kinetic model.

According to the data obtained from the intraparticle diffusion kinetic model, the constant I_d > 0, assuming that both external mass transfer and intraparticle diffusion were considered as the rate limiting step. The results obtained with the film diffusion kinetic model showed that the adsorption process was not controlled by the diffusion through the liquid film.

4.4.3.3 Effect of temperature of thermodynamic parameters

i) Effect of temperature

The effect of temperature on the adsorption of metal ions on the zeolite-sorbitol system has been investigated at 18, 22, 26 and 30^{o}C. The isotherms are depicted in the Figure 4.44.

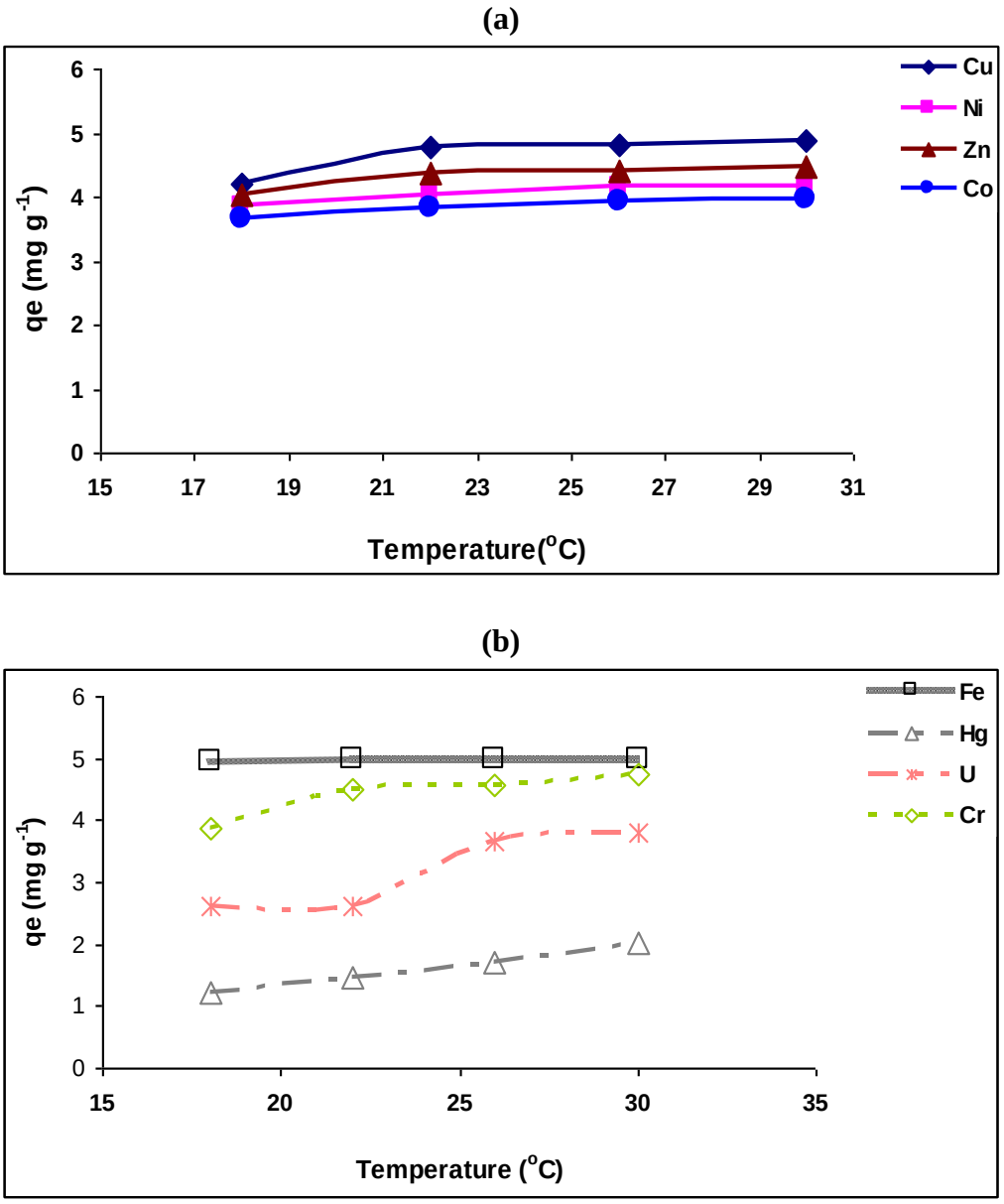


Figure 4.44 Effect of temperature on adsorption of (a) Cu, Ni, Zn, Co and (b) Cr, Fe, Hg and U onto zeolite-sorbitol in single component solutions (Ci = 100 mg L^{-1}, pH 3, agitation rate = 150 rpm, contact time = 12 h)

The results show that the adsorption of Hg, Cr and U was affected by temperature change. In fact, an increase in metal uptake was obtained with an increase in temperature. The adsorption capacity did not change with an increase in temperature for Co, Fe, Co, Ni and Zn.

ii) Thermodynamic parameters

The results for the thermodynamic parameters are listed in Table 4.38.

Table 4.38 Thermodynamic parameters for the adsorption of metal ions onto zeolite-sorbitol

	Ea kJ mol^{-1}	Δ ***H^o*** kJ mol^{-1}	Δ ***S^o*** J(K mol)$^{-1}$	Δ***G^o*** kJ mol^{-1}			
				291.15 ^{o}K	**295.15** ^{o}K	**299.15** ^{o}K	**303.15** ^{o}K
Cu	58.66	-135.1	-431.3	-6.806	-7.683	-8.196	-9.504
Ni	12.62	-29.06	-85.72	-3.442	-3.523	-3.962	-4.104
Zn	41.97	-96.65	-313.5	-3.468	-4.784	-5.037	-5.341
Co	20.80	-47.90	-152.7	-2.469	-2.942	-3.224	-3.428
Fe	-123.2	283.6	1021	-18.04	-14.26	-13.75	-13.71
Hg	20.92	-48.17	-168.8	1.773	2.169	2.854	0.984
U	10.29	-23.70	-75.64	-1.202	-0.228	-2.498	-1.676
Cr	27.78	-63.98	-204.9	-2.993	-3.376	-3.692	-4.289

The results show that the activation energy was less than 40 kJ mol^{-1} for Ni, Co, Hg, U and Cr, suggesting a physisorption process. Besides, Zn and Cu, with Ea > 40 kJ mol^{-1} followed a chemisorption process. Fe, with a negative E_a value, prefers to bind at sites with low energy barriers. The enthalpy change was negative for all the metal ions, meaning that the process was exothermic. A decrease of temperature would favour the process. The Gibbs free energy was negative for the metal ions studied, suggesting a feasible and spontaneous process. ΔG^o increases with an increase in temperature.

The negative values of entropy indicate the decrease of the degrees of freedom of metal ions at the adsorbent-metal interface. Iron exhibited a positive value of entropy, showing its affinity for the zeolite-sorbitol. The rate of adsorption of metal ions on zeolite-sorbitol increased with increasing temperature except for Fe and Hg as shown in Table 4.39.

Table 4.39 Rate of adsorption of metal ions onto zeolite-sorbitol

Rx rate (h^{-1})				
	291.15 ^{o}K	**295.15** ^{o}K	**299.15** ^{o}K	**303.15** ^{o}K
Cu	0.239	0.264	0.278	0.316
Ni	0.127	0.137	0.148	0.151
Zn	0.137	0.174	0.179	0.186
Co	0.111	0.122	0.128	0.132
Fe	0.621	0.485	0.461	0.454
Hg	0.043	0.033	0.029	0.023
U	0.062	0.081	0.090	0.110
Cr	0.124	0.133	0.141	0.156

Conclusion

The natural bentonite used in this research is crystalline with Si/Al molar ratio of 2.67. TGA/DTA analysis showed a weight loss of around 10% of hydration water and the material was found to be stable over 500^{o}C. FTIR analysis depicted the main peak of Si-O-Si and the surface charge was slightly negative below pH 4.

The results of equilibrium studies revealed that operational conditions such pH, contact time initial solution pH and concentration, the presence of competing cations etc, are able to affect the adsorption capacity and efficiency of natural bentonite. The maximum adsorption capacity was reached at pH 5 for U, Ni, Cu,Cr and at pH 7 for Zn and Co. The maximum adsorption capacity obtained at the pH range 5 to 7 for all the metals studied is probably due to adsorption as well as precipitation process since most of the metals hydrolysed at this pH range. Therefore, the efficiency of natural bentonite for metal adsorption is dependent on the initial solution pH.

The adsorption data fitted well the Langmuir and Dubinin-Radushkevich models, suggesting monolayer coverage on a heterogenous surface with ion exchange as the principal mechanism as suggested by the magnitude of the mean free energy (Es). The metal affinity based on the distribution coefficient was in the following sequence: Fe > Cu > Cr > Co > Ni > Zn > U > Hg.

The adsorption of Cu, Ni, Zn, Co, Cr, Fe, Hg and U ions followed the pseudo second-order kinetics. The calculated rate constants of the adsorption showed that adsorption of Fe was

faster (15 times more than U ions) and also marked by negative activation energy, indicating binding on sites with low energy. The metal adsorption was endothermic and spontaneous. The adsorption of mercury was not spontaneous as ΔG^o was positive with a very low adsorption rate. The entropy change (ΔS^o) of the adsorption of heavy metal ions was in the range of 87- 486.9 J (mol K^{-1}), showing an increase of randomness at the solid-liquid interface during the adsorption.

The adsorption capacity of natural bentonite was enhanced by the surface modification microbial component as histidine. The synthesized bentonite-histidine showed the main groups as N-H, COO-, Si-O and O-H on its surface, which was negative at a pH range from 2 to 8. Although the surface area decreased from 73.82 to 61.25 $m^2 g^{-1}$, bentonite-histidine was more efficient in metal adsorption mostly at low pH due to the presence of N-H. At pH < 4, histidine acts as a proton "shuttle", the amine group is protonated and, in the presence of the silicon oxide, zwitterions are formed which are less subjected to leaching compared to metal ions.

Maximum adsorption capacity was obtained even at low pH (2) with an increase of adsorption capacity, mostly for U and Hg. The formation of complexes between the metal ions and the bentonite-histidine depends on the amino groups present on the adsorbent. The rate of metal adsorption on bentonite-histidine was greater than that of natural bentonite at high concentration of metals due to the structure of bentonite-histidine.

Adsorption capacity (mg g^{-1}) of metal ions on bentonite-histidine increased by 9%, 12%, 8%, 22%, 26%, 50%, 52% and 25% for Cu, Co, Cr, Fe, Hg, Ni, Zn and U, respectively. Complexation and ion exchange in bentonite-histidine contribute to improve the adsorption capacity. The adsorption equilibrium data fitted the Langmuir and Freundlich isotherms and the affinity of the metals towards the biosorbent obtained from the distribution coefficient followed the order: Fe, Cu, Zn, Ni, Co, Cr, Hg and U.

The kinetics of adsorption followed the pseudo second-order model with rate constants higher than those of natural bentonite. The negative values of ΔG^o indicate the feasibility and the spontaneity of the adsorption process. The values of activation energy, enthalpy change were greater than those obtained at the same temperature for the natural bentonite, probably due to the formation of the complex between the metal ions and the amine groups attached on the

bentonite structure. The process was endothermic with entropy changes indicating the randomness at the interface of the sorbent.

The modification of the bentonite surface by L-cysteine occurs through the $-NH_3^+$ moiety and the FTIR spectrum depicted the presence of N-H, S-H, COO-, Si-O and O-H groups.
The maximum adsorption capacity was obtained at a low pH of 2. In fact, the presence of functional groups such as –NH–,–SH– and COO^- provided by the cysteine molecule, contribute to enhancing the adsorption capacity of natural bentonite. At low pH, $-NH_2^+$ or $-SH_2^+$ are protonated simultaneously and compete with protons for the negative charge. Also, -HS (a soft base) has an affinity for soft metals such as Hg while hard bases such as NH_2 and COO^- will preferably bind to hard metals. Studies performed on the metal complexes of cysteine indicate that the preferred binding mode of Cu, Fe and Zn with cysteine is bidentate (sulphur and nitrogens atoms).

Freundlich and D-R isotherms described the adsorption equilibrium, suggesting that the adsorption occurred on a heterogeneous surface. The affinity of the metal ions for the bentonite-cysteine followed the sequence: Cr > Fe> Zn> Ni> Co> Hg > Cu > U. The values of the distribution coefficients were high for Cr, Fe and Zn which indicated the presence of stronger bonds. Beside the HSAB theory, the metals affinity towards the biosorbent will also depend on the amount and the accessibility of the functional groups or binding sites. The kinetics of adsorption is well described by the pseudo second-order model with a higher adsorption rate for Fe.

The metal adsorption on bentonite-cysteine was spontaneous and exothermic with low activation energy, indicating physisorption. The negative entropy changes imply a decrease of degrees of freedom of the metal ions at the interface with the bentonite-cysteine system.
The change in temperature did not affect the adsorption capacity of the metal ions, except for zinc, although the rates of adsorption tend to decrease with increasing temperature. The maximum adsorption rate for uranium and mercury was reached at 295K.

The bentonite-sorbitol had a surface area of 25.02 $m^2\ g^{-1}$. The FTIR spectrum confirmed the presence of an O-H, Si-O with a negatively-charged surface at the pH range 2 to 8. The uptake of Cu, Co, Cr, Fe, Ni and Zn was maximum and constant from pH 2 to 12 whereas the uptake of Hg and U was low at pH < 5. The maximum uptake was obtained at pH 7. The

binding capacity of metals onto bentonite-sorbitol depends on the nature and amount of functional groups on the surface of the biosorbent according to the HSAB principle. Competition for the binding sites by protons decreases the metal uptake at low pH.

The adsorption capacities of metal ions increase with an increase in initial metal concentration. A slight decrease of Ni and Cu occurs at 200 mg L^{-1} while the saturation points were not reached up to 500 mg L^{-1} for Cu, Co, Cr, Fe, Hg, Ni, Zn and U. The adsorption data fitted well The Freudlich and D-R isotherms, predicting adsorption on a heterogeneous surface. The metal affinity towards the bentonite-sorbitol followed the sequence: Cr > Fe > Co > Cu > Ni > Zn > U > Hg.
The kinetics of adsorption is described by the pseudo second-order as well as Elovich models. The rise of temperature increases the adsorption capacities and the adsorption rate of metal ions on bentonite-sorbitol. The uptake of Fe, Cr and Cu was not affected by the changes in temperature though. The adsorption was exothermic and spontaneous with activation energy > 40 kJ mol^{-1}, implying a chemisorption process. The negative entropy changes correspond to a decrease in the degrees of freedom of the metals at the interface with bentonite-sorbitol.

Since bentonite-mannitol has similar characteristics to bentonite-sorbitol as they are isomers, similar results were obtained and the above conclusions are valid for the adsorption of metal ions onto a bentonite-mannitol sorbent.

Natural zeolite studied in this work had a Si/Al molar ratio of 1.08 and a surface area of 0.692 m^2 g^{-1}. The surface was negatively charged for the pH range from 2 to 8 and the FTIR analysis showed the peaks of Si-O-Si, O-H and H-O-H. TGA/DTA analysis showed thermal stability of natural zeolite over a temperature of 500^{o}C with 17% of free water lost up to 400^{o}C.

The adsorption of Cu, Co, Cr, Fe, Hg, Ni, Zn and U on natural zeolite was strongly influenced by the pH of the solution. In general, metal adsorption increased with an increase of pH with a maximum adsorption capacity obtained at pH 5 for all the metals studied. At low pH, the protons compete with the metal ions for the binding sites. At high pH, there is a combination of adsorption and precipitation of metals hydroxides.

The adsorption of heavy metal ions at different concentrations increased linearly until equilibrium was reached. The uptake of metal ions takes place in zeolite by adsorption and ion exchange processes. Ion exchange is based on several factors such as: type of counter ion to be exchanged, size of the pore opening in zeolite, ion exchange equilibrium in aqueous solution and ion exchange of zeolite.

Langmuir, Freundlich as well as D-R isotherms were found to fit the equilibrium data, except for uranium, whose fit did not obey the Freundlich isotherm. Equilibrium isotherms are considered a better tool for obtaining the selectivity series. Based on the distribution coefficient, the selectivity of metal ions was as follows: Fe> Zn > Cu > Ni > U > Cr > Co > Hg.

Maximum adsorption of metals was achieved within 30 minutes following the pseudo second-order and Elovich kinetic models, implying chemisorption as the rate-limiting step. The uptake of Hg and U increased with increase in temperature and maximum adsorption was reached at 299 K while maximum adsorption was obtained at 291 K for the other metals.

The thermodynamic constants, Gibbs free energy (ΔG^{o}), enthalpy change (ΔH^{o}) and entropy change (ΔS^{o}) were calculated to evaluate the thermodynamic feasibility of the process and to confirm the nature of the adsorption process. The adsorption of Fe, Zn, Co and U was by physisorption with activation energies < 40 kJ mol^{-1}. The process was exothermic for Cu, Ni, Co, Hg and Cr, whereas an endothermic process was observed for the other metals. The spontaneity of the adsorption of metal ions onto natural zeolite was confirmed by the negative values of Gibbs free energy.

The surface area of the zeolite-histidine synthetised in this work was about 0.545 m^2 g^{-1}. The FTIR spectrum showed the peaks of: N-H, Si-O-, COO- and O-H proving the surface modification of natural zeolite. The surface charge of the zeolite-histidine sorbent was negative for the pH range 2 to 8.

The uptake of metal ions by zeolite-histidine was maximal even at low pH due to the presence of functional groups such as N-H and COO-. The amount of metals bound to the biosorbent increased with increase in initial metal concentration.

The Langmuir model effectively described the sorption data with all R^2 values >0.95. The Freundlich and D-R isotherms also described the experimental data over the range of

concentrations studied, suggesting surface heterogeneity and exponential distribution of active sites and their energies.

The order of stability of the metal-biosorbent complexes was found to be: U >Hg > Zn > Cu > Co > Fe > Ni > Cr, which can be attributed to adsorption combined with ion exchange mechanism and, ionic attraction of positively-charged metal ions and negatively-charged hydroxyl and carboxylic groups.

The adsorption kinetics followed the pseudo second-order model with R^2 close to unity for all the metals studied. The rate constants were in the following sequence: U >Hg > Fe > Cu > Zn > Cr > Co > Ni. This sequence was similar for uranium and mercury which form the most stable complexes. The adsorption was endothermic and spontaneous with activation energies indicating chemisorption.

Zeolite-cysteine synthetized in the present work has a surface area of 0.423 m^2 g^{-1} with the presence of functional groups confirmed by the presence of groups such as: N-H, S-H, COO-, Si-O and O-H. The surface was negatively-charged for the pH range 2 to 8. A drastic increase of adsorption capacities of Hg and U were obtained at low pH compared to their adsorption on natural zeolite. This is probably due to the presence of functional groups on the surface of the biosorbent such as: –NH–, –SH– and COO^- provided by the cysteine molecule. The maximum adsorption capacity was reached at pH 6 for Ni and Cr ions as a result of the combination of precipitation and adsorption.

The adsorption capacity increased with the increase of metal concentration in solution and was described by the Freundlich isotherm. The isotherm of adsorption could also be predicted by the D-R isotherm. The stability of the metal-adsorbent complexes, as given by the Langmuir isotherm, was in the following sequence: Cu > Hg > Fe > Cr > Co > Zn > Ni > U.

The kinetics of adsorption is described by the pseudo second-order model with rate constants higher for Fe, U and Hg. The adsorption of metal ions on zeolite-cysteine was spontaneous and exothermic on binding sites with low energy. The rates of metal adsorption on zeolite-cysteine increased with an increase in temperature.

The zeolite-sorbitol was characterized by a surface area of 0.555 m^2 g^{-1} and was negatively-charged for the pH range 2 to 8. The following groups were identified by FTIR: Si-O- and O-H groups.

The maximum uptake of Fe, Hg and U was reached at pH 5 whereas the adsorption capacities for the rest of the metals were constantly maximal for the pH range 2 to 12. The adsorption

capacity increased with an increase in initial metal concentration and followed the Freundlich and D-R isotherm, except for Ni.

The selectivity of metals by the zeolite-sorbitol according to the distribution coefficient was in the order: Co > Zn > Cr >Ni > Hg > U >Fe > Cu. The Langmuir isotherm showed that Ni forms the strongest complex with zeolite-sorbitol.

The adsorption capacities did not change much with increases in temperature and the process was found to be exothermic. Low values of activation energies indicated that adsorption occurs on binding sites with low energy. The spontaneity of the process confirmed the feasibility of the biosorption with an increasing rate with temperature.

As for the bentonite-mannitol, similar conclusions could be drawn from observations made for zeolite-mannitol.